Functional consequences of jaw adductor hypertrophy on prey capture in clarifd catfishes

Proefschrift voorgelegd tot het behalen van de graad van Doctor in de Wetenschappen aan de Universiteit Antwerpen te verdedigen door



Promotor: Prof. dr. Peter Aerts Co-promotor: dr. Anthony Herrel





Faculteit Wetenschappen Biologie

Functional consequences of jaw adductor hypertrophy on prey capture in clariid catfishes

Functionele consequenties van kaakspierhypertrofie voor de voedselopname bij clariide katvissen

Proefschrift voorgelegd tot het behalen van de graad van doctor in de Wetenschappen aan de Universiteit Antwerpen te verdedigen door

Sam VAN WASSENBERGH

Promotor prof. dr. Peter Aerts Co-promotor dr. Anthony Herrel

Antwerpen, 2006

Promotor: Prof. dr. Peter Aerts

Universiteit Antwerpen

Co-Promotor: dr. Anthony Herrel

Universiteit Antwerpen

Overige leden van de promotiecommissie:

Prof. dr. Erik Matthysen Universiteit Antwerpen

Prof. dr. Ronny Blust Universiteit Antwerpen

Prof. dr. Raoul Van Damme Universiteit Antwerpen

Prof. dr. Dominique Adriaens Universiteit Gent

Prof. dr. Johan van Leeuwen Wageningen Universiteit

Phd defence: 19 may 2006, Auditorium S1, Campus "Drie Eiken", University of Antwerp.

Van Wassenbergh, S. (2006) Functional consequences of jaw adductor hypertrophy on prey capture in clariid catfishes. Doctoral thesis, Laboratory for Functional Morphology, University of Antwerp, Universiteitsplein 1, B-2610 Wilrijk, Belgium.

Subject headings: catfish / jaw muscles / suction / feeding / scaling / trade-offs / modulation / sternohyoideus / terrestrialization

Cover picture of Gymnallabes typus (head length 22 mm), © Sam Van Wassenbergh

Table of Contents

Chapter 1:	Introductionp. 5
Chapter 2:	A test of mouth-opening and hyoid-depression mechanisms during prey capture in a catfish using high-speed cineradiography
Chapter 3:	Scaling of suction feeding performance in the catfish <i>Clarias gariepinus</i> p. 35
Chapter 4:	Scaling of suction-feeding kinematics and dynamics in the African catfish, <i>Clarias gariepinus</i> p. 57
Chapter 5:	A dynamic model of mouth closing movements in clariid catfishes: the role of enlarged jaw adductorsp. 79
Chapter 6:	Effects of jaw adductor hypertrophy on buccal expansions during feeding of air breathing catfishes (Teleostei,Clariidae)
Chapter 7:	No trade-off between biting and suction feeding performance in clariid catfishesp. 127
Chapter 8:	Interspecific variation in sternohyoideus muscle morphology in clariid catfishes: functional implications for suction feeding
Chapter 9:	Modulation and variability of prey capture kinematics in clariid catfishes
Chapter 10:	Catfish strikes on landp. 177
References	p. 184
Summary in 1	Dutch/Nederlandse samenvattingp. 193
Acknowledge	ements/Dankbetuigingp. 199
Curriculum V	7itaa a 201

Chapter

Introduction

1.1 Functional trade-offs in the feeding system of aquatic animals

The cranial musculo-skeletal system of fishes must fulfil a number of crucial biological functions. It has to cope with capturing, processing and transporting prey, breathing water or air, participating in sensory perceptions, providing protection for the major sense organs and brains, and serving as a streamlined bow in locomotion. Logically, each of these functions calls for specific, structural and dynamical requirements to the animal's cranial system. Consequently, it is not surprising that the skull of fishes is an extremely complex apparatus, consisting of more than sixty interconnected and mobile skeletal parts that can be moved by the action of an approximately equal number of muscles (Barel et al., 1976; Anker, 1978).

The transmission of force and velocity between coupled elements of the fishes' head has been studied previously, mainly in percomorph fishes (Percidae) with (in contrast to most catfishes) a pronounced laterally flattened head (Elshoud-oldenhave and Osse, 1976; Otten, 1982; Aerts and Verraes, 1984; Muller, 1987; 1996; Westneat, 1990; 1994; 2004; Aerts, 1991; De Visser and Barel, 1996; Bergert and Wainwright, 1997; Durie and Turingan, 2004, Konow and Bellwood, 2005). Still, even for essential functions such as mouth opening or depression of the hyoid apparatus, relatively little is known about the underlying mechanisms causing these movements. To understand the basic mechanisms of prey capture in catfishes, **CHAPTER 2** of this thesis will deal with the linkage mechanics involved in lower jaw and hyoid movement.

In such strongly integrated and functionally divers systems, the individual units of the system must inevitably take part in several functions. The most striking example of functional overlap in the cranial system of fishes during two different functions is probably suction feeding and respiration (Roth and Wake, 1989). Although the magnitude and timing of the movements of the structures involved in feeding and respiration are clearly

different, nearly all skeletal element causing the bucco-pharyngeal volume increase during suction feeding (lower jaw, hyoid, cleithrum, operculum and branchiostegal membrane) are also used in generating the flow of water through the gills (Liem, 1985).

Cranial elements taking part in more than one function are not only found when focussing on feeding and respiration. Also within the process of prey capture, elements are used in several, functionally distinct aspects of prey capture. For example, the lower jaw and the suspensorium (suspending the lower jaw to the neurocranium) are essential in exerting bite forces onto prey (Herrel et al., 2002), which is often used by fishes for crushing hardshelled prey, tearing pieces out of large prey or holding prey tightly between the jaws (e.g., Grubich, 2000; Korff and Wainwright, 2004; Alfaro and Westneat, 1999). On the other hand, fast lower jaw depression and abduction (lateral rotation) of the suspensorium contribute to the flow of water into the mouth generated during suction feeding, which enables fishes to draw more distant prey towards and into the mouth (e.g., Lauder, 1985; Aerts, 1990; Gibb and Ferry-Graham, 2005; Wainwright et al., 2001; Van Leeuwen and Muller, 1984).

Any evolutionary change (either structural, functional or behavioural) in one of the components of such an integrated system will likely influence all functions in which this component cooperates. An important consequence of this is that natural selection will probably not result in an optimisation of one of the multiple functions, because this can have a negative influence on the other functions (that probably have other optimisation criteria). Such evolutionary 'trade-offs' are often observed in nature: a certain change in one aspect of the system increases the performance of a given function, but at the same time reduces the organism's efficiency in performing an other, morphologically coupled function (e.g., Pasi and Carrier, 2003; Schondube and Del Rio, 2003; Vanhooydonck and Van Damme, 2001; Van Damme et al., 2002).

1.2 Jaw closer hypertrophy in Clariidae

Within the family of the air-breathing catfishes (Clariidae), a remarkable evolution in one of the components of the cranial system can be observed: several species have developed extremely large (or hypertrophied) jaw adductor muscles (Cabuy et al., 1999; Devaere et al., 2001; Herrel et al., 2002). Such hypertrophy of the jaw muscles has evolved at least four times independently in this group of fishes, originating from a *Clarias*-like ancestor (Jansen et al., 2006). As shown by Herrel et al. (2002), the species *Clarias gariepinus*, *Clariallabes longicauda*, *Gymnallabes typus* and *Channallabes apus* can be viewed as a morphological series with gradually increasing hypertrophy of the jaw adductors (Fig. 1). The species with the most extreme jaw adductor hypertrophy (*Channallabes apus*) has a *musculus adductor mandibulae* A2A3' with a physiological cross-sectional area of almost 7 times the value for the species with the least developed jaw adductors, *Clarias gariepinus* (Fig. 2). The differences between

these jaw-closing muscles in maximal bite force that theoretically can be generated are of the same order of magnitude (Herrel et al., 2002; Fig. 2).

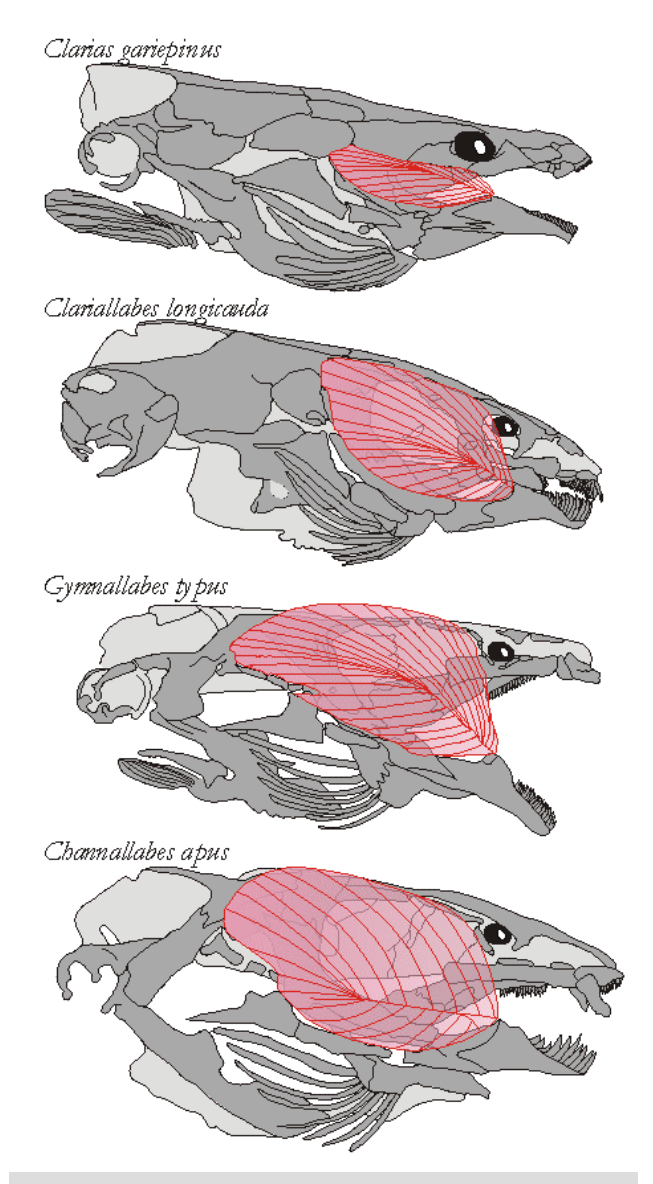


Figure 1: Lateral view on the osteocranium and the jaw adductor muscles (in *pink*) of four clariid species with increasing size of the jaw adductors (from top to bottom). Drawings are modified after Cabuy et al. (1999) for *Clarias gariepinus* and *Gymnallabes typus*, Van Meir (2001) for *Clariallabes longicauda* and Devaere et al. (2001) for *Channallabes apus*. Note that bones cover part of the muscle complex in *Clarias gariepinus*.

Why different lineages of clariid catfishes have developed such large jaw closing muscles in course of their evolution is unclear. The most obvious possibility is that jaw adductor hypertrophy has evolved as an adaptation for durophagy, enabling these catfishes to crush hard prey by producing large bite forces (Fig. 2). Indeed, studies demonstrating the relationship between the size of the jaw adductors, the maximal amount of bite force that can be generated (Herrel et al., 2002; Fig. 2) and the proportion of hard prey (especially beetles) included in the diet (Huysentruyt et al., 2004) support this idea.

1.3 Consequences of jaw muscle hypertrophy

Apart from the query why jaw adductor hypertrophy evolved (the link with ecology), an equally important question is: What are the consequences of this drastic change in jaw adductor morphology onthe mechanical functioning of the cranial system during feeding? Observations of clariid catfishes in their natural habitat have shown that feeding involves more than just exerting bite force on prey (Bruton, 1979). Food is

sucked into the mouth by enlarging the volume of the buccopharyngeal chamber, followed by snapping the jaws onto the prey. For several aspects of this prey capture process, direct or indirect consequences of the hypertrophy of the jaw adductors can be expected. These consequences can either be positive (improving the performance of a certain function) or negative (in trade-off with bite performance).

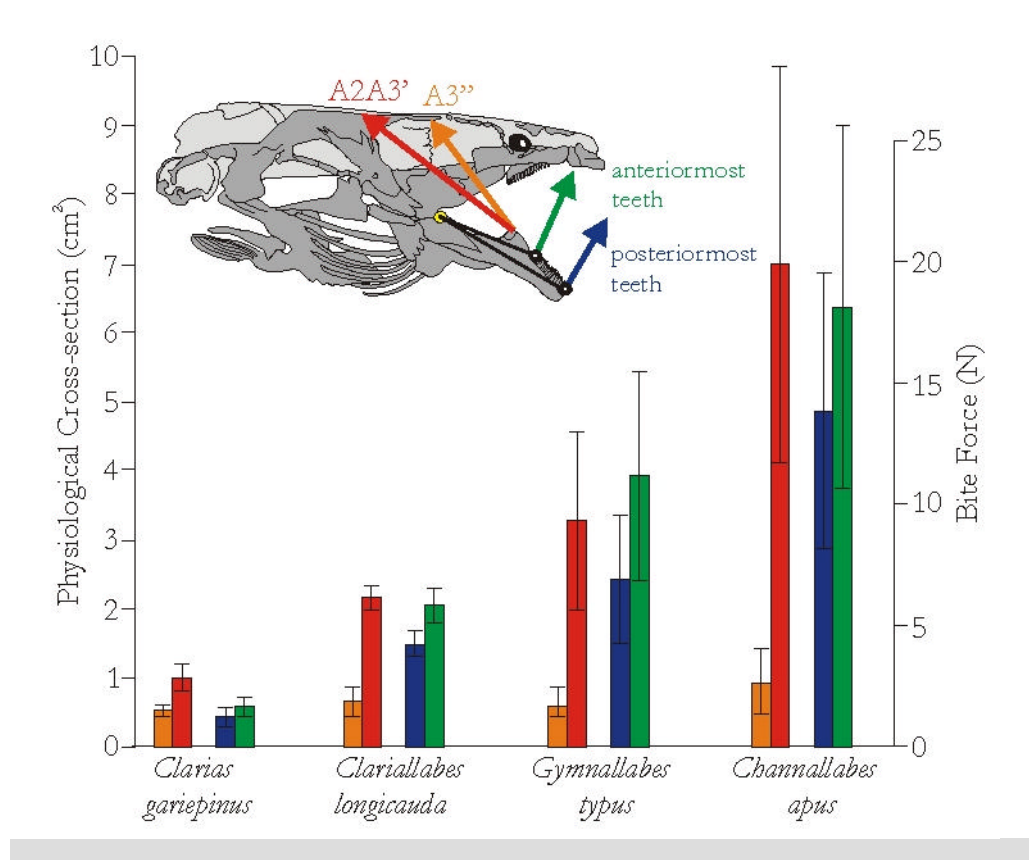


Figure 2: Single side physiological cross-sectional areas of the two parts of the jaw adductor muscle complex: the superficial *m. adductor mandibulae* A2A3' (*orange*) covering the smaller and more internal *m. adductor mandibulae* A3" (*red*). The bite force calculated for two positions along the lower jaw (at the posteriormost teeth, in *blue*; and at the anteriormost teeth, in *green*) and perpendicular to the lower jaw's output lever are shown in the graph (Herrel et al., 2002). For these static bite force calculations, all cranial lengths were scaled to 39 mm and the gape angle was set to 10 degrees.

A potential positive consequence of increasing the size of the jaw adductors is faster mouth closing after the prey has been drawn towards the mouth by suction. An analysis of the diet of Clariidae has shown that, besides including larger fractions of hard prey into the diet, the species with enlarged jaw adductors continue preying on fishes (Huysentruyt et al., 2004), which are usually fast and agile prey. Therefore, rapid snapping of the oral jaws onto the prey can be important to reduce the chance of prey escape and thus increasing the

catfishes' prey capture success. The value of having enlarged jaw muscles on the speed of jaw closure will be addressed in **CHAPTER 5**.

The enlarged jaw muscles tightly cover the suspensoria, which are (especially in the hard-biting species) firmly connected to the neurocranium (Cabuy et al., 1999; Devaere et al., 2001). Consequently, the jaw adductor hypertrophy could interfere with the lateral expansion of the buccal cavity occurring during suction generation, in which the suspensoria are abducted (i.e. rotated away from the medial body axis). This suspensorium-abduction can be hindered by either visco-elastic deformation of the jaw muscles or by the strongly interdigitated connection with the neurocranium. The potential effect of jaw adductor hypertrophy on the magnitude of lateral expansion during suction feeding will be studied in **CHAPTER 6**.

As hypothesised above, certain aspects of suction feeding kinematics may be hindered by the presence of the large jaw muscles. Still, this does not necessarily imply that the overall suction feeding performance (i.e. the amount of force exerted on the prey by displacing a parcel of water in front of the mouth relative to the fishes' head) is reduced: for example, a smaller amount of lateral expansion could be compensated for by increasing the amount of ventral expansion. Several studies have indeed proposed that the anatomical changes enhancing biting forces could decrease suction performance (Barel, 1983; De Visser and Barel, 1996; 1998; Bouton et al., 1999). However, no experimental data have yet demonstrated these predictions. In **CHAPTER 7**, the suction performance in clariid catfish species with different biting performance will be compared.

One of the levels at which suction performance can be increased considerably, is by increasing the magnitude and/or speed of the depression of the hyoid apparatus. Furthermore, no mechanical interference can be expected between the size of jaw adductors and the lowering of the mouth floor by depressing the hyoid. Therefore, if catfishes with hypertrophied jaw adductors need to increase their suction performance, modifications to the hyoid depression system are probably the most obvious option. In **CHAPTER 8**, I will focus on the mechanics of hyoid depression and how morphological variation in the sternohyoideus muscle (the hyoid depressor muscle) is related to the way the hyoid is depressed in the species presented in Figure 1.

Huysentruyt et al. (2004) showed that the species with jaw adductor hypertrophy have a less diverse diet. According to a hypothesis by Liem (1984), such trophic specialists are expected to be less flexible in their feeding capacities compared to species feeding on a wide range of different prey (trophic generalists such as *Clarias gariepinus*). In **CHAPTER** 9, I will quantify the variability in prey capture kinematics in response to different prey types and different prey positions and tested Liem's hypothesis within this group of fishes.

At the University of Ghent, a remarkably feeding behavior of *Channallabes apus*, the species with the most extreme jaw adductor hypertrophy, was discovered: this animal appeared to be able to capture food presented out of the water, on top of a piece of floating wood.

Given its muddy habitat in the swamps of tropical Africa, expanding the foraging zone to the area outside of its small, acid puddles probably increases the range of potential prey for this species drastically. The large amount of terrestrial beetles found in stomachs of these catfishes (Huysentruyt et al., 2004), seems to support that *Channallabes apus* actually is capable of feeding out of the water. In **CHAPTER 10**, this unusual feeding behavior will be analyzed and discussed.

1.4 Scaling effects

As our study species (Clarias gariepinus, Clariallabes longicauda, Gymnallabes typus and Channallabes apus) differ considerably in adult cranial size, a better knowledge on the biomechanical consequences of size on the suction feeding process in Clariidae is more than welcome. Accounting for scaling effects when results are compared between catfishes of different sizes will be necessary in different parts of this thesis. Therefore, I will analyze prey capture kinematics in an ontogenetic series of the African catfish (Clarias gariepinus), a species that can grow up to 1.5 m in total length in CHAPTER 3 and CHAPTER 4.

Although scaling relationships on aquatic feeding kinematics have been studied previously (Richard and Wainwright, 1995; Cook, 1996; Hernandez, 2000; Wainwright and Shaw, 1999; Robinson and Motta, 2002), the size-related effects of kinematics on performance (displacing the prey towards the mouth) and the biomechanical causes of the observed changes in suction feeding kinematics (decreasing speed of cranial expansion with growth) remain unclear. Consequently, the presented scaling analyses are more than just a tool to account for confounding size-effects in comparative studies, but are an important and challenging research topic.

Chapter 2

A test of mouth-opening and hyoid-depression mechanisms during prey capture in a catfish using high-speed cineradiography

Sam Van Wassenbergh – Anthony Herrel – Dominique Adriaens – Peter Aerts

The Journal of Experimental Biology 208, 4627-4639 (2005)

Summary

Detailed morphological analyses have identified a number of different mechanical pathways by which the morphologically complex cranial system of fishes can achieve mouth opening and hyoid depression. However, many of these proposed mechanisms remain untested. Furthermore, very little is known about the precise timing of activity of each of these mechanisms, and about the magnitude of each mechanism's total contribution to its proposed function. In the present study, all mouth opening and hyoid depression mechanisms described for *Clarias gariepinus*, an air-breathing catfish, are analysed. High-speed X-ray videos were recorded during prey capture of three catfish implanted with small, radio-opaque markers in the cranial elements potentially involved. A kinematic analysis was performed from which data were used as input in planar four-bar models. This analysis shows that the opercular mouth-opening mechanism initiates mouth opening, but is not able to cause the complete mouth-openings as observed on the X-ray videos. The latter is accomplished through the protractor hyoidei muscles, which couple hyoid depression to lower jaw depression in a four-bar system and also reinforce lower jaw

depression by shortening during the final stage of mouth opening. Although the anguloceratohyal ligament was previously hypothesised to play a part in mouth opening, our results show that it probably does not, but rather functions as a hyoid-elevator during mouth closure. Finally, hyoid depression is exclusively achieved by the four-bar mechanism involving neurocranial elevation and pectoral girdle retraction, generally without any reinforcement by shortening of the sternohyoideus muscle. In contrast to the results from a recent analysis on sunfish, the catfish's sternohyoideus gradually elongates during hyoid depression.

2.1 Introduction

Fishes are known to have a morphologically complex and highly kinetic skull (Ferry-Graham and Lauder, 2001). The cranial musculo-skeletal system of adult teleost fishes consists of about 60 interconnected skeletal parts that are moved by an approximately equal number of muscles (Aerts, 1991). Since the early 20th century, functional morphologists have identified a large number of distinct, kinematic couplings between the elements of the head. They examined, for instance, couplings (or linkages) involved in protrusion of the jaws (Van Dobben, 1937; Alexander, 1970a; Motta, 1984; Westneat and Wainwright, 1989; De La Hoz, 1994; De La Hoz et al., 1994; Waltzek and Wainwright, 2003, Ferry-Graham et al., 2001; Hulsey and Wainwright, 2003, Konow and Bellwood, 2005; Wainwright et al., 2005), depression of the lower jaw (Van Dobben, 1937; Otten, 1982; Aerts and Verraes, 1984; Westneat, 1990; 1994; 2004; Gibb, 2003; Durie and Turingan, 2004, Konow and Bellwood, 2005), depression of the hyoid (Elshoud-oldenhave and Osse, 1976; Muller, 1987; 1996; Bergert and Wainwright, 1997) and abduction of the suspensorium (Elshoud-oldenhave and Osse, 1976; Aerts, 1991; De Visser and Barel, 1996). Considerable insight into the behaviour of these systems has been achieved by modelling these as planar four-bar linkages, i.e. closed and intrinsically movable chains of four bars of which one is immobile (Muller, 1996). In this way, understanding has been gained in the transmission of force and velocity between coupled elements of the fishes' head.

An additional aspect of the functional complexity of the cranial system in fishes is that some essential functions during feeding and respiration, such as opening the mouth or rotating the hyoid ventrally, can be achieved by more than one mechanism at the same time. According to morphological studies, the majority of adult teleosts are theoretically able to depress their lower jaw using four mechanisms (Diogo and Chardon, 2000), which are illustrated in Fig. 1 for *Clarias gariepinus*, the species studied here: (1) the opercular fourbar mechanism in which dorso-caudal rotation of the opercular bone (realised by contraction of the levator operculi muscle) retracts the interopercular bone and a ligament connecting this bone to the lower jaw (Fig. 1A), (2) a hyoid four-bar mechanism in which lower jaw depression is generated by a ligament between the hyoid and the lower jaw (*ligamentum angulo-ceratohyale*) that is pulled ventro-caudally when the hyoid is depressed (Fig.

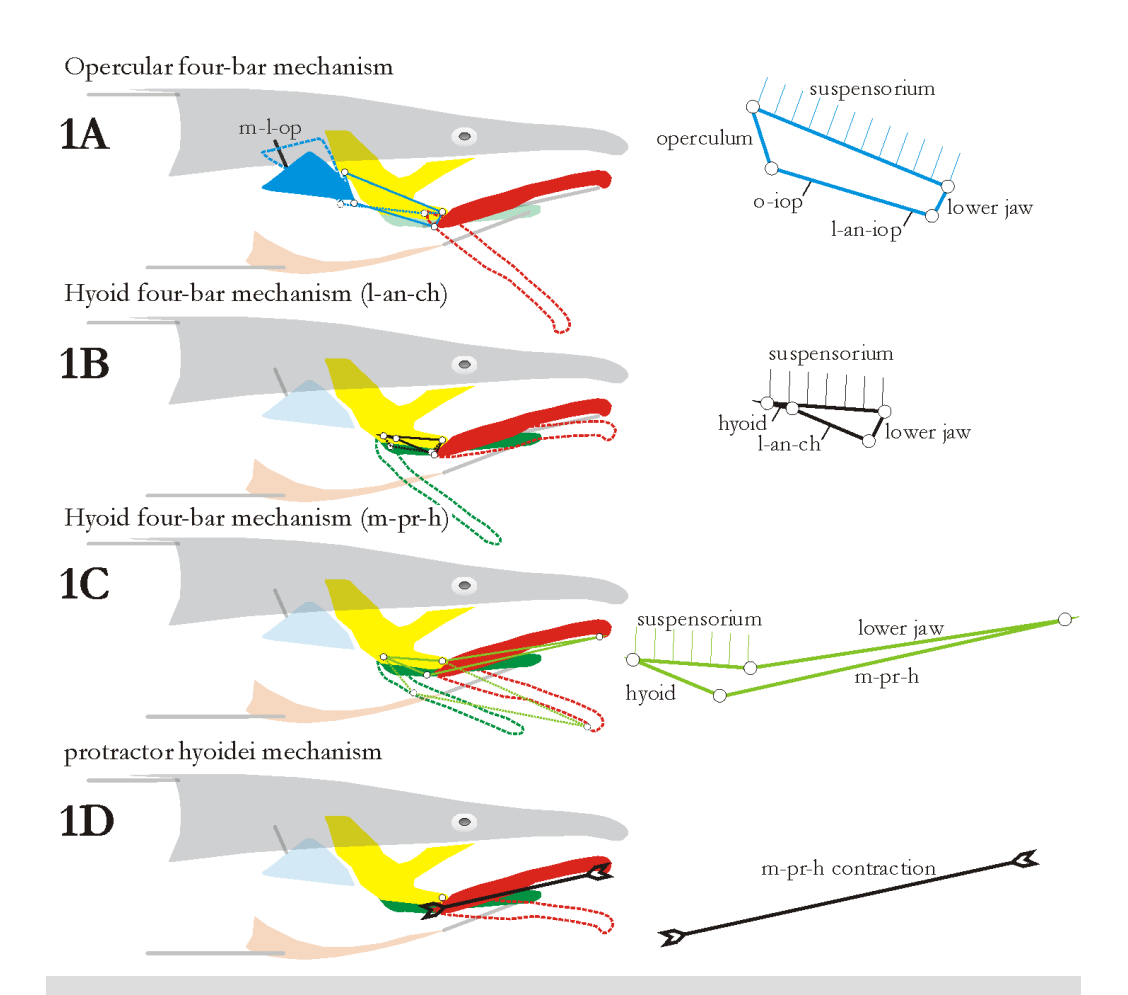


Figure 1: Schematic representation of the four potential mouth-opening mechanisms (A-D) in *Clarias gariepinus*. The involved functional elements of the cranial system are represented by different colours: lower jaw (red), hyoid (green), suspensorium (yellow), operculum (blue), cleithrum (yellow) and neurocranium (grey). Dark and light colours represent elements that are involved and not involved, respectively, in a particular mechanism. Broken lines correspond to positions of cranial elements and four-bar chains after activity of the mechanisms. A more detailed representation of the four-bar systems is given on the right, in which the fixed link is represented by short perpendicular lines. Abbreviations: l-an-ch = ligamentum angulocerotohyale, l-an-iop = ligamentum angulo-interoperculare, m-l-op = musculus levator operculi, m-pr-h = musculus protractor hyoidei, o-iop = os interoperculare.

1B) (3) a second hyoid four-bar mechanism in which the coupling between the hyoid and the lower jaw is established by the protractor hyoidei muscles (Fig. 1C) and (4) contraction of the protractor hyoidei itself (Fig. 1D), which will reinforce the action of the previous mechanism in case of ongoing hyoid depression.

A similar situation occurs for the depression of the hyoid apparatus, which can be achieved by two mechanisms (Fig. 2): (1) by a four-bar mechanism involving neurocranial elevation and pectoral girdle retraction (Fig. 2A; see also Muller, 1987; Bergert and Wainwright, 1997) and (2) by contraction of the sternohyoideus muscle, which will reinforce the action of the first hyoid depression mechanism in case neurocranial elevation and/or pectoral girdle retraction is taking place (Fig. 2B). Both cases, however, at least require a fixation of the pectoral girdle by the hypaxial muscles.

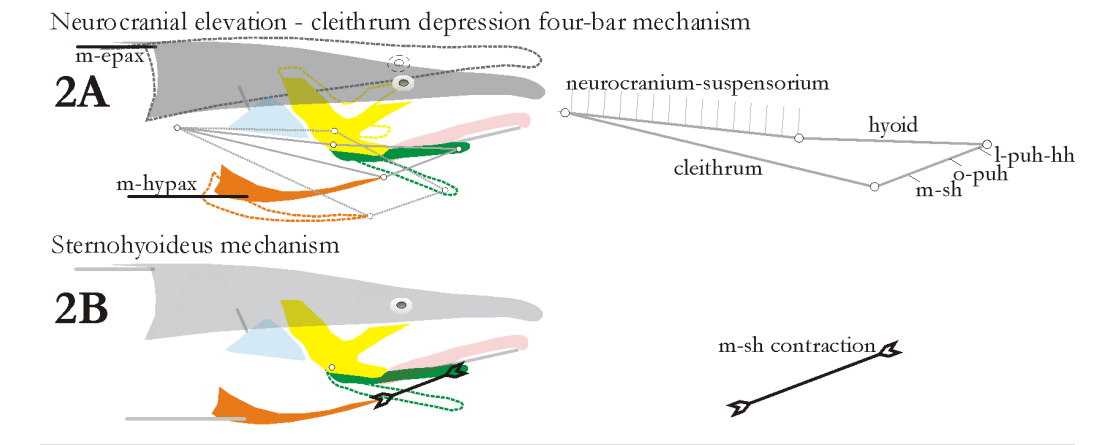


Figure 2: Schematic representation of the two potential hyoid-depression mechanisms (A, B) in *Clarias gariepinus*. Colours and symbols correspond to those used in Fig.1. Abbreviations: l-puh-hh = ligamentum parurohyalo-hypohyale, m-epax = epaxial muscles, m-hypax = hypaxial muscles, m-sh = musculus sternohyoideus, o-puh = os parurohyale.

Despite the large amount of literature on mechanisms of mouth opening and hyoid depression in fish, very little is known on how these different mechanical pathways operate in vivo when carrying out their proposed functions. Do all mechanisms contribute simultaneously during the entire mouth opening or hyoid depression? Or are there mechanisms that only perform their proposed function during the initial phase of lower jaw or hyoid motion, while others are active at later instants? Concerning the opercular mouth-opening mechanism, for example, it has been suggested that this mechanism has a role in initiating lower jaw depression in cichlids (Aerts et al., 1987; Durie and Turingan, 2004). For some other fish, however, kinematic studies have reported opercular rotations continuing until the mouth reaches its maximal gape (e.g. Elshoud-Oldenhave and Osse, 1976; Lauder, 1982; Konow and Bellwood, 2005), which could imply that the opercular mouth opening mechanism is active for longer than just during the initial stages of mouth opening. A theoretical modelling of ontogenetic shifts in efficiencies of both the opercular and hyoid four-bar linkage systems has focused on their complementary contributions to mouth opening (Adriaens et al., 2001). Yet, no study to date has actually demonstrated the

precise timing by which the opercular mechanism contributes to mouth opening. The same is true for the other mechanisms (Figs 1, 2), which, furthermore, have been addressed in considerably fewer studies compared with the opercular mechanism (Westneat, 1990; Westneat, 1994).

In the present study, the mouth opening and hyoid depression mechanisms are analysed during prey capture in an African air-breathing catfish, *Clarias gariepinus*. By using planar four-bar models with kinematic data input from high-speed X-ray video recordings, we test the activity of all potential mechanisms described for both functions in this species (Adriaens et al., 2001). In particular, we will focus on the timing of the action and the relative contribution of each of the mouth-opening and hyoid-depression mechanisms.

2.2 Materials and Methods

2.2.1 Study animals

Clarias gariepinus (Burchell,1822) is an air-breathing catfish (Fam. Clariidae) with an almost Pan-African distribution that is also found in rivers and lakes of the Middle East and Turkey (Teugels, 1996). This species was chosen because multiple mechanisms of mouth opening and hyoid depression have been suggested previously based on morphological studies (Adriaens et al., 2001). As jaw protrusion is absent in Clariidae and other catfishes (Alexander, 1965), C. gariepinus also has the advantage over many other teleosts in that jaw protrusion mechanisms do not interfere with lower jaw depression mechanisms, which will simplify the analysis.

Three adult catfish were used in the experiments, with cranial lengths of 70.2, 94.1 and 74,5 mm (defined as the distance between the rostal tip of the premaxilla and the caudal tip of the occipital process). These individuals will be referred to as, respectively, catfish A, B and C. These catfish were aquarium-raised specimens obtained from the Laboratory for Ecology and Aquaculture (Catholic University of Leuven, Belgium). The animals were kept in separate 20 l test aquaria and were trained to capture food inside a narrow, projecting corridor (25 cm length, 8 cm width, 15 cm water height) of the aquarium. The thin Plexiglas walls (2 mm) of the corridor minimised the amount of X-ray absorption.

2.2.2 Radio-opaque marking

In order to increase the quantification accuracy of movements of cranial bones (see further), small metal markers were inserted subcutaneously, touching the bones at specific positions of interest, using hypodermic needles. Prior to implantation of these radio-opaque markers, the animals were anaesthetised with MS222 (Sigma Chemical Company, St. Louis, MO, USA). In this way, 13 markers were inserted and used to track the

movements of the lower jaw, hyoid, operculum, cleithum and neurocranium in each individual (Fig. 3). Occasionally, a single marker was expelled from the skull between the marking period and the recording sessions. This was the case for the rostral tip of the cleithrum in two individuals (cranial lengths of 74,5 and 94.1 mm). These individuals also have two markers on the operculum instead of one opercular and one suspensorial marker as shown for the individual in Figure 3.

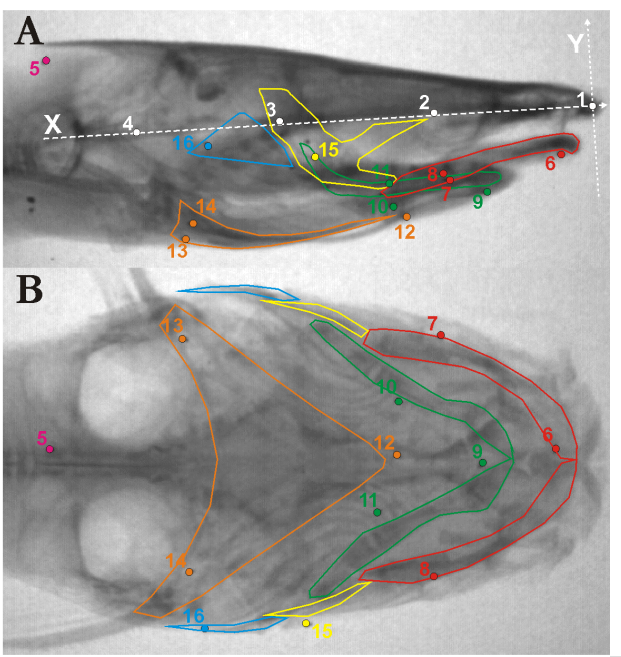


Figure 3: Position of the inserted radio-opaque markers (colour circles) and additional landmarks (white circles) digitized to define the fishbound frame of reference (white dashed lines) imposed on a lateral (A) and dorsoventral (B) X-ray image of Clarias gariepinus (70.2 mm cranial length). Contours of the lower jaw (red), hyoid bars (green), cleithrum (orange), suspensorium (yellow) and operculum (blue) are shown. markers are: (1) the upper jaw tip, (2-3-4) landmarks on the roof of the buccal cavity, (5) anterior of the neurocranium, close to the occipital process, (6) lower jaw tip, (7-8) more caudal points on the left and right lower jaw, (9) rostral tip of the hyoid, (10-11) approximate middle along left and right hyoids, near the origin of

the protractor hyoidei muscles (12) tip of the cleithrum, (13-14) caudal points on the left and right side of the cleithrum, near the base of the pectoral fins, (15) suspensorium and (16) operculum. Landmark (1) was taken as origin (0,0) and the X-axis is parallel to the least-squares linear regression through points (1-2-3-4).

Radio-opaque markers were implanted left and right at the basis of the lower jaw, hyoid and cleithrum (Fig. 3) as this procedure allows a more accurate measurement of kinematics in the case of minor rotations of the fish along its medio-sagittal axis during the feeding event (Van den Berg, 1994). Note, however, that prey capture sequences were discarded in cases where our catfish showed substantial rotation along axes other than parallel to the camera lens, or if initially the mid-sagittal plane of the fish diverged significantly from perpendicular to the camera lens axis.

After the recording sessions, the animals were killed by an overdose of MS222. Next, additional markers were inserted (single side only) onto some critical points in the four-bar mechanisms for mouth opening and hyoid depression. These points are the articulations between suspensorium-operculum, operculum-interoperculum, interoperculomandibular ligament and anguloceratohyal ligament-retroarticular process of mandible, mandibulum-

quadratum, suspensorium-hyoid and hyoid-anguloceratohyal ligament. During this post-recording marking, the precise positions of the four-bar joints for each individual were determined by careful observation, manipulations of structures, and some dissections (e.g., removing the branchiostegal membrane to pinpoint the hyoid linkages).

2.2.3 X-ray video recording and digitisation

High-speed X-ray videos and photographs were recorded using a Philips Optimus X-ray generator coupled to a 14-inch image intensifier with two zoom modes (10 and 6 inch) and a Redlake Motion Pro camera (1248 x 1024 pixels). Videos were made in lateral view and were recorded at 250 frames per second, using the 6-inch zoom function (Fig. 4). Three prey types were used: (1) pieces of cod fillet and (2) unpeeled North Sea shrimps attached to a plastic-coated steel wire, and (3) small, spherical pieces of shrimp meat which were loosely attached to the tip of a needle. For each individual, 20 recordings were analysed (5, 5 and 10 sequences respectively for each prey type).

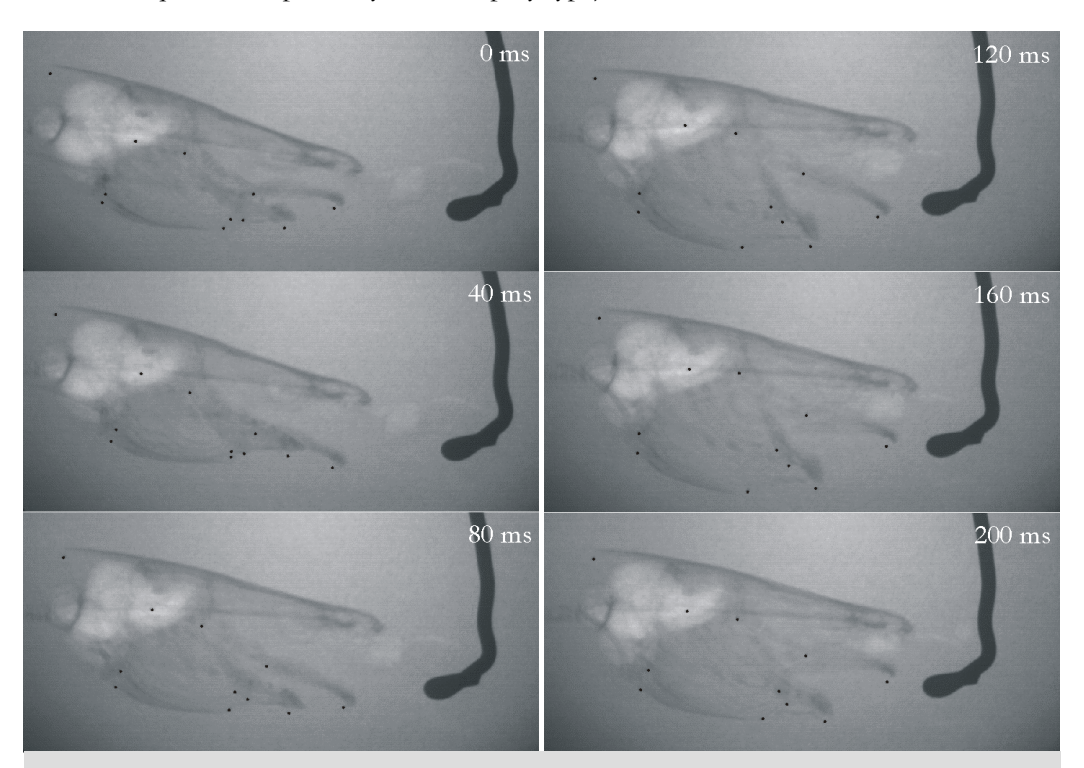


Figure 4: Selected X-ray video frames from a representative prey-capture sequence (0-240 ms) of a *Clarias gariepinus* individual (70.2 mm cranial length, Catfish A) equipped with radio-opaque markers during feeding on an attached shrimp.

The sixteen anatomical landmarks shown in Fig. 3 were digitised frame-by-frame from the high-speed X-ray videos using Didge (version 2.2.0, Alistair Cullum, Creighton University, Omaha, USA). The coordinates of all landmarks were recalculated to a frame of reference moving with the neurocranium. In this frame, the upper jaw tip was taken as origin and the horizontal axis is parallel to the roof of the buccal cavity (see Fig. 3). This digitisation and recalculation of reference frame was also done on the X-ray photographs with the additional markers on the four-bar joints (see above) together with the original, pre-recording markers. As the cleitrum can be distinguished reasonably well on the X-ray videos (Fig. 4) the tip of the cleithrum could still be digitised accurately in case the marker at this location was absent.

Angles in the first (upper right) and fourth (lower left) quadrant of the reference frame (Fig. 3) are, respectively, negative and positive. Consequently, kinematic profiles of mouth opening (mechanically identical to lower jaw depression in Clariidae) and hyoid depression will give rising curves. On the other hand, mouth closing and hyoid elevation will be represented by descending curves.

2.2.4 Muscle lengths

The origin-to-insertion length (in the sagittal plane) of the sternohyoideus muscle (mechanism Fig. 2B) was calculated as the distance between the tips of the cleithrum and the hyoid (landmarks 12 and 9 of Fig. 3). Note that a part of the short parurohyale bone is included into this 'sternohyoideus length'. The length of the protractor hyoidei muscles (mechanism Fig. 1D) was directly calculated from the XY-coordinates of the landmarks near its origin and insertion (landmarks 10-11 and 6 of Fig. 3). These muscle origin-to-insertion lengths will be presented as a percentage of the average muscle length observed for each individual. If muscle-shortening velocities are higher than 5% s-1 after 5 Hz Butterworth filtering (see below), shortening velocities exceed the observed level of noise for these measurements. In that case only, muscle shortening is assumed to be significant.

2.2.5 Four-bar models

The terminology of four-bar systems used in this paper will adhere to the one used in mechanical engineering. Consequently, the fixed bar is called the 'frame'. The two bars connected to the frame are named 'follower' and 'crank'. The crank is the input link, i.e. the link on which the input force is acting. The crank and the follower are connected to the ends of the 'coupler'. As a given four-bar chain has only one degree of freedom, its entire configuration depends on the angle between crank and frame (referred to as 'input angle'). In this way, the angle between follower and frame (referred to as 'output angle') was calculated in function of the input angle according to Aerts and Verraes (1984). As most often there existed two solutions for output angle (see Aerts and Verraes, 1984), a

graphical check was performed (intersecting circles using CorelDRAW) to determine the anatomically correct solution. To refer to one of the mouth-opening or hyoid-depression mechanisms, we will use its number as presented in Fig. 1 or Fig. 2 from this point on.

In order to calculate rotations of the lower jaw or hyoid caused by the action of a four-bar system and to compare this data to the observed lower jaw and hyoid rotations, four types of data were collected with respect to each four-bar mechanism: (1) the coordinates of the four corners (point-joints) of the four-bar system, (2) the fixed angle between the four-bar's crank and the line connecting the two radio-opaque markers on the bone serving as crank, which is necessary to translate measured positions of these markers with respect to the cranium to instantaneous positions of the crank in the four-bar system, (3) the rotation of this segment (i.e. the line connecting the markers on the crank) over time and (4) the fixed angle between the four-bar's follower and the line interconnecting the two markers on the lower jaw (for mouth opening four-bars) or on the hyoid (for hyoid depression four-bars). With these data, the initial four-bar configuration, changes in the input and output angles of the four-bar system, and the corresponding positions of the lower jaw or hyoid with respect to the fixed, fish-bound frame (Fig. 3) due to action of the four-bar system were calculated.

For mechanism 1A (Fig. 1A), the XY-coordinates of all four-bar corners were obtained from the post-recording marking (see above). For the individual lacking one of the two radio-opaque markers on the operculum (Fig. 3), the fixed coordinate of the operculum-suspensorium joint was used instead. For mechanism 1B (Fig. 1B), the position of hyoid-attachment of the angulo-ceratohyal ligament with respect to the hyoid was determined based on the morphological data (Adriaens et al., 2001). To calculate the angle of the lower jaw, hyoid and cleithrum with respect to the X-axis, the line interconnecting the tip landmark (respectively landmarks 6, 9 and 12 of Fig. 3) and the average between the coordinates of the left and right caudal landmarks on these structures (respectively landmarks 7-8, 10-11 and 13-14 of Fig. 3) were used.

For mechanism 2A (Fig. 2A) and mechanism 1C (Fig. 1C) the position of the centre of rotation of the cleithrum and the hyoid, and the length of the crank were calculated for each video sequence separately. This was done by using the kinematic data from the markers inserted at two positions (tip and caudal) on the cleithrum or hyoid.

In these four-bar linkage models, the suspensoria are assumed to be immobile with respect to the neurocranium. Although *Clarias gariepinus* shows some abduction (lateral swing) of the suspensoria during the expansive phase of suction feeding, the total lateral expansion is only a small fraction of the observed ventral expansion of the cranial system in this species (Van Wassenbergh et al., 2004). Furthermore, as the suspensoria are relatively short in this dorsoventrally flattened fish (Fig. 1), abduction of the suspensoria will only have a small influence on the relative position of the four-bar point-joints in a lateral view. As a consequence, this assumption seems justified and will probably not influence the results significantly.

Because of the short distance between the landmarks determining opercular rotation, digitisation noise had to be reduced by filtering. Therefore, a fourth order, zero phase-shift Butterworth filter was used according to Winter (2004), with cut-off frequencies between 10 and 20 Hz, depending on the nature of the data-noise. This filtering procedure was also performed prior to differentiation (e.g., calculating velocities), and where the tip of the cleithrum had to be digitised without marker (see above). Thus, with the exception of lower jaw movements predicted by the opercular mechanism (Fig. 1A) and the hyoid movements predicted by mechanism 2A (Fig. 2A) in two out of the three individuals, all data presented as angle *versus* time are (or directly use) unfiltered kinematic data.

The coupler of two of the four-bar systems (Figs 1C, 2A) consists of a muscle. In contrast to ligaments or bones, muscle cannot be considered as a link of constant length (as assumed in four-bar models). Therefore, in addition to calculating four-bar model output with the starting length of the muscle (at time 0), the four-bar simulations were performed using the minimal and maximal lengths for that muscle during a given prey capture sequence. To do so, the length of the coupler was lengthened or shortened without changing the input angle of the four-bar system. Consequently, only the output angle and the predicted lower jaw or hyoid angle will change by adjusting the coupler's length in this way.

2.2.6 Data interpretation and statistics

As mentioned earlier, the result of the action of a certain four-bar model will be presented as a predicted lower jaw or hyoid angle. This model output can be directly compared to the observed lower jaw or hyoid kinematics. However, for mechanisms 1A and 1B the length of the coupler is constant (Fig. 1A,B), while this is not required in mechanism 1C and 2A (Figs 1C, 2A). Thus, the data interpretation depends on the type of the four-bar system considered (i.e. with or without constant length coupler).

If the coupler can be assumed to have a constant length, then the four-bar system will contribute to mouth opening if the predicted lower jaw angle coincides with the observed lower jaw angle. If not, from a morphological point of view this means that the coupler's ligament (l. angulo-interoperculare in mechanism 1A or l. angulo-cerotohyale in mechanism 1B) is not tight and little or no force will be transmitted by this mechanism. 'Coinciding' and 'not coinciding' are distinguished by performing one-way analyses of variance (ANOVA) with a repeated-measures design, with the observed and predicted lower jaw/hyoid angle as independent variables. By adjusting the amount of data points included in the analyses, the time at which both curves become significantly distinct (P < 0.05) is determined. These statistics were performed using SPSS v. 12.0 (SPSS Inc., Chicago, IL, USA)

If the coupler is a muscle and thus has a variable length, the data interpretation is more complex. Four-bar simulations with muscle at its starting length show how the lower jaw or hyoid would behave in case that the muscle would keep its initial length throughout the entire prey capture sequence. Four-bar simulations with muscle at its maximal length show

the minimal mouth opening or minimal hyoid depression that is exclusively the result of the four-bar action, without any reinforcement by muscle shortening. Because we cannot exclude the possibility that *m. protractor hyoidei* or *m. sternohyoideus* lengthen during expansion *a priori*, four-bar simulations with muscle at its minimal length were also added (see above). These four-bar simulations show the mouth opening or hyoid depression in the case of full and constant reinforcement by muscle shortening throughout the entire sequence. In other words, the simulations at maximal and minimal length muscle reveal the boundaries of the four-bar mechanism, while muscle shortening (Figs 1D,2B) cause the fluctuation between these boundaries. For example, if the *m. sternohyoideus* shortens gradually and reaches its minimal length at the instant of maximal hyoid depression, the predicted hyoid angle from the four-bar model with the muscle at starting length shows how many degrees of hyoid rotation are due to mechanism 2A at that instant, while the difference between the actually observed hyoid angle and this four-bar prediction is due to sternohyoideus shortening.

For mechanism 1D (Fig. 1D), we cannot discern *active* muscle shortening from *passive* muscle shortening whenever mechanisms 1A or 1B are also contributing to mouth opening. However, if muscle shortening is the only explanation for the observed lower jaw or hyoid movement, it can be safely considered as an *active* muscle shortening. Note, in this respect, that despite several attempts by the author, EMG-measurements during preycapture in *C. gariepinus* were not successful due to the erratic behaviour of this species.

Most results will be presented as mean kinematic profiles per individual. In order to account for strike-to-strike variability and to avoid the potential confounding effects on kinematic means, the time axis of each prey capture sequence was scaled to the total duration of mouth opening (or hyoid depression) of that sequence. Consequently, timings of mouth opening and hyoid depression mechanisms will be expressed as a percentage of mouth opening duration, with 0% being the start of mouth opening and 100% the time of maximal gape. Linear interpolations are used to extract data at 2% intervals on this new, relative time scale. Another advantage of this procedure is that effects of differences in body size on the speed of prey capture kinematics (see Van Wassenbergh et al., 2005) are removed, thus simplifying the comparison between individuals.

When comparing the characteristics of different types of mouth opening (see below), twoway, mixed model ANOVAs were used. In these statistics, the effects of mouth opening type (fixed factor) are tested, with individual as a random factor. A sequential Bonferroni correction was applied (to adjusts the significance level according to the number of tests that were carried out) in case of consecutive univariate testing.

2.3 Results

2.3.1 Mouth opening types

Based on the shape of the kinematic profiles of mouth opening during prey capture in C. gariepinus, two types of mouth opening could be distinguished (Fig. 5). In most of the analysed prey-capture sequences (67 %) an additional deceleration-acceleration can be discerned during mouth opening. In the other cases (33% of total), the shape of the mouth opening profile roughly approximates the ascending part of a sinusoidal function, with only a single acceleration and deceleration phase (Fig. 5). When occurring, the additional acceleration starts on average at 64.4 \pm 9.3 % (mean \pm standard deviation) and ends at 84.0 \pm 4.8 % of mouth opening. As distinct mouth opening profiles can be caused by differences in the action of the mouth-opening mechanisms, these two types of mouth opening will be treated separately. The dominant mouth opening type (which includes an additional deceleration-acceleration) will be referred to as 'type 1', while the less frequently occurring type (single deceleration-acceleration) is designated 'type 2'.

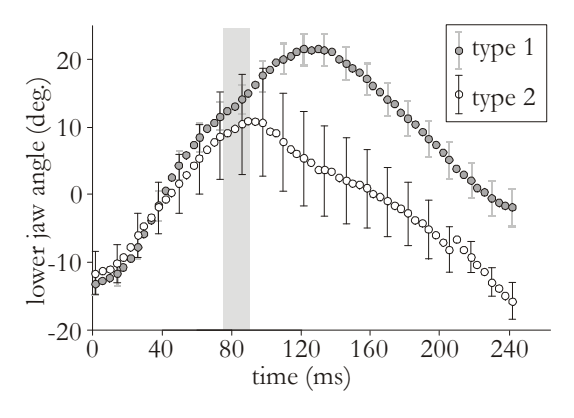
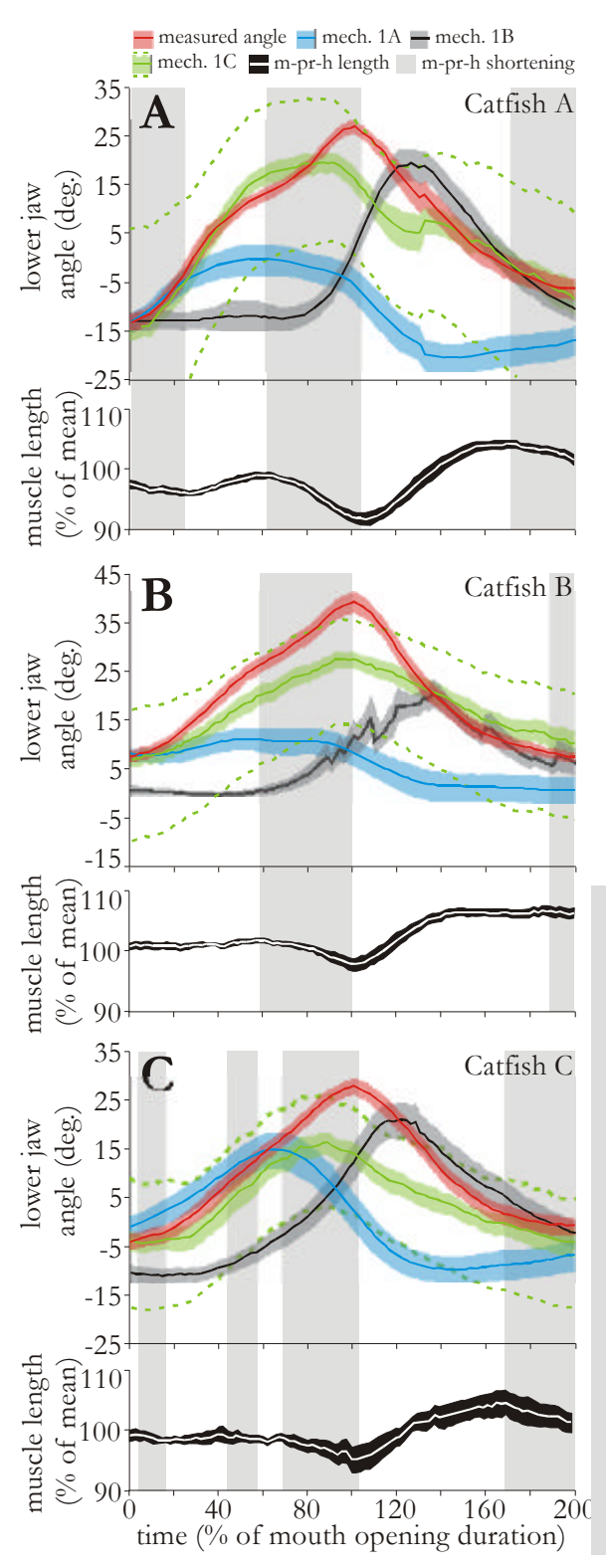


Figure 5: Kinematic profiles of the two mouth-opening types observed in *C. gariepinus*, as illustrated for one individual (catfish A). Values are means ± S.E.M. (*N* =15 for 'type 1'; *N*=5 for 'type 2'). The grey bar indicates the period of the additional acceleration which can be observed during 'type 1' mouth opening. See text for further information.

While both mouth opening types could be discerned for each individual, the distinction between both types was most prominent in catfish A (Fig. 5). In this individual, these mouth-opening types also differed in maximal lower jaw depression angle. The additional acceleration of the 'type 1' mouth openings occurred approximately at the time the 'type 2' mouth openings reach its maximal gape (Fig. 5). In catfishes B and C, however, no differences between the average kinematic profiles of 'type 1' and 'type 2' could be discerned (P=0.12 for B and P=0.67 for C)

2.3.2 Mechanism 1A

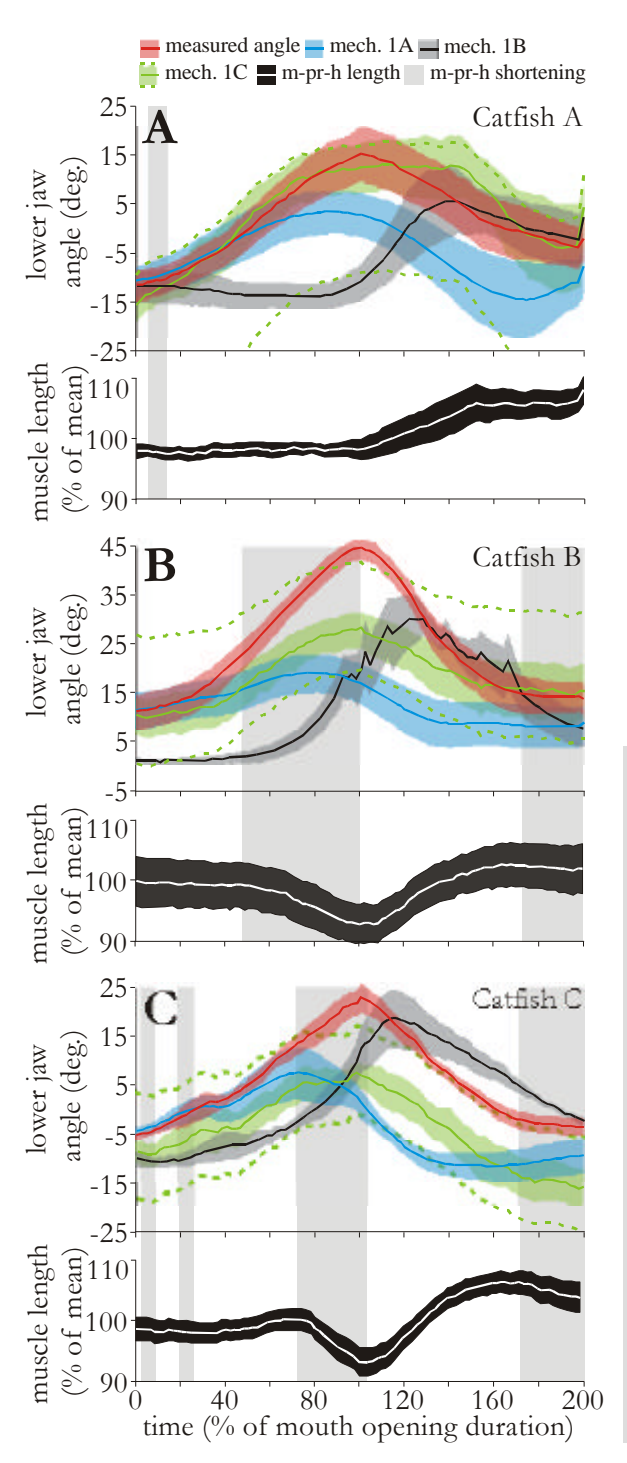
Mechanism 1A (Fig. 1A) is limited to the initial phase of mouth opening, as illustrated by the match between the observed lower jaw angle and the lower jaw angle predicted by the



movement of this four-bar system during that time (Figs 6, 7). The time after the start of mouth opening to the moment at which this mechanism finishes its contribution to mouth

opening varies among individuals, reflecting the inter-individual variation in opercular rotation. On average, this mechanism is active during the first 30%, 14% and 74% of the 'type 1'mouth opening phase (Fig. 6) for, respectively, catfish A, B and C. This relative duration of mechanism 1A tends to be longer during the 'type 2' mouth openings, with 96%, 30% and 76% respectively, but this is not statistically different from the results for 'type 1' (ANOVA, $F_{1,2} = 2.08$, P = 0.29).

Figure 6: Mean mouth-opening (0%-100%) and mouth-closing (100%-200%) profiles with the calculated four-bar model output for each of the mouth opening mechanism during 'type 1' mouth openings (A-C, top), together with length of the protractor hyoidei (m-pr-h; A-C, bottom). Separate graphs are shown for each individual: A (N =15), B (N = 12) and C (N = 13). Grey bars cover the time in which the protractor hyoidei shorten. The shaded areas accompanying each curve indicate S.E.M. The broken, green curves give average four-bar model output of mechanism 1C with the protractor hyoidei at minimum length (upper curve) and at maximum length (lower curve) as coupler. Colour codes are indicated in the key above the figure. Mech. 1A, 1B, 1C, see Fig. 1.



2.3.3 Mechanism 1B

Mouth opening mechanism 1B (Fig. 1B) is not active during any time of the mouth opening phase (Figs 6, 7). The only instants at which the lower jaw angle predicted by the activity of this four-bar mechanism coincides with the observed lower jaw angle during mouth opening, are instants near the start of jaw opening, when mechanism 1B-output does not cause any lower jaw rotation. Apart from these instants, lower jaw angles are consistently underpredicted (i.e. more elevated towards the neurocranium) by this mechanism during mouth opening (Figs 6, 7).

Figure 7: Mean mouth opening (0%-100%) and closing (100%-200%) profiles with the calculated four-bar model output for each of the mouth opening mechanism during 'type 2' mouth openings (A-C, top), together with length of the protractor hyoidei (m-pr-h; A-C, bottom). Separate graphs are shown for each individual: A (N = 5), B (N = 8) and C (N = 7). Grey bars indicate the time during which the protractor hyoidei shorten. The shaded areas accompanying each curve indicate S.E.M. The broken, green curves give average four-bar model output of mechanism 1C with the protractor hyoidei at minimum length (upper curve) and at maximum length (lower curve) as coupler. Colour codes are indicated in the key above the figure. Mech 1A, 1B, 1C, see Fig. 1.

During mouth closing, however, the lower jaw profile predicted by mechanism 1B (Fig. 1B) generally converges towards, and finally becomes adjacent to the observed lower jaw angle (Figs 6, 7). Consequently, four-bar modelling predicts that only during mouth closing, the angulo-ceratohyal ligament becomes fully stretched and potentially couples hyoid to lower jaw movement. This situation, in which the observed and predicted lower jaw angles can no longer be distinguished statistically, takes place after 114%, 124% and 110% of mouth opening duration for the 'type 1' mouth openings, and after 118%, 124% and 108% for 'type 2' mouth openings in, respectively, catfish A, B and C.

2.3.4 Mechanism 1C

Without shortening of the protractor hyoidei muscles, mechanism 1C (Fig. 1C) alone would already be responsible for a large amount of lower jaw depression during hypaxial retraction of the pectoral girdle (Figs 6, 7). The average lower jaw rotations due to this mechanism are 32.7, 20.6 and 20.1 degrees ('type 1' mouth opening) for catfish A, B and C respectively (Fig. 6), corresponding to 81.7%, 63.5% and 64.1% of the total observed lower jaw depression. The predicted maximal lower jaw angle by this four-bar mechanism is reached close to the time of maximal mouth opening (100%), more specifically at 86%, 96% and 88% for the three individuals studied. For the mouth opening profiles of 'type 2', the absolute amount of lower jaw rotation that would be generated by this mechanism alone, tends to be lower (ANOVA, $F_{1,2} = 21.6$, P = 0.043), with 25.0, 17.1 and 13.1 degrees for catfish A, B and C respectively (Fig. 7). However, the relative contribution to the total lower jaw depression is not (ANOVA, $F_{1,2} = 0.48$, P = 0.56). Again, maximal values of the lower jaw angles predicted by this mechanism are reached near the time of maximal gape (112%, 100% and 98%; Fig. 7).

2.3.5 Mechanism 1D

Mechanism 1D (Fig. 1D), shortening of the protractor hyoidei muscles (abbreviated m-pr-h), will reinforce lower jaw depression caused by mechanism 1C. Relatively slow and brief m-pr-h shortening could sometimes be discerned during the first instants of mouth opening (Figs 6, 7). However, the relative contribution of this initial muscle shortening is limited, as mechanism 1C (four-bar system modelled without muscle shortening) still predicts the observed lower jaw accurately during this stage. Furthermore, in one of the three individuals studied (catfish B) no significant changes in the length of the m-pr-h were measured during the first half of the mouth opening phase (Figs 6B, 7B). As also mechanism 1A is active during this period, these muscle shortenings can either be passive or active.

A more extensive and faster shortening of the m-pr-h was observed during the final half of mouth opening. More specificy, this muscle starts shortening at 62%, 60% and 68 % until, respectively, 104%, 102% and 104% of mouth opening ('type 1') in catfishes A, B and C

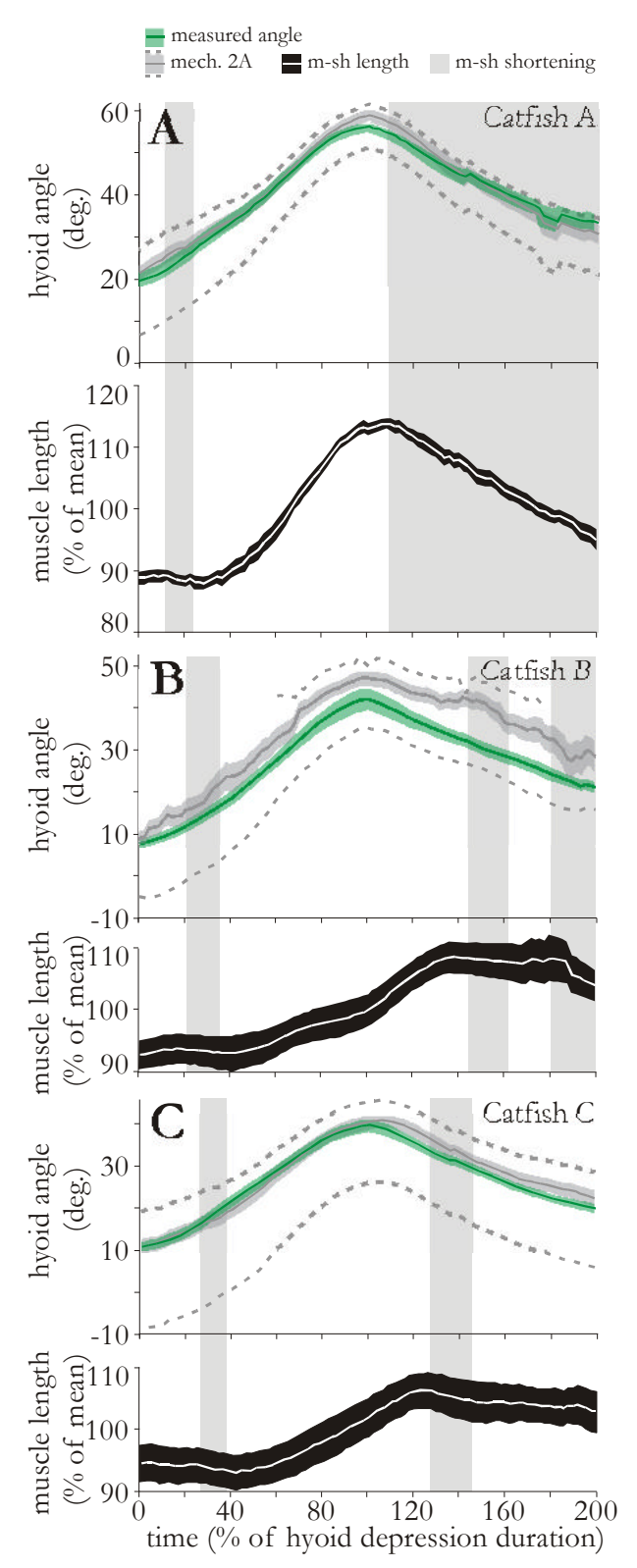
(Fig. 6). In contrast to the limited m-pr-h shortenings during the first half of mouth opening, mechanism 1D now contributes significantly to mouth opening. As mechanisms 1A and 1B are not active during this period, and the predicted lower jaw profile by the action of mechanism 1C starts diverging from the observed lower jaw angle, active m-pr-h shortening must be responsible for depression of the lower jaw in surplus to the mechanism 1C-output (Figs 6, 7). This 'surplus' is on average 7.3, 11.9 and 11.3 degrees at the time of maximal mouth opening ('type 1') in our three catfishes.

For mouth openings of 'type 2', the results for catfish B and C (Figs 7B, 7C) are similar to those during 'type 1' mouth opening, with respectively, m-pr-h shortening from 48% to 100% (16.6 degrees surplus to mechanism 1C) and from 72 to 104% (14.9 degrees surplus to mechanism 1C). However, for catfish A, the individual with the most diverging 'type 1' and 'type 2' profiles (see Fig. 5), no m-pr-h shortening could be discerned, not even during the last half of mouth opening (Fig. 7A). Consequently, only mechanism 1C causes lower jaw depression after the opercular mechanism (Fig. 1A) has ended its contribution during these sequences, without reinforcement by m-pr-h shortening.

2.3.6 Mechanism 2A

The four-bar system 2A (Fig. 2A) alone (i.e. without sternohyoideus shortening) is able to cause the entire hyoid rotation observed in *Clarias gariepinus* (Fig. 8). More specifically, 107.3%, 114.7% and 103.2% of the total hyoid depression is predicted by this mechanism if the sternohyoideus muscle maintains its initial (prior to expansion) length for, respectively, individuals A, B and C (Fig. 8). For individuals A and B, this corresponds to total hyoid rotations that are significantly higher than the observed hyoid rotations (P < 0.001 and P = 0.003). For individual C (Fig. 8C), the four-bar model output of mechanism 2A is not significantly different for the observed values from the start of hyoid depression until maximal hyoid depression (P = 0.92).

The four-bar simulation with the sternohyoideus at maximal length predicted maximal hyoid angles of 51.4, 32.6 and 26.3 degrees, which corresponds to 86.6%, 79.4% and 53.7% of the total observed hyoid rotation in, respectively, catfish A, B and C. If the sternohyoideus reached its minimal length (measured during the entire expansion-compression cycle) at the moment of maximal retraction of the cleithrum, then the four-bar system calculates hyoid angles of 61.5, 50.9 and 45.4 degrees. This corresponds to 114.2%, 125.1% and 119.5% of the observed maximal hyoid angle, or a surplus of 5.2, 10.4 and 5.7 degrees in hyoid rotation.



2.3.7 Mechanism 2B

Mechanism 2B (Fig. 2B), shortening of the sternohyoideus muscle (abbreviated m-sh), will reinforce the hyoid depression caused by mechanism 2A. However, shortening of the m-sh during hyoid depression is limited in magnitude and restricted to a short period (Fig. 8). This period lasts (on average) form 12% until 24% (catfish A), 22% until 36% (catfish B) and 26% until 38% (catfish C) of the total hyoid depression duration. During these

Figure 8: Mean hyoid depression (0%-100%) and elevation (100%-200%) profiles with the calculated four-bar model output for hyoiddepression mechanism 2A (A-C, top), together with length of the sternohyoideus muscle (m-sh; A-C, bottom). Separate graphs are shown for each individual (N=20). The shaded areas accompanying each curve indicate S.E.M. Note that these S.E.M. values are larger in case the radio-opaque marker is absent at the tip of the cleithrum (B, C). The lower and upper broken, grey lines represent the output of the four-bar model with, respectively, a fully elongated sternohyoideus muscle and the sternohyoideus at minimum length. The latter curve is partly not displayed in B when there were no analytical four-bar solutions in more than half of the cases. Grey bars indicate the period during which the sternohyoideus shortens. Colour codes are indicated in the key above the figure. Mech. 2A, see Fig. 2.

periods of m-sh shortening, the m-sh only shortens approximately 1% of its mean length. After this period, the muscle starts elongating (Fig. 8; see also Fig. 4). This elongation lasts approximately until maximal hyoid depression is reached (Fig. 8A,C), or even continues after peak hyoid depression in one individual (Fig. 8B). For all individuals, the m-sh is generally longer at the moment of peak hyoid depression than it is at the start of hyoid depression (Fig. 8).

2.4 Discussion

2.4.1 Mouth-opening mechanisms

The results of the present study show that during the first instants of mouth opening, opercular rotation causes lower jaw depression (through mechanism 1A; Fig. 1A). However, as also some shortening of the protractor hyoidei muscles (mechanism 1D, Fig. 1D) also occurs during this time (Figs 6, 7), this does not necessarily imply that the opercular mouth-opening mechanism is the only mechanism used by *Clarias gariepinus* for initiating mouth opening. Unfortunately, we cannot distinguish whether these short bursts of protractor hyoidei shortening near the start of mouth opening are caused by muscle activity, or if they are merely the consequence of the rotating lower jaw caused by the opercular mechanism. Thus, initial mouth opening is performed by the opercular mechanism (Fig. 1A), possibly assisted by protractor hyoidei shortening (Fig. 1D).

As hypothesised previously for cichlid fishes (Aerts et al., 1987; Durie and Turingan, 2004), the contribution of the opercular mechanism to mouth opening in *C. gariepinus* is limited to the initial phase of mouth opening. The opercular mechanism generally has no effect on mouth opening during the second half of the mouth-opening phase in this catfish (Figs 6, 7). Given that lower jaw depression is resisted by forces resulting from the sub-ambient pressure inside the mouth cavity, and the inertia of the lower jaw is very low compared to these forces (Aerts et al, 1987; Van Wassenbergh et al., 2005), the inertia of the lower jaw will probably not result in any lower jaw rotation due to past force-input by the opercular mechanism.

The timing of rotation of the opercular bone with respect to mouth opening, however, is apparently not always identical when comparing different species. In our study species, the operculum stops its dorso-caudal rotation relatively early during the expansive phase of suction feeding. In other fishes, however, the maximal opercular rotation is reached near the moment of maximal mouth opening (Elshoud-Oldenhave and Osse, 1976; Lauder, 1982; Konow and Bellwood, 2005). Note, in this respect, that hyoid retraction and depression can interfere with opercular movement in some teleost species due to the presence of a ligament connecting the hyoid (epihyals or ceratohyals) to the interopercular bones (e.g. Anker, 1986). This ligament is typically present in Ctenosquamate fishes (i.e.

Scopelomorpha and Acanthomorpha, which does not include catfishes; Stiassny, 1996) and may cause passive opercular rotation when the hyoid basis and interopercular are displaced dorso-caudally during the head expansion phase. In that case, observing opercular rotation does not necessary imply an active contribution of the opercular mechanism (Fig. 1A) to mouth opening. Yet, the angelfish *Pomacanthus semicirculatus*, for example, does not have this ligament connecting the hyoid to the interopercular and still performs opercular rotations approximately until the time of maximal gape (Konow and Bellwood, 2005). Consequently, the presented results concerning duration of activity of the opercular mechanism in *C. gariepinus* may not reflect a pattern that is common to all teleost fishes.

Shortly after the start of mouth opening, the hyoid begins rotating ventrally and the protractor hyoidei coupling between the hyoid and the lower jaw becomes an important mouth-opener (mechanism 1C; Fig. 1C). Even without any protractor hyoidei shortening (mechanism 1D reinforcing the activity of mechanism 1C; Fig. 1D), this mechanism alone would be responsible for a large amount of mouth opening (approximately 70% of the total observed lower jaw rotation).

After the opercular mechanism (Fig. 1A) ceases to be active (on average after 45% of the mouth opening time), further mouth opening in *C. gariepinus* is exclusively achieved through the protractor hyoidei muscles (abbreviated m-pr-h). This is done in a combination of four-bar mechanism 1C (Fig. 1C; ventral rotation of the m-pr-h origin by means of hyoid depression) and m-pr-h shortening (Fig. 1D). Mechanism 1C continues its contribution until maximal mouth opening, and is actively reinforced by m-pr-h shortening during this time. The m-pr-h now generally shortens 5 to 10% of its mean length (Figs 6, 7), which causes an extra 10 to 15 degrees of lower jaw rotation in addition to the contribution of mechanism 1C (see above).

2.4.2 Mechanical basis of the two mouth-opening types

Two types of kinematic mouth-opening profiles were discerned in *C. gariepinus*: profiles that only have a single acceleration-deceleration and, the most commonly (67% of all cases), in which an additional deceleration-acceleration could be discerned (see Fig. 5). Surprisingly, such unusual characteristics of the mouth-opening kinematics have not yet been observed in other fishes, despite the large amount of studies measuring mouth-opening kinematics (see Ferry-graham and Lauder, 2001 for a review). Two options are possible: (1) mouth opening in the African catfish *C. gariepinus* is mechanically distinct from all previously studied fish. (2) The present marker-based, high-speed cineradiographic analysis generates kinematic profiles of higher resolution than most studies based on more common high-speed videography, and therefore allows discernment of more subtle variations in kinematics. This second option is not unlikely, since no such unexpected mouth opening patterns were noticed during a preceding kinematic analysis of prey capturing *C. gariepinus*, in which images were obtained using a regular high-speed video

camera and manual, point-by-point digitisation of anatomic landmarks was done without the help of markers (Van Wassenbergh et al., 2004).

The present analysis of the mouth-opening mechanism may explain the mechanical causes of such distinct mouth-opening types. For one individual of this study (referred to as catfish A), mouth openings of each type are clearly driven by distinct mouth-opening mechanics. If there is no additional deceleration-acceleration, than maximal mouth opening is reached without any shortening of the protractor hyoidei muscles (Fig. 7A). In the other case ('type 1' mouth opening; Fig. 5), the protractor hyoidei do shorten, and the decelerating lower jaw is speeded up almost precisely at the time this muscle shortening starts (Fig. 6A). In addition, this individual can apparently modulate its maximal gape by opening the mouth with or without protractor hyoidei shortening during the second half of mouth opening (Fig. 5). This is in accordance with our observation that *C. gariepinus* is able to modulate maximum gape without changing the magnitude of hyoid depression when this species is given prey of different sizes: as the opercular mechanism (Fig. 1A) only initiates mouth opening and mechanisms 1B and 1C (Fig. 1B,C) directly depend on the (equal) amount of hyoid depression, only protractor hyoidei shortening can achieve this.

However, in the two other individuals (referred to as catfishes B and C), mouth-openings of both types were more similar in magnitude. The kinematic profiles from the different types could not be distinguished statistically and, in general, also protractor hyoidei shortening occurred in mouth-openings without the additional acceleration-deceleration (Fig. 7B,C). Yet, in most cases, the start of the characteristic additional acceleration coincides with the start of protractor hyoidei shortening (Fig. 6B,C). As a result, although no distinctive mechanical basis for both mouth-opening types was found for these individuals, it is still likely that the observed phenomenon is related to the timing and/or speed of protractor hyoidei shortening.

2.4.3 Function of the angulo-ceratohyal ligament

The angulo-ceratohyal ligament (abbreviated l-an-ch) connects the hyoid to the lower jaw (Fig. 1B). Previous functional morphological analyses have proposed that this ligament plays a part in mouth opening (see also Fig. 1B): the l-an-ch pulls the retro-articular process of the lower jaw backward during hyoid depression, which causes the lower jaw to depress (Diogo and Chardon, 2000; Adriaens et al, 2001). However, the results of the present study show that this ligament (being part of four-bar mechanism 1B; Fig. 1B) probably does not contribute at all to mouth opening in *C. gariepinus* (Figs 6, 7). The observed underprediction of the lower jaw angle (Figs 6, 7) during mouth opening in our analysis corresponds to a situation in which the length of the l-an-ch (four-bar coupler link) is shorter than prior to mouth opening (Fig. 9A). Unless the short l-an-ch is extremely elastic, this means that very little force will be transmitted to the lower jaw's

retro-articular process during mouth opening. Note that in the case where l-an-ch was indeed be considerably elastic, the jaw adductors would probably need to be activated continuously when *C. gariepinus* is resting with its mouth closed. This is very unlikely, also given the fact that fully anaesthetised catfish do not show any signs of mouth opening. Manipulating the ligaments during dissections also proves it to be very poorly elastic.

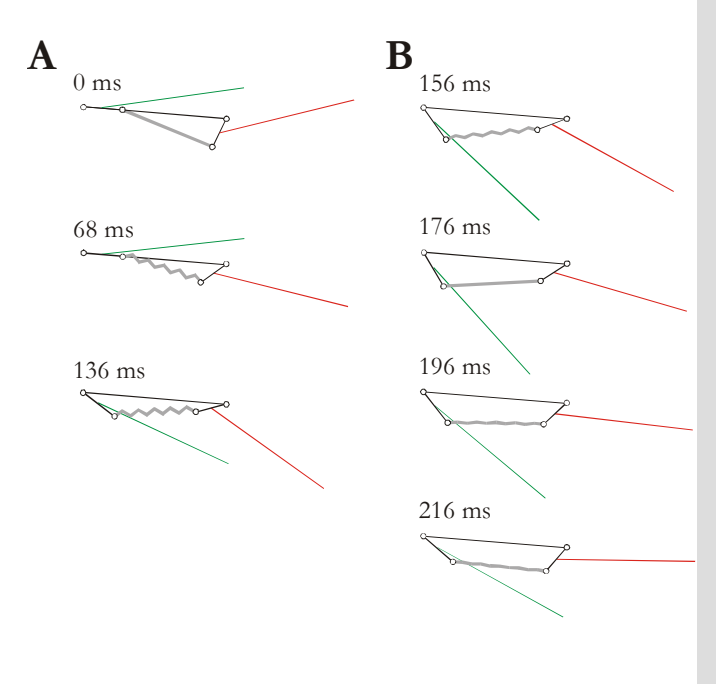


Figure 9: A representative prey capture sequence of C. gariepinus showing reconstruction of four-bar kinematics of mechanism 1B (Fig. 1B) during mouth opening (A) and mouth (B). closing Both observed hyoid angle (green line) and lower jaw angle (red line) were used as input, whereas the length of the coupler link (i.e. the anguloceratohyal ligament; thick grey line) was adjusted to fit the observed hyoid and lower jaw kinematics. Note that the angulo-ceratohyal ligament shortens during mouth opening, but stretched again during mouth closure during which it helps to elevate the hyoid.

During mouth closing, however, our results indicate that the l-an-ch first increases in length to a point where it reaches its initial (i.e. prior to mouth opening) length (Fig. 9B). Next, hyoid and lower jaw kinematics are tightly coupled by the four-bar mechanism in which the l-an-ch functions as a coupler link (Figs 6, 7). In contrast to mouth opening, the input-force of the action by this four-bar system (Fig. 1B) no longer originates from the hyoid, but from the lower jaw (activity of the jaw adductor musculature during jaw closing). If we reverse the four-bar system described in Figure 1B (crank becomes follower and *vice versa*) then the results of Figures 6 and 7 can be interpreted as follows: hyoid elevation kinematics is accurately predicted by four-bar system 1B (Fig. 1B) with the measured, instantaneous lower jaw positions as input. In other words, the results of the present paper show that the l-an-ch functions as a hyoid-elevator: the l-an-ch linkage with the lower jaw is generally able to cause approximately 15 to 20 degrees of hyoid elevation in *C. gariepinus*.

A ligament coupling lower jaw adduction to hyoid elevation can be important for a suction feeding fish's prey capture success. If a prey capture attempt is unsuccessful, then the hyoid will be automatically elevated. This will help in preparing a following attempt,

because it is crucial to start a suction feeding act with a compressed buccal cavity (De Visser and Barel, 1996). These results also shed a different light on the function of the jaw adductors, which apparently not only power mouth closing, but indirectly also have an important role in hyoid elevation in the catfish studied. Note also that the protractor hyoidei coupling (Fig. 1C) may cooperate in hyoid elevation (see Figs 6, 7).

2.4.5 Hyoid-depression mechanisms

Hyoid depression in *C. gariepinus* is exclusively the result of the mechanism (2A) involving neurocranial elevation and pectoral girdle retraction, caused by contraction of the epaxial and hypaxial musculature (Fig. 2A; Fig. 8). In this mechanism, the sternohyoideus muscle (abbreviated m-sh) transmits the movement of the cleithral bone (part of the pectoral girdle) to the hyoid (Muller, 1987). Surprisingly, the m-sh does not shorten during hyoid depression and will therefore not reinforce the action of four-bar mechanism 2A (Fig. 2). In general, the m-sh even tends to elongate during hyoid depression (Fig. 8). Given the gradual nature of the measured m-sh elongation, this muscle clearly transmits the force from cleithral retraction during an eccentric contraction.

Even without the expected reinforcement by m-sh shortening, mechanism 2A (Fig. 2A) still causes the hyoid to depress extensively: the total hyoid rotation often exceeds 60 degrees. Given the final hyoid configuration after rotations of this magnitude, any further depression of the hyoid by m-sh shortening would probably cause a considerable caudal displacement of the hyoid tip, but relatively little lowering of the mouth floor and thus little extra volume-increase of the buccal cavity (causing additional water inflow). This may explain why m-sh shortening, or even keeping the m-sh at the same length, is not needed for this species to perform successful prey captures.

On the other hand, m-sh shortening during hyoid depression would theoretically increase the speed of hyoid depression, and indirectly also the speed of mouth opening (through the mechanism shown in Fig. 1C). In fact, our results indicate some limited m-sh shortening during the prey-captures in which the fastest hyoid depressions are generated: if the kinematic data from the five sequences with the fastest hyoid depressions are pooled, then two of the tree individuals (A and B) show, respectively, 3% and 4% m-sh shortening between 52% to 85% and 20% to 54% of the mouth opening phase. However, even in these sequences, the final m-sh length at maximal hyoid depression is considerably larger than its length at the start of hyoid expansion. Furthermore, in one individual (C) the m-sh elongation pattern during the fastest hyoid depressions did not differ from all other sequences (Fig. 8C).

Therefore, we hypothesise that the m-sh in *Clarias gariepinus* is not powerful enough to perform a constant, concentric contraction when it is being retracted by the cleithrum. This depression of the cleithrum is powered by the hypaxial and epaxial muscles, which together have a much larger mass than the m-sh (Herrel et al., 2005). Consequently, a lot

of force will be needed to just to resist elongation when the powerful hypaxials and epaxials contract, let alone the m-sh should manage to contract during this time. Note, however, that other clariid species (e.g. *Clariallabes longicauda*) have a much larger the cross-sectional area of the m-sh compared to *Clarias. gariepinus* (Van Wassenbergh et al., 2004). Therefore, it is not impossible that this morphological difference will be reflected by a different pattern of m-sh length-changes during hyoid depression, especially given the fact that maximal hyoid depressions are also larger in these species (Van Wassenbergh et al., 2004).

Note also that shortening of the sternohyoideus during hyoid depression has been observed in the sunfish *Micropterus salmoides* (Carroll, 2004). Consequently, the hyoid depression mechanics discussed in this study for *Clarias gariepinus* certainly do not apply to all teleost fishes. Logically, the same is also true for the mechanics of the sternohyoideus observed in the above-mentioned sunfish from the study by Carroll (2004).

Chapter 3

Scaling of suction feeding performance in the catfish Clarias gariepinus

Sam Van Wassenbergh – Peter Aerts – Anthony Herrel

Physiological and Biochemical Zoology 79, 43-56. (2006)

Summary

Ontogenetic changes in the absolute dimensions of the cranial system together with changes in kinematics during prey capture can cause differences in the spatiotemporal patterns of water flow generated during suction feeding. Because the velocity of this water flow determines the force that pulls prey towards and into the mouth cavity, this can affect suction feeding performance. In this study, size-related changes in the suction-induced flow patterns are determined. To do so, a mathematical suction model is applied to video recordings of prey capturing Clarias gariepinus ranging in total length from 111 to 923 mm. Although large C. gariepinus could be expected to have increasing peak velocities of water flow compared with small individuals, the results from the hydrodynamic model show that this is not the case. Yet, when C. gariepinus becomes larger, the expansive phase is prolonged, resulting in a longer sustained flow. This flow also reaches farther in front of the mouth almost proportionally with head size. Forward dynamical simulations with spherical prey that are subjected to the calculated water flows indicate that the absolute distance from which a given prey can be sucked into the mouth as well as the maximal prey diameter increase substantially with increasing head size. Consequently, the range of potential prey that can be captured through suction feeding will become broader during

growth of *C. gariepinus*. This appears to be reflected in the natural diet of this species, where both the size and the number of evasive prey increase with increasing predator size.

3.1 Introduction

Suction feeding is the most commonly used prey capture mechanism in aquatic vertebrates (e.g., Lauder, 1985; Ferry-Graham and Lauder, 2001). To generate suction, animals rapidly expand their bucco-pharyngeal cavity, resulting in a flow of water into the mouth (Muller et al., 1982; Muller and Osse, 1984; Aerts et al., 2001; Ferry-graham et al., 2003). During successful strikes, this water flow exerts enough drag force onto the prey to accelerate it towards the mouth, where it is caught between the oral jaws or completely engulfed and transported through the mouth cavity. Because drag forces increase with the velocity of the water flow, generating a sufficiently high suction flow speed is a critical aspect of prey capture success in suction feeders (Svänback et al., 2002).

Because the dimensions of the bucco-pharyngeal cavity change through ontogeny, the hydrodynamics of suction feeding will most likely change as well. Obviously, animals with a larger head will be able to displace a larger amount of water by expanding their larger feeding apparatus. However, scaling effects on the speed of the suction-induced flow are less obvious. If we consider an isometrically growing animal fully expanding its bucco-pharyngeal apparatus in a constant period of time, the following relationships apply: (1) the rate of bucco-pharyngeal volume-change will increase proportional with the cube of the body length, while (2) the surface area of the mouth aperture, through which the water has to flow, only increases with the square of the body length. Consequently, if we assume that the flow velocity is proportional to the ratio of rate of volume-change to the area of the opening through which it flows (Muller et al., 1982; Van Leeuwen and Muller, 1984), suction flow speed at the mouth aperture would increase linearly with body size. Thus, large animals seem to have a considerable advantage over small animals when it comes to generating high suction flow speeds.

On the other hand, like most other movements of the musculo-skeletal system, cranial expansions are subject to scaling effects on the velocity of movement as well. Large animals will inevitably become slower in performing a movement that is similar relative to its body size (Hill 1950; Schmidt-Nielson, 1984). In addition, muscle physiology experiments have demonstrated the slowing down of the maximal intrinsic muscle contraction velocity during growth within a single species (James et al., 1998) and also across a broad sample of species with increasing adult body size (Medler, 2002). Consequently, it is not surprising that during feeding in teleost fishes (Richard and Wainwright, 1995; Wainwright and Shaw, 1999; Hernandez, 2000) and sharks (Robinson and Motta, 2002), the time it takes to complete a given expansion of the jaws or hyoid apparatus increases as animals become larger (but see Reilly, 1995).

Because of the opposing effects of the increase in expansion volume relative to mouth aperture (increasing flow speed) and the relative slowing down of movement during growth (decreasing flow speed), it is hard to predict how suction feeding performance will change during ontogeny. Although there are several studies on how prey capture kinematics of aquatic vertebrates change through ontogeny (Richard and Wainwright, 1995; Hunt von Herbing et al., 1996; Cook, 1996; Wainwright and Shaw, 1999; Hernandez, 2000; Robinson and Motta, 2002), none of these have addressed how the observed changes in feeding kinematics may result in changes in the suction-induced flow. However, the characteristics of this flow are critical determinants of the capture success during a suction event.

Thus, the aim of this article is to compare the velocity of the suction flow during prey capture in a broad size range of African catfish (*Clarias gariepinus*) and use this to evaluate scaling effects on suction performance. As there is considerable information available on the natural diet of *C. gariepinus* (Bruton, 1979) we can further examine whether changes in suction performance are reflected in changes in the diet during growth in this species.

3.2 Material and Methods

3.2.1 study animals

Clarias gariepinus is an air-breathing catfish (Fam. Clariidae) with an almost Pan-African distribution that can also be found in rivers and lakes of the Middle East and Turkey (Teugels, 1996). It has a broad diet that includes mostly fishes, shrimps, crabs, insect nymphs, beetles and snails (Bruton, 1979). While this species shows different kinds of foraging behaviours, such as individual bottom feeding, surface feeding or group hunting, prey are generally captured by a combination of suction feeding and biting (Bruton, 1979; Chapter 6). Juvenile C. gariepinus specimens already have a fully ossified cranial system that appears to be generally similar in shape to the adult configuration at the ontogenetic stage of 127 mm standard length (Adriaens and Verraes, 1998). Adults can grow up to 1.5 m total length (Teugels, 1986), making this species particularly suitable for studying scaling effects.

In this study, we used 17 individuals of between 110.8 and 923.0 mm in total length. Because the cranial length (defined as the distance between the rostal tip of the premaxilla and the caudal tip of the occipital process) can be measured more precisely and excludes variability in the length of body and tail, we will further use this metric to quantify size. The individuals used were either aquarium-raised specimens obtained from the Laboratory for Ecology and Aquaculture (Catholic University of Leuven) or specimens obtained from aquacultural facilities (Fleuren & Nooijen BV, Someren, The Netherlands). All animals were kept in a separate aquarium during the course of the training and recording period. In general, it took about two weeks to train the catfish to feed regularly in a restricted part of the aquarium.

3.2.2 video recordings of prev captures

Video sequences were recorded of *C. gariepinus* capturing pieces of cod (*Gadus morhua*) that were pinned onto a plastic coated steel wire. In order to obtain a similar feeding situation for both the small and large individuals, the size of the prey was scaled according to the size of the catfish (diameter between 25% and 35% of cranial length). The recordings were made using a Redlake Imaging Motionscope digital high-speed video camera at 250 frames per second (for individuals with cranial lengths between 28.01 and 71.00 mm), a JVC GR-DVL9800 camera at 100 fps (for the individuals with cranial legnths of 94.13 and 130.0 mm) or a Panasonic F15 at 50 fps (for the 210.2 mm cranial length individual). The feeding sequences were recorded simultaneously in lateral and ventral view, using a mirror placed at 45°. Two floodlights (600 Watt) provided the necessary illumination. Only those prey capture sequences that were approximately perpendicular to the camera lens were selected and retained for further analysis.

Ten recordings were analysed for each individual. From these video sequences, the velocity of hyoid depression was determined. This was done by measuring the distance between the eye and the tip of the hyoid for each consecutive frame (using Didge, version 2.2.0; Alistair Cullum). For species with a dorso-ventrally flattened head such as *C. gariepinus*, the depression of the hyoid apparatus is likely the most important expansive event of suction (Alexander, 1970b; Lauder, 1985). Consequently, the sequences in which an individual shows the highest velocity of hyoid depression most likely correspond to the sequences in which suction effort is maximised. Therefore, for each individual, only the two sequences with the highest and second highest peak velocity of hyoid depression were further analysed using the suction model detailed below.

3.2.3 Suction model

To calculate the water velocities inside the mouth cavity and in front of the fishes' mouths, we used the ellipse model of Drost and van den Boogaart (1986). Using this method, estimation of the flow volume can be considerably improved over previous model estimations (Drost and van den Boogaart, 1986). It has shown to give accurate predictions of flow velocities in suction feeding larval carp (*Cyprinus carpio*; Drost and van Den Boogaart, 1986) and in the snake-necked turtle (*Chelodina longicollis*; Aerts et al., 2001). Also for suction feeding of *C. gariepinus*, we have indications that this model gives good predictions of the actual flow velocity. Preliminary results of a high-speed X-ray video analysis of *C. gariepinus* capturing small, spherical pieces of shrimp (6 mm diameter) charged with a small steel marker (0.5 mm diameter) show maximal prey velocities of 1.2 m/s. After applying the suction model (see below for details) to the same individual, the two analysed sequences gave maximal flow velocities of 1.13 and 1.60 m/s. Assuming that

small prey behave approximately as a part of the fluid, these findings suggest that also for *C. gariepinus* the model output is (at least) realistic.

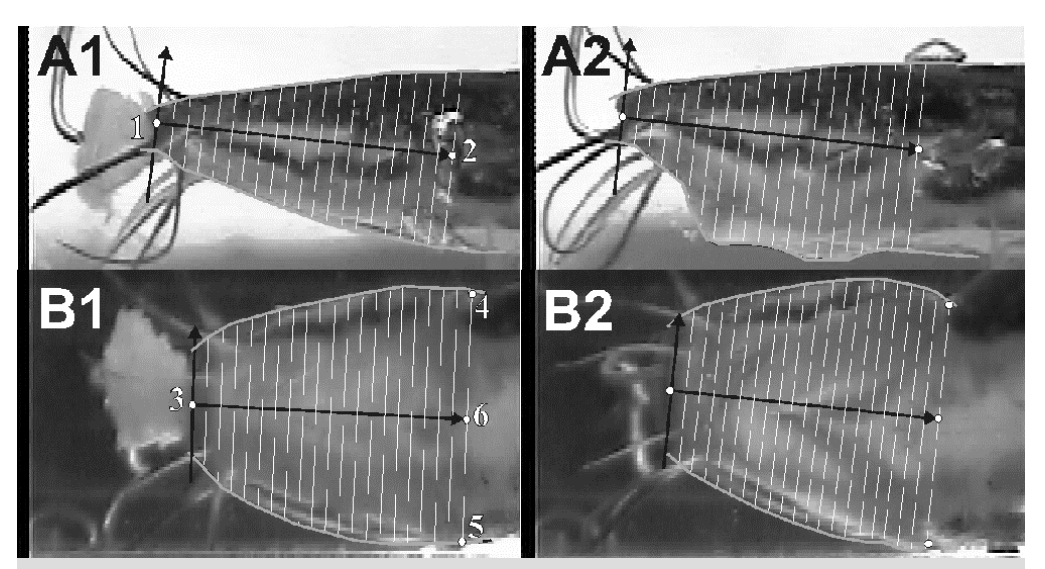


Figure 1: Selected frames from a prey capture sequence of Clarias gariepinus recorded simultaneously in lateral (A1, A2) and ventral view (B1, B2), illustrating the measurements that were made, and used as input variables in the suction model (A1, B1: before the start of suction, A2, B2: after prey intake). The gray lines represent the curves that fitted through the digitised coordinates of the contours of the head. The black arrows represent the fish-bound frame of reference of which the longitudinal axis runs from landmarks (white points with numbers) 1 to 2 in lateral view (see A1) and from landmarks 3 to 6 in ventral view (see B2). The positions of the landmarks digitised are (1) the upper jaw tip at the side of the mouth opening, (2) the anterior tip of the base of the pectoral fin, (3) the middle of the mouth aperture, (4) and (5) the anterior tips of the bases of the right and left pectoral fins and (6) the middle between landmarks 4 and 5. The distance along the longitudinal axis from mouth aperture to pectoral fin base was divided into 21 equally spaced intervals for which the height (white lines in A1 and A2) and the width (white lines in B1 and B2) of the head were calculated. These values constituted the minor and major axis of the ellipse base area of an elliptical cylinder. In our model, the volume changes over time of this these 21 serially arranged flattened cylinders, were assumed to correspond to volume changes of the mouth cavity.

In our suction model, the head of the catfish, from mouth aperture to pectoral fin, is approximated by a series of 21 elliptical cylinders. Each elliptical cylinder has an ellipse-shaped base area from which the length of the major and minor axis, respectively, correspond to the height and width of the head at any given position (Figs. 1, 2). Changes in the length of both axes were deduced from the recorded videos. To do so, upper and lower contours of the catfishes' head were digitised frame by frame (50 points each) in the lateral and ventral view. At the same time, the coordinates of a longitudinal axis connecting the upper jaw tip to the middle between left and right pectoral fin bases were

digitised (for more information, see Fig. 1). Next, the contour coordinates were recalculated in a new frame of reference moving along with the fish, with the upper jaw tip as origin and the longitudinal axis as X-axis. The coordinates of each curve were then fitted with tenth-order polynomial functions, using the XIXtrFun add-in for Microsoft Excel (Advanced System Design and Development, Red Lion, PA, USA). With these functions, at 21 equally spaced intervals along the longitudinal axis (starting with mouth aperture until pectoral fins), the distance between the corresponding coordinates of the upper and lower contours were calculated (Fig. 1). With these data, changes in the width and height of the ellipses over time as well as changes in the volume of the elliptical cylinders were calculated. For each elliptical cylinder, the profiles of length and width versus time were filtered with a fourth-order Butterworth zero phase-shift low-pass filter in order to reduce digitisation noise (cut-off frequency of 30, 12 and 6 Hz for videos recorded at 250 Hz, 100 Hz and 50 Hz). Figure 2 gives an idea of how the volume of the catfishes' head is represented in the model.



Figure 2: Three-dimensional illustration of the head-volume of *Clarias gariepinus* as modeled by a series of elliptical cylinders. The compressed (above) and expanded (below) volumes correspond to the images shown in Figure 1.

The internal dimensions of the mouth cavity of C. gariepinus in rest are approximated using X-ray images from lateral and ventral view X-ray videos of a preserved specimen (Fig. 3). recording of these X-ray videos, the specimen was held vertically while a saturated Barium-solution was poured in the mouth. Using this radio-opaque fluid, the boundaries of the mouth cavity could accurately be distinguished, and the internal area of the mouth cavity could be determined for all positions along the longitudinal axis at the base of each flattened cylinder (Fig. 1). Again, internal areas were approximated by ellipses consisting of the height and width of the measured distance between upper and lower contours of the internal volume on

the lateral and ventral X-ray images at these positions (Fig. 3). To account for the presence of the gill apparatus, the length of the major and minor axes of ellipses in the gill region were (arbitrarily) reduced by 10%. It was assumed that this situation (i.e. the internal volume of the mouth cavity of the preserved specimen at rest) reflects the moment prior to start of the suction event. Subsequently, changes in the height and the width of the head over time (calculated as in Fig. 1), will cause changes in the width and height of the

internal mouth volume ellipses. Because internal volume data were collected for one individual only, we are forced to assume that the dimensions of the bucco-pharyngeal cavity are proportional to the measured external dimensions of the head in *C. gariepinus*. The X-ray videos were made with a Philips Optimus X-ray generator coupled to a Redlake Imaging Motionpro digital high-speed camera.

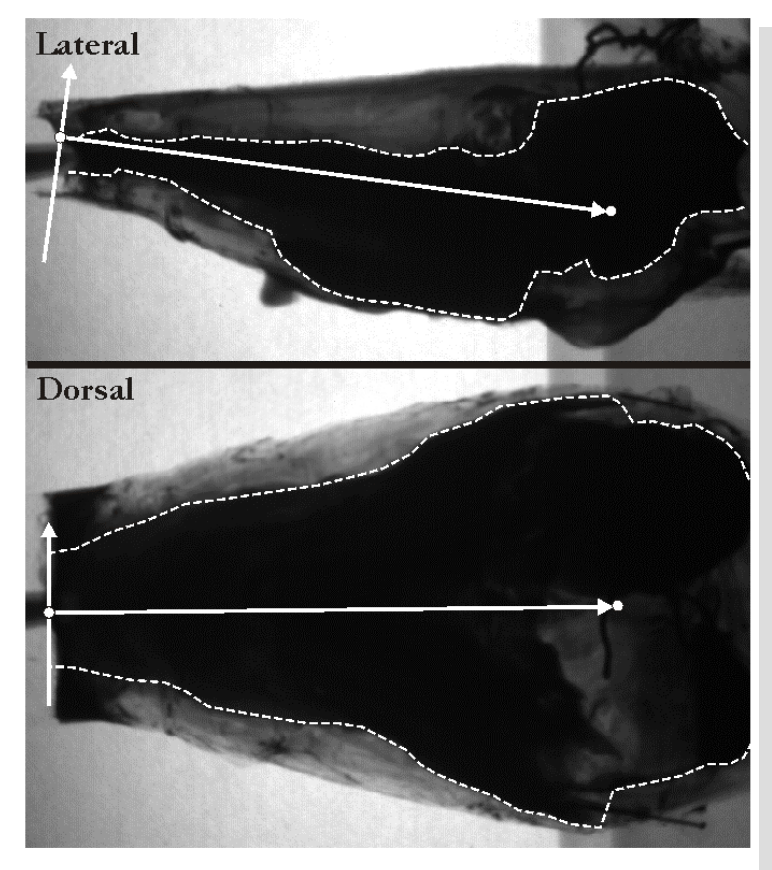


Figure 3: Lateral and dorsal X-ray photographs used to measure the internal dimensions of the unexpanded mouth cavity of a preserved Clarias gariepinus specimen (cranial length = 94.13 mm). The internal contours of the mouth cavity (dashed lines) were quantified by filling the mouth with a radio-opaque Barium-solution.

The same frame of reference (white arrows representing the axes) as in the external video analysis (see Fig. 1) was used determine the height and the width of the mouth cavity at the positions specific along the longitudinal axis defined in Fig 1.

If we assume that the volume of the tissues in the head remains constant, changes in the volume of the head correspond to equal changes in the volume of the mouth cavity. According to the

continuity principle, any change in volume must be filled instantaneously with water and thus generate a flow relative to the fishes' head. Thus, at each cross-section of the mouth cavity, the total water volume passing through this cross-section in a given amount of time depends on the total volume increase posterior to this cross-section. In this way, the average flow velocity during a given time increment can be calculated at each of the modelled ellipse-shaped cross-sections of the mouth cavity by dividing the volume increase posterior to this ellipse by the area of the ellipse (average for that time increment). This holds as long as the opercular and branchiostegal valves are closed. If not, the modelled

system becomes undetermined (Muller et al., 1982; Muller and Osse, 1984; Drost and van den Boogaart, 1986). In general, valve opening can be detected shortly after *C. gariepinus* reaches maximal oral gape. However, for several of the recorded prey capture sequences, it was problematic to pinpoint exactly the frames in which the transition from closed to opened valves occurred. Therefore, we used the model output only from the start of mouth opening until the time of maximal gape.

To calculate flow velocity in front of the mouth, the following formulae from Muller et al. (1982) is used:

$$v = \frac{v_m h^3}{(d^2 + h^2)^{1.5}}$$

, with ν the flow velocity in the direction of the longitudinal axis, ν_m the flow velocity at the mouth aperture (both v and v_m in the earth bound frame), h the radius of the mouth opening (assumed to be circular) and d the distance from the mouth at which the velocity is calculated. In this way, the flow around the mouth opening is modeled as a circular vortex filament (see Muller et al., 1982). Given the relatively slow forward movement of C. gariepinus during prey capture (average peak forward velocity of 0.096 m/s), the complexity of the model and the data-interpretation could be reduced by assuming that the observed cranial expansions occur in stationary catfish. The diameter of the mouth opening is calculated as the mean of height and width of the mouth. The height of the mouth was measured by digitizing the interior sides of the upper and lower jaw on the Because this external flow velocity decreases approximately lateral view images. proportional with the cube of the distance away from the mouth, flow velocity will rapidly drop in front of the expanding mouth cavity. Recent experiments using the particle image velocimetry technique have demonstrated that this indeed is the case for suction feeding fishes (Ferry-Graham et al., 2003).

3.2.4 Quantification and comparison of flow characteristics

Because the model gives a spatiotemporal pattern of water flow velocities (Fig. 4), specific quantifications of the characteristics of this pattern are needed in order to compare the model output for the different-sized catfish. These quantifications are illustrated in Figure 4, together with an example of the model output. Four types of variables were defined: (1) peak suction flow speeds: the maximal flow speeds at specific positions (fixed positions expressed in millimeters, as well as relative distances expressed in numbers of cranial lengths) along the longitudinal axis (-15 mm, 0 mm, +15 mm, -0.168 cranial lengths and +0.168 cranial lengths; negative positions are in front of the mouth, positive positions are inside of the mouth); (2) external suction distance: the maximal distance in front of the mouth at which specific flow speeds (0.2, 0.4, 0.6 and 0.8 m/s) take place; (3) internal suction distance: the maximal distance inside of the mouth cavity (measured from the

mouth aperture) in which specific flow speeds (0.2, 0.4, 0.6 and 0.8 m/s) can still occur; (4) suction duration: the amount of time during which specific flow speed levels (0.2, 0.4, 0.6 and 0.8 m/s) can be sustained at the mouth aperture. An illustration of how these variables are determined from the model output is shown in Figure 4. Because we are interested only in maximal suction performance, the highest value for each of these variables from the two modeled prey capture sequences per individual was used for in the subsequent regression analyses.

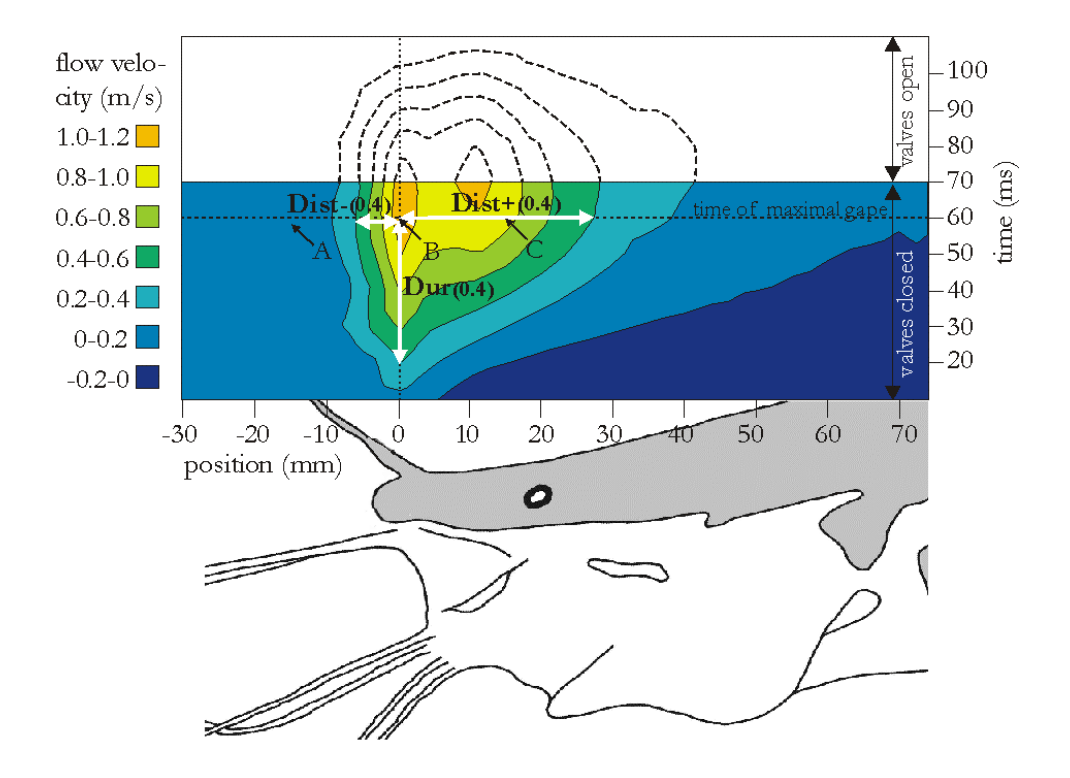


Figure 4: Spatiotemporal flow velocity patterns (in fish bound frame of reference) outside and inside the buccal cavity (position is illustrated by the drawing below the graph), as predicted by the model for a prey capture sequence of a 94.1 mm cranial length *Clarias gariepinus*. Note that the model is unreliable after valve opening and therefore, only the flow pattern before the time of the maximum gape was used. Variables quantifying peak suction flow speed, suction distance, and suction duration are indicated by arrows in the center of the graph. Dist-(0.4) and Dist+(0.4) represent respectively maximal distance outside and inside the mouth that is subject to a flow velocity of 0.4 m/s or more. Dur (0.4) gives the duration in which a flow velocity of 0.4 m/s is sustained before the time of maximum gape at the level of the mouth aperture. A and C are respectively peak flow velocity at a position of 0.168*cranial length outside and inside of the mouth aperture. B indicates the peak flow velocity at the mouth aperture.

Additionally, the forward velocity (in earth-bound frame of reference) of the catfish during prey capture was analyzed. Although this is not directly an aspect of the inertial suction process (displacing water relative to the fish by expanding the bucco-pharyngeal volume), any size-dependent changes in the attack strategy can influence scaling effects on prey capture performance. For example, a study by Cook (1996) showed that a juvenile cottid fish (*Clinocottus analis*) shifts from a ram-dominant feeding mode (more relying on fast swimming towards the prey) to a suction-dominant feeding mode during ontogeny. In this case, by focussing on only the flow patterns relative to the fish, an important behavioural component of prey capture performance could be overlooked. Therefore, the average peak horizontal velocity in the direction of the prey, as well as maximum peak horizontal velocity (out of all 10 sequences per individual) were analysed for scaling effects. These velocities were determined from the digitized coordinates of the middle of the eye, after noise filtering (Butterworth low-pas filtering) and differentiation versus time.

Because growth is an exponential phenomenon, all data were \log_{10} -transformed values (one data point for each individual) and plotted against the \log_{10} of cranial length. Next, least squares regressions were performed on these data. Because the model output (dependent data) likely has a much greater error than measurements of cranial length (independent data), least squares regressions are appropriate in this case (Sokal and Rohlf, 1995). The slopes of these linear regressions with 95% confidence limits were determined in order to evaluate changes in aspects the flow regime in relation to changes in body size. A slope of 0 means that the variable is independent of cranial length. Slopes of 1 and -1 denote that the variables respectively increase or decrease proportional to cranial length, while a slope of 2 stands for a variable increasing with the square of cranial length. The significance level of P = 0.05 was used throughout the analysis. Because the existing statistical methods that account for multiple testing (e.g., sequential Bonferroni correction) are incorrect in ignoring the number of significant tests in the analysis (Moran, 2003), we did not reduce the significance level in case of high percentages of significant results at P = 0.05 (see, e.g., Table 1).

3.2.5 Simulations of prey displacement

A number of forward dynamical simulations were performed for a hypothetical prey that is subjected to the calculated spatiotemporal flow velocity patterns. In these simulations, drag forces resulting from the suction-induced water flow move the prey. The following equation of motion is used:

$$(m_{prey} + m_{added}) \times a_{prey} = \frac{1}{2} C_d A \mathbf{r} v_r^2 + \frac{3}{2} \mathbf{r} V_{prey} a_{fluid}$$

, where m_{prey} is the mass of the prey, m_{added} an added mass component, a the acceleration of the prey, C_{d} the shape dependent drag coefficient, A the frontal area of the prey (area projected onto a plane perpendicular to the direction of fluid flow), \mathbf{r} the density of the

fluid (1000 kg/m³), v_r the linear velocity of the water flow relative to the prey, V_{prey} the volume of the prey and a_{fluid} the acceleration of fluid at the position of the prey.

Because the hydrodynamic properties of natural prey are immensely diverse, it is impossible to account for this diversity. For example, the difference in frontal area A and $C_{\rm d}$ for a fish parallel or the same fish perpendicular to the flow is considerable. Therefore, only a standardized, spherical prey with the same density as the fluid (gravitational force and hydrostatical lift will cancel each other out) was used in the simulations. This prey is presented at a specific position in front of the fish's mouth at the longitudinal axis used in the suction model, and is immobilized until the time corresponding to one frame after the start of the cranial expansion (first time for which flow velocity can be calculated). Because the suction model output gives flow velocities only at discrete positions along the longitudinal axis (intervals of 0.042 cranial lengths) rather than a continuous function, linear interpolations were used to calculate flow velocity at any given position. The simulations were stopped at one frame after the time of maximal gape (end of suction flow calculations). The added mass of a spherical particle with the same density of the surrounding water equals half the mass of this particle (Daniel, 1984). The drag coefficient of a sphere depends on its Reynolds number ($Re = D \mathbf{r} v_r / \mathbf{h}$); with D the diameter of the sphere, ρ the density of the water, v_r the flow velocity relative to the sphere and h the dynamic viscosity of water (0.001 kg m⁻¹ s⁻¹; Vogel 1994) and is approximated by the following formula from White (1991):

$$C_d = 24/R_e + 6/(1+R_e^{0.5}) + 0.4$$
 (0< Re< 2*105)

Because the results will show that the horizontal velocity of *C. gariepinus* towards the prey does not change significantly with size (see further), this was not taken into account in the modeled predator-prey interaction.

We assumed that the modeled flow velocity at the position of the center of the sphere is uniform over the entire sphere, and that the flow itself is not influenced by the presence of the prey. These assumptions will hold only for small prey relative to the size of the mouth opening. Thus, it should be kept in mind that these simulations merely predict how a standardized prey would behave in a given, modeled flow pattern, rather than giving realistic predictions of prey displacement in course of a suction feeding sequence. The goal of these simulations is to evaluate how the differences in flow pattern characteristics could potentially be translated to differences in prey movement. Because the objective of the present study is to compare fishes of different sizes, these simplifications seem justified.

3.3 Results

The flow velocity patterns predicted by the suction model clearly change with increasing fish size. The most conspicuous changes can easily be illustrated by comparing the model

output for small and large fish (Fig. 5). When *C. gariepinus* becomes larger, the duration of the expansive phase becomes longer, resulting in a prolonged time during which suction can be generated (Fig. 5). Secondly, in larger individuals, flow reaches farther away from the mouth aperture both outside and within the mouth cavity (Fig. 5).

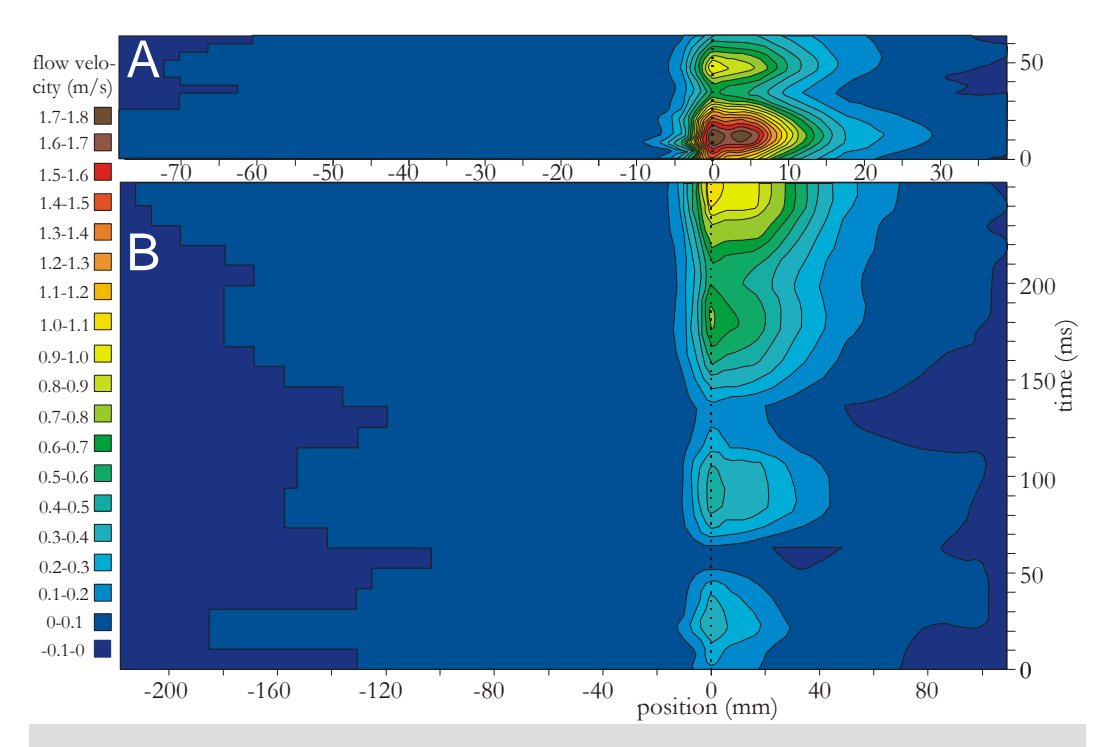


Figure 5: Examples of representative spatiotemporal flow velocity patterns from individuals of 46 mm (A) and 130 mm (B) cranial length. The dotted line (at 0 mm position) corresponds to the mouth aperture (see also Fig. 4). Note that the horizontal axis (position) is scaled according to the cranial lengths of the two individuals.

3.3.1 Maximal suction velocities

Although the slope of the least squares regression suggests a decrease in the peak flow velocities at the mouth aperture (Fig. 6), this relation is statistically not significant (P = 0.061). Also for the peak flow velocities at fixed absolute distances from the mouth aperture proportional to cranial size (Fig. 6A), no significant changes with changing cranial size can be demonstrated (Table 1).

In contrast, a different result is found when comparing peak suction flow speeds at distances from the mouth aperture (Fig. 6B). For flow 15 mm inside the mouth, peak flow speed scales with a slope of 0.94, which is an almost proportional increase with cranial length. An even more rapid increase of maximal flow velocity with head size is found in

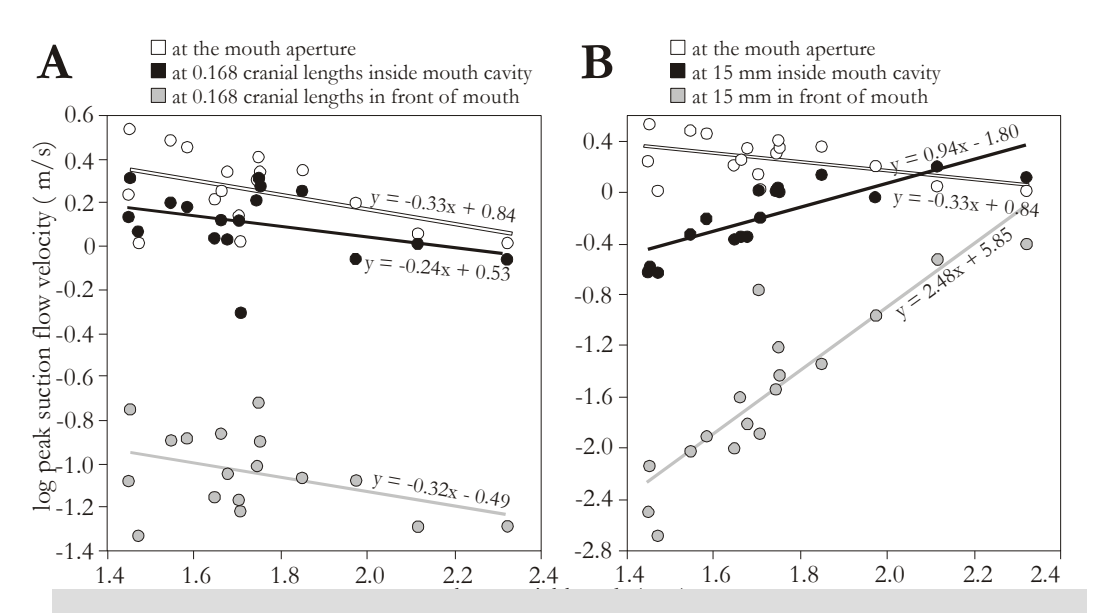


Figure 6: Log-log plots of peak suction flow velocities against cranial length, as predicted by the suction model for the positions as represented in the legend above each graph. Least squares regression lines with equations are shown for each variable. While graph \mathcal{A} represents scaling relationships at distances relative to the size of the catfishes' cranium, graph \mathcal{B} gives scaling relationships of maximal flow velocities at fixed, absolute distances away from the mouth aperture. See Table 1 for a summary of these data.

front of the mouth opening (Fig. 6B). Fifteen millimeters in front of the mouth, peak flow speed increases with cranial length to the exponent 2.47.

3.3.2 Suction distance

Suction distance in front of the mouth (Fig. 7A) and inside of the mouth cavity (Fig. 7B) show very similar scaling relationships. A close correspondence is also found between scaling of the different flow velocities (Fig. 7; Table 1). In general, scaling exponents vary around 0.8, which means an increase of suction distance roughly proportional with size. However, because all 95% confidence limits include the slope of 1 (Table 1), suction distance doesn't decrease significantly relative to the fishes' head size.

3.3.3 Suction duration

Before maximum gape, the low suction-induced flow speeds (0.2 m/s and 0.4 m/s) are sustained for a longer time in larger *C. gariepinus* individuals (Fig. 8). This increase is almost proportional to body length (regression slopes of 0.88 and 0.80 respectively). For the higher flow velocities (0.6 m/s and 0.8 m/s), the sustainable duration seems to scale differently (slopes of 0.58 and 0.25 respectively; Fig. 8). However, a much larger inter-

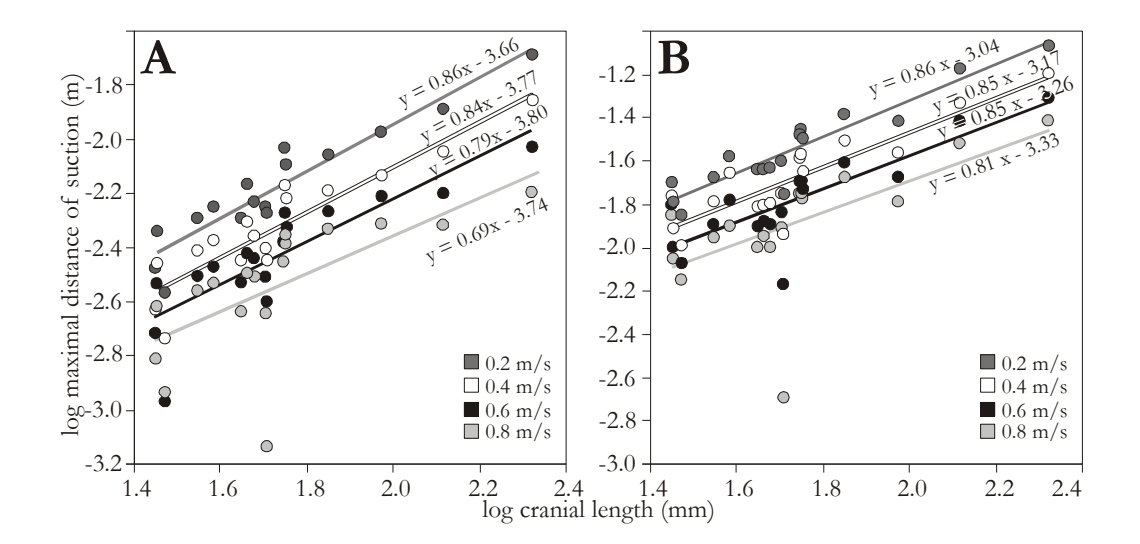


Figure 7: Log-log plots of maximal external (A) and internal (B) suction distance against cranial length, as predicted by the model for 4 levels of flow velocity (legends in the lower right-hand corner of each graph). Least squares regression lines with equations are shown for each variable. All distances are measured from the mouth aperture (see also Fig. 4). See Table 1 for a summary.

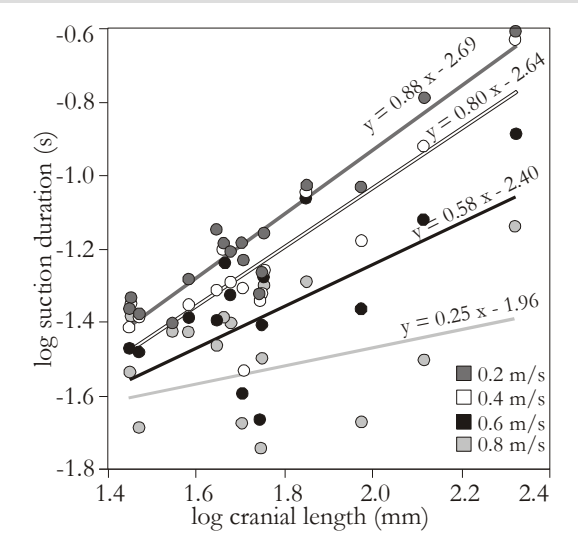


Figure 8: Log-log plot of suction duration against cranial length, as predicted by the model for four levels of flow velocity (legend in the lower right-hand corner of the graph). Least squares regression lines with equations are shown for each variable. Suction duration is measured at the mouth aperture (see Fig. 4). See Table 1 for a summary.

individual variability in the model output occurs for these two variables. As the error of the slopes is considerable, both a scaling-independent relationship (slope 0) and a scaling proportional to body size (slope 1) cannot be excluded for the duration of the two highest

Table 1: Scaling relationships of 17 variables quantifying the spatiotemporal flow pattern from suction modeling of *C. gariepinus*.

1 1								
			9.	95% confidence limits				
Variable	Slope	R^2	P	lower	upper			
Peak flow velocity:								
15 mm outside	2.47	.79	<.0001	1.78	3.18			
.168 CL outside	32	.16	.1089	73	.08			
Mouth aperture	33	.21	.0614	69	.02			
15 mm inside	94	.65	<.0001	.56	1.31			
.168 CL inside	24	.13	.1627	60	.11			
Maximum outside								
distance								
.2 m/s flow	.86	.89	<.0001	.69	1.03			
.4 m/s flow	.84	.84	<.0001	.64	1.04			
.6 m/s flow	.79	.72	<.0001	.52	1.06			
.8 m/s flow	.69	.44	.0037	.26	1.12			
Maximum inside								
distance								
.2 m/s flow	.86	.90	<.0001	.70	1.02			
.4 m/s flow	.85	.82	<.0001	.63	1.07			
.6 m/s flow	.85	.76	<.0001	.59	1.10			
.8 m/s flow	.81	.45	.0033	.32	1.31			
Duration:								
.2 m/s flow	.89	.88	<.0001	.71	1.07			
.4 m/s flow	.80	.73	<.0001	.53	1.07			
.6 m/s flow	.58	.19	.0841	09	1.26			
.8 m/s flow	.25	.3	.4875	.49	.98			

Note. P denotes the probability of the slope differing from 0. Outside and inside refer to the positions in front of the fish and internal of the buccal cavity, respectively. All distances are with regard to the mouth aperture (see Fig. 4). N = 17. CL = cranial length.

 $R^2 = 0.71$: 95% confidence interval between

flow velocities that were compared in this study (Table 1).

3.3.4 Attack velocity

No significant change in the peak horizontal velocity in the direction of the prey during prey capture was found with changing cranial size (Fig. 9). For the average peak velocity and the maximal peak velocity (out of 10 strikes per individual), slopes of the linear regressions were 0.16 with 95% confidence limits between -0.16 and 0.46 for both variables (N = 17; $R^2 =$ 0.08). However, when expressed as relative velocities (in cranial lengths/s), small fishes are considerably faster compared to large fish (slope = -0.84, N = 17; -1.14and -0.54).

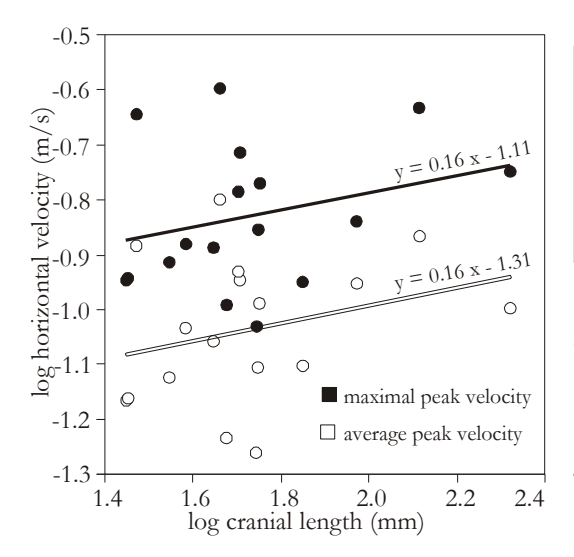


Figure 9: Log-log plot of the peak horizontal velocity of *C. gariepinus* during prey approach against cranial length. Data are shown for the maximum and average values (legend in the lower right-hand corner of the graph).

3.5 Discussion

3.5.1 Scaling of spatiotemporal flow characteristics

The model predicts that maximal flow speed during suction of *Clarias gariepinus* does not increase with increasing size of

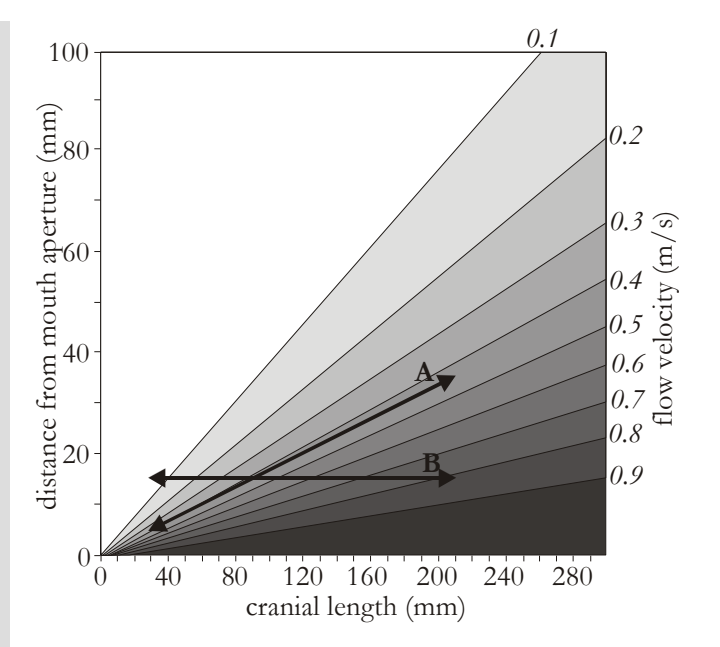
the cranial system. Moreover, the results of the model even show a decreasing trend with increasing size (Fig. 6A; Table 1). Two factors can contribute to this result. First, when *C. gariepinus* becomes larger, a relatively smaller expansion of the mouth cavity might occur during the expansive phase. For example, if a catfish of double length only expands to a four times larger volume (half of its capacity expected from isometry) in the same amount of time, then the model will predict equal flow speeds. Second, when *C. gariepinus* grows, scaling effects on prey capture kinematics may cause the slowing down of the cranial expansions, as shown in other fish taxa (Richard and Wainwright, 1995; Hunt von Herbing et al., 1996; Cook, 1996; Wainwright and Shaw, 1999; Hernandez, 2000). For example, if it takes twice as long for the double-size catfish to generate a given volume-expansion, flow velocities will also stay equal.

For *C. gariepinus*, a combination of these two factors appears to apply. First, smaller individuals generate a relatively larger expansion of their mouth cavity. If we plot the total volume change (model output at the time of maximum gape *minus* volume at the start of prey capture) against cranial length in a log₁₀- log₁₀ graph, we did not find the expected isometric slope of 3, but 2.31 (95% confidence limits: 1.70 and 2.91). Second, the duration of the expansive phase (defined here as time until maximum gape) increases considerably with rising cranial size (slope of 0.86 for the 34 analysed sequences, 95% confidence limits: 0.62 and 1.09). Separately, neither of these two factors are enough to explain the observed result for peak flow velocity (Fig. 6A). However, the combination of a less extensive cranial expansion and a longer time to create this expansion for the larger *C. gariepinus*, cause the peak flow speed to remain constant when compared to the smaller individuals of this species.

In contrast, at fixed absolute distances away from the mouth aperture, large *C. gariepinus* individuals do have a substantial advantage over small ones when it comes to generating higher suction flow velocities (Fig. 6B). It should be noted that for such variables, the

observed scaling relationships depend on how fast the flow velocity drops at a certain distance away from the mouth aperture. Figure 10 illustrates this situation for a theoretical flow velocity pattern in front of the mouth, which is determined by the formula from Muller et al. (1982) (see Material and Methods). For this flow pattern, scaling relationships depend on the distance from the mouth aperture, but also on the size-range of animals used in the study (Fig. 10). For example, if we had selected a distance further away from the mouth, less steep scaling regressions would be found. Also for the peak suction velocities at relative distances in front of the mouth aperture, the observed scaling effects depend on the fraction of cranial length is chosen, but are independent of the used size-range of fish (Fig. 10). This is just to show that almost any extrapolation of the observed scaling effects for variables of peak flow speeds distant from the mouth aperture will likely be incorrect. Although not representative of the scaling relationships of the entire flow pattern, each of these variables does have a clear biological relevance in determining the magnitude of the drag forces that pull the prey toward, and into the mouth at a given point along the longitudinal axis of the expansive system.

Figure 10: Theoretical illustration of the decreasing flow velocity exterior of the mouth opening in relation to cranial size, resulting from the circular vortex filament model of Muller et al. (1982) for a flow velocity at the mouth aperture of 1 m/s and a mouth opening radius of 0.2 times cranial length. Arrow A represents the data range included in the peak flow velocity scaling relationships at relative distance of 0.168 cranial lengths away from the mouth opening (given in Fig. 6A). Arrow B corresponds to the data range from the scaling relations of peak flow speed at fixed absolute distance of 15 mm. Arrows that are parallel to A or B, but at another position on the graph can easily cross a different number of isovelocity lines. This indicates that scaling effects depend on the chosen distance and, only for B, also on the size range of animals used in the analysis.



Suction distance in *C. gariepinus* scales slightly less than proportional to cranial size (Fig. 7). For the external suction distance (in front of the mouth opening), this scaling relationship is a result of the circular vortex filament model (Muller et al., 1982) included in our model calculations. Inherent to this model, the maximal

distances to which low suction flow velocities reach, shows a relatively faster increase with increasing absolute mouth opening size (Fig. 10) when compared with high flow velocities. Consequently, this trend is also observed in the scaling data of *C. gariepinus* (Fig. 7; Table 1). For the internal suction distance (inside the mouth cavity), with similar peak flow velocities at the mouth aperture, we would expect an increase proportional to cranial length. Although the results are not statistically different from these expectations (Table 1), the scaling exponents tend to be somewhat lower. Most likely, this is related to the decreasing trend in the peak values of flow velocity at the mouth aperture (Fig. 6).

The fact that suction duration increases during growth (Fig. 8) is obviously related to the prolonged time between the start of the cranial expansion and the time at which this expansion is completed. As mentioned earlier, the time between the onset and offset (time of maximum gape) of the model increases almost proportionally with cranial length. As a result, specific flow velocities can be kept up for a considerably longer time when *C. gariepinus* becomes larger (Figs. 5, 8).

3.5.2 Scaling of suction performance

Although it is obvious that data describing patterns of water flow during prey capture are critical for understanding the impact of movements of the head on the water surrounding the prey (Ferry-Graham and Lauder, 2001), induced water velocities are merely proximate measures of suction feeding performance (Wainwright et al., 2001). Indeed, the calculated variables quantifying the changes in the spatiotemporal flow velocity pattern with changing head size (Figs 6-8) do not directly predict the outcome of the interaction between the moving water, prey, and predator. However, if the flow velocity in function of time and position is known, movement of a hypothetical prey subjected to this flow can be reconstructed. Indeed, forward dynamic simulations of prey displacement allow us to explore the importance of the size-related changes in flow velocity for prey displacement.

The maximal distance to which flow reaches away from the mouth aperture was found to scale slightly less than proportional to cranial size (Fig. 7A). However, this does not directly mean that prey can be caught from farther away, because such prey have to be moved over a larger distance and for a longer period of time. In other words, a very short, far-reaching burst of flow velocity may not be sufficient to achieve prey transport from its outermost points. To evaluate this, a spherical prey of 4 mm diameter was introduced into the calculated flow patterns. Next, the maximal distance away from the mouth opening for which this prey could still reach the mouth aperture during the course of the expansive phase was calculated. The results of these simulations are given in Figure 11A. Consistent with the scaling relationships of maximum flow distance in front of the mouth aperture (Fig. 7), the calculated maximum distance from which the 4-mm sphere can reach the mouth opening at the time of maximal gape scales with an exponent of 0.86 (N = 17; $R^2 = 0.87$; 95% confidence intervals between 0.68 and 1.04). This indicates that the ability to

capture prey from farther away from the mouth by suction feeding in *C. gariepinus* increases with cranial size. The simulations even predict that this distance of suction increases nearly proportional with cranial length (Fig. 11A). This is not entirely surprising if we consider that behavioral observations have shown that this species often initiates prey capture upon contact with the barbels (Bruton 1979; *Chapter 6*), and that the length of these chemosensitive structures projecting from the mouth increases along with size of the cranium.

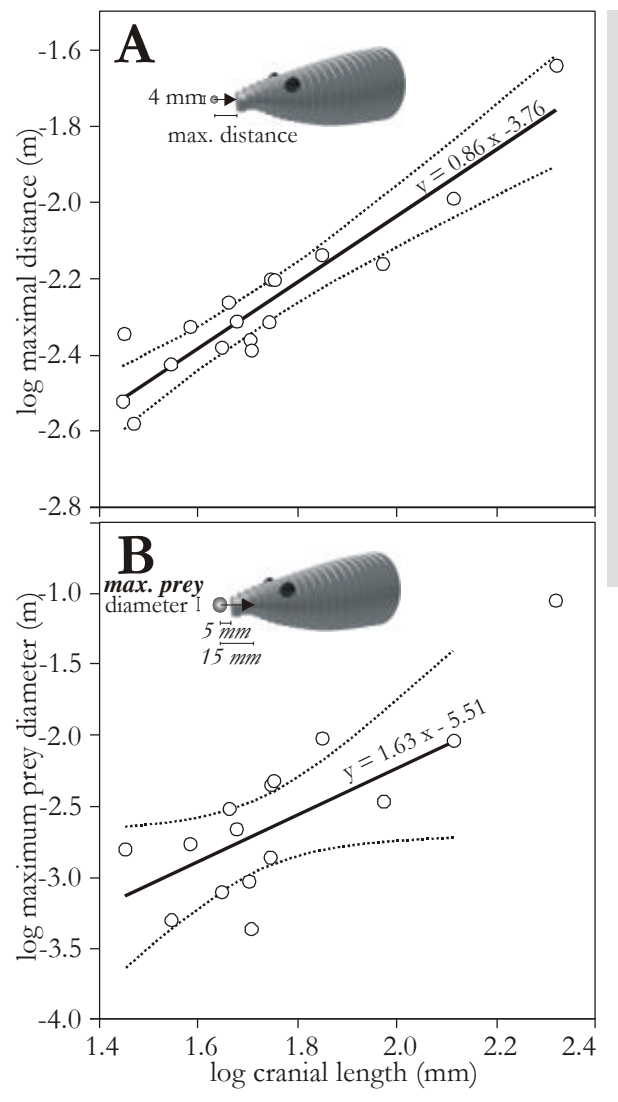


Figure 11: Log-log plots of maximal prey distance (A) and maximal prey size (B) versus cranial length, as predicted by forward dynamic simulations of spherical prey moving in the deduced flow fields. In graph A, the hypothetical prey has a fixed diameter length of 4 mm. In B, the starting distance was set at 5 mm in front of the mouth. Least squares regression lines with equations and 95% confidence limits (dotted lines) are shown. Note that in B, the value for the largest individual was not included in the regression, since a sphere of 90 mm close to the mouth will interfere with the expansions.

Large fish have a larger absolute gape compared to small individuals of the same species. This allows these large individuals to feed on larger prey compared to small ones (Schael et al., 1991; Huskey and Turingan, 2001; Manghagen and Heibo, 2001). However, when prey size increases, its moment of inertia will increase as well. Consequently, higher suction-induced drag forces on the prey will be necessary to accelerate larger prey to a given

velocity. To evaluate for *C. gariepinus* how the maximal size of prey is limited by the scaling effects on the suction flow pattern, spherical prey were presented into the calculated flow patterns at a distance of 5 mm in front of the mouth aperture. Next, the maximal diameter of the prey for which this prey could still reach the position of 10 mm inside of the mouth

cavity (measured from the mouth aperture) during the course of the expansive phase, was calculated. The results of these simulations are given in Figure 11B. The maximal size of the sphere that can still perform this movement, scales to cranial length with an exponent of 1.63 (N=14; $R^2=0.41$; 95% confidence intervals between 0.41 and 2.86). These simulations suggest that during growth of *C. gariepinus*, its ability to capture larger prey by suction feeding increases substantially. According to the model's predictions, maximal prey size would even increase faster than proportional to cranial size, if these prey are sucked from the same absolute distance from the mouth (Fig. 11B).

So far, it seems that the flow patterns generated by C. gariepinus increase the efficiency to capture prey by suction feeding during ontogeny from juveniles to large adults (Fig. 11). Moreover, our results indicate that whenever a fish swims at a certain distance in front of the mouth of a C. gariepinus individual, it will have a reduced chance of escaping when it concerns a large catfish compared to a small catfish. This increased suction performance appears also to be reflected in the dietary data from the literature on C. gariepinus. Bruton (1979) compared stomach contents from different size classes of C. gariepinus from a South-African lake, and found increasing proportions (dry weight) of fish and decreasing proportions of insects and mollusks in the diet with increasing predator size. Moreover, individuals larger than 700 mm total length included only fish in their diet (Bruton, 1979). As the success of capturing fast and evasive prey (such as fish), depends more on maximal suction feeding performance compared to other prey, the observed shift in the diet may be a direct consequence of the scaling relationships presented here. Furthermore, while the presented scaling results indicate an increase (with increasing head size) in the maximum size of prey that can be drawn into the mouth cavity by suction (Fig. 11B), the diet study of Bruton (1979) also found the size of the most common prey (Sarotherodon mossambicus) increasing linearly with predator length. Thus, changes in suction feeding capacity seem to be reflected in the properties of the natural diet of *C. gariepinus*.

At this point, we have only focused on *absolute* differences in suction feeding performance, that is, when small and large fish feed on prey of the same absolute size or at the same absolute distance from the mouth. However, small fish will probably aim at smaller prey and will also be able of approaching prey closer compared to large fish. Hence, suction performance was also compared for a situation that is similar relative to the predators' size, that is, with prey size and initial distance from the mouth in proportion to cranial length. In that case, the simulations show that the small fishes clearly outperform the larger fishes (Fig. 12).

There are several reasons for this negative scaling relationship (Fig. 12). First, prey inertia increases with the cube of the prey's length, while drag forces only increase with the square of prey length. This means that when prey size increases in proportion with predator size, higher drag forces (and thus higher suction flow velocities) are needed for the larger predators to generate similar prey accelerations compared to smaller predators. If we exclude this factor from the simulations by artificially scaling mass and added mass to the

cube of cranial length, there is still a significant decrease in realized relative prey displacement with increasing cranial size (slope = -0.782, N = 17; $R^2 = 0.41$; 95% confidence intervals between -0.01 and -1.55), though less strong (Fig. 12). This remaining negative scaling relationship must be caused by scaling effects on the suction-induced flow velocity. Indeed, our results have show that peak values of suction flow velocity tend to decrease (Fig. 6A) and that also the distance to which a given flow velocity can reach away from the mouth aperture does not scale proportional to head length (Fig. 7). Both of these results can contribute to the decreasing performance when prey capture situations are isometrically upscaled with head size.

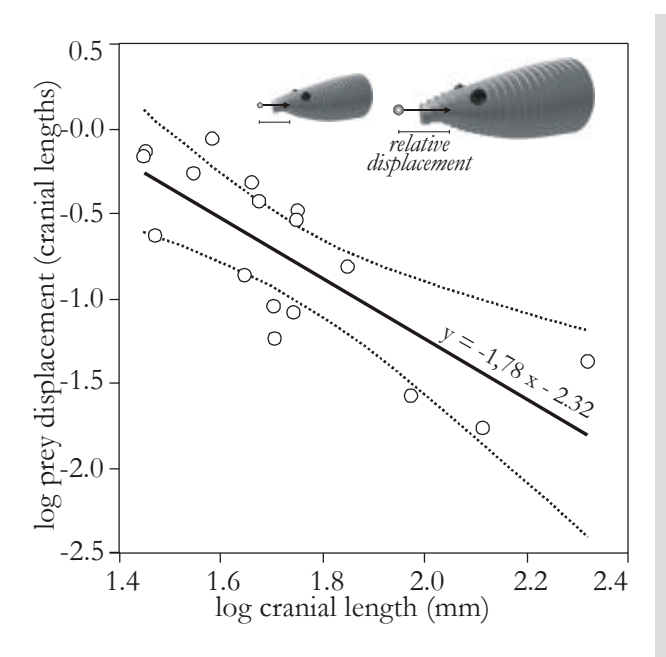


Figure 12: Log-log plot of total relative prey displacement (in numbers of cranial lengths) against cranial length, as predicted by forward dynamic simulations of spherical prey moving in the calculated flows. In order to create a situation with similar conditions relative to the size of each individual, initial prey distance in front of the mouth and diameter were adjusted proportion to cranial length (respectively 10% and 5% of cranial length). Least squares regression lines with equations and 95% confidence limits (dotted lines) are shown ($R^2 = 0.62$; 95% confidence intervals between -1.01 and -2.54).

Because relative forward velocity of the predator also decreases with size (Fig. 9), these simulations potentially even underestimate the scaling effects on prey capture performance in this situation. On the other hand, if the spherical prey is representing a prey fish prior to its escape response, a decrease in speed, acceleration and maneuverability during the subsequent escape of this prey with increasing prey size can be expected (Domenici, 2001), which may cancel out the relatively faster approach from the predator. Not only evasiveness and size of prey, but also behavioral aspects of both predator (e.g., foraging mode) and prey (e.g., predator perception capacity) will be important, as these determine potential scaling effects on the distance from which the predator is forced to initiate its prey capture. This illustrates that the study of scaling relationships of prey capture performance is extremely complex, as several aspects of the predator-prey interaction can have an influence on the outcome of a suction feeding event.

As long as we have no idea on how suction distance, prey size and predator size are interrelated, the ecological relevance of mathematical simulation with isometrically scaled prey size and distance can be questioned. Yet, our simulations do demonstrate that small *C. gariepinus* are not at all the poor suction feeders as may appear from Figure 11. If they specialize on prey with a size in proportion to their own size and if the initial distance can be reduced accordingly, their prey capture success will still be very high. Still, the results from the simulations with varying absolute distances and prey sizes (Fig. 11) illustrate their limitations when it comes to feeding on prey that are larger or further away. In this way, scaling effects on suction-induced flow velocities will restrict smaller individuals to a smaller subset of the potential prey spectrum in the environment, when compared to the larger individuals.

Chapter 4

Scaling of suction feeding kinematics and dynamics in the African catfish, Clarias gariepinus

Sam Van Wassenbergh – Peter Aerts – Anthony Herrel

The Journal of Experimental Biology 208, 2103-2114. (2005)

Summary

Scaling effects on the kinematics of suction feeding in fish remain poorly understood, at least partly because of the inconsistency of the results of the existing experimental studies. Suction feeding is mechanically distinct from most other type of movements in that negative pressure inside the buccal cavity is thought to be the most important speedlimiting factor during suction. However, how buccal pressure changes with size and how this influences the speed of buccal expansion is unknown. In this paper, the effects of changes in body size on kinematics of suction feeding are studied in the catfish Clarias gariepinus. To do so, video recordings of prey-capturing C. gariepinus ranging in total length from 111 to 923 mm were made, from which maximal displacements, velocities and accelerations of several elements of the cranial system were determined. By modelling the observed expanding head of C. gariepinus as a series of expanding hollow elliptical cylinders, buccal pressure and power requirement for the expansive phase of prey capture were calculated for an ontogenetic sequence of catfish. We found that angular velocities decrease approximately proportional with increasing cranial size, while linear velocities remain more or less constant. Although a decreasing (angular) speed of buccal expansion with increasing size could be predicted (based on calculations of power requirement and

the expected mass-proportional scaling of available muscular power in *C. gariepinus*), the observed drop in (angular) speed during growth exceeds these predictions. The calculated muscle-mass-specific power output decreases significantly with size, suggesting a relatively lower suction effort in the larger catfish compared to the smaller catfish.

4.1 Introduction

Changes in body size have important consequences for the mechanics of musculo-skeletal systems (Hill, 1950; Schmidt-Nielsen, 1984). One of these consequences is that larger animals need more time to carry out the same movement (e.g., downstroke of the wings during flight or leg extension during jumping) compared to smaller animals (Askew et al., 2001; Bullen and McKenzie, 2002; Schilder and Marden, 2004; Toro et al., 2003). Because of the importance of scaling relationships for the ecology, behaviour, performance and evolution of animals (e.g. Carrier et al., 2001; Walter and Carrier, 2002; Hutchinson and Garcia, 2002; Davenport, 2003), theoretical models have been proposed (e.g. Hill, 1950; Richard and Wainwright, 1995). These models provide quantitative predictions of scaling of kinematics in geometrically similar animals.

Although most scaling studies have addressed animal locomotion, several experimental studies have focussed on scaling of prey capture kinematics in aquatic suction feeding vertebrates (Richard and Wainwright, 1995; Reilly, 1995; Cook, 1996; Hernandez, 2000; Wainwright and Shaw, 1999, Robinson and Motta, 2002). Surprisingly, the results of these studies are largely inconsistent. For example, the time to open the mouth increases with body length by $L^{0.592}$ in Micropterus salmoides (Wainwright and Shaw, 1999), $L^{0.333}$ in Gynglymostoma cirratum (Robinson and Motta, 2002) and L^{0.314} in Danio rerio (Hernandez, 2000) and is in independent of body size in Salamandra salamandra (Reilly, 1995). Furthermore, none of the existing geometrical-similarity models are able to explain the observed results in most cases. Based on the intrinsic dynamics and energetics of contracting muscle, the model of Hill (1950) predicts that similar movements (e.g. a limb rotating a certain angle) should be carried out in times directly proportional to the linear dimensions (~ L1). On the other hand, the model of Richard and Wainwright (1995) predicts that durations of kinematic events are independent of body size ($\sim L^0$) by assuming that the shortening velocity of a muscle is directly proportional to muscle length (or the number of sarcomeres in series). Consequently, the influence of size on the velocity of movements of the feeding system during suction remains a poorly understood phenomenon.

The maximal velocity of a given movement is determined by the equilibrium of forces in the equation of motion for this specific movement. Most of these forces will be subject to size-effects. The magnitude of drag force, for example, depends on the surface area of the structures moving through a given fluid and will therefore increase with size. How these external forces scale with animal size, and how this balances with the available muscular

power, energy or stress-resistance of bones, will often determine the performance of a given movement (e.g. Hill, 1950; Wakeling et al., 1999).

During the expansive phase of suction feeding, a negative (sub-ambient) pressure is created inside the buccal cavity (see, for example, Van Leeuwen and Muller, 1983; Lauder, 1985). As estimated by Aerts et al. (1987), the force exerted by this negative buccal pressure on the expanding lower jaw, is the most important factor to be overcome by the contraction of the mouth opening muscles. Additionally, a recent study has demonstrated a correlation between the force available from the epaxial musculature and buccal pressure magnitudes in centrarchid fishes (Carroll et al., 2004). This also suggests that intra-buccal pressure is the most constraining factor for the maximal performance of the cranial system of suction feeders. So, if the maximal speed of movements by the cranial musculo-skeletal system during suction is mainly limited by buccal pressure, then scaling effects are probably the results of the size-dependency of buccal pressure.

In their theoretical model of suction feeding in fish, Muller et al. (1982) have shown that peak sub-ambient buccal pressure increases drastically (approximately $\sim L^{4.5}$) if an expanding fish head (modelled as an expanding cone) is artificially lengthened, without changing the speed of expansion. Therefore, due to scaling effects on buccal pressure, suction feeders may be forced to decrease the speed of buccal expansion when they become larger (resulting in pressure magnitudes that their cranial muscles are capable of generating). Moreover, the existing scaling models (Hill, 1950; Richard and Wainwright, 1995) may not be able to explain scaling of suction feeding kinematics because the more important effects of changes in pressure with size are not taken into account in these models.

In the present paper, the scaling of prey capture kinematics in the African catfish *Clarias gariepinus* is investigated. Next, the relationships between speed of buccal expansion, cranial size and muscular power requirement are explored by hydrodynamic suction modelling combined with inverse dynamic modelling in *C. gariepinus*. Finally, we evaluate the hypothesis that scaling of suction feeding kinematics may be determined by the size-effects imposed on buccal pressure magnitudes.

4.2 Materials and Methods

4.2.1 study animals

Clarias gariepinus (Burchell,1822) is an air-breathing catfish (Fam. Clariidae) with an almost Pan-African distribution that is also found in rivers and lakes of the Middle East and Turkey (Teugels, 1996). It has a broad diet that includes mostly fishes, shrimps, crabs, insect nymphs, beetles and snails (Bruton, 1979). While this species shows different kinds of foraging behaviours, including bottom feeding, surface feeding or group hunting, prey are generally captured by a combination of suction feeding and biting (Bruton 1979; Chapter 6). Juvenile C. gariepinus specimens already have a fully ossified cranial system that appears to be generally similar in shape to the adult configuration at the ontogenetic stage of 127 mm standard length (Adriaens and Verraes, 1998). Adults can grow up to 1.5 m total length (Teugels, 1986), making this species particularly suitable for studying scaling effects.

In the present study we used 17 individuals between 110.8 and 923.0 mm in total length. As the cranial length (defined as the distance between the rostal tip of the premaxilla and the caudal tip of the occipital process) can be measured more precisely and excludes variability in the length of body and tail, we use this metric to quantify size. The individuals used were either aquarium-raised specimens obtained from the Laboratory for Ecology and Aquaculture (Catholic University of Leuven, Belgium) or specimens obtained from aquacultural facilities (Fleuren & Nooijen BV, Someren, The Netherlands). However, catfish from both origins did not show different growth patterns of the feeding apparatus (see Herrel et al., 2005). All animals were kept in a separate aquarium during the course of the training and recording period. In general, it took about two weeks to train the catfish to feed in a restricted part of the aquarium.

4.2.2 video recordings of prev captures

Video sequences were recorded of *C. gariepinus* capturing pieces of cod (*Gadus morbua*) that were pinned onto a plastic coated steel wire (Fig. 1). In order to obtain a similar feeding situation for both the small and large individuals, the size of the prey was scaled according to the size of the catfish (diameter between 25% and 35% of cranial length). The recordings were made using a Redlake Imaging Motionscope digital high-speed video camera at 250 frames per second (for individuals with cranial lengths between 28.01 and 71.00 mm), a JVC GR-DVL9800 camera (PAL recording system) at 100 fps (for the individuals with cranial lengths of 94.13-130.0 mm) or a Panasonic F15 at 50 fps (for the 210.2 mm cranial length individual). The feeding sequences were recorded simultaneously in lateral and ventral view, using a mirror placed at 45°. Two floodlights (600 Watt) provided the necessary illumination. Only those prey capture sequences that were approximately perpendicular to the camera lens were selected and retained for further analysis.

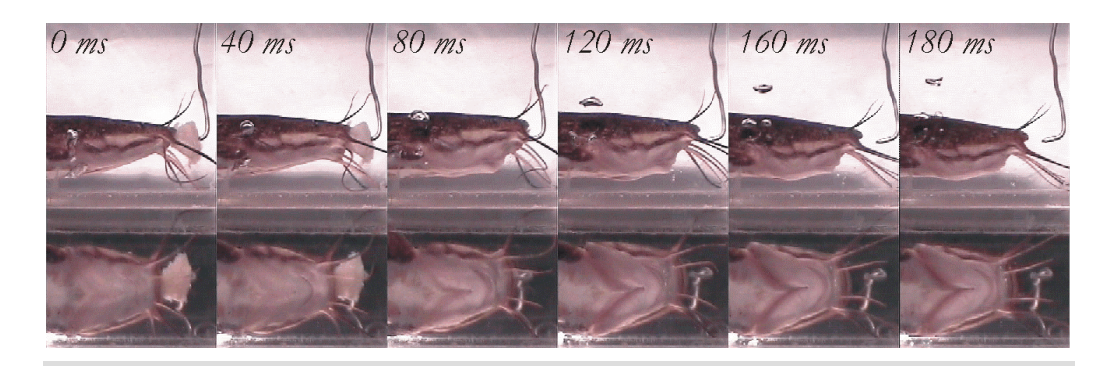
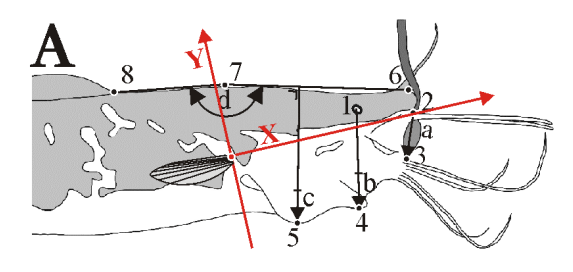
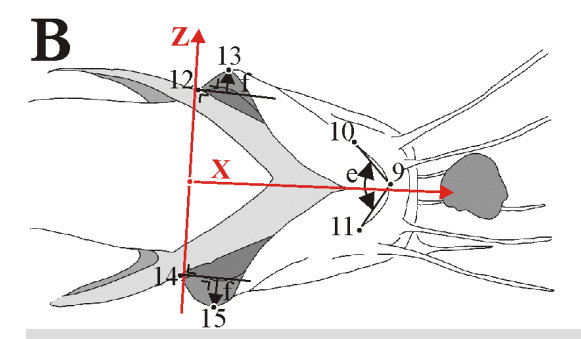


Figure 1: Selected video frames from a representative prey capture sequence for one individual of *Clarias gariepinus* (30.2 cm total length) feeding on an attached piece of cod. Lateral view (top frames) and ventral view (bottom frames) are recorded simultaneously.

4.2.3 Kinematic analysis





Ten recordings were analysed for each individual. Specific anatomical landmarks were digitised using Didge (version 2.2.0, Alistair Cullum, Creighton University, Omaha, USA) from which kinematic variables describing the position of the hyoid, branchiostegal lower jaw, membrane and neurocranium calculated (see Fig. 2). From kinematic plots, timings of kinematic events (maximum and end of the analysed head part movements) were determined, with time 0 being the start of lower jaw depression. After data filtering (4th order Butterworth zero phase-shift low-pass filter) and differentiation versus time,

Figure 2: Anatomical landmarks digitized (black points) with the calculated kinematic variables (arrows) on the lateral (A) and ventral (B) high-speed video images of *Clarias gariepinus*. The landmarks are: (1) middle of the eye, (2) upper jaw tip, interior side, (3) lower jaw tip, interior side, (4) tip of the hyoid, (5) most ventrally positioned point of the branchiostegal membrane, (6) rostral tip of the skull roof, (7) caudal tip of the skull roof, (8) anterior tip of the caudal fin, (9) hyoid symphysis, (10,11) most caudally discernible points on the hyoid bars, (12,14) base of pectoral spine and (13,15) lateral tip of the branchiostegal membrane. The measured linear variables are: gape distance (a), hyoid depression (b), branchiostegal depression (c) and lateral branchiostegal expansion (f, average between left and right). The angular variables are: neurocranial elevation (d) and lateral hyoid abduction (e). The red lines represent the coordinate system moving with the head of the catfish.

velocities and accelerations were calculated. As we are mainly interested in maximal performance, the maximal values per individual (i.e. largest excursions, highest peak velocities and accelerations) were used in the regression analysis. Only for the timing variables were the averages from the 10 analysed sequences for each individual used in the regressions to enable comparison with previous scaling studies (Richard and Wainwight, 1995; Robinson and Motta, 2002).

As growth is an exponential phenomenon, all data were log₁₀ transformed values (one data point for each individual) and were plotted against the log₁₀ of cranial length. Next, least squares linear regressions were performed on these data. As the kinematic variables or the model output (see below; dependent data) likely have a much greater error than measurements of cranial length (independent data), least squares regressions are appropriate in this case (Sokal and Rohlf, 1995). The slopes of these linear regressions with 95% confidence limits were determined in order to evaluate changes in prey capture kinematics in relation to changes in body size. A slope of 0 indicates that the variable is independent of cranial length. Slopes of 1 and –1 denote that the variables respectively increase or decrease proportional to cranial length, while slopes different from these values stand for a variable changing more than proportionally with cranial length.

Each regression was tested for statistical significance by an analysis of variance (ANOVA). T-tests were performed to compare the observed regression slopes against expected values (Zar, 1996). The basic assumptions of normality and linearity were met in the presented data. The significance level of P = 0.05 was used throughout the analysis.

4.2.4 Suction modelling and calculation of buccal pressure

First, spatio-temporal patterns of water velocities inside the mouth cavity were calculated with the ellipse model of Drost and van den Boogaart (1986). This model has been shown to give accurate predictions of flow velocities in suction feeding larval carp (*Cyprinus carpio*) (Drost and van Den Boogaart, 1986) and in the snake-necked turtle (*Chelodina longicollis*) (Aerts et al., 2001). This model also gives good predictions of the actual flow velocity for suction feeding of *C. gariepinus*. Results of a high-speed X-ray video analysis of *C. gariepinus* capturing small, spherical pieces of shrimp (6 mm diameter) charged with a small metal marker (0.5 mm diameter) show maximal prey velocities of 1.2 m/s. After applying the suction model (see below for details) to the same individual, the two analysed sequences gave maximal flow velocities of 1.13 and 1.60 m/s (*Chapter 3*). Assuming that small prey behave approximately as a part of the fluid, these findings suggest that the model output is also realistic for *C. gariepinus*.

In our suction model, the head of the catfish, from mouth aperture to pectoral fin, is approximated by a series of hollow elliptical cylinders (Fig. 3). Each cross-section of this structure consists of an external ellipse and an internal ellipse. The length of the major and minor axis of the external ellipses correspond, respectively, to the height and width of the

head at any given position, while the internal ellipse axes approximate the width and height of the bucco-pharyngeal cavity (further referred to as buccal cavity or mouth cavity). Changes in the length of the external ellipse axes were deduced from the recorded videos. To do so, upper and lower contours of the catfish's head were digitised frame by frame (50 points each) in the lateral and ventral view. At the same time, the coordinates of a longitudinal axis connecting the upper jaw tip to a point equidistant between the base of the right and left pectoral fin were digitised (Fig. 2). Next, the contour coordinates were recalculated in a new frame of reference moving with the fish, with the upper jaw tip as origin and the longitudinal axis above as the X-axis. The coordinates of each contour curve (upper, lower, left and right contours of the head) were then fitted with 10th order polynomial functions, using the XlXtrFun add-in for Microsoft Excel (Advanced System Design and Development, Red Lion, PA, USA). Next, the distance between the corresponding coordinates of the upper and lower contours, and between the left and right contours were calculated at 201 equally spaced intervals along the longitudinal axis. For each external ellipse, the profiles of length and width versus time were filtered with a 4th order Butterworth zero phase-shift low-pass filter in order to reduce digitisation noise (cutoff frequency of 30, 12 and 6 Hz for videos recorded at respectively 250 Hz, 100 Hz and 50 Hz; see above).

The internal dimensions of the mouth cavity of C. gariepinus at rest are approximated using X-ray images from lateral and ventral view X-ray videos of a preserved specimen with closed mouth (94.13 mm cranial length; 302.0 mm total length). During recording of these X-ray videos, the specimen was held vertically while a saturated Barium-solution was poured in the mouth (for illustration see Chapter 3, p.41). Using this radio-opaque fluid, the boundaries of the mouth cavity could accurately be distinguished, and the internal area of the mouth cavity determined for all positions along the longitudinal axis. To account for the presence of the gill apparatus, the length of the major and minor axes of ellipses in the gill region were (arbitrarily) reduced by 10% (see Chapter 3). It was assumed that this situation (i.e. the internal volume of the mouth cavity of the preserved specimen at rest) reflects the moment prior to start of the suction event. Subsequently, changes in the height and the width of the head over time (external ellipses), will cause changes in the width and height of the internal mouth volume ellipses. As internal volume data were collected for one individual only, we are forced to assume that the dimensions of the buccal cavity are proportional to the measured external dimensions of the head in C. gariepinus. This means that allometry in the external dimensions of the head is assumed to be reflected in a similar allometry of the bucco-pharyngeal cavity. The X-ray videos were made with a Philips Optimus X-ray generator coupled to a Redlake Imaging MotionPro digital high-speed camera.

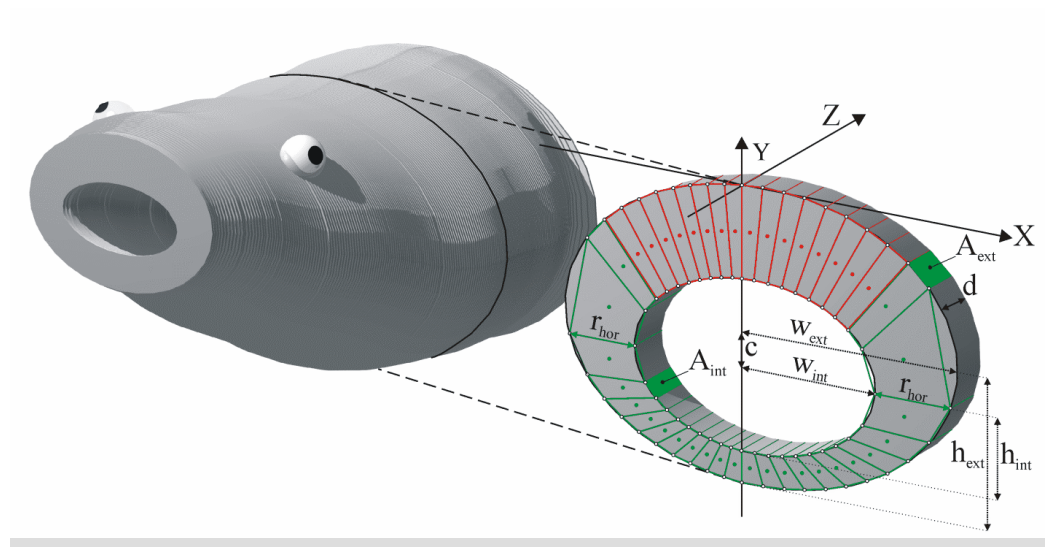


Figure 3: Three-dimensional representation of the model used for calculation of power requirement of suction feeding in *C. gariepinus*. The model consists of a 201 serially arranged hollow elliptical cylinders (left). Each cylinder consists of an external ellipse bordering the fish's head and an internal ellipse bordering the buccal cavity (right). Movement of the centres of mass (red and green dots) of 40 subdivisions of the modelled head volume (red and green segments) with respect to a fixed frame of reference (*XYZ*) were computed during the expansive phase for each cylinder. The 16 segments that approximately correspond to the neurocranium are indicated in red. Note that depth *d* is exaggerated for clarity. See text for further explanation and definition of symbols.

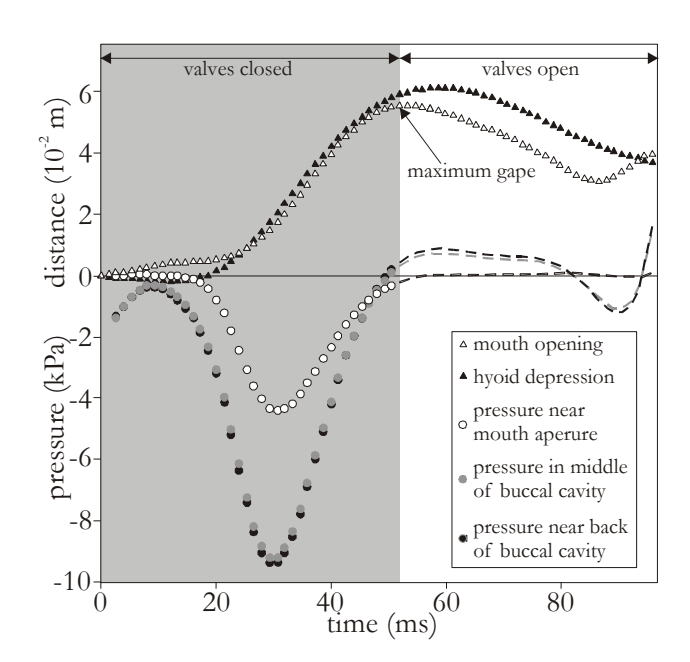
According to the continuity principle, any change in volume must be filled instantaneously with water and thus generate a flow relative to the fish's head. So, at each cross-section of the mouth cavity, the total water volume passing through this cross-section in a given amount of time depends on the total volume increase posterior to this cross-section. In this way, the mean flow velocity during a given time increment can be calculated at each of the modelled ellipse-shaped cross-sections of the mouth cavity by dividing the volume increase posterior to this ellipse by the area of the ellipse (average for that time increment). This holds as long as the opercular and branchiostegal valves are closed. If not, the modelled system becomes undetermined (Muller et al., 1982; Muller and Osse, 1984; Drost and van den Boogaart, 1986). In general, branchiostegal valve opening can be detected shortly after *C. gariepinus* reaches maximal oral gape. However, for several of the recorded prey capture sequences, it was problematic to pinpoint precisely the frames in which the transition from closed to opened valves occurred. Therefore, we only used the model output from the start of mouth opening until the time of maximal gape.

Next, pressure inside the expanding modelled profile with closed valves was calculated according to Muller et al. (1982):

$$\frac{\Delta p}{\mathbf{r}} = \int_{x}^{l} \left[\frac{\partial u}{\partial t} + u \frac{\partial u}{\partial x} \right] dx + \left| \frac{u_{l}}{(a+1)} (x-l) + \frac{u_{l}}{(a+1)} (u-u_{l}) \right| + \frac{1}{2} \left[\frac{1}{(a+1)^{2}} - 1 \right] u_{l}^{2} + \frac{a}{(a+1)} (u_{l}h_{l})' \tag{1}$$

where Δp is the pressure (difference from hydrostatic pressure), \mathbf{r} the density of water (1000 kg/m³), x the position along the longitudinal axis (x = 0 at the pectoral fin base; x = l at the mouth aperture), u the instantaneous flow velocity of water in x direction, u the instantaneous flow velocity of water in the mouth aperture in a frame of reference moving forward with the head (see Fig.2), u the ratio between u_m (instantaneous flow velocity of water in mouth aperture in earth-bound frame) and ($u_m - u$), and u0 the instantaneous radius of the mouth aperture (assumed to correspond to the average between the half width and the half height of the ellipse at this position). The prime sign denotes that the first derivate against time is taken for this function. A representative example of pressures calculated for u0. u1 gariepinus is shown in Figure 4.

Figure 4: Example of buccal pressures calculated for a prey capture sequence of a 35.20 mm cranial length C. gariepinus. Pressures for three positions inside the buccal cavity (circles), as well as mouth opening (open triangles) and hyoid depression (filled triangles) versus time are given. Note that these calculations are only valid when the opercular and branchiostegal valves are closed (grey background)(i.e. approximately until maximal gape is reached).



4.2.5 Inverse dynamic calculation of required muscular power

The power required for expanding the series of hollow elliptical cylinders was calculated by inverse dynamics. First, for each hollow cylinder, a new frame of reference is defined with the top of the external ellipse-cross section as origin, X the width, Y the height and Z the depth (Fig. 3). By doing so, the mid-sagittal part of the skull is entirely motionless in the model, while movement during expansion of the elliptical cylinders will predominantly occur in the ventral and lateral parts of the head. The external ellipses and internal ellipses are now respectively given by the following equations:

$$y = \pm (h_{ext} / w_{ext}) \sqrt{w_{ext}^2 - x^2} - h_{ext}$$
 (2)

$$y = \pm (h_{int} / w_{int}) \sqrt{w_{int}^2 - x^2} - h_{ext} - c$$
 (3)

where h_{ext} and w_{ext} are, respectively, the half height and half width of the external ellipse, h_{int} and w_{int} are, respectively, the half height and half width of the internal ellipse and c the distance between the centres of the external and internal ellipses. c was determined from the lateral-view X-ray picture of a 94.13 mm cranial length C. gariepinus specimen with a Barium-filled buccal cavity and will logically be constant throughout the expansion. The distance from the internal to the external ellipse following the horizontal axis of the internal ellipse (r_{hor}) can be calculated by:

$$r_{hor} = \sqrt{(1 - c^2 / h_{ext}) w_{ext}^2} - w_{int}$$
 (4)

Next, the volume between the internal cylinders and the external cylinders was divided into 40 segments (Fig. 3). To do so, at 20 equally spaced intervals along the horizontal axis of the internal ellipses (X-coordinates from $-w_{int}$ to $+w_{int}$) the corresponding Y-coordinates were calculated using Eq. 3. The same was done for the external ellipses (X-coordinates from $-w_{ext}$ to $+w_{ext}$) using Eq. 2. The area between the external and internal ellipse at a given cross-section is now approximated by a series of quadrangles connecting every two adjacent points on the external ellipse with the two corresponding points on the internal ellipse (see Fig. 3). After defining depth d as the distance between the cross-sections used in the model, we can calculate the volume, the surface area bordering the buccal cavity (A_{int}) and the surface area bordering the outside of the fish's head (A_{ext}) for each segment (Fig. 3). We assumed that the mass of this volume has the uniform density of 1000 kg/m³, which also implies neutral buoyancy. The xyz-coordinates of the centre of mass (COM) of any given segment were approximated by taking the average x, y and z of the eight corners of the segment.

Thirdly, the linear velocity (ν), acceleration (a) and direction of motion of the COM, as well as the inclination of A_{ext} and A_{int} , were calculated. As the expansion is symmetrical for the left and right sides of the head, these and the following calculations were performed for a single side. Consequently, final output values (required muscular force; see further) were doubled. Additionally, as the dorsal part of the head (almost static in the model) is taken in by the bony neurocranium, no calculations were performed for this region (see colour scheme in Fig.3).

To calculate the force required from muscular activity, \vec{F}_{muscle} , the following equation of motion was used:

$$m \cdot \vec{a} \cdot (1 + c_{added}) + \vec{F}_{pressure} + \vec{F}_{drag} + \vec{F}_{muscle} = 0 \tag{5}$$

where m is the mass, \vec{a} the linear acceleration, c_{added} the added mass coefficient, $\vec{F}_{pressure}$ the force resulting from pressure differences between the inside and the outside the buccal cavity and \vec{F}_{drag} the force from hydrodynamic drag. Note that forces resulting from friction between head parts and from deformation of tissues (e.g., stretching of the jaw adductor muscles during mouth opening) are not included. As these forces will probably become important only at the end of cranial expansion, it is assumed that these forces are small compared to the other forces during expansion. The orientation of $\vec{F}_{pressure}$ is perpendicular to the average inclination of the planes bordering the buccal cavity (A_{int} , see Fig. 3) and the outside of the head (A_{ext} , see Fig. 3). It's magnitude depends on $\vec{D}p$ (at a given time and position along the medio-sagittal axis) and surface area. The average surface area of A_{int} and A_{ext} was used for calculating the magnitude of $\vec{F}_{pressure}$. We used the value of 1 for c_{added} (added mass coefficient for cylinders according to Daniel, 1984), though the importance of changes in this value on the model output will be discussed (see Discussion). \vec{F}_{drag} is parallel to the direction of motion and it's magnitude was calculated by:

$$F_{drag} = 1/2 c_d \mathbf{r} A_{ext-projected} v^2$$
 (6)

where c_d is the drag coefficient, \mathbf{r} the density of water (1000 kg/m³), $A_{ext-projected}$ the area of the external surface of the bar projected onto a plane perpendicular to the direction of motion and v the velocity of the COM. A value of 1 was used for the shape-dependent c_d , corresponding approximately to drag on an infinite flat plate (Hughes and Brighton, 1999). By using the projected area $A_{ext-projected}$, F_{drag} decreases sinusoidal with the angle of attack of the surface moving through the water, which is in accordance with experimental measurements (Munshi et al., 1999; Bixler and Riewald, 2002).

Finally, total power required from cranial and post-cranial muscles ($P_{required}$) was calculated by:

$$P_{required} = \sum (\vec{F}_{muscle} \cdot \vec{v}) \tag{7}$$

Required power will be expressed as a muscle-mass-specific power by dividing $P_{required}$ (calculated as above) by the mass of a subset of the muscles contributing to the expansions

of the cranial system. From all individual catfish used in the present study, the single sided mass of the protractor hyoideus, sternohyoideus, levator arcus palatini, levator operculi and the part of the hypaxials that is anterior to the pectoral fin basis were measured and summed (Herrel et al., 2005). As this measure of muscle mass is only a fraction of the total mass of the muscles active during the expansive phase of suction feeding (for example the epaxial muscles are not included), the presented muscle-mass specific power and mechanical work will overestimate the actual values. They should therefore be regarded as relative, rather than as real values. However, we can use these values for analysing the scaling relationships of these variables because it can safely be assumed that the mass of the used sample of muscles will show a similar scaling with cranial size as the total muscle mass contributing to suction.

4.3 Results

4.3.1 Linear kinematic variables

Maximum linear displacements of the lower jaw, hyoid and branchiostegal membrane during prey capture of C. gariepinus increase significantly with increasing cranial size (Table 1, Fig. 5A,B). This increase does not differ significantly from a size-proportional increase (slope 1; P > 0.25). Therefore, no departure from isometry can be distinguished for these variables.

Maximum peak linear velocities of mouth opening, mouth closing, hyoid depression and branchiostegal movements do not change significantly with cranial size (Table 1, Fig. 5C,D). Maximum peak linear accelerations, however, decrease significantly with increasing cranial length (Table 1, Fig. 5E,F). This decrease is almost (and statistically not different from) a decrease proportional to cranial size (P > 0.07).

4.3.2 Angular kinematic variables

Maximum angular displacements of the neurocranium (elevation) and the hyoid (lateral abduction) do not change significantly with cranial size (Table 1, Fig. 6A,B). This also means that no departure from isometry can be distinguished for these variables.

Maximum peak angular velocities of hyoid abduction and neurocranial elevation decrease significantly with increasing cranial length (Table 1, Fig. 6C,D). In general, this decrease approximates (and is not statistically different from) a decrease proportional to cranial size (P > 0.13).

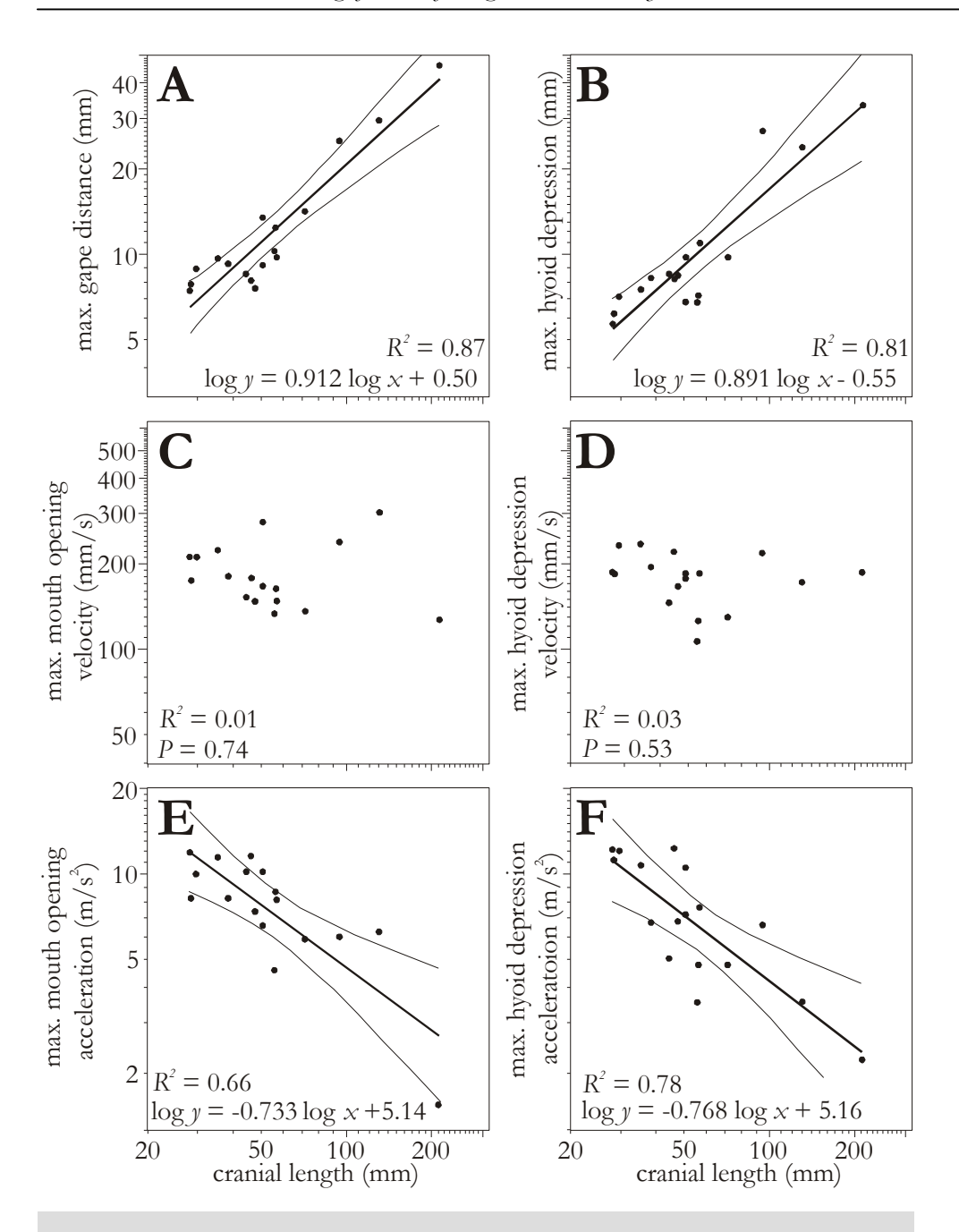


Figure 5: Log-log plots of maximal linear displacement (A-B), velocity (C-D) and acceleration (E-F) *versus* cranial length, for mouth opening (A, C, E) and hyoid depression (B, D, F).

Table 1: Scaling relationships for 27 kinematic variables of prey capture in Clarias gariepinus.

Variable	Slope	R²	95% conf. limits					
maximum linear displacements (mm)								
gape distance	0.912*	0.87	0.715	1.109				
hyoid depression	0.891*	0.81	0.657	1.125				
branchios tegal depression	0.921*	0.93	0.781	1.061				
lateral branchios tegal expansion	0.924*	0.74	0.619	1.230				
maximum angular displacements (°)								
lateral hyoid abduction	-0.191	0.19	-0.406	0.024				
neurocranial elevation	-0.207	0.10	-0.551	0.138				
maximum peak linear velocities (mm/s)								
mouth opening velocity	-0.041	0.01	-0.302	0.220				
mouth dosing velocity	0.043	0.00	-0. 32 6	0.411				
hyoid depression velocity	-0.067	0.03	-0.290	0.156				
branchios tegal depression velocity	-0.171	0.14	-0.402	0.060				
lateral branchios tegal expansion velocity	0.223	0.09	-0.173	0.618				
maximum peak angular velocities (°/s)								
lateral hyoid abduction velocity	-0.951*	0.83	-1.186	-0.716				
neurocranial elevation velocity	-1.223*	0.84	-1.519	-0.926				
maximum peak linear accelerations (mm/s²)								
mouth opening acceleration	-0.733*	0.66	-1.025	-0.441				
mouth dosing acceleration	-0.779*	0.67	-1.077	-0.480				
hyoid depression acceleration	-0.767*	0.66	-1.070	-0.465				
acceleration of branchiostegal depression	-0.952*	0.76	-1.245	-0.659				
timing variables (s)								
time to maximum gape	0.927*	0.91	0.771	1.082				
time to end of mouth dosure	0.940*	0.92	0.790	1.090				
time to maximal hyoid depression	0.997*	0.93	0.849	1.145				
time to end of hyoid elevation	0.899*	0.85	0.693	1.106				
time to maximum branchiostegal depression	1.068*	0.92	0.900	1.236				
time to end of branchiostegal elevation	1.121*	0.84	0.853	1.388				
time to maximum lateral branchiostegal expansion	0.992*	0.95	0.869	1.115				
time to end of lateral branchios tegal expansion	0.936*	0.95	0.812	1.060				
time to maximum lateral hyoid abduction	1.002*	0.94	0.859	1.146				
time to maximum neurocranial elevation	1.052*	0.87	0.828	1.276				

Note. All variables used in the least squares regressions were log10 transformed. Timing variables are relative to the start of mouth opening (time 0). Slopes differing significantly from 0 at P=0.05 are indicated by *. These slopes were also significant at P<0.0001.

4.3.3 Timings

The scaling coefficients (slopes) of timings of the analysed kinematic events are very similar to each other (Table 1). In general, the time from the start of mouth opening until the start, maximum excursion or the end of all analysed movements, increases approximately proportional to increasing cranial length (P > 0.29).

4.3.4 Buccal pressure

The magnitudes of peak sub-ambient pressure (i.e., maximal instantaneous pressures averaged over the entire buccal cavity calculated by the present hydrodynamic modelling) do not change significantly with size (slope = -0.25, N = 17; $R^2 = 0.06$; 95% confidence interval between -0.77 and 0.28; P = 0.337) (Fig. 7A). A similar scaling relationship is found for the magnitudes of the highest (per individual) average buccal pressure (averaged over position and time from start to maximal gape): the linear-regression slope is negative (slope = -0.46, N = 17; $R^2 = 0.21$; 95% confidence interval between -0.99 and 0.03), though not statistically different from 0 (P = 0.066) (Fig. 7B).

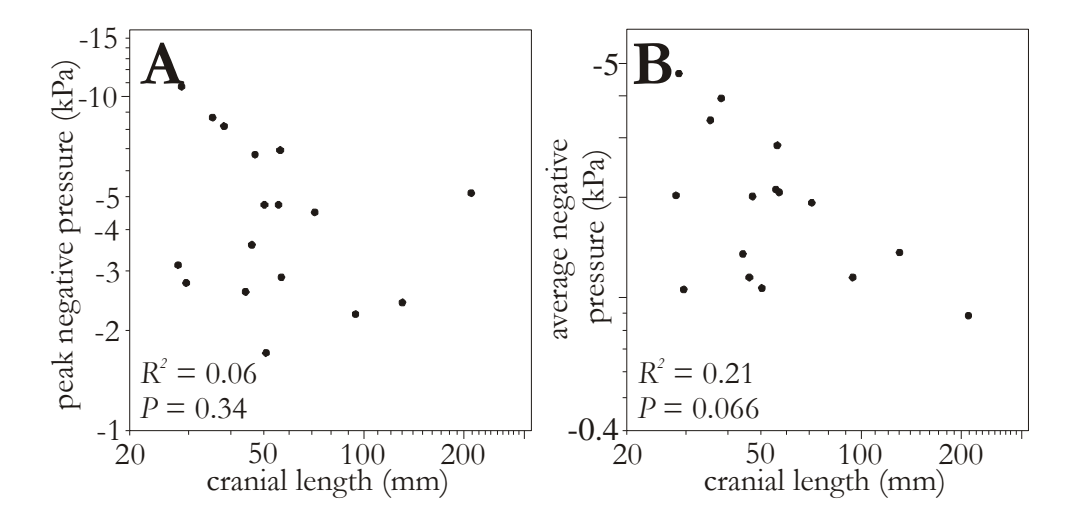


Figure 7: Log-log plots of maximal peak negative buccal pressure (A) and maximal average buccal pressure (B) *versus* cranial length. These buccal pressures are averaged over the entire buccal cavity (from mouth aperture to pectoral fin) and were calculated with hydrodynamic models (Drost & Van den Boogaert, 1986; Muller et al., 1982). Note that no significant changes were found for these pressures in relation to cranial size.

4.3.5 Required power

The maximal peak power required from the muscular system (calculated by the present hydrodynamic modelling and inverse dynamics) increases significantly (P=0.048) with increasing cranial length (slope = 0.97, N=17; $R^2=0.24$; 95% confidence interval between 0.01 and 1.92). This is also the case for the maximal average power (average from start to maximal gape), which shows a significant (P=0.021) increase with increasing size (slope = 1.08, N=17; $R^2=0.31$; 95% confidence interval between 0.19 and 1.97).

However, when expressed as muscle-mass-specific power (expressed in Watts per kg muscle), it is also decreases highly significant (P<0.0001) with increasing cranial length (Fig. 8). This is true for the highest (per individual) instantaneous muscle-mass-specific required power (slope = -2.49, N = 17; R^2 = 0.65; 95% confidence interval between -3.48 and -1.49), as well as for the highest (per individual) average (from start to maximal gape) muscle-mass-specific power (slope = -2.37, N = 17; R^2 = 0.64; 95% confidence interval between -3.36 and -1.39).

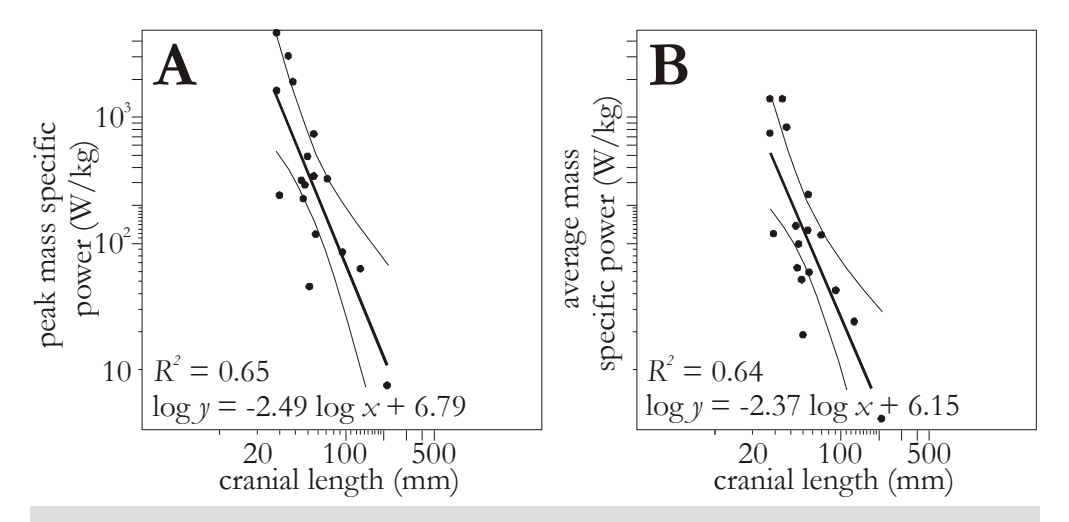


Figure 8: Log-log plots of peak muscle-mass-specific power requirement (A) and average muscle-mass-specific power requirement (B) *versus* cranial length, as calculated using the model presented in this paper. Note that peak-mass-specific power decreases significantly with increasing cranial size.

4.4 Discussion

During ontogeny, when *C. gariepinus* becomes larger, important changes in the speed of movements of the cranial structures during suction feeding occur (Figs. 5, 6; Table 1). In general, angular velocities decrease approximately proportional with increasing cranial size while linear velocities remain more or less constant (Table 1). These results are not consistent with the previous studies on scaling of suction feeding in vertebrates (Richard and Wainwright, 1995; Reilly, 1995; Hernandez, 2000; Wainwright and Shaw, 1999, Robinson and Motta, 2002). Angular velocity does decrease in these studies, but at a smaller rate than proportional to body length. Therefore, the results of the present study add to the relatively large interspecific variability in scaling coefficients of aquatic feeding kinematics, which have already been observed among previous studies.

By applying biomechanical modelling to the experimentally observed prey capture kinematics in C. gariepinus, a more detailed insight into the mechanics of suction feeding in relation to body size can be achieved. In this way, we may be able to explain the observed scaling relations in prey capture kinematics for this species. In particular, we focus on the potential importance of buccal pressures in limiting the maximal speed of buccal expansions during suction and how this is influenced by size. Results from the model presented in this paper show that the pressure gradient induced by expanding the buccal cavity, is theoretically responsible for the largest fraction (>80 %) of the total force required from muscular contractions during this expansive phase of suction feeding (Fig. 9). This is in accordance with the findings of Aerts et al. (1987) and Carroll et al. (2004). This also implies that the output of our model (required muscular power) is not very sensitive to changes in the less important factors: inertia (<20% of total required muscular force) and hydrodynamic drag (<2% of total required muscular force). Consequently, the assumptions and approximations that were made in modelling these factors are not critical. For example, tripling the added mass coefficient (eadded) in the model of a representative prey capture event increases the required power in general by less than 3%.

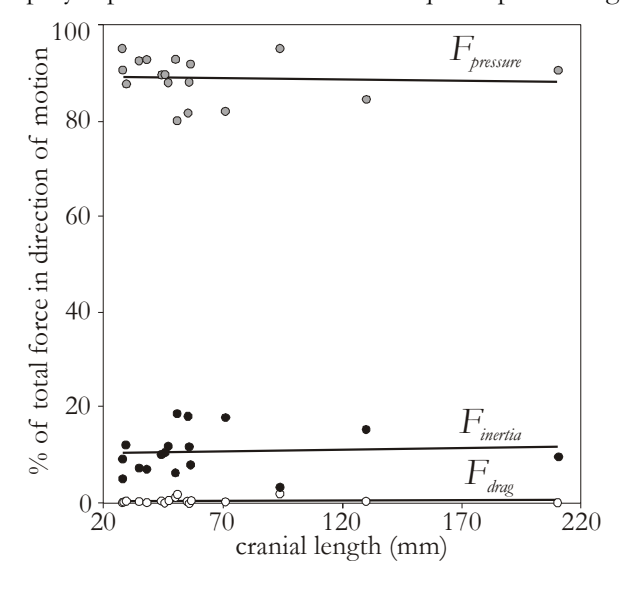


Figure 9: Relative contribution of forces in the direction of motion as a result of buccal pressure $(F_{pressure}),$ acceleration mass and added $(F_{inertia})$ and hydrodynamic drag (F_{drag}) to the total force, as estimated by dynamic modelling. Note that forces due to friction between head parts and from deformation of tissues are not included in the model. No significant changes with size are found.

4.4.1 Scaling relationships predicted by the model

Assuming that the maximal power output during suction feeding is proportional to the mass of the muscles involved in this process, the presented model can be used to generate specific predictions concerning the scaling of kinematics in C. gariepinus. If the linear dimensions of the model are increased isometrically without changing the rate of buccal expansion (i.e. constant angular velocities), the calculated negative buccal pressure magnitudes increase approximately proportional to the square of cranial length (~ CL2). As we have shown that sub-ambient buccal pressure is the most important factor in resisting cranial expansion in our model (see above), and given the fact that also the surface area of the modelled cranial apparatus to which these pressures apply (~ CL²) and linear velocity of expansion (e.g., velocity of the hyoid tip) will also increase in this situation (~ CL), it was not surprising that our model also shows that power requirement (i.e. required force $\sim CL^4$ multiplied by linear velocity $\sim CL$) increases approximately by CL^5 . However, the power available from the muscles (i.e. force \sim muscle cross-sectional area multiplied by linear velocity ~ fibre length) only increases by CL3 in the case of isometric growth, or by $CL^{3.4}$ if accounting for the positive allometry observed in C. gariepinus (Herrel et al., 2005). For this situation, which corresponds to the predictions of the theoretical scaling model of Richard and Wainwright (1995), the required power will exceed the available power during growth. This "deficit" in power will increase proportional with CL2 (isometry) or with CL1.6 (C. gariepinus allometry) during growth, forcing C. gariepinus to decrease its speed of buccal expansion.

By increasing the time to carry out a given buccal expansion (abbreviated T), buccal pressure and power requirement decreases. In order to balance the available and required power, T would have to increase during growth of C. gariepinus in a way that the calculated power "deficit" because of growth ($\sim CL^2$; see above) can be compensated for. By adjusting the expansion time T in our model, we found the buccal pressure changing approximately $\sim T^{-2}$ and power requirement $\sim T^{-3}$. Consequently, in case of isometric growth, equilibrium between the available and required power for buccal expansion is reached when the expansion time T is increased by $CL^{2/3}$. This corresponds, for example, to angular velocities scaling proportional to $CL^{2/3}$, and linear velocities scaling with $CL^{1/3}$. Accounting for the positive allometry of muscle mass in C. gariepinus, this equilibrium will be reached when the (angular) speed of buccal expansion changes in proportion with $CL^{1.6/3}$.

However, these theoretical predictions are not confirmed by the experimental data. The observed decrease in the speed of buccal expansion with growth is considerably larger (\sim CL^{-1} , Table 1) than the expected scaling relationship (\sim $CL^{-1.6/3}$). In other words, the larger C. gariepinus are slower than predicted, or vice versa. As a consequence, the model output of muscle-mass-specific power requirement decreases significantly with increasing size (Fig. 8).

4.4.2 The model of A.V. Hill

Scaling relationships found for prey capture kinematics in C. gariepinus apparently match the prediction by the scaling model of A.V. Hill (1950), in which it was stated that geometrically similar animals should carry out similar movements in times directly proportional to their linear dimensions. In this model, inertial forces (and not hydrodynamic pressures) are assumed to be dominant. If the time to fulfil a given movement does not change with size, then the kinetic energy $(E_k = \frac{1}{2} m \cdot v^2)$ required to accelerate a specific mass (for example a limb) scales as length L^5 ($m \sim L^3$ and $v^2 \sim L^2$). In contrast, the work a muscle can do is expected to increase merely by L^3 , leaving a "deficit" in available work increasing by L^2 . This "deficit" can be overcome by increasing the time to carry out this movement in proportion to the increasing length, by which the required energy for this movement is in proportion to the total muscle mass.

The forces resulting from buccal pressures calculated for suction feeding in C. gariepinus apparently scale similar to the inertial forces outlined by A.V. Hill: these forces both increase approximately by L^4 in case of constant speed, and by the square of speed in case of constant size. Consequently, the size and speed dependence of the energetic demands for suction feeding in C. gariepinus are expected to be identical to the acceleration of a limb. Nevertheless, there are still two reasons why this model (Hill, 1950) does not explain the results for C. gariepinus. First, one of the assumptions of Hill (1950) is that the muscles are optimized to work at a "reasonable" energetic efficiency. This assumption does not necessarily apply to occasional, explosive movements such as suction feeding. Furthermore, the mechanical energy or work required for a single suction feeding cycle (which only takes fractions of a second to be completed) is very low compared to the energetic content of prey (Aerts, 1990). For example, if we assume that the total work for buccal expansion in C. gariepinus equals twice the work calculated by our model from start to maximum gape, total work is about 0.0034 J for the smallest, and 0.3 J for the largest individuals used in this study. On the other hand, the energy content of a small fish prey (1 g wet mass) is approximately 6000 J (Cummins and Wuycheck, 1971). Consequently, as the energetic efficiency of buccal expansion is probably an unimportant aspect of the biology of fishes, we believe that the assumption of the model of Hill (1950), i.e. the size independency of muscle-mass-specific work, is not a good starting point for predicting scaling patterns of an extremely short and anaerobic action such as suction feeding in fishes. Note, in this respect, that the maximal power of muscle P has a different speed dependency than does mechanical work, E(E = | P dt). As a result, different scaling relationships must be predicted if the muscle-mass-specific power instead of muscle-massspecific work is assumed to be size-independent. In the case of suction feeding, maximal power seems a more appropriate speed-limiting factor than muscular energetics (see also Carroll, 2004).

Second, *C. gariepinus* does not fulfil the assumption of geometric similarity. Herrel et al. (2005) measured, for example, a significant positive allometry in the mass (in general

approximately $\sim L^{3.4}$) and a negative allometry in the fibre length of the cranial muscles ($\sim L^{0.7}$). As a result, whereas scaling of prey capture kinematics is well predicted by the model of Hill (1950), the size-independency of muscle-mass-specific work (an intrinsic assumption of his kinematic predictions) is not observed (Fig. 10).

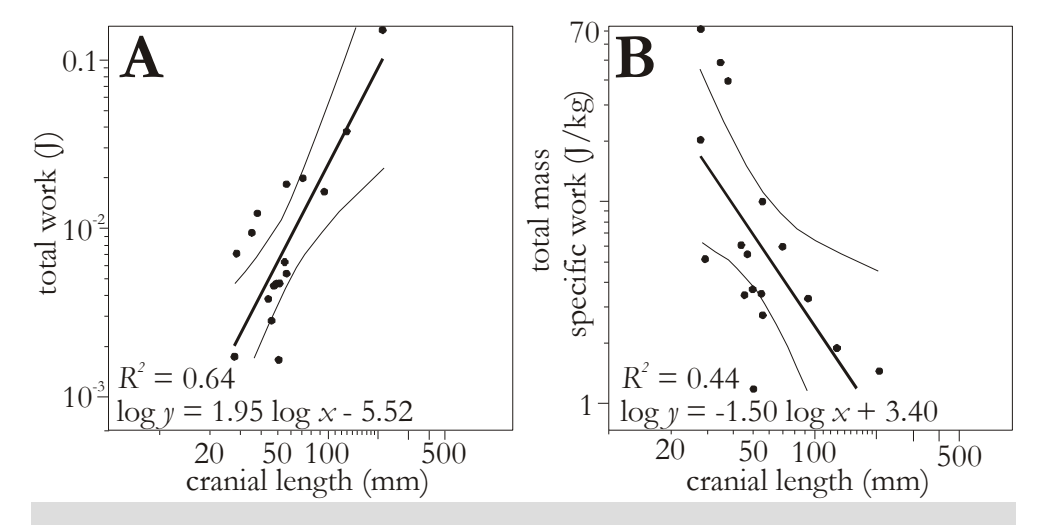


Figure 10: Log-log plots of total work (A) and muscle-mass-specific work (B) from the start of mouth opening until maximum gape *versus* cranial length, as calculated using the model presented in this paper. Note that, while total work increases significantly with increasing cranial size (A), the muscle-mass-specific work output decreases significantly with increasing cranial size (B).

4.4.3 Why are large catfish slower than predicted?

If we assume that the muscle-mass-specific power output capacity of the muscles involved in buccal expansion does not change with size, the results indicate that larger fishes perform sub-maximally compared to the smaller fishes, in a way that a smaller proportion of the available power is used (Fig.8). This still leaves us with the question why larger C. gariepinus show this apparently reduced suction effort, despite being presented with similar prey of which the size was adjusted according to the size of the catfish. Possibly, faster buccal expansions are not needed for large catfish in order to perform successful prey captures on the experimental prey types. Indeed, it was recently demonstrated for C. gariepinus that the actual suction performance (maximal prey distance and size) increases substantially with size, despite the observed decrease in the speed of buccal expansion (Chapter 3). For example, it was estimated that the maximal size of a prey that can still be successfully drawn into the mouth by suction, increases faster than proportional to cranial size, if these prey are sucked from the same absolute distance from the mouth (Chapter 3). The observation by Bruton (1979) that larger C. gariepinus include a relatively larger amount of evasive prey (i.e. fish) into their natural diet also indicates this increase in suction

performance with size. Consequently, the immobile prey of which the size is scaled according to predator size may not have been the ideal situation to induce a comparable suction effort in both small and large *C. gariepinus*. If, as appears to be the case for *C. gariepinus*, some taxa of aquatic suction feeders tend to perform increasingly sub-maximally when becoming larger, this may potentially also explain the large variability observed in the literature on scaling relationships of prey capture kinematics in this group of animals.

4.4.4 Conclusions

Model calculations have shown that negative buccal pressures are responsible for the largest part of the power (more than 80%) required for expanding the buccal cavity during prey capture in *C. gariepinus*. The size dependency of buccal pressures and the forces required for suction feeding will force *C. gariepinus* to become relatively slower during growth, if not the required power would exceed the expected available power from its muscles (proportional to muscle mass). In this way, we expected *C. gariepinus* to decrease the (angular) speed of movement of its cranial structures during suction proportion to cranial length $CL^{0.53}$. However, the experimental data show that (angular) speed decreases more rapidly with size than predicted: approximately proportional to CL^{1} (Table 1). According to our model, this would imply a significant decrease in the muscle-mass-specific power output. Our data therefore suggest that suction effort employed by the fish to capture similar prey decreases with size. Suction performance, however, does not (*Chapter 3*), leaving the possibility for larger *C. gariepinus* not to use their full muscular capacity while still performing successful prey captures on the experimental prey types we used in this study.

Chapter 5

A dynamic model of mouth closing movements in clarid catfishes: the role of enlarged jaw adductors

Sam Van Wassenbergh – Peter Aerts – Dominique Adriaens – Anthony Herrel

Journal of Theoretical Biology 234, 49-65. (2005)

Summary

Some species of Clariidae (air breathing catfishes) have extremely large (hypertrophied) jaw closer muscles. Besides producing higher bite forces, the enlarged muscles may also cause higher accelerations of the lower jaw during rapid mouth closure. Thus, jaw adductor hypertrophy could potentially also enable faster mouth closure. In this study, a forward dynamic model of jaw closing is developed to evaluate the importance of jaw adductor hypertrophy on the speed of mouth closure. The model includes inertia, pressure, tissue resistance and hydrodynamic drag forces on the lower jaw, which is modelled as a rotating half-ellipse. Simulations are run for four clariid species showing a gradual increase in jaw adductor hypertrophy (Clarias gariepinus, Clariallabes longicauda, Gymnallabes typus and Channallabes apus). The model was validated using data from high-speed videos of prey captures in these species. In general, the kinematic profiles of the fastest mouth closure from each species are reasonably well predicted by the model. The model was also used to compare the four species during standardized mouth closures (same initial gape angle, travel distance and cranial size). These simulations suggest that the species with enlarged jaw adductors have an increased speed of jaw closure (in comparison with the nonhypertrophied C. gariepinus) for short lower jaw rotations and when feeding at high gape angles. Consequently, the jaw system in these species seems well equipped to capture relatively large, evasive prey. For prey captures during which the lower jaw rotates freely over a larger distance before impacting the prey, the higher kinematic efficiency of the C.

gariepinus jaw system results in the fastest jaw closures. In all cases, the model predicts that an increase in the physiological cross sectional area of the jaw muscles does indeed contribute to the speed of jaw closure in clariid fish.

5.1 Introduction

By closing the mouth rapidly, predators may reduce the chance of prey escape. Especially when feeding on quickly moving, elusive prey, a fast snapping of the oral jaws onto the prey can be an important aspect of the predator's prey capture success (Wainwright and Richard, 1995). In fishes, such fast mouth closings also contribute to overall suction feeding performance as it excludes the reversal of flow of water (and prey) sucked into the buccal cavity (Muller and Osse; 1984; Muller et al., 1982). Hence, several experimental studies on prey capture kinematics of adult fishes have reported extremely rapid mouth closures occurring even within 20 milliseconds (Aerts, 1990; Gibb, 1995; Lauder, 1980b; Lauder and Norton; 1980).

In Actinopterygian fishes, the *musculus adductor mandibulae* complex powers these jaw closing movements. According to Newton's second law of motion, increased forces generated by this muscle complex during lower jaw adduction will cause higher accelerations. Consequently, a given jaw closing velocity can be reached in less time. The importance of an increased force from the jaw muscles to the speed of mouth closing has also been illustrated experimentally in unloading experiments in humans (Nagashima et al., 1997; Slager et al., 1997, 1998; Van Willigen et al., 1997). In these studies, during which resistance to a forceful isometric bite is suddenly withdrawn, significantly higher mouth closing velocities are reached when prior to mouth closure (and consequently also during mouth closure) higher bite forces are exerted.

Some species of Clariidae (air breathing catfishes) have extremely well developed (hypertrophied) adductor mandibulae muscles (Cabuy et al., 1999; Devaere et al., 2001; Herrel et al., 2002) (Fig. 1-p.7). The biological role of this jaw adductor hypertrophy, which is assumed to be a derived feature that originated several times independently in clariids (Teugels and Adriaens, 2003), is still unclear. Diet analyses (Huysentruyt et al., 2004) found a remarkably large proportion of hard prey types in the species with the most extreme jaw adductor hypertrophy. On the other hand, most species also include small, agile prey such as fishes into their diet. Furthermore, a kinematic study of prey capture in a clariid species with a moderate degree of jaw adductor hypertrophy (*Clariallabes longicauda*; Fig. 1-p.7) has demonstrated that even non-evasive prey types (which could be caught with minimal movement of the oral jaws) are caught using considerable expansions of the cranial system followed by a fast snapping the jaws on the prey (*Chapter 6*).

Biomechanical modelling has demonstrated that the enlarged jaw muscles in clariid catfishes drastically increase the maximal biting force of these species under fully static conditions (i.e. without any movement involved; Herrel et al., 2002). As increased forces from the jaw muscles can also result in larger moments of force that drive the lower jaw rotation during jaw closure, higher accelerations can be expected as well. Thus, besides enhancing the performance during static jaw closure (e.g., crushing hard prey or tearing pieces from large prey) the enlargement of the jaw adductor muscles could also be used to power fast snapping of the jaws.

The main objective of the present study is to test whether the observed increase in the dimensions of the jaw adductor muscles in clariid catfishes could be used to develop increased velocities of mouth closure. To test this idea, a forward dynamic model of jaw closing is developed and validated using experimental data from prey capture in clariid catfishes. By comparing simulated jaw closing events from clariid species with jaw closer dimensions ranging from relatively slender (*Clarias gariepinus*) to extremely large (*Channallabes apus*) (Fig. 1-p.7) under standardised conditions (same initial gape angle, travel distance and absolute cranial size), the role of the jaw adductor enlargement in generating higher mouth closing velocities is evaluated. Additionally, the effects of changes in several aspects of the oral jaw apparatus (e.g. cross-sectional area, pennation angle, fibre length, orientation of the jaw adductors, dimensions of the lower jaw, length and inclination of the lower jaw in-lever) on the speed of mouth closure can be assessed using this model.

5.2 Materials and Methods

5.2.1 The model

The lower jaw adduction is modelled as a rotation of a half-elliptic surface (Fig.2). Detailed morphological analyses (Adriaens and Verraes, 1997; Cabuy et al., 1999, Devaere et al., 2001) have shown that the lower jaw of clariid catfishes closely resembles the shape of a half-ellipse. Also in other teleost fishes, for example Cichlidae, this resemblance has been noticed and has subsequently been used in modelling studies (Aerts et al., 1987). As the space between left and right lower jaws is largely taken up by skin and muscles (m. protractor hyoideus, m. intermandibularis, m. hyohyoideus inferior), a half-elliptic surface is chosen over a half-elliptic bar as a model for the rotating lower jaw.

Upward rotation of the lower jaw is caused by the contraction of the jaw adductor muscles. We modelled the instantaneous force output of these muscles during mouth closure, taking into account the physiological characteristics of contracting muscle (activation rise time, force-velocity relationship, force-length relationship, passive parallel elastic forces). By modelling the lower jaw and its inertial properties together with forces that cause (jaw muscle force) and resist (drag, pressure differences, tissue resistance) jaw closing movements, adduction of the lower jaw can be simulated. Simulations were run with a

time step of 0.01 ms. Until the next simulated point, the acceleration was kept constant. To avoid circularities in the formulae, the acceleration at time t is calculated based on the velocity and gape angle at t –0.01 ms. At the start of the simulation (–0,01 ms before the start of jaw closing, i.e. time 0), an acceleration of 0 radians/s² was imposed.

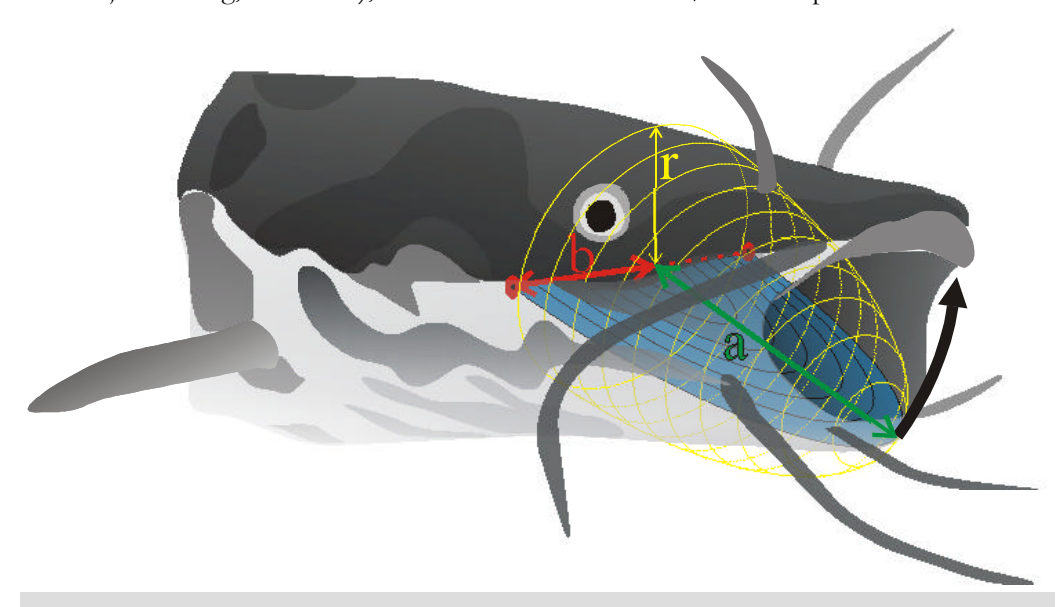


Figure 2: Representation of the half-elliptic surface (in blue) as a model of the lower jaw in C. *gariepinus*, with a the length (in green) and b the half width of the ellipse at the axis of rotation (in red). The half-ellipsoid added mass component with radius r is shown in yellow.

5.2.1.1 Equation of motion

In a dynamic equilibrium situation, the equation of angular motion for the rotating jaw is determined by the sum of all moments of force acting on the system. The following equation of motion was used:

$$I\ddot{a} = M_m + M_d + M_{pr} \tag{1}$$

where I is the moment of inertia of the lower jaw with respect to the quadratomandibular axis of rotation, \ddot{a} the angular acceleration of the lower jaw, M_m , M_d and M_{pr} are the moments of force from respectively the jaw muscles, hydrodynamic drag and pressure differences between inside and outside the buccal cavity, together with tissue resistance. As the density of the lower jaw and its surrounding soft tissues is approximately the same as the density of the water, gravitational forces and hydrostatic lift are assumed to counter each other, and are not considered further.

5.2.1.2 Inertia of the lower jaw

When an object moves through water, it will put in motion a significant amount of water as well. Therefore, an added mass component was included in the model (Fig. 2). As added mass, a volume of water with the shape of a half-ellipsoid comprising the half-ellipse was taken. This was done in accordance with studies on fish swimming hydrodynamics (Vogel, 1994). At each point along the length axis of the lower jaw, the radius of this half-ellipsoid equals the half width of the half-ellipse. The moment of inertia (*I*) of a half-elliptic surface and its half-ellipsoid added mass rotating around the minor axis (*b* in Fig. 2) can be calculated after expressing the mass distribution as a function of the distance from the axis of rotation. We simplified the calculations by assuming that the mass of each cylindrical segment of the ellipsoid at a given distance from the axis of rotation, is centred in the middle:

$$I = (2/15) \,\mathbf{p} \,\mathbf{r} \,a^3 b^2 \tag{2}$$

where \mathbf{r} is the density of water (1000 kg/m³), a the length of the lower jaw and b the half width of the lower jaw. The assumption was made that the added mass component remained constant during the entire mouth closing phase.

5.2.1.3 Drag

We accounted for drag forces on the lower jaw surface that were generated by the rotation of the lower jaw itself, as if it were moving in motionless water. Drag forces (F_d) are given by the following formula:

$$F_d = -(1/2) C_d A \mathbf{r} v^2$$
 (3)

where C_d is the shape dependent drag coefficient, A the area of the half ellipse, \mathbf{r} the density of the fluid (1000 kg/m³) and v the linear velocity of fluid flow. The drag coefficient of 2 from Lasher (2001) was used (flow normal to a flat plate). During rotation, the linear velocity of a given point on the half elliptic surface depends on its distance to the axis of rotation. Therefore, when calculating the moment of force from drag, the area of the half ellipse was expressed as a function of its distance from the axis of rotation (x):

$$M_{d} = -\int_{0}^{a} (b/a) \sqrt{a^{2} - x^{2}} (\mathbf{w}x)^{2} \mathbf{r} x dx$$
 (4)

with a the length and b the half width of the half ellipse, w the angular velocity of rotation and r the water density. Under these conditions, the moment of force from drag forces on a rotating half elliptic surface is given by:

$$M_d = -(2/15) \, \mathbf{r} \, \mathbf{w}^2 \, a^4 b \tag{5}$$

5.2.1.4 Buccal pressure and tissue resistance

The buccal cavity will decrease in volume during jaw closure. This usually results in a positive pressure inside the buccal cavity (Van Leeuwen and Muller, 1983). Although the magnitudes of these pressures are typically much lower than the negative pressures during the expansive phase (generating suction), they could still have an important effect on the movements of the lower jaw. Besides this positive intra-oral pressure, movements of the jaws are also dampened by the surrounding soft tissues (Koolstra and Van Eijden, 1996). Unfortunately, estimates of pressures inside the buccal cavity during prey capture of catfish, as well as data on the effect of tissue resistance on jaw movements are lacking. Therefore, a factor is added into the model that includes both forces from positive buccal pressures and soft tissue resistance. Both pressure and tissue resistance are likely to increase when the lower jaw is lifted towards the roof of the buccal cavity as the buccal cavity is increasingly reduced in volume and tissues connecting the hyoid apparatus to the lower jaw (musculus protractor hyoideus) are stretched.

In Van Leeuwen and Muller (1983), estimates of buccal pressure at specific positions along the sagittal axis of the head are presented for a variety of fish species. As positive pressure peaks at the end of prey capture strongly depend on the approaching speed of the predatory fish, the peak pressure of +1 kPa halfway the buccal cavity in the slowest fish (Onchorynchus mykiss; Van Leeuwen and Muller, 1983) is likely the best assessment of buccal pressure during jaw closure in a catfish, which also approach the prey relatively slowly (Chapter 6). We (arbitrarily) assumed that dampening as a result of tissue resistance would be of the same order of magnitude. This factor also includes some resistance to lower jaw rotation as a result of friction at the jaw joint. Thus, the following formula was used to account for intra-oral pressure and soft tissue resistance:

$$M_{pr} = -0.40373 \, (\mathbf{p} / 2) \, a^2 b \, P \tag{6}$$

where (0.40373*a) is the distance from the rotation axis of the center of area of the half-ellipse, $(a*b*\pi/2)$ the total area of the half-ellipse. In this formula, pressure P is a function that starts at 0 Pa (beginning of mouth closure), increases linearly with decreasing gape angle, and reaches the peak value of +2 kPa at the end of mouth closure. This pressure profile is assumed to be uniform over the half-elliptic surface representing the lower jaw.

5.2.1.5 Oral jaw apparatus

The lever system of the lower jaw and the jaw muscles is schematically represented in figure 3. As the upper jaw of catfishes is fixed to the neurocranium, no protrusion of the jaws occurs in this group of fishes (Alexander, 1965). Consequently, the mouth is opened and closed by a simply rotation the lower jaw around the quadratomandibular joint. The adductor mandibulae muscle complex of clariid catfishes consists of two parts: an external A2A3' part and a smaller, medial A3" part (Adriaens and Verraes, 1996). Whereas the

A2A3' part is a bipennate muscle, the A3" is not. For fast jaw closure, a bilateral symmetrical activity of these jaw muscles can be assumed. As in that case, left and right transversal force components are expected to cancel each other out, only the sagittal orientation of both jaw muscle parts (A2A3' and A3") was taken into account. As the origin of the jaw muscles is fixed to the neurocranium, the orientation of the lines of action of these muscles is solely determined by the degree of lower jaw depression. Biometric data on all variables represented in figure 3 were taken from the literature (Cabuy et al., 1999; Devaere et al. 2001; Herrel et al., 2002) for all four species (Fig. 1; Table 1). All linear biometric variables were scaled to cranial length (defined as the distance between the rostral tip of the premaxilla and the caudal tip of the occipital process), assuming isometric scaling of the morphological variables in Table 1.

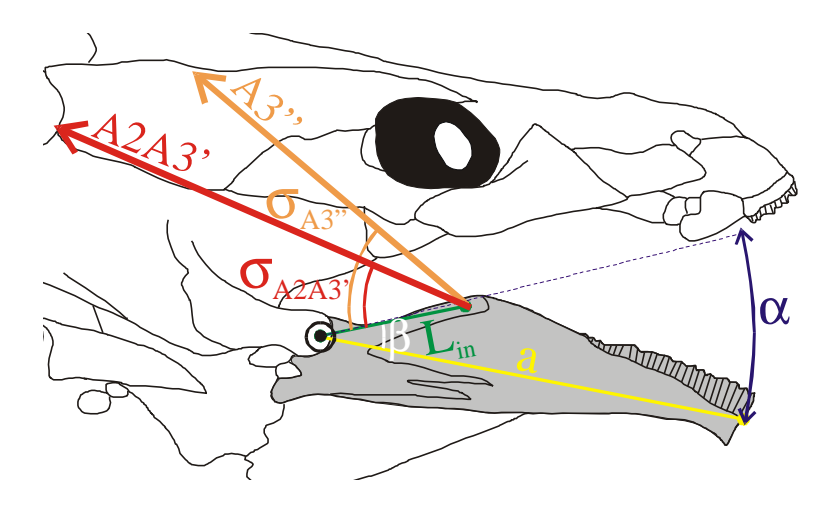


Figure 3: Schematic representation of the lower jaw lever system in Clariidae in lateral view. The *musculus adductor mandibulae* A2A3' and A3" are represented by their lines of action (red and orange respectively). Both muscles insert on the coronoid process of the lower jaw (in grey). The distance from the jaw muscle attachment to the centre of rotation of the lower jaw (L_{in} , lower jaw in-lever, green line) and the lower jaw length axis (a, yellow line) are shown. b is the angle between the in-lever (L_{in}) and out-lever (a) (also referred to as the inclination of the lower jaw in-lever). $S_{A2A3'}$ and $S_{A3''}$ are the angles between L_{in} and the lines of action of respectively A2A3' and A3" (also referred to as the inclination of the jaw muscles with regard to the in-lever).

Table 1: Biometric data of the lower jaw lever system

		Species				
Variable	Muscle	Clarias gariepinus	Clariallabes longicauda	Gymnallabes typus	Channallabes apus	
$egin{array}{c} a \ b \ L_{in} \ eta \end{array}$		0.2869 0.2145 0.0750 23.66	0.3027 0.2624 0.1197 31.26	0.3797 0.2686 0.1373 24.97	0.3609 0.2558 0.1456 43.64	
$\sigma (\alpha = 0^{\circ})$	A2A3' A3"	39.35 57.40	51.35* 59.08*	49.30 63.47	61.27 76.93	
Muscle length ($a = 0^{\circ}$)	A2A3' A3"	0.2588 0.2086	0.3887* 0.2910*	0.4304 0.2710	0.4086 0.2877	
PCSA	A2A3' A3"	0.01194 0.00626	0.02563* 0.00776*	0.03907 0.00702	0.08351 0.01124	
Average pennation angle	2 A2A3'	27.35	44.37*	50.72	35.14	
Average fibre length	A2A3' A3"	0.115 0.125	0.104* 0.098*	0.113 0.093	0.135 0.117	

Note. a = lower jaw length, b = half width lower jaw, $L_{in} =$ length of lower jaw in-lever, $\sigma =$ angle between L_{in} and the jaw muscle line of action, $\alpha =$ mouth opening angle (see also Fig. 3), PSCA = physiological cross sectional area (both sides included). All length values are in numbers of cranial lengths. All angle variables are in degrees. The given muscle lengths are distances of origin to insertion in the sagittal plane. *data for *Clariallabes melas*. Data on muscle dimensions and orientations are from Herrel et al. (2002). Other data are obtained from Adriaens and Verraes (1996) (*C. gariepinus*), Liesbeth van Meir (personal communication) (*C. longicanda*), Cabuy et al. (1999) (G. typus) and Devaere et al. (2001) (*C. apus*). Note also that the A3" muscle is not pennate.

5.2.1.6 Muscular torque

At each point in time, the moment exerted by the jaw muscles (M_m) is a function of gape angle and the force generated by the jaw muscles $(F_{A2A3'})$ and $F_{A3''}$:

$$M_{m} = F_{A2A3'} \sin(\mathbf{s}_{A2A3'}) L_{in} + F_{A3''} \sin(\mathbf{s}_{A3''}) L_{in}$$
 (7)

where s will decrease with increasing gape angle (Fig. 3). The instantaneous muscle force depends on several dynamical muscle properties. In our model, we accounted for the force-velocity dependence (F_{FV} factor), force-length dependence (F_{FL} factor), parallel elastic forces (F_{Par} factor) and a "rise time" of activation of the muscle (F_{Ad} factor):

$$F_{Muscle} = F_{Max} * F_{FV} * F_{FL} * F_{Act} + F_{Par}$$
 (8)

where F_{Max} (maximal force along the line of action of the muscle) is given by the following formula:

$$F_{Max} = PCSA * F_{MaxFibre} * \cos(\mathbf{q})$$
(9)

with *PCSA* the physiological cross section area of the muscle (volume divided by average fibre length), $F_{Max\ Fibre}$ the maximal isometric force that can be generated by the muscle fibres and \boldsymbol{q} the average pennation angle of the muscle fibres. The value of 19 N/cm² (Akster et al., 1985) was used for $F_{Max\ Fibre}$, as this is the highest value from experimental measurements of contractile properties of fast fibred fish head muscles out of several studies (Akster et al., 1985; Flitney and Johnston, 1979; Granzier et al., 1983; Johnston, 1982, 1983).

When a pennate muscle is stretched, the pennation angle of muscle will decrease and subsequently the component of force parallel to the line of action of the muscle will increase (see equation 9). Therefore, during lower jaw movements, F_{Max} depends on the degree of lower jaw depression. For calculating the relation between length of the muscle (origin to insertion) and average pennation angle, we followed Narici (1999):

$$\mathbf{q}_{2} = \tan^{-1} \left(\frac{FL_{1} \sin(\mathbf{q}_{1})}{FL_{1} \cos(\mathbf{q}_{1}) + (L_{2} - L_{1})} \right)$$
(10)

with FL = average fibre length, \mathbf{q} = average pennation angle and L = origin to insertion muscle length, at two muscle elongation positions (subscript 1 and 2). As FL, \mathbf{q} and L in a closed mouth situation is known for the four clarids from Herrel et al. (2002), these variables can be calculated for each muscle length by the above formula. Next, the instantaneous fibre length can be calculated using the following equation:

$$FL_2 = FL_1 \sin(\boldsymbol{q}_1) / \sin(\boldsymbol{q}_2) \tag{11}$$

5.2.1.7 Force-velocity factor

Once a muscle fibre starts shortening, the maximal force that can be generated by this fibre will decrease. The relationship between contraction velocity of muscle fibres and their force output is characterized by the following Hill's equation:

$$F_{FV} = (V_{Max} - v)/(V_{Max} + G v)$$
 (12)

where F_{FV} is the force-velocity factor, V_{max} the maximal unloaded contraction velocity, v the fibre shortening velocity at a given time and G a constant determining the shape of the Hill-curve, with G roughly being equal to 4 in vertebrate muscle (Hill, 1970; Alexander, 2003). The value of 8.4 muscle lengths per second from Johnston and Brill (1984) was used for V_{max} , as this is the highest value for fast-fibred fish muscles out of numerous studies (reviewed in Aerts et al., 1987).

5.2.1.8 Force-length factor

The relationship between normalized force (F_{FL}) and muscle fibre lengths (FL) has been approximated for mammalian skeletal muscle (Woittiez et al., 1984; Epstein and Herzog, 1998) and accords to the following equation

$$F_{FL} = -6.25 \left(\frac{FL}{FL_0}\right)^2 + 12.5 \left(\frac{FL}{FL_0}\right) - 5.25 \tag{13}$$

,with FL_0 the optimal fibre length. To include this force-length relationship in our model, we made the following assumption: the optimal fibre length for jaw muscles from a given species is reached when the muscles are stretched according to a mouth opening of mean maximum gape angle decreased with 10°. In this situation, the jaw muscles are well adapted to work within the range of fibre lengths with favourable sarcomere-overlap and, unlikely to reach the unstable, descending limb of the force-length curve ($F_{FL} > 1.1$).

5.2.1.9 Muscle activation rise time

Maximal activation of muscle is not reached instantaneously, but is gradually built up. The shortest time to peak twitch force from *in vitro* studies on contractile properties of fast fibred fish muscles was used (20 ms; James et al., 1998). To reach maximal activation after 20 ms, a sinusoidally rising activation profile was used:

$$F_{Act} = 0.5 - 0.5 \cos(\mathbf{p} \ t / T_r) \tag{14}$$

with F_{Aa} the muscle activation factor, T_R the activation rise time (20 ms) and t the time (between 0 to 20 ms). After 20 ms, full stimulation of the muscles was maintained (F_{Aa} = 1). Activation of left and right muscles is assumed to be identical.

5.2.1.10 Parallel elastic force

A parallel elastic force increasing with muscle length and proportional to maximal isometric force of the jaw muscles is included in the model (F_{Par}). In our model, F_{Par} increases linearly starting from the situation when muscles are stretched to the mean maximal gape angle (for that species) decreased with 5°. In our model, F_{Par} reaches 0.03 times F_{Max} when muscle fibres are stretched to 1.5 times the optimal fibre length. This value was determined for human jaw muscles by Koolstra and Van Eijden (1996).

5.2.2 Kinematic analysis

In order to test the model predictions, mouth closing movements during prey capture in the four species represented in figure 1 (p.7) were analysed. In total 16 individuals were used in the experiments (8 *Clarias gariepinus*, 4 *Clariallabes longicauda*, 2 *Gymnallabes typus* and 2 *Channallabes apus*). The *C. gariepinus* specimens were either aquarium-raised specimens of which larval stages were initially obtained from the Laboratory for Ecology and Aquaculture (Catholic University of Leuven) or specimens obtained from aquacultural facilities (Fleuren & Nooijen BV, Someren, The Netherlands). Cranial lengths (CL) of these catfish were 28.01, 28.39, 44.4, 46.1, 47.5, 47.5, 51.7 and 56.2 mm. The *C. longicauda* individuals (CL = 32.4, 34.7, 35.7, 49.0) and *C. apus* individuals (CL = 22.6, 24.2) were caught in Northern Gabon. The *G. typus* specimens (CL = 20.80, 22.15) were imported from the western region of tropical Africa. Animals were kept separate in 20 L test aquaria and were trained to capture food presented inside a narrow, projecting corridor (25 cm length, 8 cm width, 15 cm water height) of the aquarium, which induced the animals to feed in a position perpendicular to the camera.

Two different prey types were used: (1) a piece of cod fillet (*Gadus morhua*) of about 3 cm³ and (2) a North Sea shrimp (*Pandalus borealis*). Both prey types were attached to a thin, plastic coated steel wire and were suspended about 5 cm above the bottom of the corridor. The cod was pinned onto the steel wire, while the shrimp was clipped around its middle.

High-speed video recordings (250 frames s⁻¹) were made from a lateral position, using a Redlake Imaging Motionscope digital high-speed video camera (shutter 1/2500). Two floodlights (600 Watt) provided the necessary illumination. Only those prey capture sequences that were approximately perpendicular to the camera lens were selected and retained for further analysis. To do so, lateral recordings in which skull roof, skull bottom or origin of the maxillary barbel of the opposite side of the fish was visible, were discarded. For each individual, 10 recordings (each consisting of 5 cod and 5 shrimp captures) were analysed.

Three anatomical landmarks were digitised on the recorded images using Didge (version 2.2.0, Alistair Cullum), and the horizontal (x) and vertical (y) coordinates for each point were exported to a spreadsheet. These landmarks are the interior sides of the upper and lower jaw tips and the approximate rotation point of the lower jaw. The latter landmark was digitised after careful examination of its relative position on the head using morphological drawings from the literature and X-ray photographs. To improve the accuracy of the digitisations, each point was digitised separately throughout the entire prey capture sequence. After data filtering (Butterworth low pass filter, cut-off frequency between 20 and 25 Hz) and differentiation, angular displacement, velocity and acceleration profiles were obtained.

5.2.3. Simulations

In order to compare the speed of mouth closure in the four species with increasing degree of hypertrophy of the jaw adductor muscles, model simulations were run using the species-specific biometric data (Table 1) for a large number of jaw closures in which the lower jaw starts rotating from a given gape angle referred to as the initial gape angle, and from which it performs a specific rotation of which the magnitude is referred to as the travel distance. As the initial gape and travel distance of jaw closures *in vivo* are highly variable and interspecific differences are often observed (Table 2), simulations were run for several initial gape angles and travel distances. The time it takes to fulfil a specific rotation was used as a relative measure of average jaw closing velocity. In simulations used in interspecific comparisons, the species cranial length was set to 30 mm, which approximates the average cranial length of the animals used in the recording sessions. To evaluate the importance of the variables used in the model (to describe the shape of the jaw system and the dynamical properties of the jaw muscles) for jaw closing speed, a sensitivity analysis

Table 2: Average start gape, end gape and travel distance of mouth closings

_	Species					
- Variable	Clarias gariepinus ^a		Gymnallabes typus ^c	Channallabes apus ^d		
Initial gape	32.0 <u>+</u> 9.4	54.7 <u>+</u> 8.8	55.6 <u>+</u> 10.2	44.1 <u>+</u> 6.3		
End gape	11.8 <u>+</u> 7.1	36.1 <u>+</u> 11.4	35.7 <u>+</u> 11.7	31.4 ± 8.6		
Travel distance	20.3 ± 7.0	18.6 ± 9.3	19.9 <u>+</u> 7.3	12.7 <u>+</u> 6.8		

Note. All values in degrees \pm standard deviation.

 $^{a}N = 80, ^{b}N = 40, ^{c}N = 20$

was performed. In this analysis, the effects of a 10% increase or decrease of these variables on the speed of jaw closure were reported.

5.3 Results

5.3.1 Model output: forces during jaw closure

Figure 4 gives an overview of the model output of the forces that are involved during a specific jaw closure of *C. apus*. Initially, muscular forces are mainly used to accelerate the lower jaw (Fig. 4B). After this phase, the model predicts that forces from jaw muscle activity are largely used to overcome the increasing positive pressure in the buccal cavity and the resistance from soft tissues. In all cases, the importance of drag forces on the rotation of the half-elliptic plate is negligible (Fig. 4B)

As the activation of the jaw muscles is initiated at time 0, the active force production starts increasing from that moment on. Consequently, mainly the elastic forces included in the model (F_{par}) contribute to the acceleration of the lower jaw during the first millisecond of jaw closure. Once the muscles become fully active (after 20 ms), parallel elastic forces

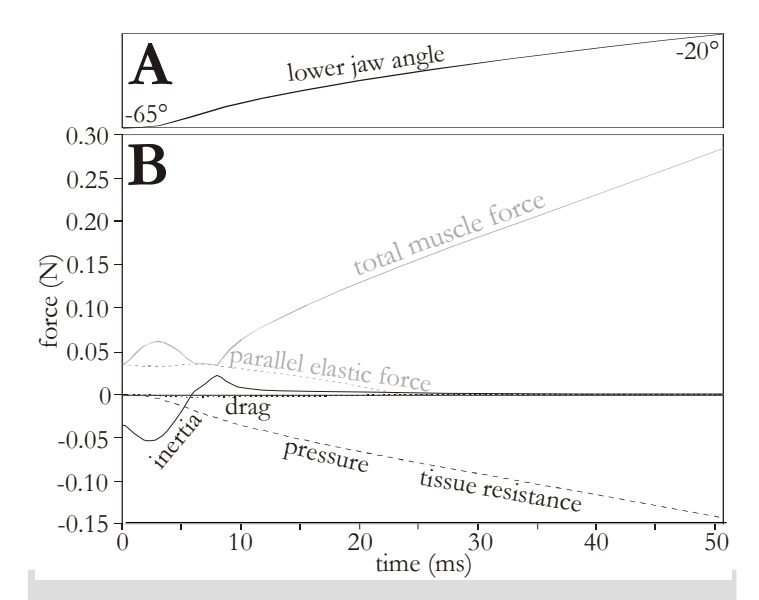


Figure 4: Model output of the forces (graph B) involved during a simulated *C. apus* jaw closure from a lower jaw angle of -65° to -20° (graph A). The direction of the calculated forces is in between the lines of action of both muscle parts (A2A3' and A3''). The total (active and passive) muscular force, (passive) parallel elastic forces and the forces needed to overcome drag, positive buccal pressures, tissue resistance and the inertia of the lower jaw are represented. Note that pressure and tissue resistance have equal magnitudes in the model. See text for further explanation.

usually become an insignificant factor and in general, their overall contribution to the jaw closure is limited. However, the model predicts that these elastic forces can be much more important when clariid catfish feed at high gape angles. This is for example the case when C. apus opens its mouth to a -65° lower jaw angle (Fig. 4). In this case C. apus will have 0.035 N of parallel elastic force when it opens its lower jaw to -65°, which is about 12% of the peak total muscle force during the following jaw closure (Fig 4B).

5.3.2 Model predictions versus experimental data

In general, simulations of jaw closing movements by

the model correspond well to the fastest jaw closures of prey captures by the four species of clariid catfish, as determined on the high-speed video recordings (Fig. 5, first row). In all cases, the shape of the simulated kinematic profiles is realistic. For example, jaw closing velocity profiles start at zero degrees per second at the time the lower jaw is put in motion, reach their peak values in the first half of the jaw closing phase, and show a gradual decrease towards the end (Fig. 5, second row). Note, however, that effects of prey impact were not modelled. Consequently, in contrast with the model simulations, jaw closing movements based on videos of prey captures are counteracted by reaction forces from the prey after prey contact and will ultimately prevent any further movement of the lower jaw. As for the observed data, the model predicts peak accelerations to be reached within the first 5 ms of the jaw closing phase. Again, due to prey impact, the negative accelerations are much more pronounced in the kinematic data when compared to the model simulations (Fig. 5, third row).

The best match between the model and the kinematic data is for *C. gariepinus* and *C. longicuada* (Fig. 5). The time to close the mouth from its initial (maximal) opening to the

moment of impacting the prey is well predicted by the model (within 10% of values from the kinematic data). Also, predictions of peak jaw closing velocities are not beyond 12% of the experimental values for these species. Peak positive accelerations, however, are apparently overestimated by the model of *C. longicauda* (Fig. 5).

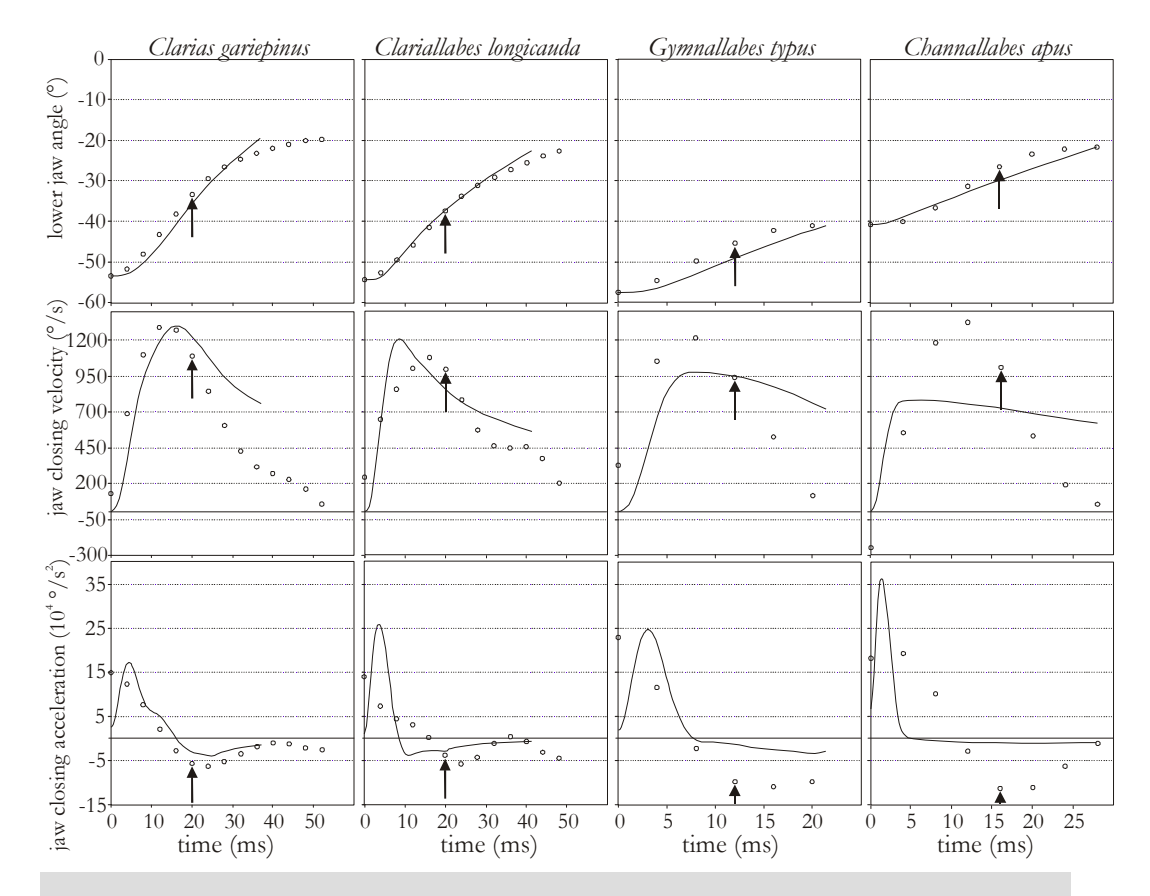


Figure 5: Comparison of filtered kinematic profiles from the prey capture sequence in which the highest jaw closing velocity is reached for each species (dots) with the model output (black line). The model simulations are initiated and stopped at angles corresponding to initial and final gape based on the kinematic analysis. Note that the model does not account for reaction forces as a result of prey impact, and thus should not follow the kinematic data after the moment of prey impact (indicated by the arrows). Also note that the error of the kinematic data points increases from plots of angles (first row) to plots of accelerations (third row), due to data-differentiation. Consequently, a better fit between experimental data and model is expected in the graphs of lower jaw angles compared to velocities or (especially) accelerations.

In *G. typus* and *C. apus*, the kinematic data show that the peak velocities of jaw closure are underestimated by the model for these species (Fig. 5). Whereas for *G. typus*, the model prediction of peak jaw closing velocity is still not more than 20% less than the result from the kinematical analysis, a considerable difference is shown for *C. apus* (peak velocity 41% underestimated). As *C. apus* is the only species for which the velocity profiles do not

accurately predict the observed *in vivo* results, we decided not to fine-tune the model to improve the fit for this species specifically (for example by increasing the maximal contraction velocity of the muscle fibres). Nevertheless, when comparing the model output between the four modelled species, this underestimation of maximal jaw closing velocity for *C. apus* will have to be considered in the interpretation of the results (see Discussion).

5.3.3 Interspecific comparison of model output

5.3.3.1 velocity of mouth closure

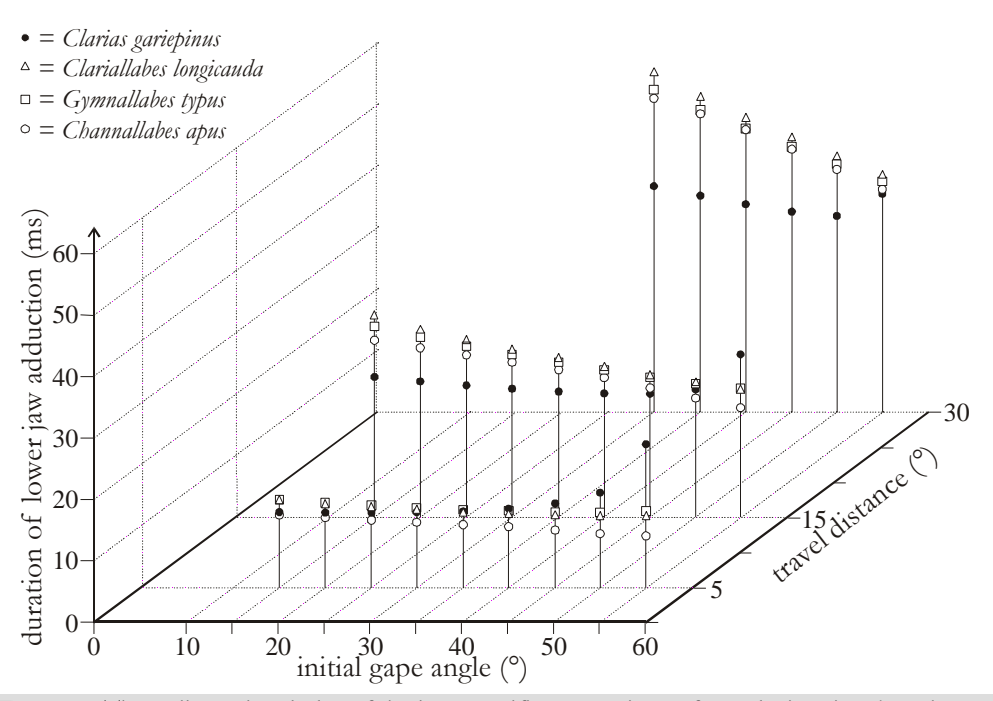


Figure 6: Three dimensional plot of the interspecific comparison of jaw closing time based on model simulations with different travel distances and starting from different gape angles. All species are represented by a single symbol (see legend on the upper left side). For all species, cranial length in the model was scaled to 30 mm.

In most cases, no positive relation could be demonstrated between the size of the jaw muscles (Fig. 1; Table 1) and the duration of mouth closure (Fig. 6). There are, however, two exceptions: (1) jaw closures of intermediate travel distance (15°) from initial gape angles above 50° and (2) jaw closures of short travel distance (5°) from initial gape angles above 40°. Still, even in these cases, *G. typus* apparently has no advantage over *C. longicauda*, despite the fact that its jaw adductors roughly have a 50% larger physiological cross-sectional area (Table 1). Furthermore, for jaw closures of long travel distance (30°) and intermediate travel distance (15°) with initial gape angles below 45°, the species

without jaw adductor hypertrophy (*C. gariepinus*) is able to carry out the fastest jaw closing movement (Fig. 6).

5.3.3.2 Moment and force from the jaw muscles

To illustrate the model output, the jaw closing velocity, muscular torque and force output are presented for two situations mimicking biting onto small and large prey: a jaw closure of long travel distance starting from a low gape angle (40° to 10°, Fig. 7) and a jaw closure of short travel distance starting from a high gape angle (55° to 50°, Fig. 8). As demonstrated in figure 6, both situations yield a different result in terms of average jaw closing velocity.

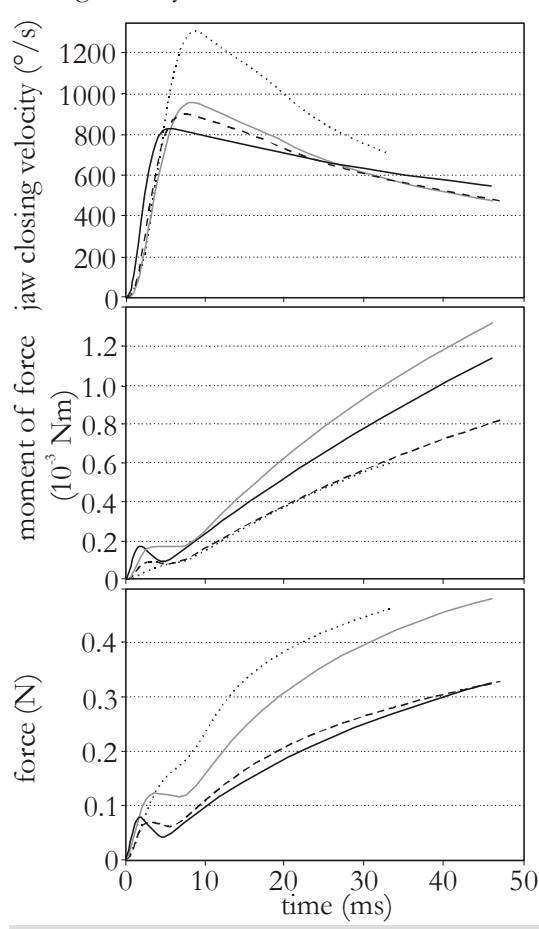


Figure 7: Model output of a jaw closure from a gape angle of 40° to 10°. Moment of force, and force include results from both jaw closer muscles (A2A3' and A3"). The lines represent *C. gariepinus* (dotted line), *C. longicauda* (dashed line), *G. typus* (grey line) and *C. apus* (black line).

For the jaw closure with long travel distance, higher jaw closing velocities are reached during the initial phase by C. longicauda (during the first 4.2 ms) and C. (during the first 4.8 ms) when compared to C. gariepinus and G. typus For the latter species, the (Fig. 7). predicted jaw closing velocity is initially approximately equal to values for C. gariepinus but becomes significantly lower after 3.5 ms. After this initial phase, however, the species with the smallest jaw muscles (C. gariepinus) is able to achieve the highest mouth closing velocity (1304 °/s) (Fig. 7). Peak velocities from C. longicauda, G. typus and C. apus respectively 26.8, 30.9 and 36.6 % lower than the maximal value for C. gariepinus. Finally, after reaching peak values, jaw closing velocities decrease (Fig. 7). Although this drop of velocity is more substantial in C. gariepinus compared to the other species, the jaw closing velocity of this species remains the highest until the end of the simulated mouth closure.

The interspecific comparison of the moment of force from both jaw muscle parts (Fig. 7), shows that initially (first 2.5 ms) the magnitude of these moments is in proportion to the size of the jaw muscles: the moments increase from *C.gariepinus*,

over *C. longicauda* and *G. typus* to *C. apus*. However, towards the end of the jaw closure, the moments generated by *C. gariepinus* are approximately equal to those of *C. longicauda*. Now,

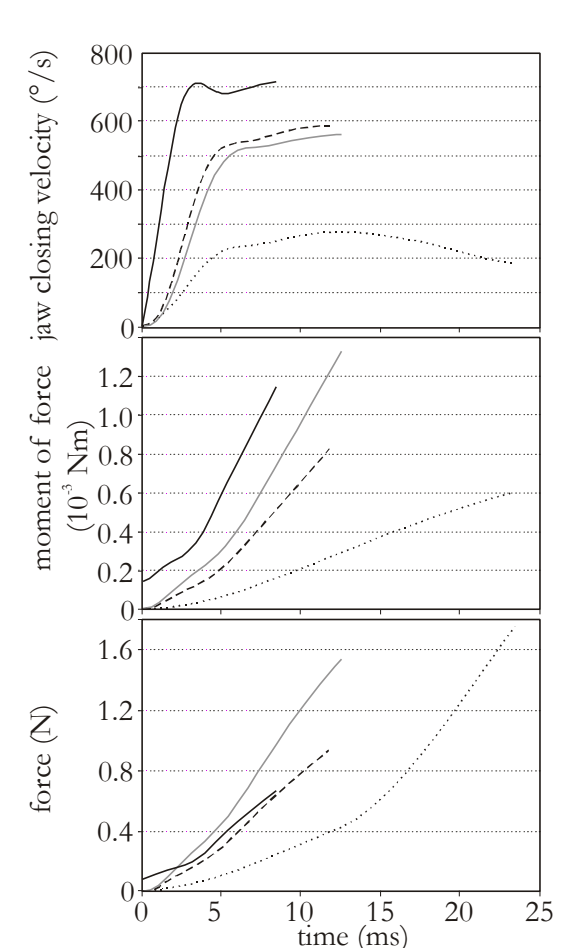


Figure 8: Model output of a jaw closure from a gape angle of 55° to 50°. Moment of force and force include results from both muscle parts (A2A3' and A3"). The lines represent *C. gariepinus* (dotted line), *C. longicauda* (dashed line), *G. typus* (grey line) and *C. apus* (black line).

G. typus instead of C. apus, reaches the highest values.

Due to differences in the constructional parameters of the jaw system (length and inclination of the lower jaw in-lever, inclination of the jaw muscles; see Table 1), the interspecific comparison of jaw muscle force profiles differs from the profiles of moments (Figs. 7-8). No higher forces are generated during the 40° to 10° jaw closure in the species with enlarged jaw adductors, except for a very short interval from 0.5 to 5.5 ms after the start of the simulated jaw closure. Furthermore, after this interval, the relatively slender muscled *C. gariepinus* reaches the highest muscle forces.

In contrast with the 40° to 10° jaw rotation (Fig. 7), *C. gariepinus* shows an impaired capactity to close the mouth quickly during a short rotation that starts at a large gape angle (Fig. 8). In this case, the highest jaw closing velocity is reached by *C. apus*, followed by *C. longicauda*, *G. typus*, and *C. gariepinus*. As a result of the short travel distance (5° rotation), velocities are still rising when the end of the simulation is reached. The moment of force profiles follow the trend of increasing jaw adductor size in the

species studied (Fig. 8). The same is true for the force profiles of *C. gariepinus*, *C. longicauda* and *G. typus*, while the extremely hypertrophied jaw muscles of *C. apus* generate forces that are lower than the less hypertrophied *G. typus* (Fig. 8).

5.3.3.3 Effects of increasing jaw muscle cross-sectional area

Previous results might suggest that hypertrophy of the jaw adductors in Clariidae (the most obvious modification of the jaw system of the species used in the present study) is of no use for generating higher jaw closing velocities, except when feeding at high gape angles and short travel distances. However, when we increase the physiological cross sectional area (PCSA) of the jaw muscles in *C. gariepinus* in the model to values equal to PCSAs from the other species, we see that the mouth can be closed significantly faster (Fig. 9A). The inverse effect is observed when the PCSA of *C. apus*, the species with most extreme jaw closer hypertrophy, is decreased to values equal to the species with less large jaw muscles (Fig. 9B).

The simulations with a range of PCSA values in the jaw system of *C. gariepinus* (Fig. 9A) and *C. apus* (Fig. 9B) reveal a clear difference in jaw closing velocity independent of the size of the cross-sectional area. Indeed, the *C. gariepinus* jaw system is able to fulfil the 40° to 10° jaw closure in about half the time the *C. apus* jaw system needs with an equal PCSA. Therefore, other interspecific differences in the jaw system besides PCSA are also important, and cancel out the potentially faster jaw closure due to jaw adductor enlargement for this specific jaw closing movement.

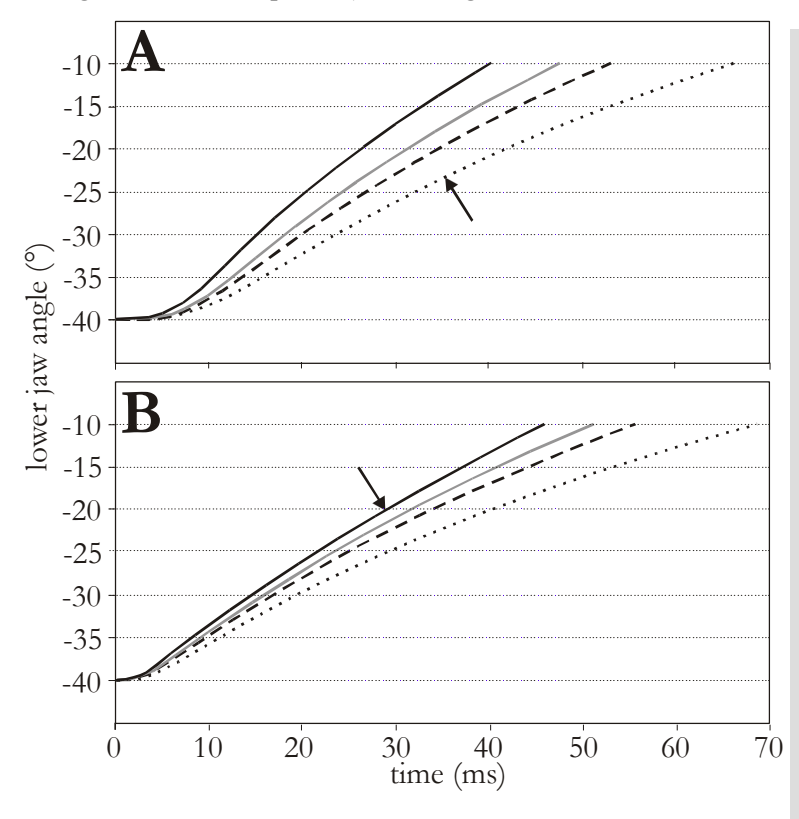


Figure 9: (A) Jaw rotation profile of *C*. gariepinus (line indicated by arrow) together with the profiles derived from a simulation where the physiological cross sectional area (PCSA) of the muscles is increased to values observed for the other species. In (B), the jaw rotation profile of C. apus (arrow) is presented together with results of simulations using a decreased value for PCSA, again corresponding to the values measured for the other species. Dotted line = PCSA of C. gariepinus, dashed line = PCSA of C. longicauda, grey line = PCSA of G. typus and black line = PCSA of C. apus.

5.4 Discussion

5.4.1 The role of enlarged jaw adductors in Clariidae

Our model simulations of jaw closing movements show different results, depending on the rotation of the lower jaw that is being considered (Fig. 6 and Fig. 7 vs. Fig. 8). In most cases (e.g. all jaw closures with initial gape angles below 45° performing rotations of larger than 10°), the jaw systems of clariid species with enlarged jaw adductors is not well suited to perform fast mouth closures (Fig. 6). The observed underestimation of peak and average jaw closing velocity before prey impact of respectively 40% and 10% in C. apus (Fig. 5) will not change this result. Even if we correct for this 10% underestimation of average jaw closing velocity in C. apus, C. gariepinus is still able to perform the fastest mouth closures.

Yet, even for the lower jaw rotations in which the species with jaw adductor hypertrophy perform much poorer than the non-hypertrophied species (e.g. the 40° to 10° rotation), the size of the jaw muscles remains an important aspect for fast mouth closing in these fishes. Indeed, if *C. gariepinus* would have had jaw muscle the size of those of *C. apus*, our model suggests that it would be able to close its mouth from a 40° to 10° gape angle within 20.1 ms instead of 33.2 ms; i.e. one third faster (Fig. 9A). The same is true for *C. apus*: a decrease in the cross-sectional area of its jaw muscles results in considerably lower speeds of jaw closure (Fig. 9B). However, when we compare the species shown in figure 1, the enlarged jaw muscles work within jaw systems that show other difference besides the differences in the size of the jaw muscles (Table 1). Consequently, while the jaw muscle enlargement speeds up jaw closure considerably, this effect is cancelled out if the different sized muscles are placed in their respective jaw systems.

On the other hand, an advantage in average jaw closing velocity (or in time to fulfil a certain lower jaw adduction) is predicted for short lower jaw rotations and prey captures with large gapes (Fig. 6). In addition, compared to the non-hypertrophied *C. gariepinus*, the kinematic analysis of prey captures in clariids with enlarged jaw adductors showed that these species typically also tend to feed at these larger gape angles and indeed use shorter lower jaw rotations to grab the prey (Table 2). We included a more detailed overview of model predictions of the advantage or disadvantage in jaw closing velocity of the hypertrophied species compared to the non-hypertrophied species and how the experimentally observed prey captures fit in these predictions (Fig. 10). In *C. longicauda*, *G. typus* and *C. apus*, about half of all analysed prey captures have the initial gape and travel distance for which the model predicts an advantage in average jaw closing velocity of 5% and more compared to *C. gariepinus* (Fig. 10). This indicates that, given their particular prey capture behaviour, the observed specialisations in the jaw system of these species are still functionally important *in vivo* when it comes to fast jaw closing.

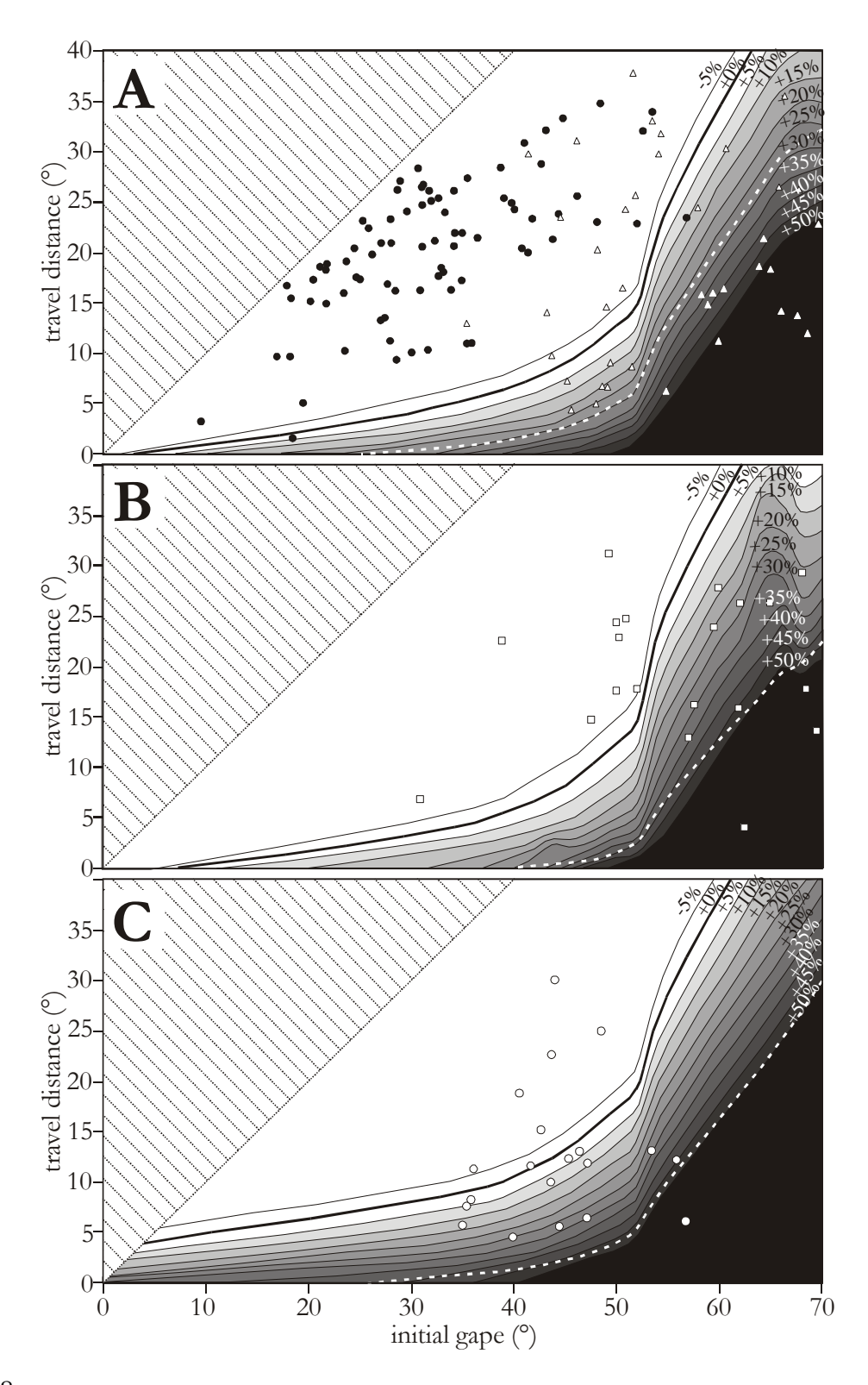


Figure 10: Characteristics of the prey captures observed in the experiments (initial gape and travel distances of the lower jaw) plotted together with lines indicating the predicted differences in average jaw closing velocity between the species with jaw adductor hypertrophy and the non-hypertrophied *C. gariepinus*. These differences are expressed as a relative increase/decrease when comparing jaw closing times from *C. longicauda* (A), *G. typus* (B) and *C. apus* (C) to the corresponding values of *C. gariepinus* (lines connecting equal values, legends are on the upper right side of each graph). For jaw closures from the white region of a graph, the model predicts a disadvantage (+0 % and lower) or very little advantage in the time needed to close the mouth (+5 % and lower) for the hypertrophied clariids compared to *C. gariepinus*. In the grey or black region of the graphs, an increase of 5% and more in average jaw closing velocity is expected. Points represent the positions of all prey captures analysed based on high speed video recordings from *C. gariepinus* (black points, graph A), *C. longicauda* (white triangles, graph A), *G. typus* (white squares, graph B) and *C. apus* (white points, graph C). The white dashed line represents the +5% in average jaw closing velocity if the jaw muscles would not be hypertrophied (PCSA of *C. gariepinus* used in the model simulations of the other species).

The species with enlarged jaw adductors thus appear "adapted" to feed at higher gape angles when compared to C. gariepinus. Biometric data also show that they have an increased inclination of the jaw muscles and a larger and more inclined lower jaw in-lever (Table 1). These characteristics of the jaw system enable the jaw muscles to continue generating torques resulting in lower jaw adduction when the lower jaw is depressed to large gape angles (Gans and De Vree, 1987). Note that when C. gariepinus starts its jaw closing movement from a gape angle higher than 52.7°, the line of action of the A2A3' jaw muscle initially lies behind the articulation of the lower jaw. Consequently, in this situation the A2A3' muscle cannot contribute to the mouth closing movement. For the other species, the gape angle by which this occurs is considerably higher (C. longicanda: 67.9°, G. typus: 66.2° and C. apus: 81.8°). This suggests that the advantage for jaw closing in these species compared to C. gariepinus is largely due to the geometry of their jaw system, and would also occur without the hypertrophy of the jaw muscles. However, the model predicts that the range of jaw closures in which this advantage occurs would be strongly restricted if all species would have jaw muscles the size of those of C. gariepinus (Fig. 10). For example, whereas for jaw closures in which C. longicauda would have a velocity advantage of 5% compared to C. gariepinus with equal sized jaw muscles, an advantage of 30% is predicted with the observed hypertrophy of the jaw adductors (Fig. 10). Thus, not only when feeding at intermediate gape angles (Fig. 9), but also for feeding at high gape angles the increased size of the jaw adductors will increase jaw closing velocity considerably. However, only when feeding at large gape angles (and also for short jaw closings at lower gape angles) the species with enlarged jaw muscles are expected to have an increased jaw closing performance over the species without jaw adductor hypertrophy included in this study (Fig. 10).

The maximal size of the mouth opening is a very important aspect of feeding in fishes as it may limit the size of the prey the can be eaten (Keast and Webb, 1966; Schael et al., 1991; Gill, 1997; Huskey and Turingan, 2001; Manghagen and Heibo, 2001). Especially for *G*.

typus and C. apus, the adult head size is much smaller than for C. gariepinus, which can grow up to more than 1.5 m total body length (Cabuy et al., 1999). Consequently, being able of feeding at high gape angles and snapping the jaws relatively fast on large, moving prey may be an important aspect of the feeding success in these species with reduced head sizes and elongated bodies. Furthermore, engulfing the prey at a high gape angle may enable these catfishes to start biting or crushing the prey at a more caudal position at the jaws, in which much larger bite forces can be exerted on the prey (Herrel et al., 2002). The fact that the teeth are positioned more caudally on the oral jaws in these species (Cabuy et al., 1999; Devaere et al., 2001), confirms the importance of biting the prey closer to the jaw articulation.

5.4.2 Disadvantage for large lower jaw rotations in species with jaw hypertrophy

As the model predicts that an increased physiological cross-sectional area (PCSA) of the jaw muscles is an important aspect for fast mouth closure within the clariid species studied (Fig. 9), the question arises why a species like *C. apus* with its 5 times higher jaw muscle PCSA compared to *C. gariepinus* (Table 1) is not able to develop increased jaw closing velocities for most of the jaw closings simulated here (Fig. 6, Fig. 10). The reason why the model predicts a considerably lower speed of jaw closure in most jaw rotations of long travel distance, despite the enlarged jaw adductors, has to be sought in the geometry of their jaw system (Table 1, Fig. 3).

Once the lower jaw starts its closing movement, fibres from the jaw muscles start shortening and, due to the force-velocity relationship, the force that can be generated by the jaw muscles drops. We noted an interspecific difference in the amount of force reduction as a result of changes in the force-velocity relationship. During mouth closure in C. apus, the force-velocity factor (F_{FV} , equation 8) causes a much faster and more extensive drop in force compared a jaw closure of C. gariepinus. C. typus and C. longicauda are intermediate in this regard. For example, during the 40° to 10° gape angle simulation (Fig. 7), the active muscle force of C. apus is reduced to 2% of the maximal active isometric force in the first 6 ms of the jaw closure. For C. longicauda and C. typus, this force drops to 7% in the first 8 ms. In C. gariepinus, however, the decrease in active muscles force is limited and reaches the value of 17% of its maximal isometric force (after 16 ms).

The relation between fibre shortening velocity and jaw closing velocity explains these results (Fig. 10). To rotate the lower jaw by a given velocity, the muscle fibres of C. apus have to contract much faster compared to the same situation in C. gariepinus. Again, C. longicauda and C. typus are intermediate between these extremes (Fig. 11). As the force-velocity factor is directly related to the shortening velocity of the jaw muscle fibres, the reduction in active force for a given jaw closing velocity increases from C. gariepinus over C. typus and C. longicauda to C. apus. This stronger decrease in force will result in smaller fractions of the peak isometric force (F_{max}) available to accelerate the lower jaw to higher

velocities. In this way, the increased acceleration potential of the enlarged jaw muscles in the catfish studied will be lost relatively early during the jaw closing phase.

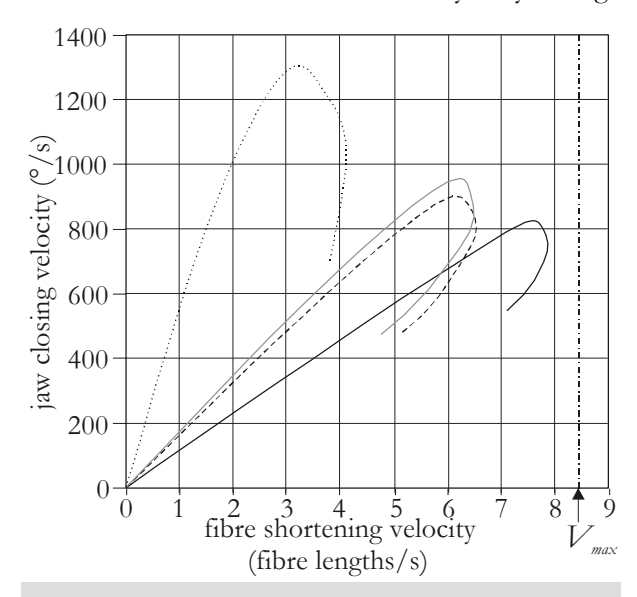


Figure 11: Relationship between the shortening velocity of fibres from the main jaw closing muscle (adductor mandibulae A2A3') and the angular velocity of jaw rotation during a jaw closure from 40° to 10° gape angle in *C. gariepinus* (dotted line), *C. longicanda* (dashed line), *G. typus* (grey line) and *C. apus* (black line). Note that the model input of maximal shortening velocity of the muscle fibres used in the model is 8.4 fibre length/s.

To facilitate further discussion, we introduce a ratio (fibre velocity transmission FVTR) ratio describing the relationship between velocity of lower jaw rotation and fibre shortening velocity. This gape-dependent variable calculated by dividing the decrease in gape angle (expressed in degrees) by the average decrease in length of the jaw muscle fibres (expressed in numbers of fibre lengths). FVTR describes how efficient velocity from the muscles fibres is transmitted to a lower jaw rotation. If we assume that the jaw muscle fibres from different species have maximal same shortening velocities and if we ignore the inertial effects of the rotating lower jaw, the FVTR induces limits on the peak angular velocity that can be

reached during jaw closure. Indeed, if the muscle fibres reach their maximal contraction velocity, the corresponding angular jaw closing velocity is solely determined by the FVTR. Furthermore, it describes to what extent the active jaw muscle force is decreased (due to Hill's force-velocity relationship) for a given angular jaw closing velocity.

Together with the increasing jaw adductor hypertrophy (Fig. 1-p.7), a trend can be observed in the species studied to increase (1) the length of the lower jaw in-lever, (2) the inclination of the lower jaw in-lever and (3) the inclination of the line of action of the jaw muscles (Table 1). These three changes in the geometrical constitution of the jaw system reduce the mechanical efficiency of the jaw system by decreasing the FVTR. Apparently, for lower jaw rotations of large travel distance, where higher angular jaw closing velocities are reached, the difference in FVTR among the species studied becomes increasingly important. Indeed, in figure 10 we see that *C. apus* nearly reaches the maximal shortening velocity of its muscle fibres in the A2A3' during the 40° to 10° simulated jaw closure. In this situation, due to its impaired mechanical efficiency in transmitting velocity of the muscle fibres to lower jaw rotation (FVTR), *C. apus* is unable to reach the peak jaw closing

velocity that was predicted by the model for *C. gariepinus*, a species with a much higher FVTR.

5.4.3 Effects of changes in the jaw system on the speed of jaw closure

To examine what changes in the biometrics of the jaw system (see Fig. 3) are most important to improve the performance of jaw closures in clariid catfishes, a sensitivity analysis was performed using the jaw system of the generalized clariid *C. gariepinus*. In this analysis, we changed this species jaw system characteristics from table 1 (and also the lower jaw width) by +10% and -10% and calculated the relative change in speed of the 40° to 10° jaw closure (Fig. 12). To examine potential functional trade-offs, we also listed the effects on static bite force, kinematic efficiency of the jaw system (FVTR) and the highest possible gape angle from which the mouth can be closed (Fig. 12).

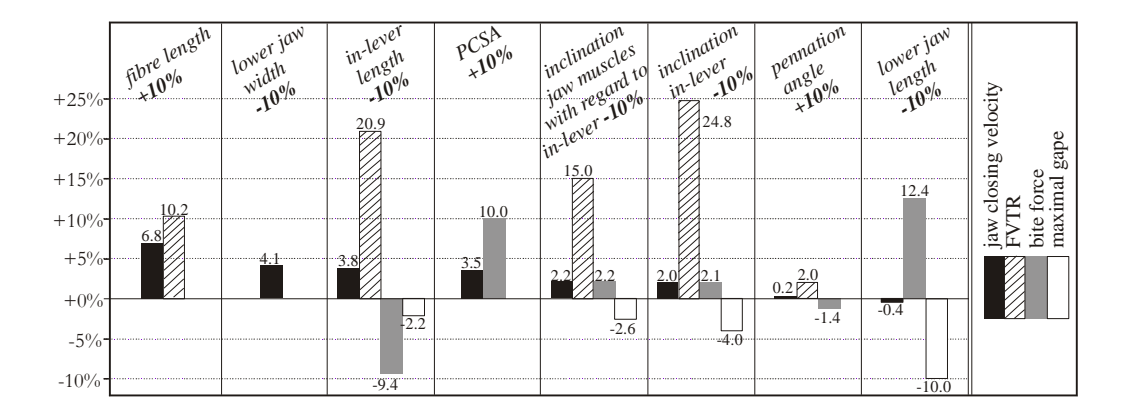


Figure 12: Sensitivity analysis of changes in the jaw system architecture (lengths and angles +10% and -10%) of a 30 mm cranial length *C. gariepinus* performing a jaw closure of 40° to 10° gape angle. Only the changes that had an advantageous effect on the speed of jaw closure are listed, as the opposite changes (-10% instead of +10% or reversed) yielded approximately the inverse relative changes. The relative changes of the following variables are given (legends on the right side of the graphs): (1) average jaw closing velocity, (2) kinematic efficiency of the A2A3' jaw muscle (average fibre velocity transmission ratio of 40° and 10° gape), (3) bite force perpendicular to the jaw tip (average 40° and 10° gape) and (4) the maximal gape distance from which the mouth can still be closed. In the model simulations with altered lower jaw length, the lower jaw rotation of which the absolute mouth opening corresponds to the 40° to 10° gape of normal jaw length are performed. Note that the combined effect of more than one of these changes is not always the sum of the separate effects.

Increasing the average fibre length of the muscles is apparently the most advantageous change in the jaw system to enhance the speed of jaw closure in *C. gariepinus* for the lower jaw rotation induced here (Fig. 12). Also important are the width of the lower jaw (a narrow lower jaw reduces the moment of inertia, as well as the impact of drag and pressure on the lower jaw rotation), the length of the lower jaw in-lever (a shorter in-lever increases the kinematic efficiency) and the physiological cross-sectional area of the jaw muscles (a higher PCSA increases the acceleration of the lower jaw). Reducing the inclination of the jaw muscles and the lower jaw in-lever is less important for speeding up jaw closure. Changes in the average pennation angle and in the length of the lower jaw hardly influence the average jaw closing velocity for this lower jaw rotation (Fig. 12).

An increase in the PCSA of the jaw muscles does not compromises other functions of the lower jaw during feeding. However, it has been shown for clariid catfishes that this morphological modification can interfere with the mechanics of suction feeding (Chapter 6). Also, spatial constraints may occur when accommodating an increased muscle volume into the cranial system and, as shown for cichlid fishes by De Visser and Barel (1996, 1998), this potentially limits the suction force that can be generated by the hyoid apparatus. In contrast, several other aspects of the jaw system in C. gariepinus may cause a direct mechanical trade-off between jaw closing performance and the maximal size of the mouth opening (Fig. 12): decreasing the length of the lower jaw in-lever, the width of the lower jaw, the inclination of the jaw muscles and the inclination of the lower jaw in-lever have positive effects on the speed of jaw closure, but limit the maximal size of the oral aperture and consequently the size of the prey that can be eaten. As predicted in previous studies (Barel, 1983; Wainwright & Richard, 1995; Westneat, 1994), our model also showed that the size of the in-lever of the lower jaw cause a trade-off between the maximal bite force that can be exerted by the lower jaw and the velocity of jaw movement. However, it should be kept in mind that these results strongly depend on the nature of the lower jaw rotation that is considered: the distance in which the lower jaw can freely travel before impacting the prey, and the position from which it starts its rotation are very important in this regard (Fig. 10).

Compared to the previously discussed effects of changes in the geometrical constitution of the jaw system in C. gariepinus (Fig. 12), altering the magnitudes of the moment of inertia, drag, tissue resistance and pressure only has relatively little influence on the speed of jaw closure. If we reduce these parameters by 10% for the 40° to 10° jaw closure in C. gariepinus, jaw closing will be respectively 0.15%, 0.03%, 1.8% and 1.8% faster. However, the contractile properties of the jaw muscle fibres are more important. For example, if the maximal shortening velocity is increased by 10%, the average speed of jaw closure will be 6.8% higher. Also the input values for G (the shape of the Hill-curve) describing the force-velocity relationship (2.5%), the maximal isometric force that can be generated by the jaw muscle fibres (3.5%) and the rise time of muscle activation (2.1%) appear to be important factors that affect the velocity of mouth closure. On the other hand, the parallel elastic forces (0.03%) and the optimal fibre length (0.21%) have less of an effect on the

speed of jaw closure in this case. Therefore, accurate estimates of the relatively important variables are more critical for the model output than for example the values from the calculations of the moment of inertia or drag, which only seem to have a minor effect on the speed of jaw closure.

5.4.4 The use of jaw closing lever ratios

Previous studies dealing with the mechanics of jaw movement in teleost fishes (Richard and Wainwright, 1995; Wainwright and Richard, 1995; Wainwright and Shaw, 1999; Westneat, 1994) have used the jaw closing lever ratio (ratio of lower jaw in-lever to outlever, or Lin divided by length of the lower jaw (a) in Fig. 3) as a comparative measure of potential speed of jaw closure. Also in ecomorphological studies (Albertson et al., 2003; Cutwa and Turingan, 2000; Turingan, 1994; Sibbing and Nagelkerke, 2001; Turingan et al., 1995; Wainwright and Richard, 1995; Westneat, 1995), lever ratios are used to evaluate feeding performance. When using jaw closing lever ratios as a measure of kinematical efficiency of the jaw system for closing, it is assumed that velocity of jaw movement is inversely proportional to this lever ratio. The amplification of velocity occurs in direct trade-off with the force exerted at the jaw tip, as force will be directly proportional to the lever ratio (Wainwright and Richard, 1995). Thus, in these studies, low jaw closing lever ratios are considered to enable a relatively rapid jaw closing, which is useful for capturing soft, mobile prey.

However, the results of our model show several limitations to the use of simple jaw closing lever ratios as a relative measure for speed of jaw closing in comparative studies:

- (1) Kinematic efficiency of transmitting velocity from the jaw muscle fibres to the tip of the jaws includes other aspects besides length of in-lever and out-lever of the lower jaw. A sensitivity analysis on a more complete measure of kinematical efficiency (fibre velocity transmission ratio ore FVTR) shows that fibre length, inclination of the jaw muscles and inclination of the in-lever are also very important parameters of the transmission system of jaw muscle to lower jaw (Fig. 12). For example, if in *C. gariepinus* the length of lower jaw in-lever is decreased by 10% (improved kinematic efficiency according to the lever theory) together with an increase in the inclination of the in-lever by 10%, the average FVTRs of the main jaw closing muscle (A2A3') will remain equal during a rotation of 40° to 10° gape angle.
- (2) Kinematic efficiency strongly depends on the gape angle: for example at a 45° gape angle, the A2A3' muscle FVTR is 974.3 °/fibre length, while at a 5° gape angle this FVTR becomes 169.2 °/fibre length. Therefore, it is important to know at which gape angles the species studied usually feeds, before evaluating the kinematical efficiency of its jaw system.

- (3) Our model illustrates that measures of efficiency of kinematic transmission (jaw closing lever ratios, or alternatively FVTR) cannot be simply translated to "speed of jaw closure". For the example shown in figure 12, the -10% change in jaw closing lever ratio only results in +3.8% average jaw closing velocity. Also relative changes in FVTR tend to overestimate the speed of jaw closure considerably in this case (Fig. 12).
- (4) Our study also demonstrates that in a comparative analysis of jaw closure velocity, the result depends on the gape angle from which the jaw closure starts and on the travel distance of the jaw closure (Fig. 11). For example, if a fish feeds on very small prey and has to adduct its lower jaw over 5° only during capture, a less kinematic efficient jaw system can even be advantageous for the speed of this specific jaw closure because of its increased force transmission (increased acceleration potential).

Yet, a simple approach is often needed to evaluate the speed of jaw movement in studies that compare trophic morphologies in a broad range of species. Especially when there is no information on the orientation and the geometrical structure of the muscles attached to the lower jaw, the use of jaw lever ratios is probably the best feasible assessment of maximal jaw velocity and can provide valuable insights into the evolution of trophic structures in fishes.

Recently, a dynamical model for the analysis of jaw movements of fishes that includes muscle dynamics has been published (Westneat, 2003). Yet, in contrast to our model and dynamical models of jaw movements in humans (Koolstra, 2002; Koolstra and Van Eijden, 1996, 1997; Peck et al., 2000; Slager et al., 1997), the relationship between muscle dynamics, external load and inertial effects (established by the equation of motion) was not included. Nevertheless, these elements are rather essential to be able to predict motions from simulated muscle contractions. This could explain, for example, why the velocity profiles from the model of Westneat (2003) show jaw rotations starting with the highest velocity at time 0 after which it decreases in a hyperbolic way. Rather unexpectedly, even though this would imply infinitely high muscle forces preceding this movement, it was stated that accurate predictions of lower jaw kinematics of labrid fishes are achieved (Westneat, 2003).

5.4.5 Validity of our model

Like most biomechanical models, the jaw closing model of clariid catfishes presented here has its limitations, as it reduces the complexity of the real process. Inevitably, several assumptions had to be made. First, the drag forces do not include flow patterns resulting from the suction feeding event preceding, and continuing during the jaw closure phase. Secondly, muscle geometry is far more complex than included in our model. For example, we used average values for fibre length and pennation angle whereas the jaw muscles

consist of fibres of different size that are placed under different angles with respect to the central tendon (Herrel et al., 2002). Thirdly, the contractile properties of the jaw muscle are taken from physiological experiments that were conducted on fish muscles other than jaw adductor muscles that were taken out of fishes from other taxonomic groups. These data could thus differ considerably from the actual contractile properties of the jaw adductor muscles of the catfishes studied in this paper. Fourthly, the magnitudes of forces resulting from pressure differences and tissue resistance in the model can be rough estimates only. However, the rather good fit between the model and the experimental data suggests that the model can be used as a tool to explore the effects of functional modifications of the jaw system in these fish, including the effects of an increased jaw muscle size on the speed of jaw closure.

Chapter 6

Effects of jaw adductor hypertrophy on buccal expansions during feeding of air breathing catfishes (Teleostei, Clariidae)

Sam Van Wassenbergh – Anthony Herrel – Dominique Adriaens – Peter Aerts

Zoomorphology 123, 81-93. (2004)

Summary

Some species of Clariidae (air breathing catfishes) have extremely well developed (hypertrophied) jaw closing muscles that increase the maximal biting force of these species. As these enlarged jaw muscles tightly cover the suspensoria, which are firmly connected to the neurocranium, we expect diminished lateral expansions during suction for species with hypertrophied jaw muscles. In turn, this could imply a reduced suction performance for these species. Compared to *Clarias gariepinus*, which has relatively small jaw closers, *Clariallabes longicanda* shows a clear hypertrophy of the jaw adductors. A kinematic analysis of prey capture in these two species is presented here. As predicted, *Clariallabes longicanda* shows less lateral expansion (average abduction of the hyoids of 19.0 degrees) than *Clarias gariepinus* (abduction of 31.1 degrees). However, our data indicate that the decrease in lateral expansion capacity in the species with excessive adductor development is compensated for by a larger and faster ventral expansion of the buccal cavity by depression of the hyoid.

6.1 Introduction

Siluriforms (catfishes) are an important component of the fish fauna of tropical limnic systems. It is a very diverse group with over 2500 described species (Teugels, 1996). Representatives of the air breathing catfishes or Clariidae are found in Africa, the Middle-East and South-East Asia. They are characterised by an elongated body, a dorso-ventrally flattened head, small eyes and a suprabranchial organ (Teugels, 1996). Within the Clariidae, several species have developed unusually large (hypertrophied) jaw closing muscles (m. adductor mandibulae A2A3'). Species like Gymnallabes typus Günther, 1867 (Cabuy et al., 1999) and Channallabes apus Günther, 1873 (Devaere et al., 2001) show an excessive growth of the jaw adductors of which the physiological cross-sectional area is respectively more than 3 and 7 times higher for a given skull length, compared the non-hypertrophied species Clarias gariepinus Burchell, 1822 (Herrel et al., 2002). According to phylogenetical studies, this hypertrophy of the jaw adductors is a derived feature for clariid catfishes (Teugels and Adriaens, 2003).

Biomechanical modeling showed that species with such enlarged jaw closers can (at least theoretically) produce a higher maximal biting force (Herrel et al., 2002). Given this increased bite performance, it was not surprising that diet analyses found an altered feeding pattern for species that possess hypertrophied jaw adductors with a special preference for coleopterans, which are hard prey (Huysentruyt et al., 2004). Moreover, also other morphological characteristics of the clariids with jaw adductor hypertrophy are regarded as adaptations related to the increased biting force (Cabuy et al., 1999; Devaere et al., 2001; see also Barel, 1983; Turingan and Wainwright, 1993). A noticeable characteristic in this respect is the stronger interdigitation of the suspensorium (hyomandibula) with the neurocranium (sphenotic and pterotic). The suspensorium (which in teleost fishes suspends the lower jaw, the hyoid bars and the opercular bone) in clariid species with jaw closer hypertrophy has a series of well-developed processes onto the neurocranium (Cabuy et al., 1999) (see Fig 1B). As during biting reaction forces of the food exert a moment about a transversal axis at the level of the suspensorium-neurocranium joint (Herrel et al., 2002), the stronger connection of these two bones may function to counter the larger moments that are caused by the increase in bite force.

Exerting bite forces onto the prey is only one aspect of feeding in Clariidae. Suction feeding is generally used to draw the prey towards the mouth (Bruton, 1979). Suction feeding in Actinopterygian fishes is characterised by a three-dimensional expansion and subsequent compression of the bucco-pharyngeal cavity, which is driven by complex movements of several musculo-skeletal elements of the cranial system (Muller et al., 1982; Muller and Osse, 1984). Unfortunately, experimental data on suction feeding mechanisms of siluriforms are almost completely lacking in the literature (but see Alexander, 1970b).

Given the morphology of the head in clariid catfishes with hypertrophied jaw adductors, we expect a diminished lateral expansion of the skull during suction feeding compared to the non-hypertrophied clariids. There are two reasons to expect this:

(1) the jaw adductor muscle almost completely covers the lateral side of the head (Fig. 1). A considerable growth of this visco-elastic mass inserting both on suspensorium and neurocranium can potentially constrain the abduction (lateral swing) of the suspensorium.

(2) The stronger connection (through interdigitating processes) of the suspensorium with the neurocranium (Fig. 1) can also limit the abduction of the suspensorium.

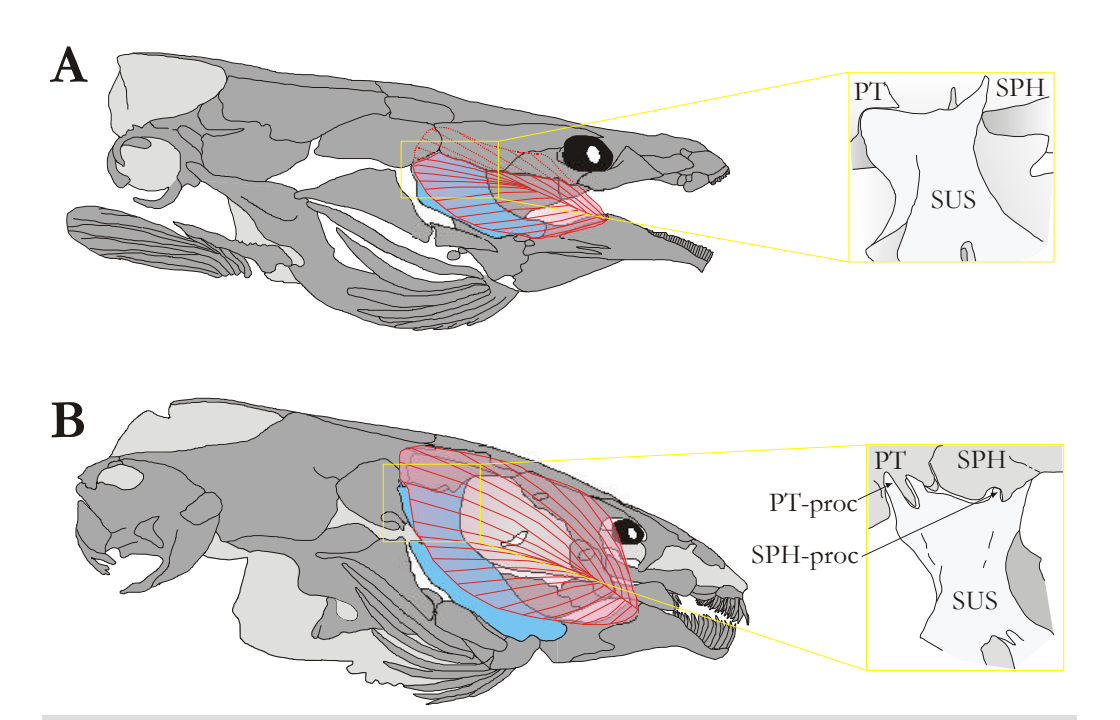


Figure 1: Lateral view on the skulls of *Clarias gariepinus* (A) (modified from Adriaens and Verraes 1996) and *Clariallabes longicanda* (B). The pink surface represents the adductor mandibulae A2A3' (hypertrophied in *Clariallabes*) which almost entirely covers the suspensorium (in blue). The physiological cross-sectional area of this A2A3' of *Clariallabes longicanda* is about twice that of *Clarias gariepinus* (Herrel et al. 2002; data for *Clariallabes melas* (Boulenger, 1887)). Note that the upper part of this jaw closing muscle of *Clarias* is covered by the skull roof. A detailed view on the articulation of the suspensorium with the neurocranium is presented on the right (part A modified from Cabuy et al. 1999), illustrating the interdigitations in *Clariallabes longicanda*. *PT* pterotic, *PT-proc* pterotic process, *SPH* sphenotic, *SPH-proc* sphenotic process, *SUS* suspensorium.

If this reduced lateral expansion actually occurs in species with jaw closer hypertrophy, we further predict either a decrease in suction performance capacity or a compensation for the decrease in lateral expansion by creating a larger and/or faster ventral expansion. As the depression of the mouth floor by the hyoid apparatus is the most important ventral expansion for generating suction (Alexander, 1970b; Lauder, 1985) this compensation will most likely take place at this level. On the other hand, the hyoid also participates in lateral

expansions by pushing the suspensoria outwards when the sternohyoid musculature is contracted. If the suspensorium abduction is hindered for the above reasons, increased abduction forces exerted by the musculus sternohyoideus and m. levator arcus palatini via the hyoid onto the suspensorium can compensate for the potentially increased mechanical resistance to this movement.

In order to test the potential consequences of jaw closer hypertrophy on the cranial expansions during suction feeding in clariid catfishes, a kinematic analysis of the prey captures by two species (*Clarias gariepinus* and *Clariallabes longicauda* Boulenger, 1902) was performed. Whereas *Clarias gariepinus* has relatively small jaw closers and a relatively flat suspensorium-neurocranium articulation (Fig. 1A) *Clariallabes longicauda* has hypertrophied jaw adductors and a strongly interdigitated suspensorium-neurocranium articulation (Fig. 1B). The interspecific differences in prey capture kinematics are determined, with special emphasis to the variables of lateral expansion and hyoid movements.

6.2 Materials and methods

6.2.1 Animals

Ten adult specimens (6 Clarias gariepinus and 4 Clariallabes longicanda) were used in the experiments. The Clarias specimens were aquarium-raised specimens of which larval stages were initially obtained from the Laboratory for Ecology and Aquaculture (Catholic University of Leuven). Specimens of Clariallabes longicanda were caught in Northern Gabon. Cranial lengths of the Clarias gariepinus specimen were 44.4, 44.7, 47.5, 47.5, 51.7 and 56.6 mm. The Clariallabes longicanda individuals had cranial lengths of 32.4, 34.7, 35.7 and 49.0 mm. Cranial length (CL) was defined as the distance between the rostral tip of the premaxilla and the caudal tip of the occipital process. The animals were kept separate in 20 L test aquaria and were trained to capture the presented food inside a narrow, projecting corridor (25 cm length, 8 cm width, 15 cm water height) of the aquarium (which forced the animals to feed in a position perpendicular to the camera). The thin Plexiglas walls (2 mm) of the corridor minimised the amount of X-ray absorption during cineradiography.

To measure the properties of the sternohyoideus muscles, 3 specimens (preserved in 70% alcohol) for each species were dissected. The muscles of both sides were removed and weighed (0.0001 g). The average muscle fibre length was approximated by taking the average of lengths of the most medially positioned fibre, a central muscle fibre and the most laterally situated fibre. Muscle and muscle fibre orientation were determined from myological drawings (Adriaens and Verraes, 1997; Van Meir, 2004). The force transmission of this muscle, resulting in suspensorial abduction was calculated according to De Visser and Barel (1996) in a two-dimensional representation of their model.

6.2.2 Prey

Previous research on feeding of fishes revealed the capacity of fishes to change (modulate) the prey capture kinematics in function of the prey type (Liem, 1980; Liem, 1993; Lauder, 1981; Wainwright and Lauder, 1986; Ralston and Wainwright, 1997; Nemeth, 1997; Ferry-Graham, 1998; Ferry-Graham et al., 2001). To reduce the chance that interspecific differences are the result of differences in behavioral modulation between both species, two different prey types were used: (1) a piece of cod fillet (*Gadus morbua* Linneaus, 1758) of about 3 cm³ and (2) a North Sea shrimp (*Pandalus borealis* Krøyer, 1838). Both prey types were attached to a thin, plastic coated steel wire and were suspended about 5 cm above the bottom of the corridor. The cod was pinned onto the steel wire, while the shrimp was clipped around its middle. These prey were selected because (1) fish and crustaceans are the most abundant prey found in stomachs of wild *Clarias gariepinus* (Bruton, 1979) and also *Clariallabes longicauda* could be trained to feed on these prey, (2) the attached prey types elicit suction feeding behavior and (3) both prey clearly differ in form and attachment strength.

6.2.3 High-speed video recordings

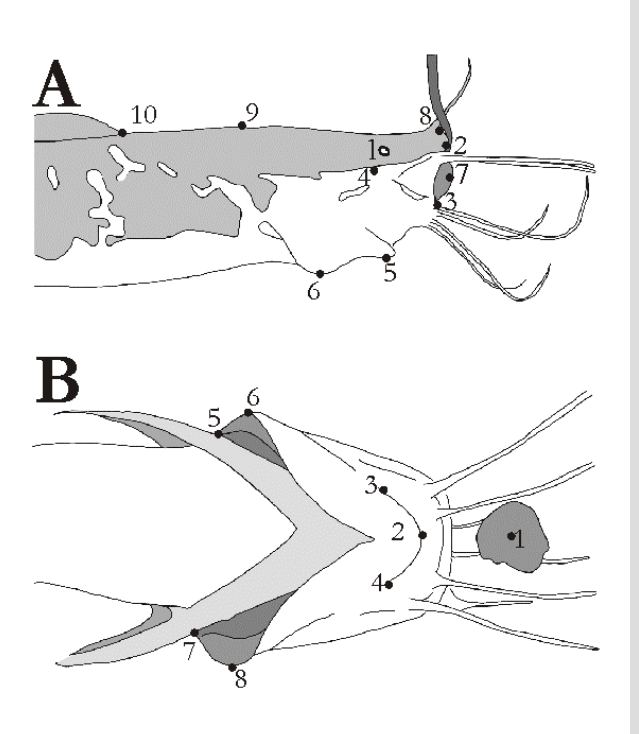


Figure 2: Anatomical landmarks digitised on the lateral (A) and ventral (B) high-speed video images of Clarias gariepinus. Identical landmarks were digitised on images of Clariallabes longicauda. A Lateral landmarks: (1) middle of the eye, (2) upper jaw tip, interior side, (3) lower jaw tip, interior side, (4) jaw articulation, (5) tip of the hyoid, (6) most ventrally positioned point of the branchiostegal membrane, (7) prey, (8) rostral tip of the skull roof, (9) caudal tip of the skull roof and (10) anterior tip of the caudal fin. The measured angular variables are: gape angle (2-4-3) and neurocranial elevation (8-9-10). The linear variables are: gape distance (2-3), hyoid depression (1-5) branchiostegal depression perpendicular distance to 8-9). B Ventral landmarks: (1) prey, (2) hyoid symphysis, (3,4) most caudally discernible points on the hyoid bars, (5,7) base of pectoral spine, (6,8) lateral tip of the branchiostegal membrane. The measured angular variable is the hyoid expansion (3-2-4). The measured linear variable is the branchiostegal expansion (distance of the segment through 6 (or 8) that intersects perpendicularly with the line through 5 (or 7) perpendicular with 5-7).

High-speed video recordings (250 frames s⁻¹) were made from a lateral and ventral position, using a Redlake Imaging Motionscope digital high-speed video camera (shutter 1/2500). Two floodlights (600 Watt) provided the necessary illumination. Only those prey capture sequences that were approximately perpendicular to the camera lens were selected and retained for further analysis. To do so, lateral recordings in which skull roof, skull bottom or origin of the maxillary barbel of the opposite side of the fish were visible, as well as ventral recordings in which the side of the skull was visible, were discarded. For each individual, 10 lateral and 10 ventral recordings (each consisting of 5 cod and 5 shrimp captures) were analysed. For one *Clarias gariepinus* individual, however, only 4 (in stead of 5) ventral recordings with cod as prey could be analysed. Anatomical points were digitised on the recorded images (Fig. 2) using Didge (version 2.2.0, Alistair Cullum), and the horizontal (x) and vertical (y) coordinates for each point were exported to a spreadsheet. To improve the accuracy of the digitisations, each point was digitised separately throughout the entire prey capture sequence.

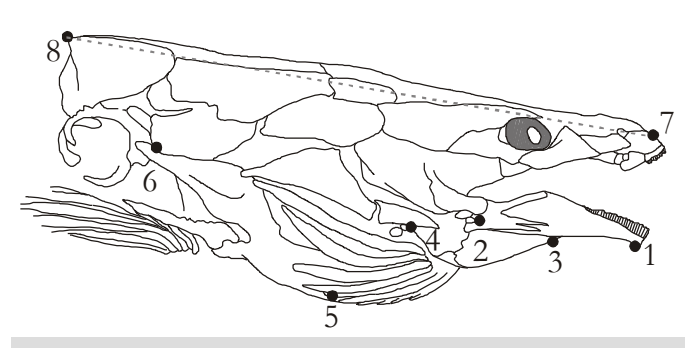


Figure 3: Positions of the radio-opaque markers used in cineradiography, as seen from a lateral view on *Clarias gariepinus* (modified after Cabuy et al, 1999): (1) rostral tip of the lower jaw, (2) the caudal tip of the lower jaw, near the articulation with the quadrate, (3) rostal and (4) caudal tip of the hyoid, (5) ventro-rostral tip of the cleithrum, (6) dorso-caudal of the cleithrum, close to the articulation with the posttemporo-supracleithrum, (7) rostral of the upper jaw and (8) caudal tip of the processus occipitalis. Points (7) and (8) are fixed neurocranium points. The dashed line represents the reference line for following angle variables; 1-2: lower jaw angle, 3-4: hyoid angle and 5-6: angle of the cleithrum.

6.2.4 Cineradiographic recordings

For two individuals of Clarias gariepinus (47.5 mm and 51.7 mm CL) and two individuals of Clariallabes longicauda (32.4 mm and 34.7 mm CL) lateral X-ray film recordings (50 frames s-1) were made on Eastman 7231 Plus-X Negative film (16 mm). Xrays were generated by a Siemens Tridoros 880 Optimatic (90 kV, 2 ms pulses). A Sirecon 2 image intensifier (17 cm diameter) with an Arriflex 16 mm ST camera (with a 70 mm lens) was placed at a distance of 1 m from the X-ray source. For each individual, 10 recordings

(5 with cod and 5 with shrimp as prey) were analysed. Before the cineradiography, small metal markers were inserted subcutaneously or into the cranial bones at specific locations using hypodermic needles (Fig. 3). During implantation of these radio-opaque markers, the animals were anaesthetised with MS222 (Sandoz). The placement of the markers was checked using dorsoventral and lateral X-ray photographs, on which also measurements of the hyoid position and length were made for both species. Cineradiographic films were

projected (Vanguard Instruments projector) on a HIPAD-digitizer, the position of each marker was digitized, and horizontal (x) and vertical (y) coordinates of each point were recorded for each frame. The coordinates were recalculated to a frame of reference moving with the neurocranium, with the horizontal axis parallel to the roof of the buccal cavity. Angles describing the position of the lower jaw, hyoid and cleithrum were measured with respect to this plane. Clockwise rotations are negative when fish are facing towards the right.

6.2.5 Kinematic variables

After digitisation of the sequences, the coordinates of each point were used to calculate the variables of interest. The kinematic plots allowed us to analyse movements of the lower jaw tip, hyoid tip, branchiostegal membrane and neurocranium on the high-speed video recordings. After data filtering (Butterworth low pass filter) and differentiation, peak velocities of jaw and hyoid movements were determined. On the cineradiographic recordings, movements of the lower jaw, hyoid, cleithrum (pectoral girdle) and neurocranium were analysed.

For the lateral high-speed video recordings, the following kinematic variables were analysed: the time (after the beginning of the mouth opening) at which (1) mouth opening, (2) hyoid depression, (3) branchiostegal depression (a) starts, (b) attains its maximal excursion and (c) ends; the displacement variables of (1) maximum gape angle (2) total hyoid depression (maximal depression minus starting position), (3) total depression of the branchiostegal membrane (maximum depression minus starting position) and (4) total neurocranial elevation; the velocity variables are (1) the maximal jaw opening velocity, (2) maximal jaw closing velocity, (3) maximal hyoid depression velocity and (4) maximal hyoid elevation velocity. Also the total duration of the entire prey capture sequence (begin mouth opening until end of recovery) was calculated from the timing variables. All timing variables of the lateral recordings are relative to the beginning of the mouth opening.

From the ventral high-speed video recordings, the following kinematic variables were analysed: the time at which (1) lateral hyoid expansion, (2) lateral branchiostegal expansion (a) starts, (b) attains its maximal excursion and (c) ends; displacements and angles including, (1) the width of the hyoids at start (angle), (2) maximal width of hyoids (angle), (3) maximal lateral expansion of the hyoids (angle, maximal width minus starting width) and (4) the lateral expansion of the branchiostegal membrane (maximal excursion minus starting position); the velocity variables of (1) average angular hyoid abduction velocity and (2) average angular hyoid adduction velocity. All timing variables of the ventral recordings are relative to the beginning of the lateral expansion of the hyoids.

Cineradiographic recordings allowed us to analyse the movements of the hyoid, the cleithrum, the lower jaw and the neurocranium. Note that there were individual differences caused by the fact that the number of discernible markers differed among individuals.

Although the same marking treatment was carried out for all of the test animals, some of the markers changed position, or were expelled from the skull between the period of marking and the recording sessions. As a result, data on hyoid movements are lacking for one *Clariallabes longicanda* individual. Marker placement was checked after each recording session.

6.2.6 Statistics

To test for effects of species and prey type on feeding kinematics, a principal components analysis (PCA) was performed on the kinematic variables of (1) the lateral high-speed video recordings and (2) the ventral high-speed video recordings. Two-way MANCOVA's were performed on the individual averages (within each prey type) of the varimax rotated principal component scores (PC-scores) of the first two principal components, with species and prey type as independent variables. After comparing the eigenvalues of the principal components with 'broken stick' values, only the first two principal components were retained for further analysis (Jobson 1992). To compensate for body size differences between the individuals, cranial length was taken as a covariate in the MANCOVA (Richard and Wainwright, 1995). Species effects were also tested univariately (ANCOVA). In that case, a sequential Bonferroni test was performed to adjust the significance level for these results. In all other cases, the significance level of P=0.05 was used. All PC-scores, as well as all kinematic variables used in (co)variance analyses were normally distributed (Kolmogorov-Smirnov test). To account for the scaling effects in interspecific comparison tests, linear displacements, angular and linear velocities were compared using two-way ANCOVA's (with cranial length as covariate). The (size-independent) angular displacement variables were compared by two-way ANOVA's. For all the analyses, the statistical package Statistica (v. 5.0, Statsoft, Tulsa) was used.

6.3. Results

6.3.1 Prey capture

The prey are captured by a combination of suction feeding and biting. In most cases, after the expansion of the skull, during which the prey is sucked towards the mouth, the jaws are placed firmly onto the prey (Fig. 4, Fig. 5). Next, the head is swung to one side, thereby tearing loose the attached pieces of food. Sometimes, when striking on a piece of cod, the suction was sufficient to draw the entire prey into the mouth. Touching of the prey with some of the barbels sometimes preceded the strike. While in most cases barbel touching was passive, occasional active touching could be discerned (one or two barbels being moved towards the prey). During prey capture, food items are approached relatively slowly. The maximum swimming speed during the strike never exceeded 0.22 m/s (N=100 including both species). As predicted for siluriforms fishes in general (Alexander, 1965), no protrusion of the upper jaws took place.

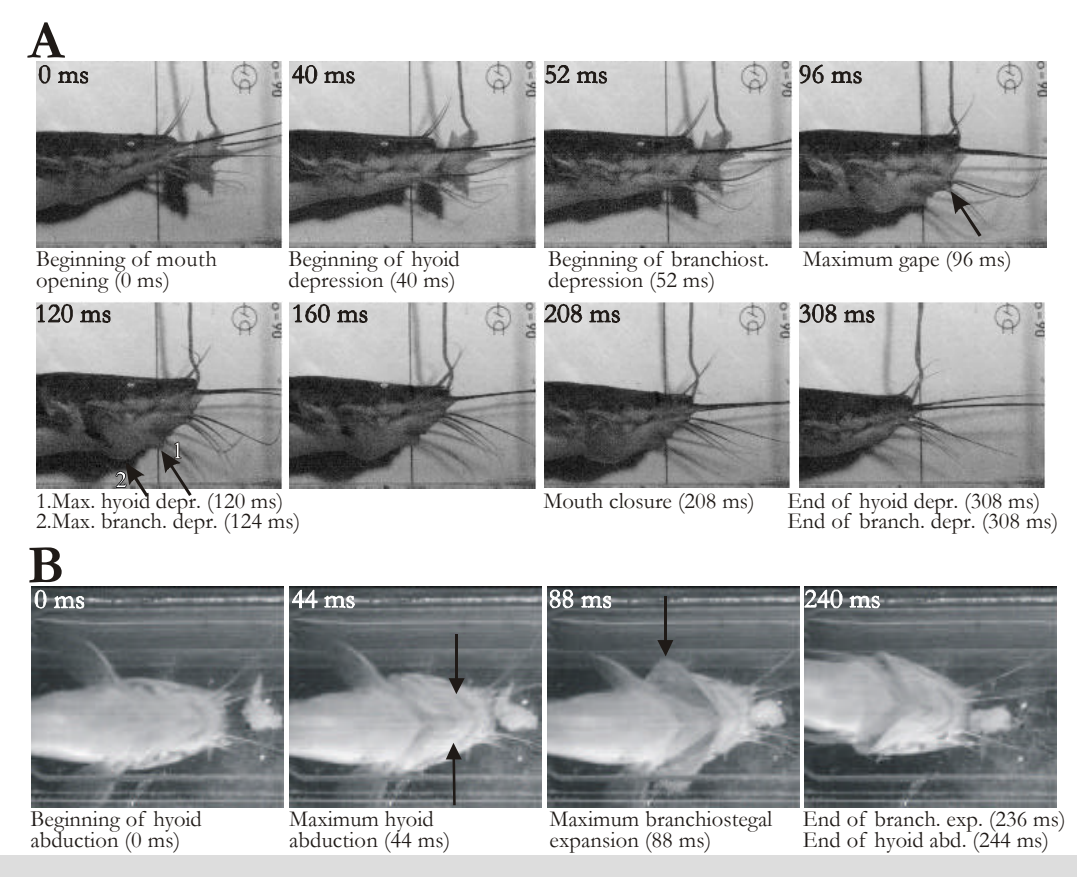


Figure 4: Selected video frames from a representative lateral (*A*) and ventral (*B*) prey capture sequence for one individual of *Clarias gariepinus* feeding on an attached piece of cod. Numbers above the frame represent time in milliseconds relative to the beginning of the mouth opening for lateral images, or the beginning of the hyoid expansion for the ventral images (time 0 ms). Below the frames, some important events are given with the exact time (between brackets) at which these took place. Arrows indicate maximal excursions of the structures indicated.

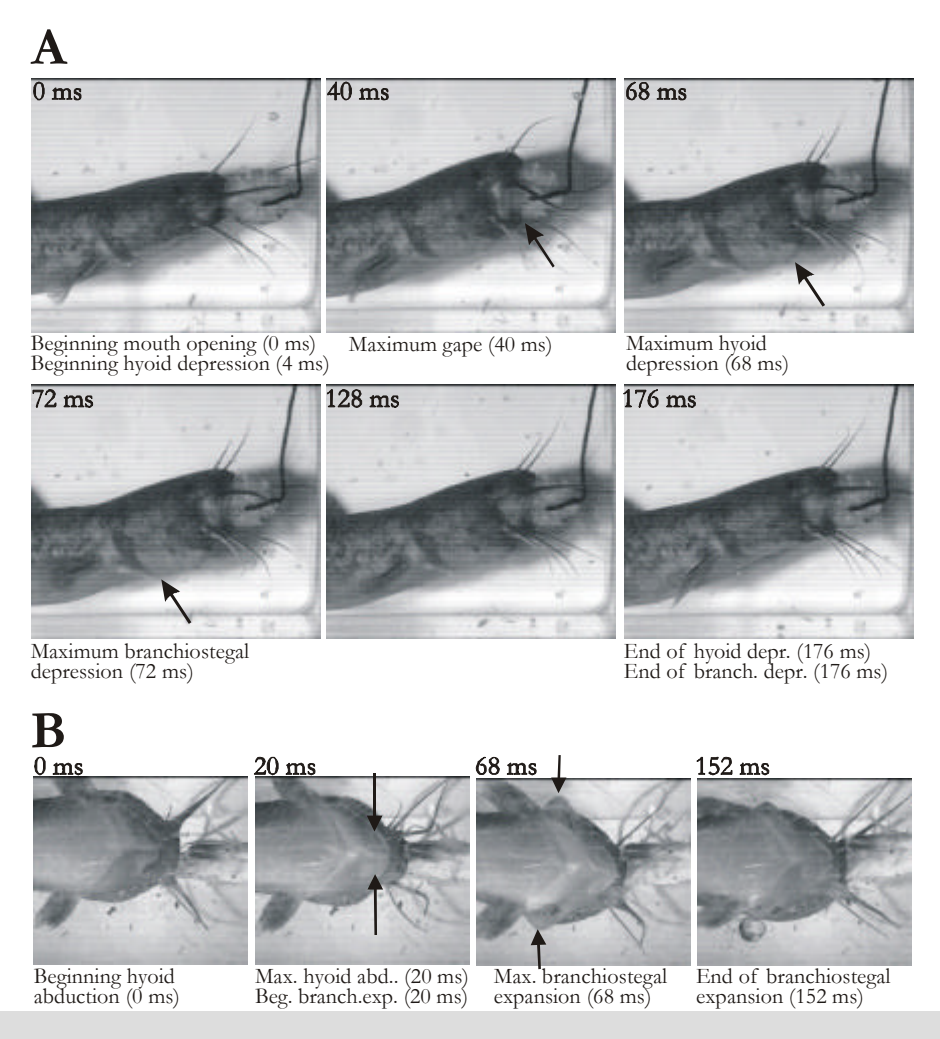


Figure 5: Selected video frames from a representative lateral (*A*) and ventral (*B*) prey capture sequence for one individual of *Clariallabes longicauda* feeding on an attached shrimp. Numbers above the frame represent time in milliseconds relative to the beginning of the mouth opening for lateral images, or the beginning of the hyoid expansion for the lateral images (time 0 ms). Below the frames, some important events are indicated with the exact time (between brackets) at which these took place. Arrows indicate maximal excursions of the structures indicated.

Both on lateral and ventral views, a rostro-caudal expansion wave is visible, which is typical for aquatic, suction feeding vertebrates (Muller and Osse, 1984; Van Leeuwen and Muller, 1984; Lauder, 1985). In *Clarias gariepinus* for example, maximum gape (on average after 75 ms) precedes maximum hyoid depression (on average after 100 ms) and maximum branchiostegal depression (on average after 110 ms) (Fig. 6). Rotation of the cleithrum (visible in the radiographic recordings) starts at the same time or shortly after the hyoid rotation. The cleithrum rotates (during retraction) -23.2 ± 1.5 degrees (mean \pm standard error) in *Clarias gariepinus* and -23.0 ± 1.3 degrees in *Clariallabes longicauda*. The opposite rotations of the hyoid and the cleithrum, by which these elements return to their initial

positions, continue after mouth closure. The ventral recordings show a clear lateral expansion of the hyoids that is shortly followed by the highly mobile branchiostegal membranes. The total duration of the prey captures (the time from the beginning of the mouth opening until the recovery of the branchiostegal expansion) is 0.225 s for *Clarias gariepinus* and 0.196 s for *Clariallabes longicauda*. *Clariallabes longicauda* tends to feed at higher maximal gapes (gape angle: $58.0 \pm 1.6^{\circ}$, gape distance: 0.179 ± 0.009 Cranial Lengths) compared to *Clarias gariepinus* (gape angle: $33.1 \pm 1.3^{\circ}$, gape distance: 0.340 ± 0.010 CL). Examples of prey capture sequences of *Clarias gariepinus* and *Clariallabes longicauda* are given in figures 4 and 5 respectively.

Prey capture kinematics of *Clarias gariepinus* and *Clariallabes longicauda* are far from stereotyped. For the same prey, individual fish show an extensive variation in the timing and magnitude of the prey capture movements. The total duration of the strike, for example, varied from 208 ms to 376 ms and from 200 ms to 456 ms for two of the *Clarias gariepinus* individuals. The maximum gape distance varied from 11.8 mm to 17.8 mm and from 10.8 to 16.2 mm for these two individuals.

This is also illustrated by the relatively large standard errors on the mean kinematic profiles of one individual (Fig 6.).

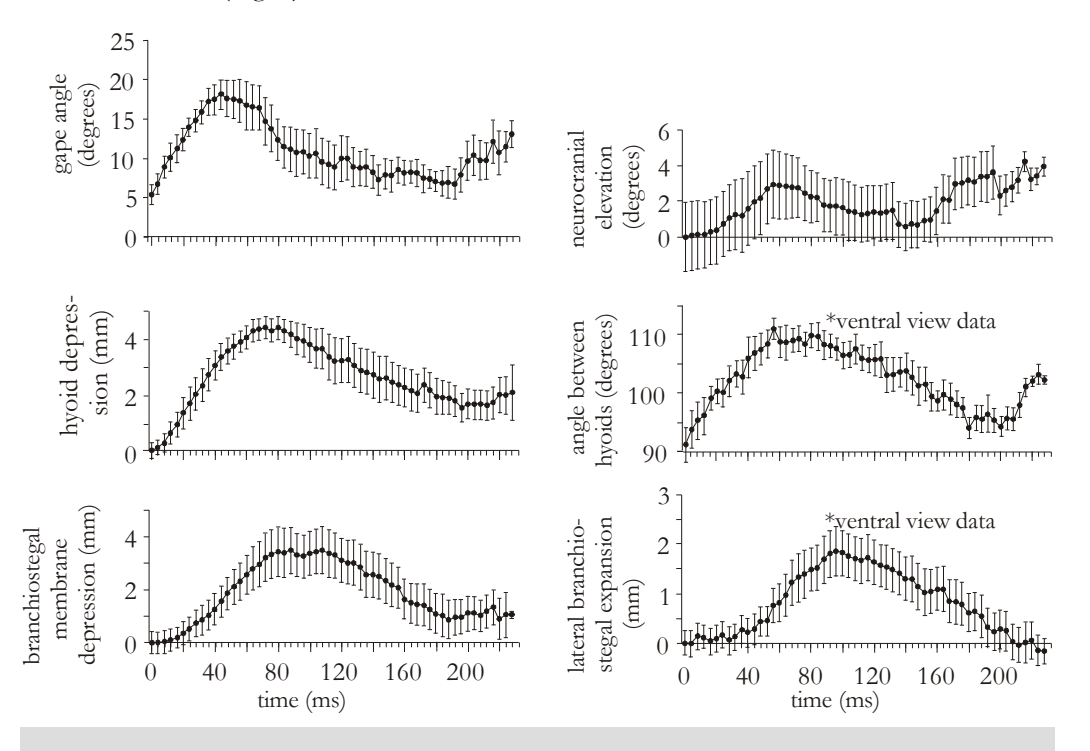


Figure 6: Mean kinematic profiles, with standard error bars, of selected kinematic variables during prey capture in one individual *Clarias gariepinus* (cranial length = 46.10 mm, total length = 182.20 mm). Ten capture events (5 fish and 5 shrimp) are included in each profile. Time zero is defined as the beginning of mouth opening.

The average neurocranial elevation is $6.3 \pm 0.8^{\circ}$ in *Clarias gariepinus* and $10.6 \pm 1.0^{\circ}$ in *Clariallabes longicauda*, although during several strikes both species reached neurocranial elevations of more than 25 degrees.

6.3.2 General interspecific comparison

To determine whether the prey captures of *Clarias gariepinus* and *Clariallabes longicauda* are kinematically distinct, the two species were compared using a principal component analysis (Fig. 7, Table 1).

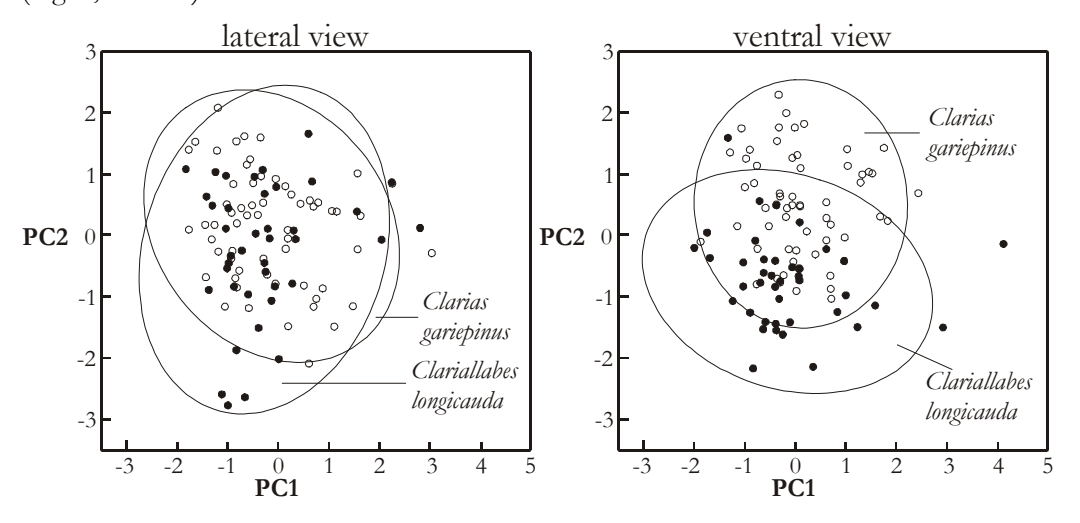


Figure 7: Plots of the principal component scores of the first two principal components (PC1 and PC2). Principal component analyses were performed on the data sets of the lateral (left graph) and ventral recordings (right graph). Principal component scores were subdivided by species (white points = *Clarias gariepinus*, black points = *Clariallabes longicauda*) and plotted with the 95% confidence limit ellipses for each species. Covariance analysis (MANCOVA) showed that *Clarias gariepinus* and *Clariallabes longicauda* do not differ significantly in lateral prey capture kinematics. However, they do differ significantly in ventral prey capture kinematics on both PC1 and PC2.

The two species do not differ significantly based on the movements observed on the lateral external images (two-way MANCOVA, Rao's $R_{2,14} = 4.02$, P = 0.26). Consequently, it is not possible to make a clear distinction between the general prey capture kinematics of both species from the lateral view data.

On the basis of the movements observed on the ventral images, however, both species do differ significantly (two-way MANCOVA, Rao's $R_{2,14} = 7.15$, P = 0.007). This difference is significant for PC1 (one-way ANCOVA, $F_{1,15} = 4.63$, P = 0.048) as well as for PC2 (one-way ANCOVA, $F_{1,15} = 13.8$, P = 0.0021). PC1 mainly represents variation in the timing of the hyoid expansion and the branchiostegal expansion, while PC2 mainly represents

variation in the starting angle between the hyoid bars and in the total dilatation of the hyoid (Table 1). Apparently, the most important differences in prey capture kinematics, by

Table 1: Results from the principal component analysis on two data sets: (a) lateral external and (b) ventral external recordings.

Lateral external			Ventral external			
	PC1	PC2		PC1	PC2	
Eigenvalue	7.85	2.46		3.59	2.48	
Percentage of total varia	ınce 46.2	14.5		32.7	22.5	
Broken stick	3.44	2.44		3.02	2.02	
Time max gape	0.804	0.283	Time max H exp	0.896	0.036	
Time end gape	0.870	0.253	Time end H exp	0.908	0.003	
Time begin H dep	0.165	0.104	Time begin B exp	0.426	0.193	
Time max H dep	0.834	0.337	Time max B exp	0.754	0.304	
Time end H dep	0.902	0.167	Time end B exp	0.793	-0.092	
Time begin B dep	0.504	0.030	Begin angle H	-0.106	-0.936	
Time max B dep	0.783	0.342	Max angle H	-0.009	-0.109	
Time end B dep	0.893	0.243	Total exp H	0.105	0.907	
Total duration	0.919	0.199	Total B exp	0.167	0.043	
Max gape	-0.036	-0.354	Average vel H exp	-0.614	0.571	
Total H dep	0.588	-0.501	Average vel H add	-0.247	0.411	
Total B dep	0.149	0.009				
Total N elev	0.059	0.121				
Peak vel M open	-0.378	-0.659				
Peak vel M closing	0.310	0.757				
Peak vel H dep	-0.278	-0.793				
Peak vel H elev	0.246	0.741				

Note. Factor loadings exceeding 0.70 are indicated in *bold. B* Branchiostegal membrane, *dep* depression, *elev* elevation, *exp* expansion, *H* hyoid, *max* maximum, *N* Neurocranium, *M* mouth, *vel* velocity.

which it is possible to distinguish prey captures of both catfish species, are the lateral movements of the hyoid bars seen from the ventral view. Indeed, Clariallabes longicauda has larger hyoid angles at the start of the prey capture sequence $(101.0 \pm 1.1^{\circ} vs. 86.4 \pm$ 1.2° for Clarias) and showed less lateral expansion of the hyoid $(19.0 \pm 1.2^{\circ} vs. 31.1 \pm$ 1.2° for Clarias) (Table 2).

6.3.3 Lateral expansions

As mentioned, Clariallabes longicauda shows less lateral expansion during suction feeding compared to Clarias gariepinus. This lateral expansion was measured by the increase in the angle between the hyoid bars (also referred to as the dilatation or widening of the hyoid) during the expansive phase of the feeding event. The average hyoid dilatation is reduced in Clariallabes longicauda (19.0 \pm 1.2°) compared to Clarias gariepinus (31.1 \pm 1.2°) (Table 2). The maximal observed values for lateral expansions are also lower in Clariallabes longicauda (41.2° vs. 51.2° for Clarias gariepinus). In Clariallabes longicauda, the hyoid starts its lateral expansion on average with a larger angle between the hyoid bars (101.0 \pm 1.1° vs. 86.4 \pm 1.2° for Clarias gariepinus, see Table 2), but merely reaches similar maximal angles (119.9 \pm 1.1° vs. 117.6 \pm 0.8° for Clarias gariepinus). The average velocities of hyoid abduction (as well as adduction velocities) tend to be larger in Clarias gariepinus (Table 2). As the dilatation of the hyoids is directly coupled to the abduction of the suspensoria, and given the configuration of the hyoids at the starting position of the feeding event, the larger and faster abduction of the hyoids can be translated into a larger and faster suspensorium abduction.

6.3.4 Hyoid movements

The hyoid movements for both species, analysed from lateral and ventral views, are compared in Table 2. For a given skull size, a more extensive lowering of the mouth floor by the hyoid is observed in Clariallabes longicauda (0.210 \pm 0.001 Cranial Lengths) compared to Clarias gariepinus (0.152 \pm 0.006 CL). The speed by which the hyoid depression lowers the mouth floor is also larger in Clariallabes longicauda. The cineradiographic recordings show angular depressions of the hyoid that start shortly after the beginning of the lower jaw depression (also observed for larval Clarias gariepinus by Adriaens et al., 2001). In Clarias gariepinus, the hyoid starts its rotation in most cases (17 out of 20) slightly elevated (12 \pm 2.2°) with respect to a plane parallel to the roof of the buccal cavity (Fig. 3) and shows an average rotation of -55.6 \pm 2.6 degrees. In Clariallabes longicauda, the hyoid starts its rotation parallel with the roof of the buccal cavity (0.0 \pm 2.5°) and rotates on average –49.8 \pm 3.5 degrees. The maximal angle of hyoid depression is on average larger in Clariallabe longicauda (49.8 \pm 3.3° vs. 43.3 \pm 2.8° in Clarias gariepinus).

Table 2: Interspecific comparison of the hyd	oid movements			
	Clarias gariepinus	Clariallabes longicauda	statistics (A or Ac) ^c	P
Lateral (high-speed video)				
Average hyoid dep. (CL)	0.152 ± 0.006	0.210 ± 0.001	Ac, $F_{1,15} = 4.63$.048
Maximal hyoid dep. (CL)	0.26	0.33	Ac, $F_{1,15} = 4.45^{\text{a}}$.049
Mean peak velocity of hyoid dep. (CL/s)	2.77 ± 0.13	5.56 ± 0.40	Ac, $F_{1,15} = 7.77$.014
Maximal peak velocity of hyoid dep. (CL/s)	5.69	12.38	Ac, $F_{1,15} = 5.77^{\text{a}}$.030
Mean peak velocity of hyoid elev. (CL/s)	1.79 ± 0.09	2.46 ± 0.21	Ac, $F_{1,15} = 1.87$.19
Maximal peak velocity of hyoid elev. (CL/s)	3.82	7.42	Ac, $F_{1,15} = 1.02^{a}$.33
Lateral (cineradiographic film)				
Average starting angle hyoid (°) ^b	12.2 ± 2.2	0.0 ± 2.5	A, $F_{1,2} = 11.5$.077
Average peak angle hyoid (°) ^b	-43.3 <u>+</u> 2.8	-49.8 ± 3.3	A, $F_{1,2} = 1.69$.32
Maximal peak angle hyoid (°) ^b	-62.5	-70.3	A, $F_{1,2} = 4.33^{\text{a}}$.17
Average total rotation hyoid (°)	-55.6 ± 2.6	-49.8 ± 3.5	A, $F_{1,2} = 12.7$.071
Ventral (high-speed video)				
Average starting angle hyoids (°)	86.4 ± 1.2	101.0 ± 1.1	A, $F_{1,16} = 20.9$.00031
Average peak angle hyoids (°)	117.6 ± 0.8	119.9 ± 1.1	A, $F_{1,16} = 1.50$.024
Average hyoid dilatation (°)	31.1 ± 0.8	19.0 ± 1.2	A, $F_{1,16} = 20.2$.00037
Maximal hyoid dilatation (°)	51.2	41.2	A, $F_{1,16} = 10.3^{\text{a}}$.0055
Average abduction velocity (°/s)	404 <u>+</u> 22	347 ± 38	Ac, $F_{1,15} = 6.46$.00226
Maximal abduction velocity (°/s)	943	1146	Ac, $F_{1,15} = 6.00^{\text{a}}$.027
Average adduction velocity (°/s)	315 ± 25	232 ± 21	Ac, $F_{1,15} = 8.87$.0094
Maximal adduction velocity (°/s)	1251	602	Ac, $F_{1,15} = 4.30^{\text{a}}$.056
^a Individual maxima for both prey types inclu	Significant P values after sequential Bon-			
^b angle with respect to the roof of the buccal	ferroni adjustement are indicated in <i>bold</i> .			
$^{\circ}$ A = ANOVA, Ac = ANCOVA	CL = cranial length			
dep. = depression, elev. = elevation		$^{\circ}$ = degrees		

6.4 Discussion

Several studies have proposed that the anatomical changes enhancing biting forces could decrease the amount of suction (Barel, 1983; De Visser and Barel, 1996; De Visser and Barel, 1998; Bouton et al., 1999; see also Ferry-Graham et al., 2001). Fishes whose jaw apparatus is highly specialised for biting are distinct in many aspects of their cranial morphology (e.g. Barel 1983) and muscle activity patterns during feeding (Alfaro et al., 2001) from fishes that only use suction feeding. This indicates a potential incompatibility of optimising both functions. Furthermore, recent models have suggested a functional trade-off between biting and suction performance mediated by modifications of the hyoid apparatus (De Visser and Barel, 1996; De Visser and Barel, 1998). In these studies, it is argued that cichlid fishes that are able to produce high biting forces cannot have the left and right hyoid bars close to one another medially. In this condition in which the hyoid bars include only a small angle, the depression of the hyoid apparatus initially causes no outward rotation of the suspensorium, suction is presumed to be most efficient. However, no experimental data have yet demonstrated these predictions. It is also unknown if the same architectural differences in the cranial system are present in other groups of fishes besides cichlids. Although never mentioned in literature, the morphological differences between species with and without jaw adductor hypertrophy illustrated in figure 1 can also have a direct effect on suction feeding mechanics by limiting lateral expansion of the buccal cavity. In the present study, we tested whether the increase of the jaw closing muscle dimensions combined with fortifications of the connection of the suspensorium to the neurocranium reduce the potential for lateral expansion of the buccal cavity in clariid catfishes.

6.4.1 Differences in lateral expansion

As predicted, the lateral expansion capacity is reduced during suction feeding in the species with hypertrophied jaw closers (*Clariallabes longicanda*) compared to the species without this hypertrophy (*Clarias gariepinus*). Most likely, this effect is caused by the striking morphological differences illustrated in figure 1. The presence of an increased jaw muscle mass covering a large part of the side of the skull, combined with the reinforced articulation of the suspensorium with the neurocranium, apparently has consequences on the buccal expansion mechanics during suction feeding in these clariid catfishes.

The average speed of dilatation of the hyoid apparatus, which is directly coupled to the lateral expansions, is also reduced in the species with the jaw adductor hypertrophy (Table 2). We suggest that this reduced abduction velocity is caused by the enlarged adductor muscles, rather than by the interdigitating bony processes at the suspensorial articulation surface. Given the visco-elastic nature of the jaw closers and the fact that this muscle extends beyond the boundaries of the suspensorium, deformation of this muscle mass as a result of suspensorium abduction will have a speed-reducing effect on this movement. On

the other hand, the "locking" of the suspensorial articulation through interdigitation processes would probably only limit the maximal rotation capacity of the suspensorium presumably without interfering with the speed of expansion. Notably, also the opposite movement, the adduction of the hyoid bars and consequent adduction of the suspensorium, has a reduced average velocity in *Clariallabes longicanda* compared to *Clarias gariepinus* (Table 2).

6.4.2 Abduction Forces

The hyoid apparatus plays a crucial role in the expansive phase of the suction feeding event, not only because of its contribution to the depression of the mouth floor and (indirectly) to the opening of the mouth, but also because it participates in the lateral expansion of the oral cavity (i.e., suspensorium abduction) (Lauder, 1985; Aerts et al., 1987; Aerts, 1991; De Visser and Barel, 1996). Contraction of the sternohyoideus muscle results in retraction and depression of the hyoid and produces important passive reaction forces at the level of the interconnection of the hyoid with the suspensorium. It is commonly assumed that during strenuous activities such as suction feeding the abduction forces originate mainly from the hyoid (Alexander, 1970b; Aerts, 1991). Therefore, the position of the hyoid is an important determinant of the distribution of the expansive forces over the expansion movements (De Visser and Barel, 1996).

When comparing the shape and the position of the hyoid apparatus of *Clarias gariepinus* and *Clariallabes longicauda*, we expect larger abduction forces to be transmitted by the hyoid onto the suspensorium in the latter species (Fig. 8). The starting configuration of the hyoids, as well as the orientation of the rotation axis of the suspensorial plane differ between both species. *Clariallabes longicauda* has a broader hyoid with a larger angle between the hyoid bars $(87.1 \pm 4.0^{\circ} \text{ vs. } 70.7 \pm 3.3^{\circ} \text{ in } \text{ Clarias gariepinus})$ and a rotation axis of the suspensorial plane that is more parallel to the mediosaggital axis of the skull $(12^{\circ} \text{ vs. } 17^{\circ} \text{ in } \text{ Clarias gariepinus})$. Both features contribute to a larger angle between the hyoid bars and the suspensorial rotation axis and by this means also to an increased transmission of the retraction force of the hyoids to forces resulting in suspensorial abduction (Fig. 8).

Not only the transmission of forces from the hyoid onto the suspensorium is expected to be larger in *Clariallabes longicauda*, but also the retraction forces itself (F_{EH} in Fig. 8). When comparing the properties of the sternohyoideus muscle, the muscle that retracts the hyoid (Table 3), a considerably higher muscle mass is found for *Clariallabes longicauda* compared to *Clarias gariepinus*. Even though the sternohyoideus muscle fibres are slightly longer and on average more inclined (Table 3), the over 4 times higher mass of this muscle (for a given skull length) will cause a more forceful retraction of the hyoid (during sternohyoideus activity) for this species (effective physiological cross section of 33.1 10-6 CL² vs. 8.6 10-6 CL² for *Clarias gariepinus*).

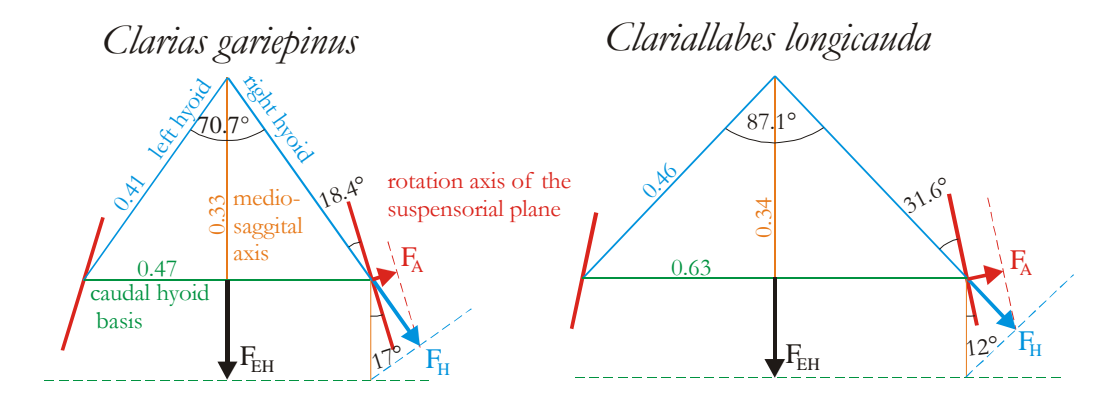


Figure 8: Schematic planar representation of the hyoid's starting configuration (blue lines) and the interconnection with the suspensorium (red lines represent the rotation axis) from a dorsoventral view in *Clarias gariepinus* and *Clariallabes longicauda*. Specific distances (in cranial lengths) and angles are given for both species. For a given expansion force in the hyoid plane (F_{EH} , black arrow), the force component along the hyoid (F_{H} , blue arrow) and the force resulting in suspensorial abduction (F_{A}) are shown. In *Clariallabes longicauda*, F_{A} at the beginning of the hyoid retraction is expected to be about 40% higher compared to *Clarias gariepinus* (see also Table 3).

Table 3: Properties of the sternohyoideus muscles of *Clarias gariepinus* and *Clariallabes longicauda*. All values are represented in cranial lengths (CL) to enable the comparison. Effective physiological cross-section = $\max x \cos(\text{fibre inclination})/\text{fibre length}$.

	Mass	Average fibre	Average muscle fibre	Effective physiological
Species	$(10^{-6} \text{ CL}^3)^a$	length (CL) ^a	inclination (degrees) ^b	cross-section (10 ⁻⁶ CL ²)
Clarias gariepinus	2.4 ± 0.2	0.267 ± 0.01	13.5	8.6
Clariallabes longicauda	10.6 ± 1.9	0.292 ± 0.09	23.9	33.1

 $^{^{}a}N = 3$

As the abduction forces exerted by the hyoid onto the suspensorium are thus larger in the species with the reduced lateral expansion (*Clariallabes longicauda*), this difference cannot be explained by differential abduction forces. This result further strengthens the notion that the lateral expansions are constrained or counteracted by structures increasing the mechanical resistance to this movement.

6.4.3 Compensating effects on buccal expansions

A reduced lateral expansion does not necessarily imply a reduced suction feeding efficiency. The observed decrease in the magnitude and the velocity of the lateral

^b Angle with respect to the mediosagittal axis of the skull, which represents the line of action of the sternohyoideus

expansion in *Clariallabes longicauda* compared to *Clarias gariepinus* can be compensated for by more extensive and faster ventral expansions (lowering of the floor of the mouth). This would not be surprising, as the simultaneous lateral expansion of the hyoid and the ventral lowering of the mouth floor by the hyoid causes a mechanical trade-off between lateral en ventral buccal expansions. If there is no lateral expansion, the hyoid apparatus will maintain its initial configuration. In that case, its full mediosagittal length can contribute to the lowering of the mouth floor. The other extreme would be a lateral expansion that abducts the hyoid apparatus so that both hyoid bars lie in each other's extensions. In that case, there will be no hyoid depression at all (see also Diogo and Chardon, 2000).

As expected, the reduced dilatation of the hyoids in Clariallabes longicauda (19.0 \pm 1.2° vs. $31.1 \pm 1.2^{\circ}$ for *Clarias gariepinus*) goes along with a more extensive depression of the mouth floor by the hyoid $(0.210 \pm 0.001 \text{ cranial lengths})$ (CL) vs. 0.152 ± 0.006 CL for Clarias gariepinus). However, the difference in mouth floor depression is too large (38%) to be explained solely by the differences in hyoid dilatation. If the hyoid apparatus with initially a similar mediosagittal length (0.33 \pm 0.02 CL in C. gariepinus and 0.34 \pm 0.03 CL in C. longicauda) is dilated as observed (Table 2) and equally depressed to an angle of -45 degrees (relative to the roof of the buccal cavity), an increase of only 7% in mouth floor depression can be expected. Therefore an additional factor, besides this mechanical consequence of the reduced hyoid dilatation, must have contributed to the increased mouth floor depression by the hyoid in Clariallabes longicauda. This factor most likely involves an increased angular depression of the hyoid apparatus. Indeed, the cineradiographic data point out that the hyoid is depressed to larger angles with respect to the roof of the skull in C. longicauda compared to C. gariepinus. The combined effect of the reduced shortening of the hyoid by lateral expansions and an increased angular depression of the hyoid can cause substantially larger mouth floor depressions.

Suction in fishes implies the generation of a water flow into the mouth cavity. Consequently, suction feeding performance can be estimated by two variables: (1) the total volume of the water drawn into the buccal cavity, which is related to the magnitude of buccal expansions, and (2) the velocity of the water entering the mouth, which is related to the rate of expansion of the buccal cavity and the size of the oral aperture (Muller et al., 1982; Van Leeuwen and Muller, 1984; Wainwright et al., 2001). As mentioned, the reduced magnitude of the lateral expansions are (at least partly) compensated for by the larger depression of the mouth floor by the hyoid. Yet, as *Clariallabes longicanda* also has a reduced average velocity of this lateral expansion (see Table 2), this can still result in a reduced velocity of the water sucked in. Moreover, *Clariallabes longicanda* feeds using larger maximal gape distances (0.340 \pm 0.010 CL vs. 0.179 \pm 0.009 CL for *Clarias gariepinus*), which also reduces the speed of water inflow. Therefore, the observed higher peak velocity of hyoid depression in *Clariallabes longicanda* (see Table 2) will be of great importance to preserve a sufficient speed of the water entering the mouth.

6.4.4 Conclusion

Buccal expansions during suction feeding clearly differ between the species without hypertrophied jaw adductors (Clarias gariepinus) and the species with hypertrophied jaw adductors (Clariallabes longicauda). The predicted consequence (i.e. the reduced lateral expansion in the species that exhibits these enlarged adductors) is confirmed, even despite the fact that the abduction forces exerted by the hyoid onto the suspensorium are larger in this species. The reduced lateral expansion is compensated for by a more extensive and faster lowering of the mouth floor by the hyoid. Therefore, the results of the present study support the notion that features of the cranial system in favour of an increased biting force (larger adductor muscles, stronger bony connections between skeletal elements) will have consequences on suction feeding mechanics (though not necessarily on suction feeding performance). Thus, morphological specialisation has consequences on other functions performed by the same system, as the same structures have to participate in different functions (e.g., prey capture, swallowing, aquatic respiration, air breathing). In other words, changing the features of one of the components of the system can alter the mechanics of several, structurally coupled functions of this system. Not only effects on prey capture mechanics, but also on other functions performed by the complex cranial system, such as aquatic respiration and air breathing can be expected. Air breathing catfishes (Clariidae), exhibiting a rich structural diversity, are particularly suitable to investigate the effects of variation in morphology (degree of jaw adductor hypertrophy) in a complex integrated system (cranial musculo-skeletal apparatus of teleost fish).

Chapter

No trade-off between biting and suction feeding performance in clarifd catfishes

Sam Van Wassenbergh – Anthony Herrel – Dominique Adriaens – Peter Aerts

Submitted to Functional Ecology

Summary

It is generally assumed that biting performance trades off with suction performance in fish because both feeding types may place conflicting demands on the cranial musculo-skeletal system. However, the functional consequences of morphological adaptations enhancing biting on the mechanics and performance of suction feeding in fish remain obscure. In this study, suction feeding performance was compared between three clariid catfish species differing considerably in their biting capacity, by measuring the velocity of a standardized prey being sucked into the buccal cavity using high-speed cineradiogaphy. In addition, buccal volume changes during prey capture were quantified by ellipse modelling. As all species were able to accelerate the prey to similar peak velocities, our results demonstrate the possibility for catfishes to increase bite performance considerably without compromising in suction performance. The amount of buccal expansion in the ventral direction is approximately equal for all species. Consequently, the system generating expansion through ventral rotation of the lower jaw, hyoid and pectoral girdle is apparently not constrained (mechanically or architectonically) by the hypertrophy of the jaw adductors. Although the less important lateral expansion, however, reduces, the effect of this on suction performance in Clariidae appears to be negligible.

7.1 Introduction

Evolution towards optimal performance is prevented whenever two ecologically relevant functions require opposing biomechanical or physiological adaptations (Stearns, 1992). Such evolutionary trade-offs are often observed in case certain components of the musculo-skeletal system have to participate in different functions: a certain change in one aspect of the system increases the performance of a given function, but at the same time may reduce the organism's efficiency in performing an other, morphologically coupled function (e.g., Vanhooydonck and Van Damme, 2001; Van Damme et al., 2002; Pasi and Carrier, 2003; Schondube and Del Rio, 2003). Identifying such conflicts in the performance of ecologically relevant functions is basic to our understanding of the evolutionary processes associated with species radiations. Furthermore, analyses on the constraints on the compatibility of functions may provide insight into the ecological potential (potential niche width) of animals (Barel, 1983).

One of the most striking examples of a complex and integrated system that has to fulfil a large number of crucial biological functions is probably the cranial musculo-skeletal system of fishes (Liem, 1980). It has to cope with capturing, processing and transporting prey, breathing water or air, participating in sensory perceptions, providing protection for the major sense organs and brains, and serving as a streamlined bow in locomotion. Logically, each of these functions calls for specific, structural and dynamical requirements to the animal's cranial system.

Different functional aspects can also be distinguished within the process of prey capture: prey can either be caught by suction feeding (generating of flow of water that drags the prey towards and into the mouth) and/or by biting (e.g., scraping algae or picking molluscs off the substrate with the oral jaws). It is hypothesised that biting a prey or sucking it directly into the mouth are two functionally conflicting ways of getting food into the buccal cavity (Barel, 1983; Bouton et al., 1999; Sibbing and Nagelkerke, 2001). It is therefore assumed that suction feeding and biting can be combined only to a certain extent, and at certain costs. This hypothesis appears to be supported by the observation that specialized biters usually possess other anatomical, functional, dietary, and behavioural features that distinguish them from species that rely primarily upon suction feeding to capture prey (Alfaro et al., 2001).

However, many fish species still seem to combine biting and suction seemingly efficiently (Turingan and Wainwright, 1993; Bouton et al., 1998; *Chapter 6*; Janovetz, 2005), and to our knowledge, no experimental study has yet directly demonstrated the proposed inverse relationship between biting and suction performance (see Bouton et al., 1998). Consequently, the underlying biomechanical basis responsible for the proposed conflicting demands on the oral jaw apparatus (for biting) and the buccal expansion apparatus (for suction feeding) remains to be demonstrated.

In this paper, suction performance is quantified and compared between species of air-breathing catfish (Clariidae) that differ in bite performance. In this group of fishes, hypertrophy of the jaw adductors is a derived feature that has evolved at least four times independently (Jansen et al., 2006) and is associated with a drastic increase in maximal bite force (Herrel et al., 2002) and a larger proportion of hard prey (mainly coleopterans) in the diet (Huysentruyt et al., 2004). Nevertheless, our observations have shown that even the species with the most extreme jaw adductor hypertrophy still apply considerable buccal expansion before impacting the jaws onto the prey and manage to drag relatively large prey into the mouth by suction. As suction feeding behaviour is thus maintained despite the considerable increase in bite performance, this group of fishes provides a unique opportunity to test the proposed trade-off between suction and biting performance in a number of evolutionary lineages. It also allows us to examine the biomechanical consequences of the morphological variation associated with increasing bite performance on the kinematics of buccal cavity expansion.

7.2 Materials and Methods

7.2.1 Species, morphology, phylogeny and bite performance

According to a recent molecular phylogenetic study (Jansen et al., 2006), species with eellike bodies, hypertrophied jaw adductors and a narrow skull roof have arisen at least four times independently within the Clariidae. Each time, a sister group relation with a non-specialized *Clarias*-like ancestor is observed. In this study, we focus on two lineages from which three clariid species were selected (Fig. 1): *Clarias gariepinus* (Burchell 1822), *Gymnallabes typus* (Günther 1867) and *Channallabes apus* (Günther 1873).

The neurocranium of *C. gariepinus* forms a broad, closed roof that partly covers the relatively small jaw adductor muscles (Cabuy et al., 1999). Its overall cranial morphology resembles that of *Heteropneustes fossilis*, which can be considered as a sister species of Clariidae (Agnese and Teugels, 2005; Diogo, 2005; Jansen et al., 2006). Biomechanical modelling has shown that the maximal bite forces that can be exerted by *C. gariepinus* are considerably less compared to the species with jaw adductor hypertrophy (Herrel et al., 2002; Fig. 1). Yet, *C. gariepinus* has a broad diet, which not only includes relatively soft prey such as insect nymphs, fish and shrimps, but also harder prey such as crabs, beetles and snails (Bruton, 1979). While this species shows different kinds of foraging behaviours, including bottom feeding, surface feeding or group hunting, prey are generally captured by a combination of suction feeding and biting (Bruton, 1979; *Chapter 6*). The individuals used in the experiments (see further) were either aquarium-raised specimens obtained from the Laboratory for Ecology and Aquaculture (Catholic University of Leuven, Belgium) or specimens obtained from aquacultural facilities (Fleuren and Nooijen BV, Someren, The Netherlands).

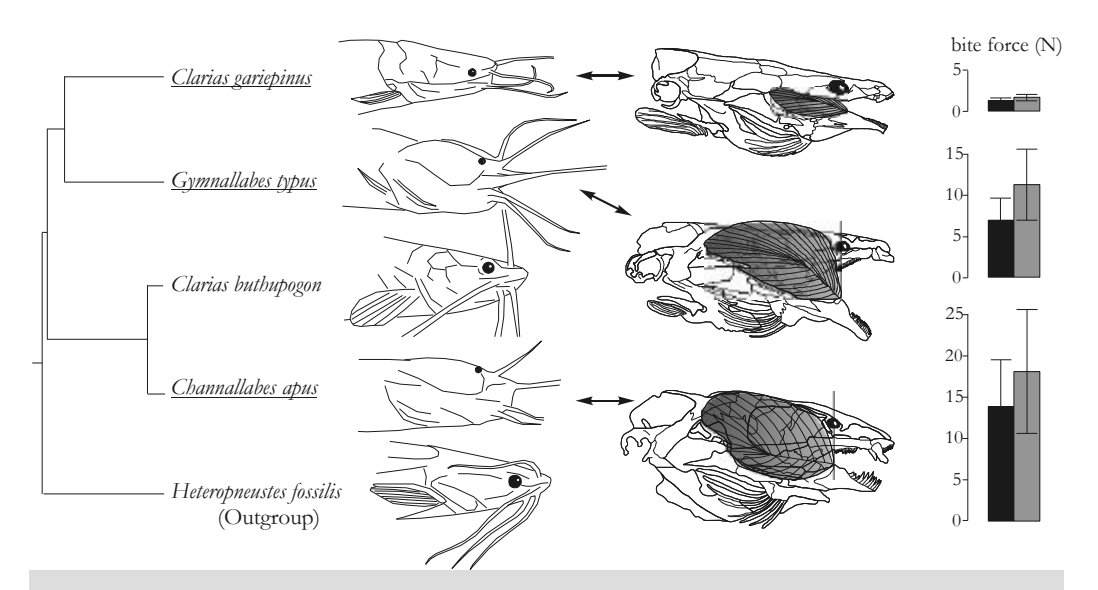


Figure 1: Partial phylogeny of Clariidae based on the consensus tree of several analyses on ribosomal DNA sequences presented in Jansen et al. (2006) indicating the species studied (Clarias gariepinus, Gymnallabes typus and Channallabes apus). Illustrations of the external head morphology (left column of drawings) showing the closed skull roofs of C. gariepinus, Clarias buthupogon and the outgroup sister species of Clariidae Heteropneustes fossilis, as opposed to the hypertrophied jaw adductors in G. typus and C. apus that fill up a large part of the head behind the eyes. This jaw adductor hypertrophy has evolved four times independently in Clariidae, of which only two lineages are illustrated here. The jaw adductors imposed on osteological drawings of the head (right column of drawings) for the three species studied clearly illustrate the jaw muscle hypertrophy in G. typus and C. apus compared to the relatively slender jaw muscles of C. gariepinus, which are partly covered by neurocranial bones. The graphs give the maximal bite force (perpendicular to the lower jaw) at the posteriormost teeth (black bars) and anteriormost teeth (grey bars) of animals with a cranial length scaled to 39 mm and at a gape angle of 10 degrees as calculated by Herrel et al. (2002).

In contrast with *C. gariepinus*, *G. typus* and *C. apus* have bulging, hypertrophied, jaw adductors and a narrow skull roof (Cabuy et al., 1999; Devaere et al., 2001; Devaere et al., 2005). This increase in jaw muscle size, the reduction of the bony skull roof, and the development of the more anguilliform body is the result of independent, convergent evolution in these two species (Agnese and Teugels, 2005; Jansen et al., 2006; Fig. 1). Except for the height of the corronoid process and the cross-sectional area of the jaw muscles (which both are larger in *C. apus*), the lever-system for jaw closing is remarkably similar in these two species with jaw adductor hypertrophy (*Chapter 5*). Additionally, bite performance in *G. typus* and *C. apus* is remarkably higher compared to *C. gariepinus* (Fig. 1). This appears to be reflected in the diet, with the species with jaw adductor hypertrophy exhibiting a special preference for coleopterans (Huysentruyt et al., 2004). *G. typus* individuals were commercially imported from the West of tropical Africa (exact location unknown), while *C. apus* were wild-caught in Northern Gabon.

7.2.2 Quantifying suction performance

The velocity and travel distance of a standardised prey that is sucked into the buccal cavity is measured using high-speed X-ray videos. These prey were spherical, 6 mm diameter pieces of meat from boiled North Sea shrimp. In order to visualise the position of the centre of the prey, a small, steel marker was inserted into the middle of each prey. These prey were attached loosely on the tip of a blunt-tip needle so that very little force is needed to release the prey from the needle. The prey-loaded needles were placed horizontally at the end of a narrow, projecting corridor (25 cm length, 8 cm width, 15 cm water height) of the 20 l test aquaria in which the catfish were trained to capture food. The thin Plexiglas walls (2 mm) of the corridor minimised the amount of X-ray absorption. X-ray videos (250 frames per second) were recorded using a Philips Optimus M200 X-ray generator coupled to a 14-inch image intensifier and a Redlake Motion Pro camera.

Although the standardised prey are relatively small, results from a previous study on prey capture kinematics (Van Wassenbergh et al., 2005) indicate that *C. gariepinus* does not reduce its suction effort while capturing this type of prey during the recording of X-ray videos compared to, for example, firmly attached shrimps (Fig. 2). Note that these shrimps often forced our catfish to perform several attempts to detach a single prey by

suction. Also for *G. typus* and *C. apus*, no modulation of prey capture kinematics in function of size, shape or attachment strength could be discerned (*Chapter 9*). Consequently, although a certain amount of strike-to-strike variability will inevitably occur (*Chapter 9*), there is no reason to assume that our experimental prey may have elicited submaximal suction performance.

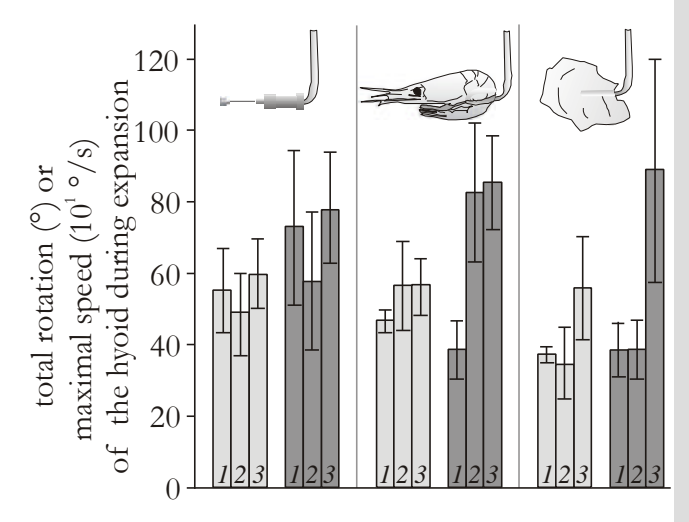


Figure 2: Comparison of the average magnitude of rotation (light gray) and average peak velocity of hyoid depression (dark gray) for three C. gariepinus individuals (bar labels) capturing three different prey (illustrated on the top of the graph) during X-ray video recording (kinematic data from Chapter 2). The graph shows that suction effort on the relatively small, spherical prey attached on the tip of a needle (left hand side of the graph) is not reduced compared to suction feeding sequences on firmly attached prey (shrimp; middle part of the graph) or large, voluminous prey pieces (fish; right hand side of the graph). N = 10, 5 and 5 for the three prey respectively (for each individual). Error bars denote standard deviations.

Prey captures were recorded for six individuals (3 C. gariepinus with cranial lengths of 70.2, 74.5 and 94.1 mm; 1 *G. typus* of 22.0 mm and 2 *C. apus* of 24.5 and 26.0 mm cranial length) in lateral view (10 sequences per fish analysed) and dorsoventral view (5 sequences per fish analysed). Only prey capture sequences that were approximately perpendicular to the camera lens were retained. The prey marker, the rostral tip of the upper jaw and three additional points equally distributed along the roof of the buccal cavity (for lateral view Xray videos) or along the medial axis of the head (for ventral view X-ray videos) were digitised frame-by-frame using Didge (version 2.2.0, Alistair Cullum, Creighton University, Omaha, USA). The position of the origin (upper jaw tip) and the inclination of an orthogonal frame of reference moving with the neurocranium were calculated. Leastsquares linear regression of the four landmarks on the line of reference (buccal cavity roof or medial line) determined the slope of the X-axis. Next prey positions were recalculated in the fish-bound frame of reference. In order to reduce digitisation noise, a fourth-order, zero phase-shift Butterworth low-pass filter was applied to the data, with cut-off frequencies adjusted according to the duration of the prey transport. Finally, three-point floating averages divided by the time between two consecutive frames (0.004 s) yielded velocities in the direction of the X and Y axes.

Prey velocities were expressed in the fish-bound frame of reference, primarily because of simplicity: this enables us, for example, to display prey trajectories and plots of prey velocity versus prey position with respect to the fish (see further). Note, however, that differences in the swimming velocity of the fish towards the prey during suction feeding can complicate the interpretation of the fish-bound frame velocity data: forward translation of the head with open mouth and closed branchiostegal and opercular valves causes a positive pressure component inside the mouth cavity (Muller et al., 1982), which reduces the effort needed to expand the head. In other words, a certain amount of compensatory suction (needed to keep the water and prey motionless in the earth-bound frame) is indirectly powered by the fish's swimming musculature, which facilitates buccal expansion. For the present study on clariid catfishes, however, the animals' velocity in the direction of the prey is always relatively low compared to the measured velocity of the prey in the earth-bound frame (average 7.9 % for the three sequences with the fastest prey movement for each individual). Consequently, although minor interspecific differences in approaching speed are observed (mean \pm standard deviation of 0.085 \pm 0.011 m/s for C. gariepinus, 0.052 ± 0.015 m/s for G. typus and 0.040 ± 0.011 m/s for C. apus), these differences will probably have little effect on the results of our study. On the other hand, if this small difference in velocity is due to the fish sucking themselves forward (due to momentum conservation), comparing fish-bound frame velocities of the prey is the most appropriate approach. Given that the head-to-body mass ratio follows the same trend as the approaching speed (highest in C. gariepinus and lowest in C. apus), the latter situation is not unlikely.

The small difference between the density of the prey (average density of 1029 kg m⁻³) and the density of the water (1000 kg m⁻³) implies that the force due to gravitation after the

prey is released from the needle is relatively low and may be neglected given that the velocity of the prey sinking in motionless water after 0.1 s (the approximate maximum duration of prey transport in our catfish) is only 0.024 ± 0.002 m/s (mean \pm standard deviation; N=20). Consequently, the velocity of the prey is almost entirely induced by suction and the prey's velocity profile will adequately reflect the amount of suction generated by the catfish. Furthermore, this gravitational factor is equal for all species and will thus not influence the results of our comparative study.

The species included in the analysis differ in absolute head size: the anguilliform species *G. typus* and *C. apus* have smaller heads compared to the more fusiform *C. gariepinus*. If suction performance is subject to scaling effects, then this may influence the results. Scaling data on suction flow velocities in the species *C. gariepinus* (*Chapter 3*) allows us to evaluate the importance of differences in head size on the output of the suction performance experiments described above. Although the results of this study generally did not show significant differences in maximal flow velocities in relation to head size, the average (and thus most likely) scaling relationship shortly posterior to the mouth aperture is a decrease in peak flow velocity with increasing size proportional to (cranial length)-0.24. To account for this, we additionally compared the prey velocity data in function of cranial length with respect to the scaling relationship of flow velocity for *C. gariepinus* (*Chapter 3*).

7.2.3 Buccal expansion kinematics

The increase in the volume of the buccal cavity is responsible for the flow of water (and prey) into the mouth. In order to evaluate potential interspecific differences in buccal expansion, the buccal volume increase during suction is modelled using a method to the one outlined by Drost and Van den Boogaart (1986). The expanding buccal volume is approximated by a series of elliptical cylinders, in which the major and minor axis of each ellipse corresponds to the width and height of the buccal cavity at a certain position along the head's mediosagittal axis. The following data is needed for this: (1) a measurement of the dimensions of the buccal cavity (i.e., the width and height at specific points along the midsagittal axis), for example from the head in compressed state and (2) measurements of the changes of these ellipse axes in time during suction feeding.

The first type of data is obtained from lateral and ventral view radiographs of an unexpanded head of each of the species in which the bucco-pharyngeal cavity is filled with a radio-opaque (Barium) fluid (Fig. 3A). The line connecting the upper jaw tip to a point equidistant between the base of the right and left pectoral fin served as mediosagittal axis. Height and width of the buccal cavity were measured at 21 points equally distributed along this axis. For *C. apus*, which lacks pectoral fins, a fixed point at the approximate position of the pectoral girdle joint was used instead. It was assumed that this situation (i.e. the buccal volume distribution for the preserved specimen at rest) reflects the moment prior to start of the suction event (Fig. 3B).

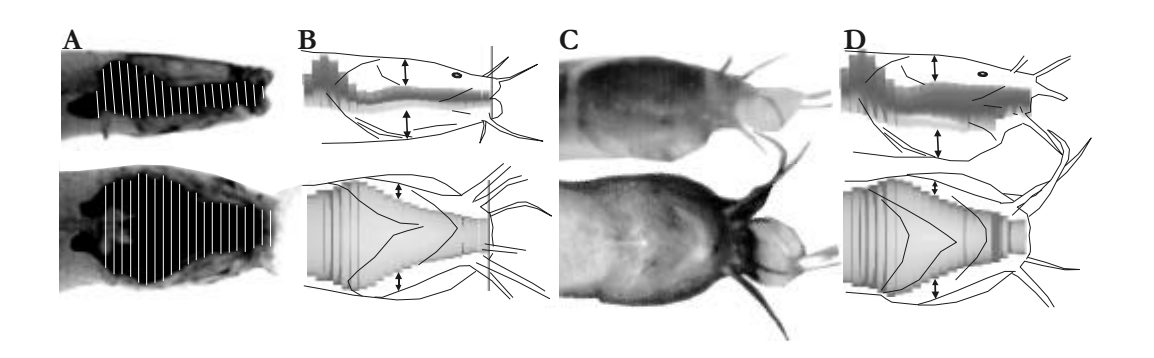


Figure 3: Illustration of the steps carried out in modeling the buccal volume increase as a series of 21 elliptical cylinders in *C. apus*. The height and width of the buccal cavity were measured at several positions using X-ray pictures of the (compressed) catfish head filled with radio-opaque fluid (A). These measurements were used to construct the elliptical cylinder model for buccal volume, which is assumed to occur inside the catfish's head prior to the start of suction feeding (B). Next, simultaneous lateral and ventral high-speed videos were recorded of catfish capturing pieces of fish (C). Finally, by assuming that the thickness of the head tissues bordering the buccal cavity does not change in time (see arrows), the increases in the radii of each elliptical cylinder during suction could be calculated (D). Note that the part of the hypertrophied jaw adductors extending laterally at the level of the eyes is not included in the external head boundaries a seen from a ventral view (see lower drawings of B and D).

To obtain the second type of data, high-speed videos were recorded for C. gariepinus (2 individuals; cranial lengths of 28.4 and 29.5 mm), G. typus (1 individual; 22.0 mm cranial length) and C. apus (2 individuals; cranial lengths of 24.5 and 26.0 mm) capturing pieces of cod (Gadus morhua) that were pinned onto a plastic coated steel wire (Fig. 2, third type of prey). The recordings were made using a Redlake Imaging Motionscope digital high-speed video camera at 250 frames simultaneously in lateral and ventral view on the feeding catfish, using a mirror placed at 45° (Fig. 3C). Two floodlights (600 Watt) provided the necessary illumination. Three feeding sequences that were approximately perpendicular to the camera lens were selected for each individual. Next, the upper and lower contours of the catfish's head were digitised frame by frame (50 points each) in the lateral and ventral view. At the same time, the coordinates of the mediosagittal axis described above were also digitised. The contour coordinates were recalculated in a new frame of reference moving with the fish, with the upper jaw tip as origin and mediosagittal axis as the X-axis. Next, the distance between the corresponding coordinates of the upper and lower contours, and between the left and right contours were extracted at 21 equally spaced intervals along the mediosagittal axis. Digitisation noise was reduced after applying a fourth order, zero phase-shift Butterworth low-pass filter (cut-off frequency of 30 Hz) to the profiles of length and width versus time. Finally, buccal volume models were calculated for each video frame by assuming that the thickness of the tissue layer between

the internal (buccal cavity) and external (head contours) boundaries of the head remains constant (Fig. 3B,D). To allow comparison between individuals of different size, all models were isometrically scaled to a length of 25 mm.

7.2.4 Statistics

In order to test whether the species differ in the maximal suction velocity of the standardised prey, the total distance travelled by the prey, and a variable combining these two aspects of suction performance (peak prey velocity x total distance of travel), one-way analyses of variance (ANOVAs) were performed. In these statistics, the distinction is made between maximal peak prey velocities and the mean peak prey velocities. The first data set includes only the two highest values per individual, while the second data set includes all measured values. In case these ANOVAs indicated an overall significant difference between species (P<0.05), further *post hoc* tests were performed to compare the means between the species individually. Given the variation in the number of individuals per species included in the analyses, Spjotvoll-Stoline tests (Tukey honest significant difference tests for unequal N) were used for this purpose.

7.3 Results

7.3.1 Suction performance

The clariid species with increased bite capacity (G. typus and G. apus) do not show a significant decrease in maximal peak velocities of standardized prey sucked into the buccal cavity (Fig. 4; Table 1). For example, the highest prey velocity (1.15 m/s) along the mediosagittal axis of the catfish's head was observed for G. apus, the species also capable of producing the highest bite forces (Fig. 1). Even the species for which the lowest maximal prey velocities are measured, G. typus (0.97 m/s; Fig. 3), still performs better on this aspect of suction performance compared with two out of the three individuals from the least specialised biter G. gariepinus (each 0.94 m/s). Also after correcting for potential scaling-effects, maximal peak velocities still do not differ significantly between the species (see Fig. 5). Only if all measured peak prey velocities are pooled (instead of selecting the two highest values per individual), G. typus performs on average poorer than G. gariepinus (Spjotvoll-Stoline test, G = 0.038) while other combinations of species do not differ significantly (Spjotvoll-Stoline test, G = 0.038) while other combinations of species do not differ significantly (Spjotvoll-Stoline test, G = 0.038)

No significant differences were found between the species in the maximum relative distance (expressed in numbers of cranial lengths) travelled by the prey from the moment of its release from the needle until the end of prey displacement (Spjotvoll-Stoline test, P always > 0.11). Also relative travel distance multiplied by peak prey velocity does not differ significantly between the species (Table 1). This variable can be considered as a

combination of the prey velocity magnitude and the distance (relative to head length) over which a certain prey velocity level is maintained.

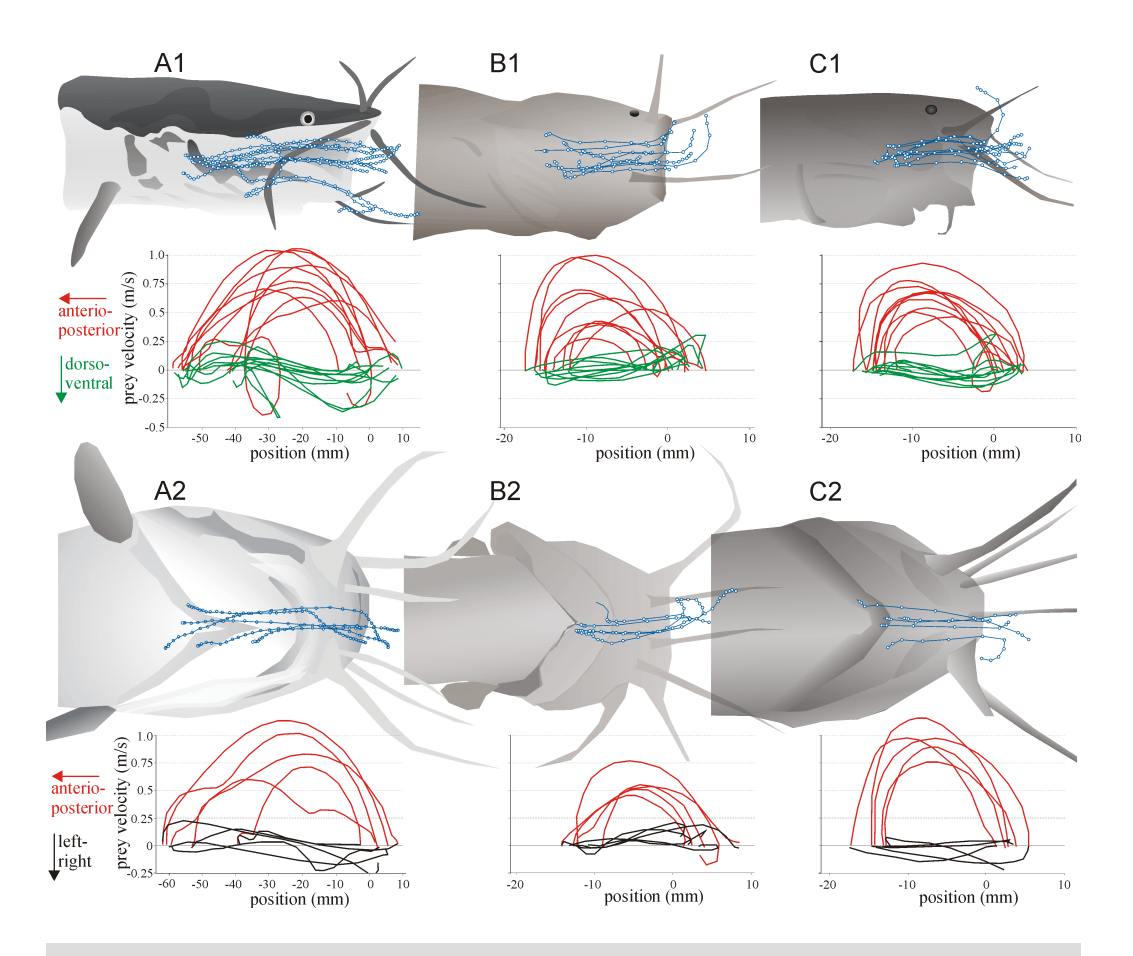


Figure 4: Lateral (A1-C1) and ventral view (A2-C2) prey trajectories (blue curves and circles) and the corresponding plots of prey velocities versus prey position (graphs) for each species' individual with the highest suction performance (**A**: C. gariepinus, **B**: G. typus and **C**: C. apus). Prey velocities and positions are in the fish-bound frame of reference. Color codes and positive directions of the velocities are explained on the left side of the graphs.

7.3.2 Buccal expansion

Increases in the volume of the buccal cavity are calculated for a number of suction feeding sequences by modelling (Fig. 6). The largest buccal volume increases are observed for *C. gariepinus* (0.76 \pm 0.10 cm³; mean \pm standard error), the smallest in *G. typus* (0.53 \pm 0.07 cm³), while *C. apus* is intermediate (0.68 \pm 0.10 cm³). However, if expansion in the lateral direction is removed (by keeping the horizontal radii constant in time), the interspecific

differences are considerably reduced (respectively 0.50 ± 0.04 , 0.43 ± 0.08 and 0.50 ± 0.07 cm³). Consequently, a substantial difference is noted in the average amount of volume increase due to lateral expansion (respectively 0.26 ± 0.07 , 0.10 ± 0.08 and 0.18 ± 0.05 cm³).

Table 1: Interspecific comparison (average \pm S.E.M.) of peak prey velocities and the total distance travelled by a standardised prey due to suction.

	Peak velocity (m/s)		Travel distance (cranial lengths)		Peak velocity x travel distance (m/s x cranial lengths)		N	
	mean	maxima	mean	maxima	mean	maxima	mean	maxima
0 1		.98 ± .04		.70 ± .02	.46 ± .02	.67 ± .03	45	6
G.typus	$.58 \pm .05$	$.975 \pm .002$	$.66 \pm .04$	$.88 \pm .10$.40 <u>+</u> .10	$.67 \pm .07$	15	2
C. apus	$.70 \pm .04$	$.99 \pm .06$	$.63 \pm .02$	$.79 \pm .04$	$.44 \pm .03$	$.70 \pm .02$	30	4
P (ANOVA)	.011	.98	.12	.046	.77	.27		

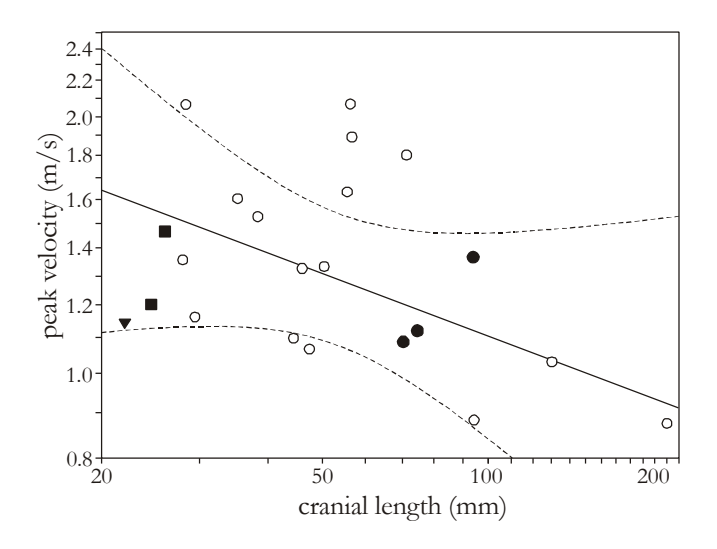


Figure 5: Logaritmic plot of peak prey velocities in function of cranial length (individual maxima of unfiltered data; filled black symbols) and the scaling relationship (least-squares regression with 95% confidence limits) of peak flow velocities (white circles) from *Chapter 3*. *C. gariepinus* is represented by circles, *G. typus* by the triangle and *C. apus* by squares. No significant interspecific difference was found for the residuals of peak prey velocities with respect to the scaling relationship (P = 0.054).

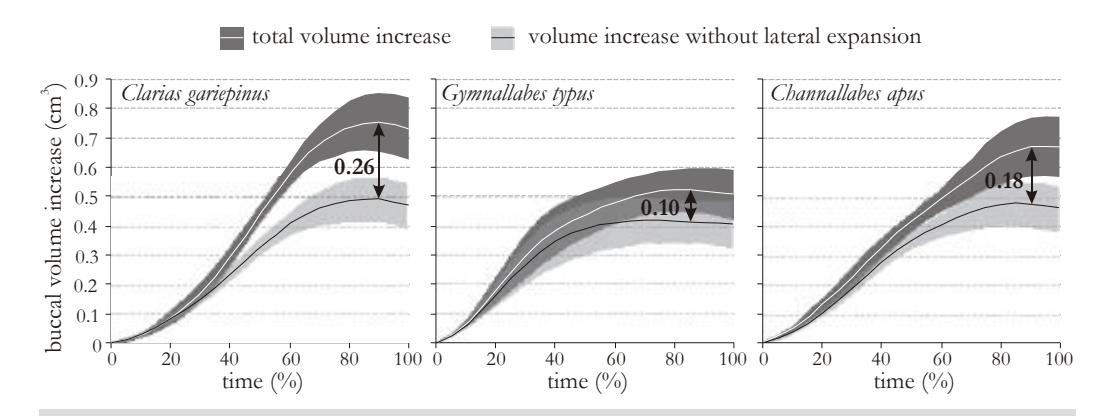


Figure 6: Increase in the volume of the bucco-pharyngeal cavity during suction feeding calculated using ellipse models (see also Fig. 3). The 100 % relative time (X-axis) corresponds to one frame after maximal volume. All models are scaled to a length of 25 mm. Besides the total volume increase (ventral and lateral expansion), also the volume increase due to only ventral expansion is shown (legend above graphs). Shaded areas indicate standard errors. The arrows denote the volume increase due to lateral expansion.

7.4 Discussion

Suction feeding and biting generally require conflicting morphological adaptations to the cranial system in fishes (Barel, 1983). The short and robust oral jaws of specialized biters (e.g., Turingan and Wainwright, 1993; Friel and Wainwright, 1999; Albertson et al., 2003) as opposed to long, highly protrusible jaws of some specialized suction feeders (e.g., Motta, 1984; Westneat, 1989, Ferry-graham et al., 2002) are a well-studied example of this. Given the diversity in food characteristics, it is therefore not surprising that the mode of feeding (suction or biting) is usually reflected in the fishes' diet, which in turn can often can be predicted fairly well from morphology (Sibbing and Nagelkerke, 2001).

However, developing a certain morphological or behavioural modification to increase bite performance (e.g., enabling the fish to crush hard prey) does not *necessarily* imply a reduced performance in capturing other, maybe less available or less preferred prey types by suction. This will only be the case if *every* possible option to increase this bite performance (e.g., increasing jaw adductor cross-sectional area, increasing the moment arms of the lower jaw closing leverage or increasing the strength of the oral jawbones) reduces suction feeding performance. Consequently, although it is obvious that the optimal design for a biter and a suction feeder are different (illustrated by the extreme morphologies of specialists), it may still be possible that *some* adaptations for biting do not compromise suction performance. Unfortunately, very little is known about potential interferences between the system causing buccal expansion and the system producing bite forces. Therefore, an important goal is to identify evolutionary pathways of specialization towards

biting or suction feeding and their respective functional consequences. We may learn from this to what extends biting and suction feeding can be combined efficiently.

The result of the present study on clariid catfishes exemplifies the possibility of increasing bite performance considerably (Fig. 1) without substantially compromising suction performance (Figs. 4,5; Table 1). The anguilliform species with hypertrophied jaw adductors *G. typus* and *C. apus* are able to produce bite forces that are, respectively, more than 5 and 11 times larger compared to *C. gariepinus* (Fig. 1; Herrel et al., 2002). On the other hand, these species still manage to accelerate a standardised prey to similar velocities during suction feeding. A logical question following these observations is: "why doesn't biting performance trade-off with suction performance in these Clariidae?"

A functionally important characteristic of Clariidae is their dorso-ventrally flattened head Alexander (1970b) recognised that fishes with this type of head shape predominantly rely on ventral expansion (i.e. depression) of the buccal cavity for suction feeding, and less on lateral expansion (i.e. suspensorium abduction). Our modelling of the volume increase of the buccal cavity during expansion in Clariidae supports this: if only ventral expansion occurred, still (on average) 74% of the total observed volume increase had been reached, while lateral expansion only would result in 20 % of the total expansion (the remaining 6% is due to the interaction between both directions of expansion). Clariidae differ in this aspect from the more laterally flattened cichlid fishes, the group for which the trade-off between biting and suction has been studied most intensively (Barel, 1983; De Visser and Barel, 1996, 1998; Bouton et al., 1998, 1999). It has been proposed for ciclid fishes that in order to accommodate thicker jaw adductor muscles (increasing bite force) the cichlid's head has to widen, which implies a lateral displacement of the touching point between the hyoid and the suspensorium. This displacement increases the angle between the hyoid bars, which in turn would reduce the optimality of the starting position of the hyoid (De Visser and Barel, 1996, 1998). However, the morphological modification causing this trade-off for cichlid fishes, i.e. widening of the head due to jaw adductor hypertrophy, does not occur in Clariidae (for illustrations see Herrel et al., 2002). In these catfishes, the neurocranial roof has been reduced to a small, medial ridge of bones, which makes room available for the jaw adductor muscles to "bulge" dorso-laterally of the head without the need for adjusting the spatial configuration of the hyoid-suspensorium apparatus. In addition, the suprapreopercle and the fourth infraorbital bones, positioned respectively at the posterior and anterior margins of the jaw adductors, have reduced considerably (Cabuy et al., 1999; Devaere et al., 2001).

As no factors of potential interference between the systems for hyoid depression (i.e. caudo-ventral rotation of the hyoid bars and the pectoral girdle, coupled by the sternohyoideus muscle) and the adaptations for increasing bite force can be identified in Clariidae, it is not surprising that no interspecific differences in the volume increase due to ventral expansion are observed in these catfishes (Fig. 6). However, especially in *G. typus* but also in *C. apus*, the contribution to the total volume increase by lateral expansion (i.e.

suspensorium abduction) does seem to be restricted with respect to the species without the hypertrophied jaw muscles, C. gariepinus (Fig. 6). Consequently, the increase in bite performance may interfere with the capacity of abduction (lateral swing) of the suspensoria. This was also concluded previously from a study comparing the prey capture kinematics of C. gariepinus with a species with a moderate degree of jaw adductor hypertrophy, Clariallabes longicauda (Chapter 6). Two reasons have been suggested to explain this reduced lateral expansion. Firstly, a considerable increase of the visco-elastic jaw adductor mass inserting both on the suspensorium and the neurocranium may passively constrain the lateral swing of the suspensorium. Secondly, a stronger and increasingly interdigitated connection of the suspensorium with the neurocranium may be needed in order to resist the large reaction forces and moments caused by the large bite forces exerted onto prey. This more firmly "locking" of the suspensorium associated with adductor mandibulae hypertrophy has been observed in all Clariidae (Cabuy et al., 1999; Devaere et al., 2001; Herrel et al., 2002) and could therefore restrict the suspensorium in rotating laterally. However, despite this reduction in lateral expansion capacity (Fig. 6), the overall effect of this on maximal suction feeding performance is apparently negligible (Figs. 4,5; Table 1).

In conclusion, the results of our study comparing species from two evolutionary lineages of Clariidae demonstrates that convergent morphological evolution toward increasing bite performance does not necessarily lead to a reduced suction feeding performance. This is in contrast to what has been proposed for other groups of fishes (Barel, 1983). Clariid catfishes have dorso-ventrally flattened heads and predominantly rely on ventral expansion of the buccal cavity to produce suction. We hypothesise that potential spatial constraints by increasing the jaw adductor size on the buccal expansion system is avoided by the narrowing of the roof of the neurocranium, enabling the jaw adductors to develop freely in the dorsolateral region of the head without interfering with the depression of the hyoid. Although a reduced capacity of lateral expansion (suspensorium abduction) is observed in the powerfully biting species (presumably due to passive resistance of the jaw adductor mass spanning the suspensorium and/or the strengthened articulation of the suspensorium with the neurocranium) the contribution of this lateral expansion to the total buccal expansion is relatively limited and, probably for this reason, does not result in a reduced suction capacity.

Interspecific variation in sternohyoideus muscle morphology in clariid catfishes: functional implications for suction feeding

Sam Van Wassenbergh – Anthony Herrel – Dominique Adriaens – Peter Aerts

Submitted to The Journal of Experimental Biology

Summary

Depression of the hyoid apparatus plays a crucial role in generating suction, especially in fishes with a dorso-ventrally flattened head shape. It is generally assumed that shortening of the sternohyoideus muscle, which connects the hyoid to the pectoral girdle, contributes to hyoid depression. However, a recent study on the clarid catfish Clarias gariepinus has shown that this muscle does not shorten but elongates during this phase through retraction of the pectoral girdle. Here, we test whether this pattern is general among clariid catfish, or if variation in the morphology of the sternohyoideus may result in a different sternohyoideus behaviour during hyoid depression. First, sternohyoideus mass, effective cross-sectional area, fibre length and fibre diameter were measured and compared for four clariid species. Next, velocity and magnitude of hyoid depression during prey capture (from high-speed videos), as well as patterns of sternohyoideus strain were analysed (from high-speed X-ray videos) in these species. While morphology and hyoid depression performance varied considerably among these species, only the species with the most massive sternohyoideus, Gymnallabes typus, showed shortening of the sternohyoideus muscle during the initial part of the expansive phase. The data for *Channallabes apus* demonstrate that increasing the magnitude of hyoid depression does not necessarily require a shortening of the m. sternohyoideus, as it shows elongation of this muscle during hyoid depression.

8.1 Introduction

To generate a flow of water into the mouth during suction feeding, aquatic animals rapidly expand the volume of their bucco-pharyngeal cavity. In teleost fishes, this expansive phase of prey capture is characterised by mouth opening, followed by simultaneous abduction (i.e. lateral swing) of the suspensorium and ventral rotation (depression) of the hyoid apparatus (Lauder, 1985). Especially in fishes with a dorso-ventrally flattened head the depression of the hyoid apparatus is assumed to cause a large fraction of the total bucco-pharyngeal volume increase during suction (Alexander, 1970b).

Despite the crucial role for hyoid depression in generating suction, relatively little is known about the underlying mechanisms causing the depression of the hyoid apparatus in fishes. The classical view is that the pectoral girdle (cleithrum) rotates caudo-ventrally with respect to the neurocranium by contraction of the hypaxial and by the epaxial muscles causing neurocranial elevation (Fig. 1). The sternohyoideus muscle (abbreviated m-sh) connects the pectoral girdle to the hyoid, and contracts while being retracted by the pectoral girdle (Fig. 1A). Hence, in this mechanism, the m-sh transmits the force from pectoral girdle rotation and actively increases the magnitude of hyoid depression by shortening (Gosline, 1971; Liem, 1980; Lauder, 1985; Bone and Marshall, 1986; Diogo and Chardon, 2000; Adriaens et al., 2001). As the numerous functional morphological studies on feeding mechanisms in fish have used high-speed video recordings to quantify prey capture kinematics (reviewed by Ferry-Graham and Lauder, 2001) the strain behaviour of the m-sh typically cannot be quantified as the pectoral girdle (including the origin of the m-sh) is hidden behind the branchiostegal membranes during most of the expansion phase. To our knowledge, only a single study has actually confirmed the "classical" hyoid-depression mechanism in the Percomorph fish Micropterus salmoides using sonomicrometry (Carroll, 2004).

However, a recent study on the hyoid-depression mechanisms in the African catfish *Clarias gariepinus* did not observe the pattern outlined above (*Chapter 2*). Although the pectoral girdle does indeed rotate considerably, the m-sh gradually *elongates* during depression of the hyoid in this species. Consequently, a different strategy has to be used by *C. gariepinus* to depress the hyoid whereby the m-sh transmits the force from pectoral girdle retraction to the hyoid while elongating (Fig. 1B; *Chapter 2*). Yet, even if we ignore the passive force that rises when the muscle increases in length, muscle can produce much higher active force in the excentric part of the force-velocity relationship (Hill, 1938). If the m-sh is the least powerful muscular part of the linkage system that causes hyoid depression (also including the epaxial and hypaxial muscles; Fig. 1), the m-sh will therefore inevitably be forced to elongate. This also implies that only relatively large and forceful m-sh will be able to produce isometric forces exceeding the forces exerted on its origin (forces from pectoral girdle retraction) and insertion (forces of resistance to hyoid depression), and therefore be potentially capable of shortening during this phase.

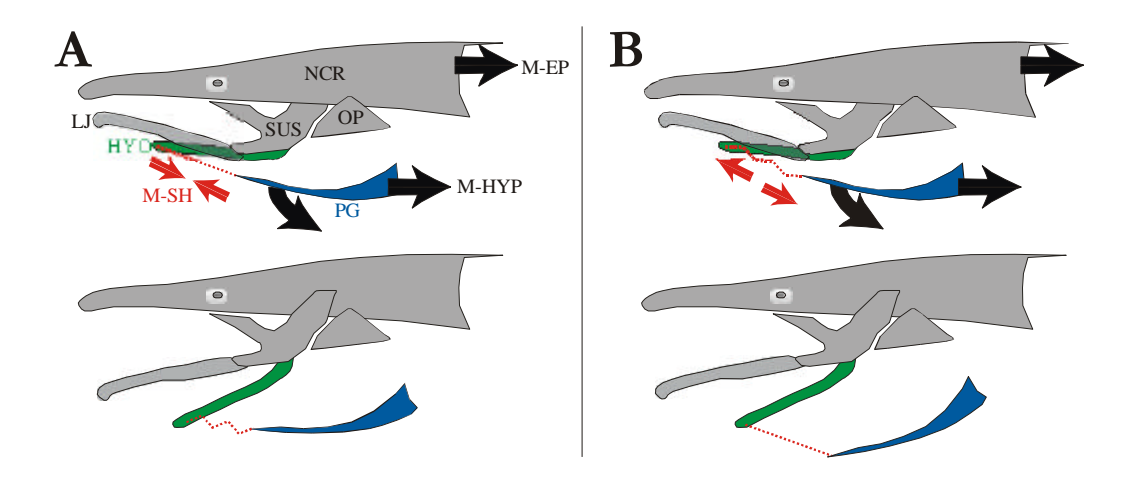


Figure 1: Schematic illustration of two potential strategies in depressing the hyoid: (A) rotation of the pectoral girdle (*blue*) as well as shortening of the sternohyoideus muscle (*red*) contribute simultaneously to the depression of the hyoid (*green*) and (B) the pattern observed in *Clarias gariepinus* (*Chatper 2*): the rotating pectoral girdle retracts and stretches the sternohyoideus that pulls the hyoid. Legend: HYO = hyoid, LJ = lower jaw, M-EP = epaxial musculature, M-HYP = hypaxial musculature, M-SH = sternohyoideus muscle, NCR = neurocranium, OP = operculum, PG = pectoral girdle, SUS = suspensorium.

Because relatively little is known about the behaviour of the m-sh during hyoid depression in fishes, the generality of each of the two alternative strategies (Fig. 1) is unknown in this large and diverse group of animals. The morphology of the m-sh may determine whether this muscle is able to contribute in powering the buccal expansion by shortening (Fig. 1A) or whether the m-sh only functions as a force transmitter and uses its passive and/or active excentric force when it is pulled backward by the pectoral girdle.

A considerable difference in the morphology of the m-sh between two species of clariid catfishes has been reported (*Chapter 6*). Remarkably, the species with the largest physiological cross-sectional area of the m-sh (*Clariallabes longicauda*) was also able to generate the largest amount of hyoid depression compared to closely related species (*Clarias gariepinus*). Possibly, the enlarged m-sh in *Clariallabes longicauda* is able to reinforce the action of the pectoral girdle on the hyoid by active shortening of its m-sh (Fig. 1A), while the more slender m-sh of *Clarias gariepinus* does not have enough power even to maintain its initial length when it is pulled backward by the large hypaxial muscle masses causing pectoral girdle rotation and the epaxial muscles causing neurocranial elevation (Fig. 1B). M-sh shortening instead of elongating during hyoid depression will increase the speed and magnitude of hyoid depression, which would probably enhance suction feeding performance considerably.

In order to test whether variation in the morphology of the sternohyoideus muscle is associated with different mechanisms of hyoid depression (Fig. 1), or if the pattern

observed for *Clarias gariepinus* (*Chapter 2*) is general within Clariidae, morphology and function of this muscle during suction feeding is studied in this group of fishes. To do so, we first examine the morphology of the sternohyoideus muscle in four species of Clariidae (Fig. 2) by measuring total mass, physiological cross-sectional area, fibre length and fibre diameter. Next, we test whether a relationship exists between the morphology and the magnitude and velocity of hyoid depression, as well as the pattern of m-sh shortening during prey capture for these species.

8.2 Materials and Methods

8.2.1 Study animals

Four species of Clariidae showing morphological differences in the cranial musculature (Cabuy et al., 1999) were included in the analyses: Clarias gariepinus, Channallabes apus, Clariallabes longicauda and Gymnallabes typus. The C. gariepinus specimens were either aquarium-raised specimens of which larval stages were initially obtained from the Laboratory for Ecology and Aquaculture (Catholic University of Leuven, Belgium) or specimens obtained from aquacultural facilities (Fleuren & Nooijen BV, Someren, The Netherlands). Specimens of C. longicauda and C. apus were caught in Northern Gabon. G. typus was commercially obtained, originating from Western tropical Africa. The number of individuals used in each of the analyses of the present study is given in Table 1. For each individual, cranial length (i.e. the distance between the rostral tip of the premaxilla and the caudal tip of the occipital process) was measured using digital callipers and used to quantify fish size. The fishes used for video recordings (see further) were kept in separate, Plexiglas aquaria and were trained to capture food in a narrow, projecting corridor of the aquarium. The thin walls (2 mm) of the corridor minimised the amount of X-ray absorption during cineradography.

	sternohyoideus	serial	high-speed	high-speed X-
	dissection	section	video	ray video
Clarias gariepinus	23 (1),(2)	2	17 (3)	3 (4)
Clariallabes longicauda	2	1	4	2
Gymnallabes typus	3 (2)	1	4 (2)	0
Channallabes apus	2	1	3	1

Table 1: Number of individuals analysed

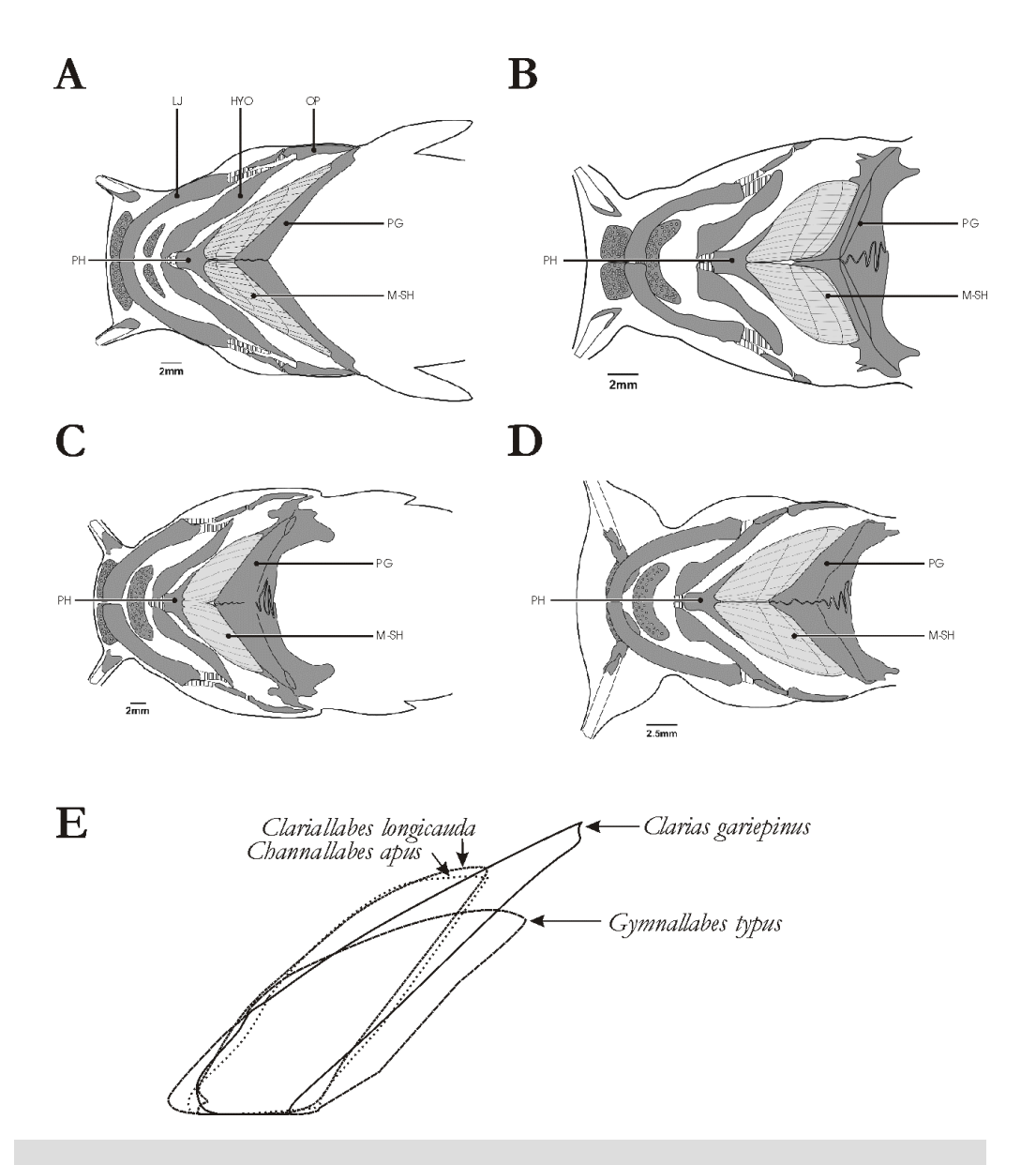


Figure 2: Ventral view morphology of the head, illustrating the position and shape of the sternohyoideus muscle in four Clariidae: (A) *Clarias gariepinus*, (B) *Channallabes apus*, (C) *Clariallabes longicauda* and (D) *Gymnallabes typus*. In (E) the left side sternohyoideus of the four species are superimposed, after scaling to the same mediosagittal length between the rostral part of the parurohyal bone and the caudal margin of the pectoral girdle. This drawing illustrates the relatively elongated sternohyoideus shape in *C. gariepinus*, the similarity between the intermediate shapes of *C. apus* and *C. longicauda*, and the relatively broad muscle of *G. typus*. Legend: HYO = hyoid, LJ = lower jaw, M-SH = musculus sternohyoideus, OP = operculum, PG = pectoral girdle, PH = os parurohyale.

8.2.2 Morphological data

To measure the properties of the sternohyoideus muscles (Fig. 2), specimens preserved in 70% alcohol were dissected. The muscles of both sides were removed and weighed using electronic scales (±0.0001 g; Mettler MT5, Switzerland). Muscle volume was obtained by dividing the mass by 1050 kg m⁻³ (Ward and Lieber, 2005). The average muscle fibre length was approximated by taking the average of lengths of the most medially positioned fibre, a central muscle fibre and the most laterally situated fibre. Similarly, the inclination of the muscle fibres with respect to medio-sagittal axis of the head (i.e. the line of action of the sternohyoideus) was determined. The effective physiological cross-sectional area was obtained by multiplying muscle volume by the cosine of the mean fibre inclination and dividing this by the mean fibre length.

Inter- and intraspecific variation of the sternohyoideus muscle fibre diameter was evaluated for all the species (*Clarias gariepinus*, *Channallabes apus*, *Clariallabes longicauda* and *Gymnallabes typus*), using serial histological sections (5 µm, Technovit 7100 embedding). Five sections were obtained using a Leica Polycut microtome. In order to test whether fibre diameter is subjected to ontogenetic scaling, two specimens of *C. gariepinus* were analysed (cranial lengths of 7.6 and 17.0 mm). For each specimen, a section in the middle of the sternohyoideus was selected on which the diameters were measured using digital images obtained through an Olympus 52 x 9 stereomicroscope, equipped with Colorview 8 CCD-camera. A total of 400 fibres were measured in the left sternohyoideus (only 273 fibres could be measured in the smallest *C. gariepinus* specimen). As fibres were cut slightly obliquely, always the minimal fibre diameter was used.

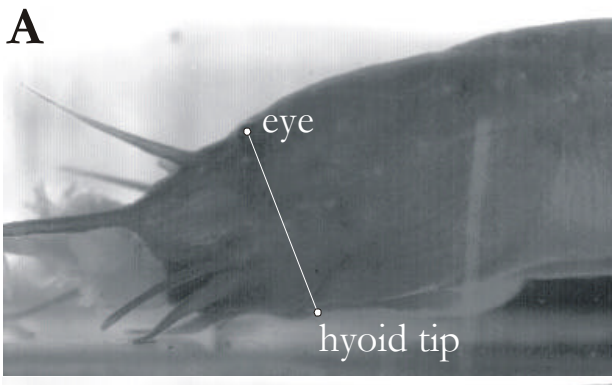
8.2.3 High-speed video

High-speed video recordings (250 frames s⁻¹) of prey capturing catfish were made from a lateral view, using a digital Redlake Imaging Motionscope (640 x 480 pixels) or MotionPro (1280 x 960 pixels) camera. Two *Clarias gariepinus* individuals of larger than 94 mm cranial length were recorded at 100 frames s⁻¹ with a JVC GR-DVL9800 camera, while we used a Panasonic F15 (50 frames s⁻¹) for the 210 mm cranial length individual. As the duration of a prey capture event is considerable higher in these large individuals, the lower recording speeds do not result in an increased experimental error when determining velocity and maximal displacement of the hyoid (see further). Two floodlights (600 Watt) provided the necessary illumination. Only those prey capture sequences that were approximately perpendicular to the camera lens were selected and retained for further analysis. Two prey types were used: (1) pieces of cod fillet (*Gadus morhua*) and (2) North Sea shrimps (*Pandalus borealis*). Both prey types were attached to a thin, plastic coated steel wire. Ten prey capture sequences were analysed for each individual, generally including five fish and five shrimp captures. For 17 out of the 23 individuals of the species *C. gariepinus*, only the first prey type (fish) was used (*Chapter 4*). However, this does not influence the results as the

magnitude and speed of hyoid depression do not differ between the two prey types for this species (*Chapter 9*).

The XY-position of the eye and the tip of the hyoid (Fig. 3) were digitized frame-by-frame using Didge (version 2.2.0, Alistair Cullum, Creighton University, Omaha, NE, USA). The distance between these two points was plotted against time. The difference between the minimal and maximal value was taken as a measure of the total hyoid depression for a given prey capture sequence. After data filtering (4th order Butterworth zero phase-shift low-pass filter) and differentiation *versus* time, linear velocities were calculated. As we are mainly interested in maximal performance, the maximal value per individual (i.e. the largest

excursion of the hyoid tip, highest peak velocity) was used in the comparative analyses.



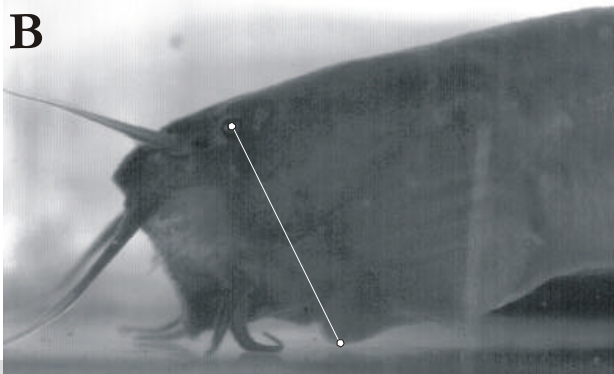


Figure 3: High-speed video frames (*Channallabes apus* feeding on a piece of fish) showing the two anatomical landmarks used to determine the magnitude of hyoid depression (distance between both landmarks) at the start of the sequence (A) and at the time of maximal hyoid depression (B).

8.2.4 High-speed cineradiography

First, small metal markers were inserted subcutaneously at specific positions of interest, hypodermic needles (Fig. 4). Prior to implantation of these radioopaque markers, the animals were anaesthetised with MS222 (Sigma Chemical Company, St. Louis, MO, USA). Next, X-ray videos and photographs were recorded using a Philips Optimus X-ray generator coupled to a 14-inch image intensifier and a Redlake Motion Pro camera (1248 x 1024 pixels). Videos were made in lateral view and were recorded at 250 frames per second, using the 6-inch zoom function. Three prey types were used: (1) pieces of cod fillet and (2) unpeeled North Sea shrimps attached to a plasticcoated steel wire, and (3) small,

spherical pieces of shrimp meat which were loosely attached to the tip of a needle. For *C. gariepinus* 20 recordings were analysed per individual (cranial lengths of 70.2, 74.5 and 94.1 mm; 5, 5 and 10 sequences respectively for each prey type). For both *Channallabes apus* individuals (cranial lengths of 24.5 and 26.0 mm) and the *Gymnallabes typus* individual

(cranial length of 22.0 mm) only the third prey type was used, with respectively 13, 14 and 6 sequences analysed. No high-speed X-ray videos could be recorded for *Clariallabes longicanda*, as no living specimens could be obtained for this species since the start of the X-ray video recordings.

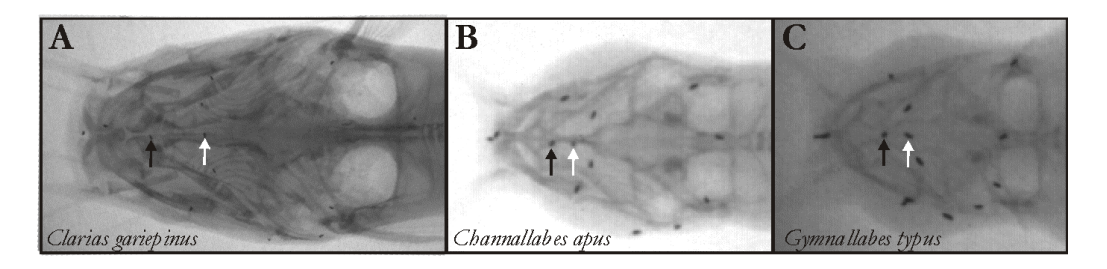


Figure 4: Positions of the inserted radio-opaque markers on a dorsoventral X-ray image of *Clarias gariepinus* (A), *Channallabes apus* (B) and *Gymnallabes typus* (C). The white arrow indicates the marker at the tip of the cleithrum. The black arrow indicates the marker near the tip (symphysis) of the hyoids.

In this way, it was possible to track the movements of two markers (Fig. 4): one at the rostral tip of the hyoid and one at the tip of the cleithrum (pectoral girdle). The distance between these two points is spanned by the sternohyoideus muscle, and may also include part of the short parurohyale bone and parurohyalo-hypohyale ligament (Fig. 2). This variable is used to determine whether or not the sternohyoideus muscle is shortening. Note, however, that the amount of bone or ligament included in this hyoid-to-cleithum distance may vary slightly between individuals. Consequently, relative muscle shortening velocities could only be obtained by approximation.

These hyoid-to-cleithum distances will be presented as a percentage of the average hyoid-to-cleithrum distance observed for each individual. In order to account for strike-to-strike variability and to avoid the potential confounding effects on kinematic means, the time axis of each prey capture sequence was scaled to the total duration of hyoid depression of that sequence. Consequently, time will be expressed as a percentage of hyoid depression duration, with 0% being the start of hyoid depression and 100% the time of maximal hyoid depression. Linear interpolations are used to extract data at 2% intervals on this new, relative time scale. In this way, also the effects of differences in body size on the speed of prey capture kinematics (*Chapter 4*) are removed, which thus simplifies the comparison between individuals.

8.2.5 Statistics

Kolmogorov-Smirnov tests were used to test the normality of the distributions and, if necessary, the data were log₁₀ transformed. As probably the most important source of variation between individuals is body size, one-way covariance analyses (ANCOVA) were performed to test whether species (independent variable) differ, using cranial length as a covariate. Only if an overall significant difference between species (P<0.05) is indicated by the ANCOVA, further post hoc tests were performed to statistically compare the means for the species used in this study. Given the variation in the number of individuals per species included in the analyses (Table 1), Spjotvoll-Stoline tests (Tukey honest significant difference tests for unequal N) were used for this purpose. To eliminate scaling effects in these post hoc tests, the data were adjusted according to the scaling relationship found for Clarias gariepinus, the species for which data are available for a broad range of individuals of different sizes (Herrel et al., 2005; Van Wassenbergh et al., 2005a). To do so, each value was divided by the power of cranial length by which this specific variable scales in C. gariepinus. This approach is analogous to an analysis of residuals, but has the advantage of using a real scaling relationship, rather than the artificial scaling relationship obtained by pooling all species to calculate the residuals. In both analyses (ANCOVA and post-hoc tests) it was thus assumed that the scaling relationships measured for C. gariepinus (Herrel et al., 2005; Chapter 4) also apply to the other species. Although unlikely to occur because of the close phylogenetic relatedness of the species, it should be mentioned that the validity of the results would be restricted to individuals of C. longicauda, G. typus and C. apus within the size-range of the individuals used for each species in the experiments in case of interspecific differences in scaling relationships.

8.3 Results

8.3.1 Cross-sectional area

The effective physiological cross-sectional area of the sternohyoideus muscle (m-sh) differs significantly between species (ANCOVA, P = 0.016). On average, Clarias gariepinus has the most slender m-sh, closely followed by Channallabes apus (Fig. 5A; Table 2). The largest values are measured for Gymnallabes typus, which is the only species for which a significantly larger cross-sectional area compared to C. gariepinus can be demonstrated (Spjotvoll-Stoline test, P = 0.008). The average difference between these two species is considerable, with G. typus more than doubling the effective m-sh cross-sectional area of C. gariepinus for animals of the same head size (Table 2). Clariallabes longicauda takes an intermediate position between C. gariepinus and G. typus and does not differ significantly from both species (Spjotvoll-Stoline test, respectively P = 0.12 and P = 0.36).

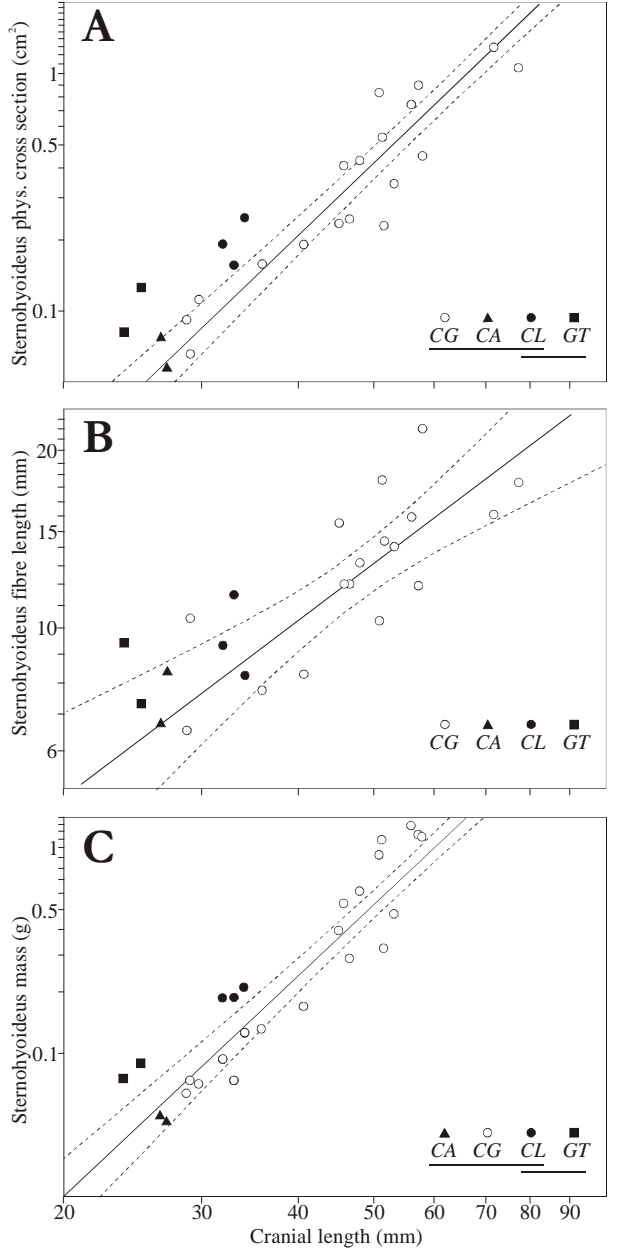


Figure 5: Logaritmic plot of the effective physiological crosssectional area (A), the fibre length (B) and the mass (C) of the sternohyoideus muscle in Clarias gariepinus (CG), Channallabes apus (CA), Clariallabes longicauda (CL) and Gymnallabes typus (GT). Symbol legends and post hoc test results (Spjotvoll-Stoline) are given at the lower right part of the graph. No significant differences in fibre length between species are found. The regression line (with 95% confidence limits) shows the scaling relationship for Clarias gariepinus. All regressions are highly significant (P < 0.0001) and slopes are 3.15 (A; $R^2 = 0.96$), 1.08 (B; R^2 = 0.65) and 3.56 (C; $R^2 = 0.94$).

8.3.2 Fibre length

Although the average length of the sternohyoideus fibres tends to increase with increasing average cross-sectional area of this muscle (Table 2), the species do not differ significantly in fibre length (ANCOVA, P = 0.52; Fig. 5B).

8.3.3 Sternohyoideus mass

Alike the cross-sectional area of the m-sh, the total mass of the muscle varies significantly in the Clariidae (ANCOVA, P = 0.03). After

correcting for size, the largest masses are observed for *Gymnallabes typus*, followed by *Clariallabes longicauda*, *Clarias gariepinus* and *Channallabes apus* (Fig. 5C; Table 2). *Gymnallabes typus* is the only species for which the m-sh masses are significantly larger compared to C. *gariepinus* (Spjotvoll-Stoline test, P = 0.037; Fig. 5C). The scaled average m-sh mass for C. *typus* is almost double that of C. *gariepinus* (Table 2).

Table 2: Scaled characteristics of the sternohyoideus and hyoid depression in Clariidae (mean \pm S.E.M.)

	m-sh <i>PCSA</i> (cm ²) x 10 ³ CL -3.15	m-sh FL (mm) x 10 ² CL ^{-1.08}	m-sh mass (g) x 10 ⁷ CL ^{-3.56}	m-sh fibre diameter (µm)	max. hyoid depr. (mm) x CL ^{-0.87}	peak speed hyoid depr. (mm s ⁻¹) x CL ^{0.09}
C.gariepinus C. longicauda G. typus C. apus	5.5 ± 0.4 6.0 ± 1.0 9.0 ± 1.0 12.1 ± 1.6	3.4 ± 0.2 3.7 ± 0.4 3.8 ± 0.4 4.6 ± 0.7	5.0 ± 0.4 4.0 ± 0.3 7.6 ± 0.3 9.43 ± 0.02	15.4 ± 0.3 25.7 ± 1.3 27.1 ± 1.4 31.1 ± 1.6	130 ± 8 190 ± 10 185 ± 9 208 ± 14	134 ± 6 170 ± 25 259 ± 19 148 ± 18

Abbreviations: CL = cranial length (in m), PCSA = effective physiological cross-sectional area, FL = fibre length, depr. = depression, m-sh = musculus sternohyoideus

8.3.4 Fibre diameter

The average fibre diameter of the sternohyoideus muscle differs significantly between species (ANOVA, P < 0.001; Table 2). Similar to the total muscle's cross-sectional area, Clarias gariepinus has the most slender muscle fibres, while fibres are on average twice as thick in Gymnallabes typus (Fig. 6, Table 2). The values for C. gariepinus are significantly lower than those for all other species (Spjotvoll-Stoline test, all P < 0.001). Channallabes apus and Clariallabes longicanda are intermediate between C. gariepinus and G. typus and differ significantly from these species (Spjotvoll-Stoline test, all P < 0.001). The maximal fibre diameters follow the same trend as the averages (Fig. 6). The results for two C. gariepinus individuals of different head size (7.6 and 17.0 mm) show that m-sh fibre diameters in this species are independent of head size for the range of sizes used in this study (Fig. 6).

8.3.5 Maximal hyoid depression

The maximal amount of depression of the tip of the hyoid apparatus during prey capture (see Fig. 3) differs significantly between species (ANCOVA, P < 0.001). Apparently, also for this hyoid depression magnitude, *Clarias gariepinus* shows the least depression of the four species (Fig. 7A; Table 2). For a given head size, *Channallabes apus* and *Gymnallabes typus* perform significantly larger hyoid depressions while suction feeding when compared to *C. gariepinus* (Spjotvoll-Stoline test, respectively P = 0.045 and P = 0.020). On average, *C. apus* is able to lower the hyoid tip 46 % more than an equally-sized *C. gariepinus* individual (Table 2). For *G. typus*, this difference is even larger, with an average increase of 59 % in total hyoid depression compared to *C. gariepinus*. Also the amount of hyoid depression measured for *Clariallabes longicanda* is more similar to *C. apus* and *G. typus* than it is to *C. gariepinus* (Spjotvoll-Stoline tests, respectively P = 0.99, P = 0.79 and P = 0.069).

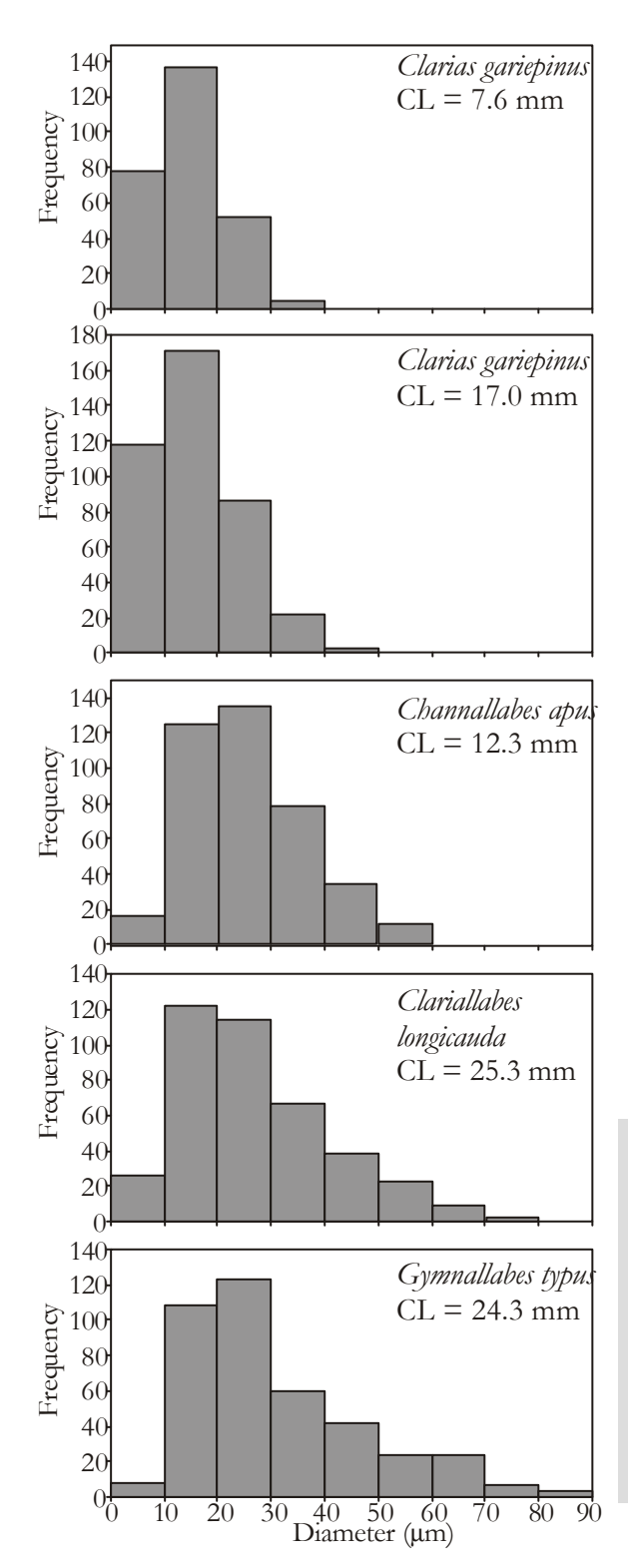
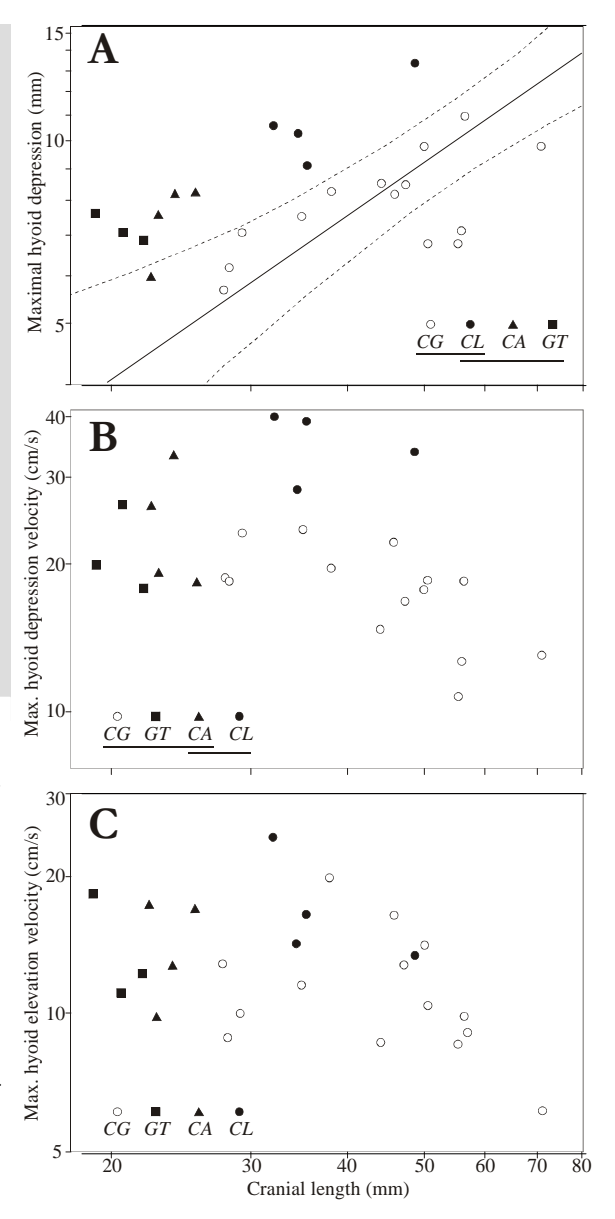


Figure 6: Histograms of sternohyoideus fibre diameter in the species studied. The upper two graphs indicate that no scaling effects exist for *Clarias gariepinus* within the range of head sizes presented here. N=400 except for the uppermost graph (N=273). The average fibre diameter differs significantly among species. More information is given in the text and in Table 2.

Figure 7: Logaritmic plot of the maximal hyoid depression (A), the maximal peak velocity of hyoid depression (B) and the maximal peak velocity of hyoid elevation (C) during prey capture in Clarias gariepinus (CG), Channallabes apus (CA), Clariallabes longicauda (CL) and Gymnallabes typus (GT). Symbol legends and post hoc test results (Spjotvoll-Stoline) are given at the lower part of the graph. Note that no significant differences in hyoid elevation velocity between the species are found (C). The regression line (with 95% confidence limits) shows the scaling relationship for Note that only Clarias gariepinus. maximal hyoid depression increases significantly with size in this species (slope = 0.87; $R^2 = 0.78$; P <0.0001).

8.3.6 Speed of hyoid depression

The maximal speed of depression of the tip of the hyoid apparatus during suction feeding (see Fig. 3) also differs significantly between species (ANCOVA, P < 0.001; Fig. 7B; Table 2). However, only one species, Clariallabes longicanda, reaches hyoid depression speeds that are significantly higher than those of Clarias gariepinus (Spjotvoll-Stoline test, P < 0.001), with on average almost twice the peak hyoid



depression velocity of the latter species. On the other hand, the speed of hyoid depression for *Channallabes apus* and *Gymnallabes typus* cannot be discerned statistically from *C. gariepinus* (Spjotvoll-Stoline test, respectively P = 0.22 and P = 0.92).

8.3.7 Patterns of sternohyoideus strain

Changes in the length of the sternohyoideus muscle during prey capture were measured (Figs. 8,9) for *Channallabes apus* and *Gymnallabes typus* and can thus be compared to the pattern observed for *Clarias gariepinus* (*Chapter 2*). The strain pattern of this muscle during

prey capture in *C. apus* is roughly similar to the pattern in *C. gariepinus* (Fig. 9A,B). During the first half of the hyoid depression phase, the sternohyoideus approximately maintains a constant length (on average during the first 36% and 44% of

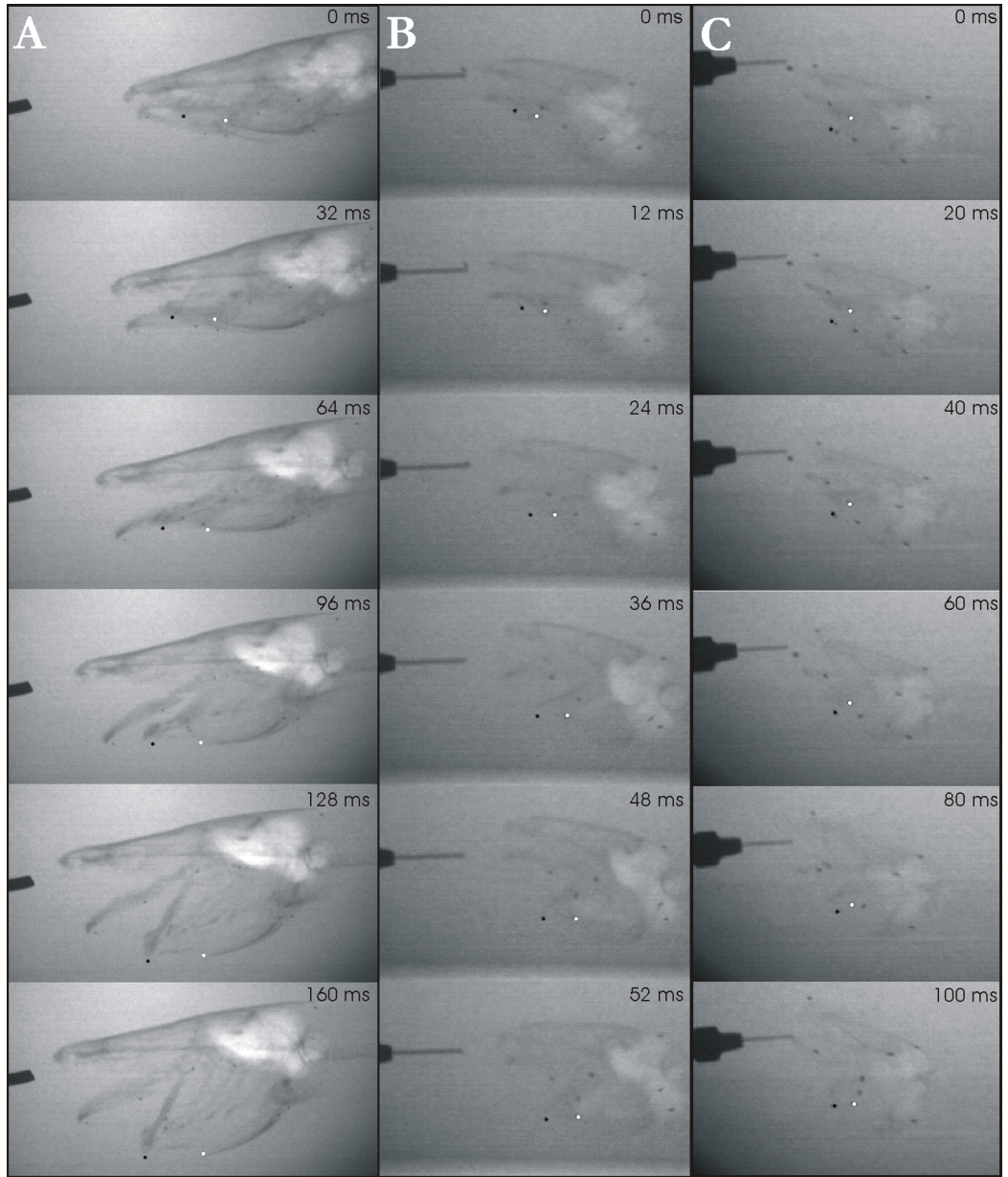
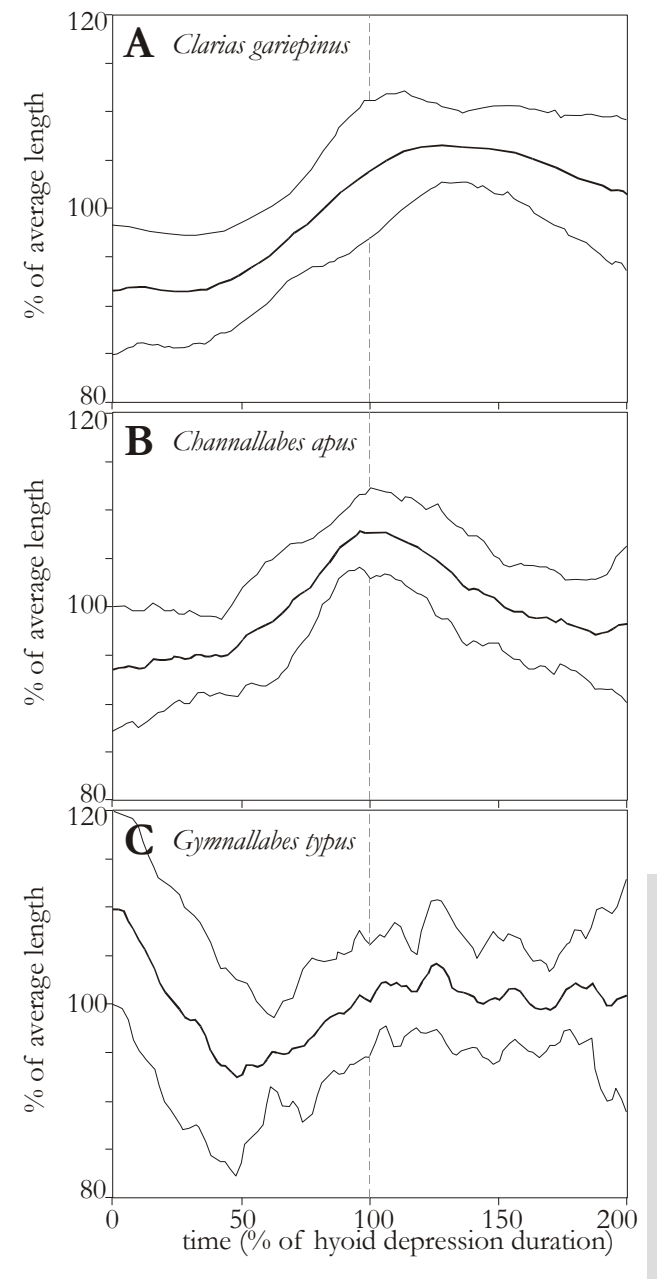


Figure 8: Selected X-ray video frames of prey capture in *Clarias gariepinus* (A), *Channallabes apus* (B) and *Gymnallabes typus* (C). The markers at the tip of the cleithrum and the tip of the hyoid are highlighted by white and black dots respectively (see also Fig. 3). Note the increasing distance between the points during hyoid depression in A and B, but not in C.

hyoid depression for, respectively, *C. gariepinus* and *C. apus*) after which the muscle starts elongating. This m-sh elongation then continues during the entire second half of hyoid depression. In contrast to *C. apus*, a limited amount of m-sh elongation can still be observed after the maximal hyoid depression is reached in *C. gariepinus* (Fig. 9A,B).



For Gymnallabes typus, however, a different pattern of m-sh length changes during prey capture is observed (Fig. 9C). In contrast to the other species (Fig. 9A,B), the m-sh shortens considerably in G. typus (approximately 17 % of the muscle's mean length) during the first half of the hyoid depression phase. Yet, muscle shortening does not continue until the end of the hyoid depression. Similarly to the other Clariids, the second half of the hyoid depression phase is characterised by m-sh elongation. However, at the instant of maximal hyoid depression, the length of the m-sh is still shorter than at the start of the hyoid depression in G. typus (Fig. 9C).

Figure 9: Mean profiles of sternohyoideus length changes for the period of hyoid depression (0% to 100% time) and elevation (100% to 200% time) during prey capture in gariepinus Clarias (A), Channallabes apus (B) and Gymnallabes typus (C). The lines accompanying above below each curve represent standard errors. See text for further information.

Discussion

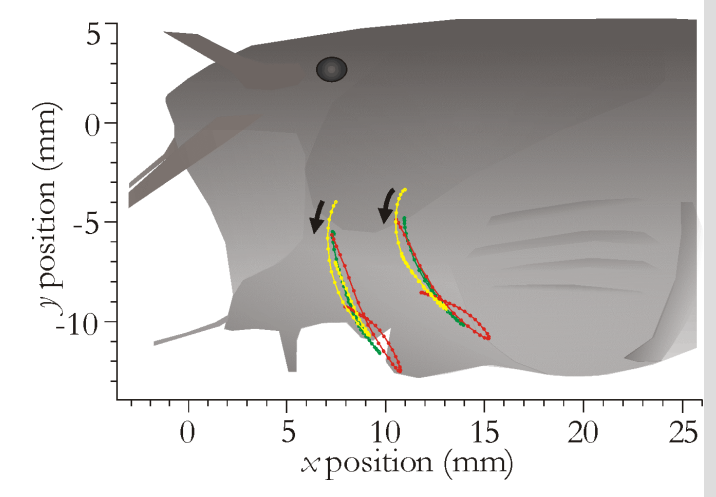
As suggested by previous work (*Chapter 6*), interspecific variation in the morphology of the sternohyoideus muscle (m-sh) exists within the catfish family Clariidae. More specifically, significant differences in the mass, cross-sectional area and fibre diameter of the m-sh are observed (Figs. 5A, 5C, 6) while m-sh fibre length is similar for all species studied (Fig. 5B). The m-sh of the species with the larger m-sh cross-sectional area also contains fibres with larger diameters (Table 2). As the average fibre diameter is generally associated with the percentage of fast glycolytic (Type IIb) fibres, a relatively large-fibred muscle is probably better in performing rapid muscle contractions compared to a smaller-fibred muscle of the same dimensions. Consequently, the combination of an increased effective cross-sectional area and larger fibres (Fig. 6), as for example observed in *Gymnallabes typus* with respect to *Clarias gariepinus* (Figs. 5A,6), may therefore result in a hyoid depression system in which the function of the m-sh is no longer limited to force transmission (as in *C. gariepinus*, Fig. 1B), but also includes powering of the hyoid expansion by shortening while the muscle is retracted by the pectoral girdle (Fig. 1A).

As the most important function of the m-sh during suction feeding in Clariidae is causing a ventral depression the hyoid (Fig. 1), the potential increase in power and speed of the more voluminous and thicker fibred m-sh could result in an increased hyoid-depression performance. Compared to *C. gariepinus*, such significantly increased muscle and fibre cross-sectional diameter of the m-sh can be found at least in one species: *Gymnallabes typus* (Fig. 7; Table 2). As expected, this species also show larger hyoid depressions compared to *C. gariepinus*. However, such increased total hyoid depression is also observed for *Channallabes apus*, a species with similar mass, fibre length and cross-sectional area of the m-sh compared to *C. gariepinus* (Table 2). Furthermore, only *Clariallabes longicauda*, and not the species with the most massive m-sh (*G. typus*) has gained significantly in peak velocity of hyoid depression (Fig. 7B). Therefore, no simple relationship exists between the morphology of the m-sh and hyoid depression performance in Clariidae.

Observing a larger or faster lowering of the bottom of the mouth cavity is indicative of a more powerful system causing hyoid depression. Indeed, any increase in the volume of the mouth cavity during suction feeding by means of hyoid depression requires an input of force exerted on the hyoid. The m-sh has an essential role in the hyoid-depression system as all force has to be transmitted to the hyoid through the m-sh (Fig.1). Yet, not only the m-sh but also two other muscles contribute in producing this force: the hypaxial and the epaxial muscles. In fact, the m-sh is only a single part of the entire system causing hyoid depression: it couples the retraction of the pectoral girdle to the hyoid (Fig. 1). Consequently, changes in the magnitude or speed of hyoid depression do not necessary imply a shift in function of the m-sh: the observed hyoid depression also depends on how the origin of the m-sh is retracted by the pectoral girdle and on the morphology of the hyoid itself.

The strength of the m-sh after activation will determine its behaviour when it is being retracted by the pectoral girdle. If the retraction of the muscle's origin is too powerful, the muscle may not be able of shortening during hyoid depression. This situation seems to occur in *Clarias gariepinus*, the species with the slenderest m-sh in our study (Fig. 9A; *Chapter 2*) and also for *Channallabes apus*, a species with a m-sh of similar mass and effective cross-sectional area, but with larger fibre diameters compared to *C. gariepinus* (Fig. 9B). Consequently, the increased magnitude of hyoid depression observed in *C. apus* (Fig. 9) with respect to *C. gariepinus* is apparently not caused by a shift in the strain pattern of the m-sh.

The data for *C. apus* therefore exemplifies that an increased retraction and depression of the anterior tip of the pectoral girdle can cause an increased hyoid depression without altering the strain behaviour of the m-sh. If we compare the displacement patterns of the hyoid and the pectoral girdle between different feeding sequences of a single species, variation in the magnitude of hyoid depression is typically associated with similar variation in the amount of pectoral girdle rotation (Fig. 10). Unfortunately, despite its apparent crucial role in generating suction in fish, the functional morphology or mechanics of the pectoral girdle has rarely been studied (e.g., Oliveira et al., 2001).



Displacement Figure 10: profiles of the hyoid tip (anterior points) and cleithrum tip (posterior points) relative to roof of the buccal cavity during three feeding sequences of Channallabes apus with different hyoid depression magnitudes (yellow < green < red) imposed on a schematic illustration of the head of C. apus at the moment of maximal hyoid expansion. figure illustrates the tightly coupled kinematics of both elements and thereby

demonstrates that the amount of hyoid depression is modulated predominantly through the amount of rotation of the pectoral girdle with respect to the neurocranium. A similar pattern was also observed in the other clariid species.

Gymnallabes typus also shows considerably greater hyoid depressions when compared to Clarias gariepinus, but unlike Channallabes apus, this species has a m-sh with almost twice the mass and more than twice the effective cross-sectional area and average fibre diameter of C. gariepinus (Table 2). The distinct m-sh morphology of G. typus appears to be reflected in a different pattern of shortening during hyoid depression, with a period of shortening

during the initial stages of hyoid depression (Fig. 9C). Yet, even this species does not show the "classical" mechanism of hyoid depression in which m-sh shortening is assumed to continue throughout the entire hyoid depression phase (Fig. 1A): after a short period of shortening, the m-sh of *G. typus* starts elongating as is observed in *C. gariepinus* and *C. apus*.

In Clarias gariepinus and Channallabes apus, the m-sh is nearly maximally elongated at the moment of maximal hyoid depression (Fig. 9A,C). This means that, compared to the situation in which the m-sh would shorten during hyoid depression, the cleithrum (pectoral girdle) has to rotate over a larger angle to cause an equal amount of hyoid depression (see Fig. 1B compared to Fig. 1A). This could have significant consequences for the recovery phase, i.e. when the hyoid and cleithrum are elevated and the buccal cavity is compressed: it may require a longer time to reposition the cleithrum unless shortening of the m-sh during the recovery phase may actually help in protracting the cleithrum. This may be important, as our observations have shown that in case of an unsuccessful suction-feeding attempt, the catfish are able to perform a subsequent prey-capture attempt shortly after. Being able to quickly reposition the cleithrum is probably an important aspect of the capability to perform consecutive prey captures. In this respect, it would be interesting to investigate how the cleithrum recovery time differs between C. gariepinus or C. apus and G. typus, the single species that does not have a fully elongated m-sh at the start of the recovery phase. Although we did not include unsuccessful prey captures in our analysis (which would particularly motivate fish to recover quickly), both C. gariepinus and C. apus show m-sh shortening during the recovery phase (Fig. 9A,B), while G. typus does not (Fig. 9C). Given that hyoid elevation velocity (and thus the speed in which the rostral end of the m-sh is protracted during this phase) does not differ significantly between the species studied (Fig. 7C), this indeed suggests that the m-sh contributes (through active contractile force and/or passive elasticity) in elevating the cleithrum and reducing the recovery time by shortening in course of the compressive phase in these species. In this way, the potential delay due to repositioning the cleithrum after this element has stretched the sternohyoideus during the expansion phase is compensated for by m-sh shortening which helps in protracting the cleithum afterwards.

Studies using electromyography (EMG) have demonstrated repeatedly that the m-sh is active during the expansive phase of suction feeding in a variety of teleost species (e.g., Lauder, 1983c; Alfaro et al., 2001; Wainwright, 2002; Carroll, 2004). As suction feeding motor patterns are considered to be evolutionary conservative in fishes (Wainwright, 2002), it is likely that also clariid catfishes activate their m-sh during hyoid depression. In this way, the pattern observed in *Clarias gariepinus* and *Channallabes apus* (Fig. 9A,B) would imply active, excentric force exerted by the m-sh on the hyoid during buccal expansion, while m-sh contraction during recovery would result from the elasticity build up by the previous elongation. Yet, the observed m-sh strain pattern in these two species leaves the possibility that the m-sh is used as a passive force transmitter during expansion, and is only activated to power cleithrum protraction during the recovery phase. If the latter situation occurs, this would not only imply a different "strategy" of the m-sh to depress the hyoid,

but even an alternative m-sh "function" compared to other fishes (see Carroll, 2004). Unfortunately, no EMG data are available for prey capturing clariid catfishes to distinguish between these two possibilities in the timing of m-sh activation. However, the data on *Gymnallabes typus* showing an early m-sh shortening period (Fig. 9C) are indicative of the traditional m-sh activation during the expansive phase of suction.

Although a mechanistic explanation was given for the diverging m-sh strain pattern of *Gymnallabes typus* compared to the other clariid species (i.e. the considerably larger m-sh mass and cross-sectional area enable this muscle to depress the hyoid by shortening during the first instants of buccal expansion), this does not explain why this species has developed this alternative pattern (Fig. 9). Preliminary results show that *G. typus* shows a highly constrained lateral expansion (suspensorium abduction) compared to the other species. Consequently, the more massive m-sh (Fig. 5) and the large maximal hyoid depression in *G. typus* (Fig. 7) may be needed to compensate for this reduced amount of suspensorial abduction. In turn, this compensation may be required to maintain an efficient suction feeding ability.

In conclusion, the species with the largest cross-sectional area of the m-sh also tend to show an increased magnitude of hyoid depression and (with exception of Gymnallabes typus) a higher maximal speed of hyoid depression (Table 2). This suggests that a thicker m-sh is able to transmit higher forces to the hyoid during suction feeding. Still, only the species with the largest m-sh cross-sectional area and mass of the four species studied (G. typus) was able to shorten its m-sh during part of the expansive phase. Consequently, the m-sh shortening pattern for Clarias gariepinus observed in a previous study (Chapter 2) is not an exception among catfishes. Increasing the magnitude of hyoid depression compared to C. gariepinus does, however, not necessarily require an alternative pattern of m-sh strain, as the m-sh force transmission from the pectoral girdle to the hyoid can apparently be performed through an excentric contraction as in Channallahes apus or a partly concentric contraction as in G. typus. Still, none of the species studied was able to show a continuing m-sh shortening during hyoid depression as often hypothesised to be the general mechanism of hyoid depression in teleost fishes (Lauder, 1985; Bone and Marshall, 1986). Our data emphasize the importance of the post-cranial muscles (epaxial and hypaxial musculature) for powering suction feeding in clariid catfishes.

Modulation and variability of prey capture kinematics in clariid catfishes

Sam Van Wassenbergh – Anthony Herrel – Dominique Adriaens – Peter Aerts

Journal of Experimental Zoology Part A: Comparative Experimental Biology (in press)

Summary

Species with narrow or limited diets (trophic specialists) are expected to be less flexible in their feeding repertoire compared to species feeding on a wide range of different prey (trophic generalists). The ability to modulate prey capture kinematics in response to different prey types and prey position, as well as the overall variability in prey capture kinematics, is evaluated in four clariid species ranging from trophic generalist (Clarias gariepinus) to species with morphological specializations and a narrow diet (Channallabes apus and Gymnallabes typus). High-speed video recordings were made of prey captures on two prey that differ in shape, attachment strength and hardness. While the observed amount of strike-to-strike variability in prey capture kinematics is similar for all species and not influenced by prey type, only the two less specialized species showed the ability to modulate their prey capture kinematics in function of the presented prey types. All species did, however, show positional modulation during the strike by adjusting the magnitude of neurocranial elevation. These results indicate that the narrow dietary breadth of trophic specialists is indeed indicative of functional stereotypy in this group of fishes. Although most studies focussing on prey processing found a similar result, the present study is one of the few that was able to demonstrate this relationship when focussing on prey capture Possibly, this relationship is less frequently observed for prey capture compared to prey processing because, regardless of prey type, the initial capture of prey requires a higher amount of variability.

9.1 Introduction

In evolutionary biology, it has been hypothesized that trophic breadth is correlated with behavioural and functional versatility or flexibility. Species with limited diets (trophic specialists) are expected to be less flexible in their feeding capacities compared to species that feed on a wide range of different prey (trophic generalists). Indeed, trophic generalists often have to switch from one prey to another and the ability of generalists to change their feeding behaviour in function of the type or position of the prey (i.e. modulation) is an important aspect of their success (e.g., Norton, 1991, 1995; Nemeth, 1997a, 1997b). In contrast, because trophic specialists restrict themselves to a limited range of prey for which they possess specific morphological and/or behavioural modifications (Ferry-Graham et al., 2002), the importance of being able to handle a wide variety of prey decreases. Although several experimental tests on fishes have supported the above hypothesis (Lauder, 1983a,b; Sanderson, 1991; Ralston and Wainwright, 1997), other studies failed to demonstrate this suggested stereotypy of specialists compared to the flexibility of generalists (Sanderson 1988; Sanderson 1990) or even showed striking examples countering this hypothesis (Liem, 1978; Liem, 1980; Liem, 1984; Norton, 1991). Yet, the reason why support for this hypothesis is found in some cases and not in others remains unclear.

In this study, the variability and modulation of prey capture kinematics is studied in four catfish species of the family Clariidae (Clarias gariepinus, Clariallabes longicauda, Gymnallabes typus and Channallabes apus) that show clear differences in the diversity of their diet (Fig. 1). Clarias gariepinus is a typical example of a trophic generalist with a broad diet of different prey ranging in size from zooplankton to fishes half its own length (Groenewald, 1964; Bruton, 1979; Yalçin et al., 2001). This species feeds in a variety of habitats and in fluctuating marginal areas of lakes and rivers. Clarias gariepinus switches from one prey to another as prey availability (density and accessibility) changes (Bruton, 1979). Clarias gariepinus is also known to use multiple feeding modes like foraging, shovelling, surface feeding and group hunting (Bruton, 1979), and different structural adaptations can be linked to different feeding types ranging from filter feeding to piscivory (Groenewald, 1964). Unlike C. gariepinus, the other clariid species used in this study (C. longicauda, G. typus and C. apus, Fig. 1) have developed unusually large (or hypertrophied) jaw adductors, and also lack elongated and numerous gill rakers (Cabuy et al., 1999). While the diet of C. longicauda, a species with an intermediate degree of jaw adductor hypertrophy is still relatively diverse, the trophic diversity is strongly reduced in the anguilliform representatives C. apus and G. typus (Fig. 1). According to Herrel et al. (2002), modifications of the feeding system (i.e. jaw adductor hypertrophy) enable these species to exert much larger bite forces onto prey (bite forces for C. apus are more than 10 times higher than C. gariepinus for a skull length of 39 mm). Given this increased bite performance, it was not surprising that dietary analyses showed an altered and more selective feeding pattern for species that possess hypertrophied jaw adductors with a special preference for coleopterans, which are indeed hard prey (Huysentruyt et al., 2004).

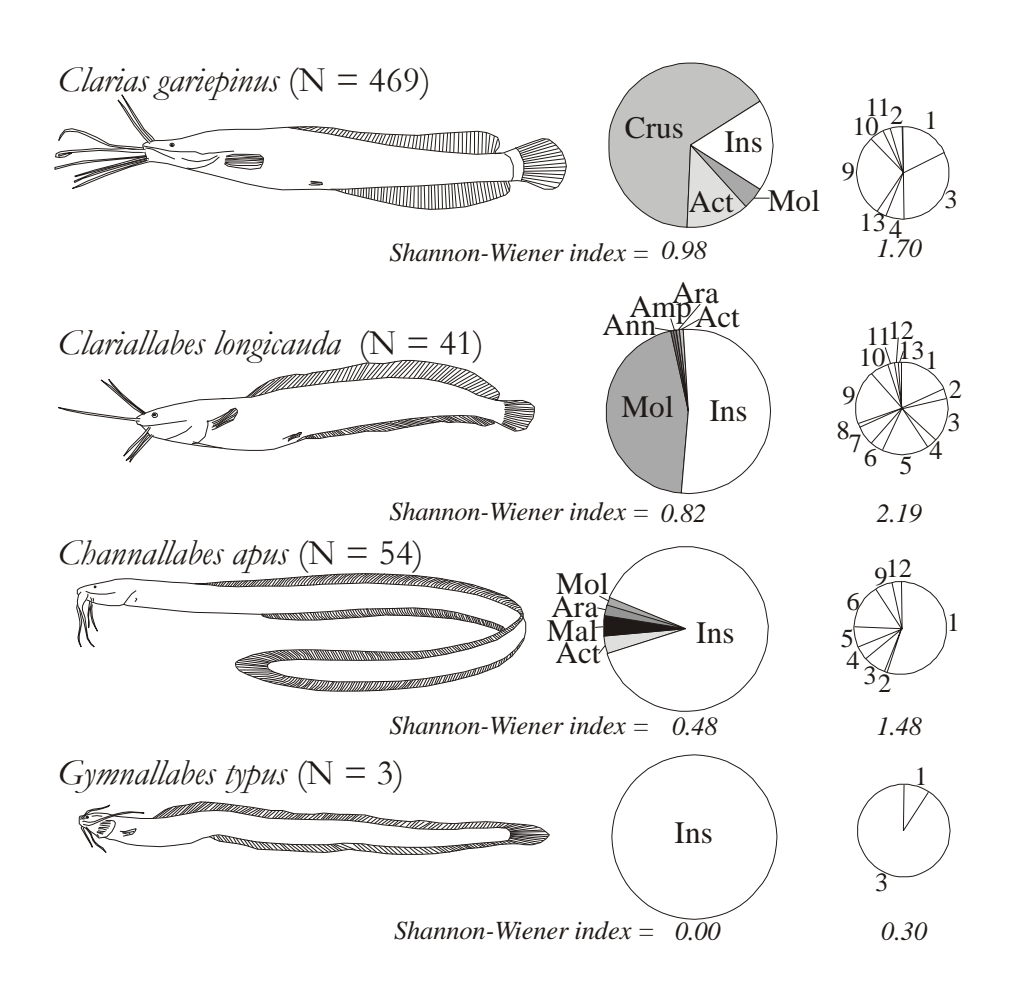


Figure 1: Dietary composition of four species of Clariidae according to the literature (Bruton, 1979 for C. gariepinus, Wyckmans, 2004 for C. longicauda and Huysentruyt et al., 2004 for C. apus and G. typus). The Shannon-Wiener index of dietary diversity was used to quantify the degree of specialization in each species, and is calculated by $-\Sigma p_i \ln p_i$, where p_i is the numerical proportion of a particular prey category. The large pie-charts in the middle give broad taxonomic groupings (see legend below). The smaller pie-charts on the right side illustrate the numerical proportions of the most important groups of insect in the diet. Drawings of C. apus and G. typus are made after Teugels and Adriaens (2003). Legend: Act = Actinopterygii, Amp = Amphibia, Ann = Annelida, Ara = Arachnida, Crus = Crustacea, Ins = Insecta, Mol = Mollusca, 1 = Colleoptera, 2 = Dictyoptera, 3 = Diptera, 4 = Hemiptera, 5 = Hymenoptera, 6 = Isoptera, 7 = Lepidoptera, 8 = Mecoptera, 9 = Odonata, 10 = Orthoptera, 11 = Trichoptera, 12 = Ephemeroptera and 13 = others. N = number of stomachs analysed with content. Although the dietary data sample of G. typus is small, similar results are found for Gymnallabes alvaresi (Huysentruyt et al., 2004). This species (closely related to G. typus) ingests Coleopterans in high proportions and has a low Shannon-Wiener index of diet diversity.

Here, we test whether the trophic generalists exhibit a greater ability to modulate their prey capture kinematics in response to different prey types when compared to the more specialized species. We also tested whether there is a relationship between the overall variability of the exhibited kinematic pattern and the degree of trophic specialization and whether the experimental prey types influence the variability of the kinematic patterns (see also Wainwright and Friel, 2000). Not only prey type, but also prey position can elicit alternative prey capture movements (Elshoud-Oldenhave and Osse, 1976; Liem, 1980; Lauder and Liem, 1980; Lauder, 1981). Therefore, we also tested the ability of these catfish species to adjust their head position with respect to the prey right before prey capture. As clariid catfishes are mainly nocturnal predators relying predominantly on chemotactile and electrical signals for prey detection (Bruton, 1979; Hanika and Kramer, 2000), such positional 'fine-tuning' during prey capture can be important in this group of fishes.

9.2 Materials and Methods

9.2.1 Animals

Seventeen adult specimens (6 Clarias gariepinus, 4 Clariallabes longicauda, 4 Channallabes apus and 3 Gymnallabes typus) were used in the experiments. The C. gariepinus specimens were aquarium-raised specimens of which larval stages were initially obtained from the Laboratory for Ecology and Aquaculture (Catholic University of Leuven). Specimens of C. longicauda and C. apus were caught in Northern Gabon. Gymnallabes typus was imported from Western tropical Africa. Cranial lengths of the C. gariepinus specimens were 44.4, 44.7, 47.5, 47.5, 51.7 and 56.6 mm. The C. longicauda individuals had cranial lengths of 32.4, 34.7, 35.7 and 49.0 mm. The measured cranial lengths for C. apus and G. typus were respectively 22.6, 23.10, 24.2, 25.80 mm and 19.20, 20.8, 22.15 mm. Cranial length (CL) was defined as the distance between the rostral tip of the premaxillary and the caudal tip of the occipital process. The animals were kept separate in 20 L test aquaria and were trained to capture the presented food inside a narrow, projecting feeding arena (25 cm length, 8 cm width, 15 cm water height) in the aquarium (which forced the animals to feed in a position perpendicular to the camera).

9.2.2 Prey

Two different prey types were used: (1) a piece of cod fillet (*Gadus morhua*) of about 3 cm³ and (2) a North Sea shrimp (*Pandalus borealis*) of approximately 4 cm in total length. Both prey types were attached to a thin, plastic coated steel wire and were suspended about 5 cm above the bottom of the corridor. The cod was pinned onto the steel wire, while the shrimp was clipped around its middle (see Fig. 2). For both prey, we measured the force

needed to detach the prey from its attachment (by pulling horizontally), the force needed to tear a piece from the prey, and force needed to penetrate the prey using a standard object (flat-tipped screw of 3 mm diameter) using a Kistler Force Transducer 9203 (range 0.1 - 500 N) and charge amplifier (type 5995).

These prey were selected because they differ in several physical properties. (1) Both prey types differ in shape: a spherical piece of fish versus a more elongated shrimp. (2) The attachment strength of both prey types differs significantly (P<0.001) implying that the piece of fish can be sucked easily from its attachment, while the firmly tied shrimp has to

Table 1: Force (mean + S.D.) needed to detach, tear or pierce the presented prey types.

	fish	shrimp
detach*	0.4 <u>+</u> 0.1	1.8 ± 0.6
tear	2.1 ± 1.1	2.0 ± 0.6
pierce*	2.1 ± 0.8	4.6 ± 0.8
$\overline{N} = 10$		-1
* significant	prey type differe	ences $(P < 0.05)$

be pulled more forcefully from its attachment (Table 1). (3) Both prey types clearly differ in their hardness: While the fish can be easily penetrated, significantly (P<0.001) higher forces are needed to pierce the shrimp (Table 1).

When feeding on attached prey types, clarid catfishes are known to use a combination of suction feeding (drawing the prey toward the mouth) followed by fast snapping of the oral jaws onto the prey (Bruton, 1979;

Chapter 6). If the prey cannot be sucked directly from its attachment, they are detached by a lateral head swing in which the prey is held tightly between the oral teeth (Chapter 6). Prey processing usually only occurs after these catfishes have returned to their favoured, hiding places in the aquarium.

Given this feeding mode and the above mentioned physical properties of both prey used in this study, several ways of modulation of prey capture kinematics in function of prey type can be expected (Fig. 2). The three types of modulation expected are: (1) modulation of gape in function of the shape and size of the prey (Fig. 2A). Reducing the oral gape as much as possible will increase prey capture performance, because it increases the suctioninduced flow speed (Alexander, 1970a; Muller et al., 1982) and also reduces the duration of the compressive phase. Note in this respect, that the depression of the hyoid apparatus in Clariidae is responsible for the largest increase in buccal volume (Chapter 7) and a reduced mouth opening will therefore only have a smaller effect on the total volume of water sucked into the mouth. (2) Modulation of suction effort in function of the attachment strength of the prey (Fig. 2B). The increased attachment strength of the shrimp makes it more difficult to draw it towards the mouth by suction feeding. Therefore, an increased magnitude and/or speed of buccal expansion are likely to increase the prey capture efficiency on this prey type. (3) Modulation of jaw closing speed in function of external texture and piercing strength of the prey (Fig. 2C). As the shrimp cannot be sucked directly from its attachment, a strong grip on this prey by the jaws prior to the lateral head swing will likely increase the prey capture success. A higher level of jaw adductor muscle activation when capturing the shrimp, resulting in faster jaw closing movements and higher biting forces at the moment of impact of the lower jaw with the prey, will most likely improve the piercing of the catfish's teeth into this type of prey.

Although both prey types are immobile food items, our observations show that both prey types are challenging for the catfish, which often needed several attempts to detach a single prey by suction, especially (but not only) during feeding on the firmly attached shrimps. The catfish sometimes even returned to their hiding places in the aquarium after failing to detach the food. We can therefore safely assume that high levels of performance are exhibited during feeding on these prey, and that the catfish are prompted to enhance their performance by showing prey-type modulation if they are capable to do so.

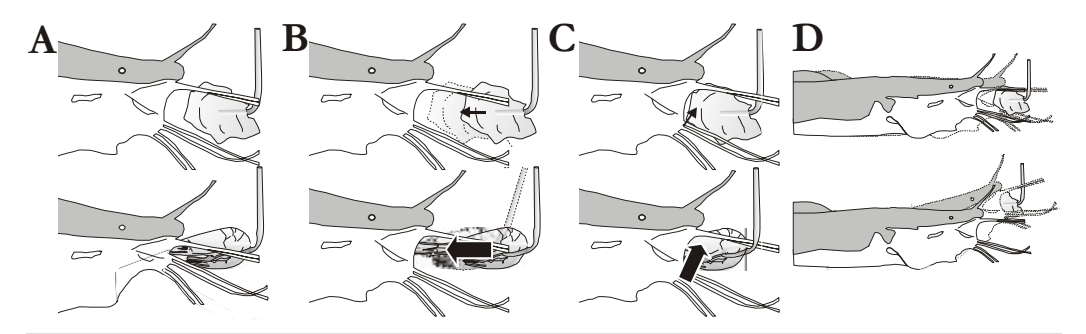


Figure 2: Illustration of the four types of modulation that are expected to increase a clariid catfishes' capture performance on the prey used in this study (attached fish and shrimp). In A, oral gape is adjusted according to the size of the prey. In B, an increased suction effort is shown when feeding on the more firmly attached shrimp. In C, the jaws are closed faster during captures on shrimp. Compared to the fish, this prey is harder to pierce the teeth into, and also needs a firmer grip to be detached during subsequent lateral head swings. While A, B and C are prey type related modulations, a 'positional' modulation is shown in D. In this, the magnitude of neurocranial elevation is adjusted according to the position of the prey.

9.2.3 High-speed video recordings

High-speed video recordings (250 frames s⁻¹) were made from a lateral and ventral position, using a Redlake Imaging Motionscope digital high-speed video camera (shutter 1/2500). Lateral and ventral views of prey captures of eight individuals were recorded separately (different prey capture sequence for each recording). All other individuals were filmed simultaneously from a lateral and a ventral view using a mirror inclined at 45 degrees. Two floodlights (600 Watt) provided the necessary illumination. Only those prey capture sequences that were approximately perpendicular to the camera lens were selected and retained for further analysis. To do so, lateral recordings in which skull roof, skull bottom or origin of the maxillary barbel of the opposite side of the fish were visible, as well as ventral recordings in which the side of the skull was visible, were discarded. For each individual, 10 lateral and 10 ventral recordings (each consisting of 5 fish and 5 shrimp

captures) were analysed. For one *C. gariepinus* individual, however, only 4 (in stead of 5) ventral recordings with cod as prey could be analysed. Anatomical landmarks were digitized on the recorded images (Fig. 3) using Didge (version 2.2.0, Alistair Cullum), and the horizontal (x) and vertical (y) coordinates for each point were exported to a

spreadsheet.

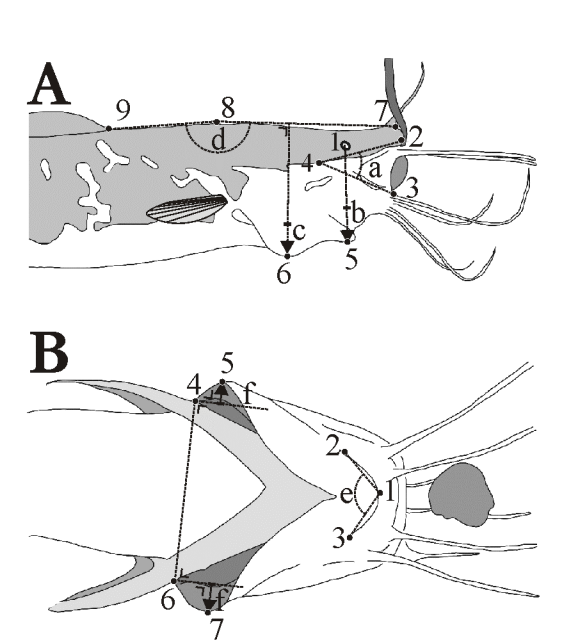


Figure 3: Anatomical landmarks digitized with the calculated kinematic variables (dotted lines) on the lateral (A) and ventral (B) highspeed video images of Clarias gariepinus. Identical landmarks were digitized on images of the other species. A Lateral landmarks: (1) middle of the eye, (2) upper jaw tip, interior side, (3) lower jaw tip, interior side, (4) jaw articulation, (5) tip of the hyoid, (6) most positioned ventrally point of branchiostegal membrane, (7) rostral tip of the skull roof, (8) caudal tip of the skull roof and (9) anterior tip of the caudal fin. The measured angular variables are: gape angle (a) and neurocranial elevation (d). The linear variables are: hyoid depression (b) and branchiostegal depression (c). B Ventral landmarks: (1) hyoid symphysis, (2,3) most caudally discernible points on the hyoid bars, (4,6) base of pectoral spine, (5,7) lateral tip of the branchiostegal membrane. The measured angular variable is the hyoid expansion (e). The measured linear variable is the branchiostegal expansion (f, average between left and right).

9.2.4 Kinematic variables

After digitization of the sequences, the coordinates of each point were used to calculate the variables of interest (Fig. 3). After data filtering (fourth order, zero phase-shift Butterworth low pass filter) and differentiation, peak velocities of jaw and hyoid movements were determined. Because for some individuals lateral and ventral views were not recorded simultaneously, the data sets of each recording view (lateral and ventral) had to be analysed separately.

For the lateral high-speed video recordings, the following kinematic variables were analysed: (1) maximum gape angle, (2) total lower jaw rotation (maximal angle minus starting angle) (3) total hyoid depression (maximal depression minus starting position), (4) total depression of the branchiostegal membrane (maximum depression minus starting position) and (5) total neurocranial elevation, (6) the maximal jaw opening velocity, (7) maximal jaw closing velocity and (8) maximal hyoid depression velocity.

From the ventral high-speed video recordings, the following kinematic variables were analysed: (1) maximal width of hyoids (angle), (2) maximal lateral expansion of the hyoids

(angle, maximal width minus starting width) and (3) the lateral expansion of the branchiostegal membrane (maximal excursion minus starting position) and (4) average angular hyoid abduction velocity (See also Fig. 3)

9.2.5 Statistics

To evaluate the ability of each species to modulate its prey capture kinematics for the different experimental prey, the statistical approach of Ralston and Wainwright (1997) was used. First, two-way analyses of variance (ANOVAs) were used to test for each species the ability to alter the kinematic variables of interest when feeding on the two different prey types. In these ANOVAs, the 'individual' factor (random effect) was crossed with 'prey type' factor (fixed effect), resulting in an individual-by-prey-type interaction. F-ratios for 'prey type' effect were calculated with the prey mean squares in the numerator and the interaction-term mean squares in the denominator. If two-way interaction between 'prey type' effects and 'individual' effects occur, there are differences in the way individuals respond to the two different prey types. In this case, separate tests for 'prey type' effects (one-way ANOVA) within each individual of the species were performed.

Second, the ability of each species to modulate its position with respect of the prey during the course of the strike was evaluated. Therefore, a Spearman rank correlation was used to test whether catfishes elevate the skull more when the head of the fish (when approaching the prey) was deeper under the prey. For each prey capture sequence, the frame preceding the start of the feeding event (mouth starts to open) was analysed. The position of the skull with regard to the prey at this moment was evaluated by extending the segment describing the position of the skull (landmarks 7-8 of Fig. 3A) towards the attached prey. The following scores were given: (1) skull segment above the prey, (2) skull segment intersects the upper part of the prey, (3) skull segment intersects the lower part of the prey (4) skull segment underneath the prey.

Third, principal components analyses (PCA) were performed on the kinematic variables of (1) the lateral high-speed video recordings and (2) the ventral high-speed video recordings. To quantify the amount of variation exhibited, centroid distances were calculated (distance between unrotated PC-scores for each prey capture and the mean position of all PC-scores for the corresponding prey type in a three-dimensional representation) and we tested whether prey type influenced the variability of the kinematic patterns within each species (two-way crossed design ANOVAs described above, performed on centroid distances from separate PCAs for each species). When testing for interspecific differences in the overall variability in prey capture kinematics, a single PCA was performed including the data sets of all the species studied. In this, distances and linear velocities were scaled according to cranial length in order to exclude the influence of size. 'Species' effects in centroid distances from the first three principal components were tested in one-way ANOVAs, followed by Spjotvoll-Stoline *post hoc* tests (only performed when the one-way

ANOVA indicated overall statistical significance). Although this approach is analogous to measuring the effect of 'prey type' on the variance of each kinematic variable, the final interpretation is strongly simplified as a single parametric test can be used to test the significance of the results (Ralston and Wainwright, 1997).

Although the significance level of P=0.05 is used throughout the analyses, the results of applying a sequential Bonferroni correction (that adjusts the significance level according to the number of tests that were carried out) in case of consecutive univariate testing are also given whenever applicable. However, as the use of this method (and other multiple testing adjustments) in ecological studies has recently been questioned (Moran, 2003), we base the discussion on the unadjusted results (see also Ralston and Wainwright, 1997). Nevertheless, as the sequential Bonferroni method has been used in several topic-related studies (e.g., Sanderson, 1991), the comparative value of our results is increased by including this into the analysis.

9.3 Results

9.3.1 Prey type modulation

The two less specialized species (C. gariepinus and C. longicauda) showed significant modulation in response to the two prey types (Table 2). C. gariepinus decreases its maximal gape angle when feeding on shrimps compared to the larger pieces of fish (ANOVA, $F_{1.5}$ = 6.31, P = 0.0075). After applying the more conservative statistical method described above (i.e. sequential Bonferroni correction), this modulation of mouth opening size in C. gariepinus is the only statistically significant modulation of the entire data set (Table 2). In general, no modulation in the magnitude or speed of the observed cranial expansion can be discerned for this species, although two out of the six individuals did show a significantly larger lateral expansion of the branchiostegal membranes during shrimp captures (ANOVA, $F_{1,8} = 6.31$, P = 0.040). In contrast to C. gariepinus, C. longicauda did not modulate its gape but showed larger hyoid depressions when feeding on the more firmly attached shrimps (ANOVA, $F_{1,2} = 17.9$, P = 0.025) as predicted. Also within *C. longicauda*, some individuals responded differently to the two types of prey (Table 2): while one individual increases its jaw closing speed when capturing shrimps (ANOVA, $F_{1,8} = 43.2$, P = 0.00017), another individual showed larger lateral expansion of the branchiostegal membrane when feeding on this prey type ($F_{1,8} = 16.7$, P = 0.0035).

However, no prey type related modulation could be demonstrated for the two most specialized species (C. apus and G. typus). A single exception was that, like some C. gariepinus and C. longicauda individuals, one out of the 4 C. apus specimens showed a larger lateral expansion of the branchiostegal membrane (ANOVA, $F_{1,8} = 11.1$, P = 0.010). An overview of the results for all species is given in Table 2.

Table 2: Means and S.E.M. of the analysed kinematic variables of prey capture	nematic variable	s of prey captur	e					
	Clanias g	Clarias gariepinus	Clariallabes	Clariallabes longicanda	Channall	Channallabes apus	Gymnalle	Gymnallabes typus
	fish	shrimp	fish	shrimp	fish	shrimp	fish	shrimp
A) gape max. gape angle (°)	35.4 ± 1.4 *	30.8 ± 1.1 *	58.5 ± 1.8	57.5 ± 1.5	47.4 ± 1.7	45.8 ± 1.3	55.9 ± 2.0	53.0 ± 1.8
B1) buccal expansion magnitudes lower jaw opening rotation (°) hyoid depression (mm) branchiostegal depression (mm) max. width of hyoids (°) lateral expansion of hyoids (°) hyangli branchiostegal expansion of hyboresis and property of the	25.9 ± 1.1 7.55 ± 0.30 6.96 ± 0.39 117.7 ± 0.7 31.8 ± 1.0 3.30 ± 0.30	23.2 ± 0.8 7.36 ± 0.29 6.06 ± 0.30 117.5 ± 0.9 30.5 ± 1.2	28.5 ± 1.5 7.12 ± 0.37 3.78 ± 0.27 121.0 ± 0.9 18.9 ± 1.2	27.3 ± 1.6 8.70 ± 0.26 4.06 ± 0.20 118.9 ± 1.3 19.0 ± 1.3	20.9 ± 1.5 5.20 ± 0.22 2.63 ± 0.12 104.8 ± 1.1 15.5 ± 1.1 105 ± 0.13. ⁽³⁾	20.1 ± 1.2 5.28 ± 0.20 3.21 ± 0.19 101.6 ± 2.6 14.6 ± 0.7	26.5 ± 2.0 5.11 ± 0.21 2.85 ± 0.16 116.9 ± 3.4 21.2 ± 1.5 1.83 ± 0.15	24.3 ± 1.5 5.23 ± 0.15 3.27 ± 0.31 109.9 ± 2.2 18.5 ± 1.6
B2) buccal expansion velocities max. jaw opening velocity (°/s) max. hyoid depression velocity (mm/s) mean lateral hyoid abduction velocity (°/s)			727 ± 46 165 ± 8 364 ± 43	4.00 ± 0.15 859 ± 58 250 ± 14 329 ± 33	533 ± 31 126 ± 9 265 ± 32	$\begin{array}{c} 2.07 \pm 0.17 \\ 617 \pm 46 \\ 160 \pm 10 \\ 287 \pm 30 \end{array}$	958 ± 61 151 ± 8 457 ± 42	762 ± 48 163 ± 8 361 ± 33
C) Jaw closing max. jaw closing velocity $(^{\circ}/s)$	411 ± 23	451 ± 25	$402 \pm 32^{(0)}$	553 ± 44 ⁽¹⁾	455 ± 37	492 ± 25	09 + 889	680 ± 33
Circuit front men differences me minted in hold (my way recessed decirce ANIONAs within each creation D < 0.05)	2000 Caro rioris Crist	Accioca A NOVA	Ac within one	(20 0 > 0 seises				

Significant prey differences are printed in *bold* (two-way crossed desing ANOVAs within each species, *P* < 0.05) * significant after sequential Bonferroni correction

(1) significant prey type-by-individual interaction

See text for further information

9.3.2 Positional modulation

For all species, differences in approach position are adjusted during the strike by altering the amount of neurocranial elevation (Fig. 4). More neurocranial elevation is shown if, while approaching the prey, the head was positioned deeper underneath the prey (Spearman rank correlation; *C. gariepinus*: R = 0.52, N = 60, P < 0.001; *C. longicauda*: R = 0.36, N = 40, P = 0.023; *C. apus*: R = 0.53, N = 40, P < 0.001; *G. typus*: R = 0.67, N = 30, P < 0.001). The largest neurocranial elevations were observed in *C. gariepinus* and *C. longicauda* (more than 25 degrees). *Clarias gariepinus* and *G. typus* even showed neurocranial

0 ms 0 ms 44 ms 72 ms (2) 124 ms 84 ms (A) 144 ms 112 ms 6 264 ms 152 ms 9 356 ms 284 ms depressions in about 10% of the analysed prey captures.

Figure 4: Positional modulation Clarias in gariepinus feeding on a piece of fish. More neurocranial elevation is shown (compare B to A) when, just before the strike (see 0 ms frame), the head is positioned deeper underneath the prey. Neurocranial elevation is illustrated by the increase in skull-to-body-axis angle (white lines). The maximal angle neurocranial of elevation in sequence B is represented by the angle between the dotted and full with line (112 ms frame). same pattern of positional modulation is observed for all other species in this study.

	Clarias gariepinus	gariepinus	Clariallabes	Clariallabes longicanda	Channallabes apus	abes apus	Gymnallabes typus	es typus
total variability ⁽ⁱ⁾ lateral	1.19 + 0.08	80.0	1.47 + 0.09	60.0	1.36 + 0.09	60 0	7.10 + 85.1	17
ventral	1.28 ± 0.08	0.08	1.39 ± 0.12	0.12	1.49 ± 0.12	0.12	1.57 ± 0.17	.17
variability within prey types (2)	fish	shrimp	fish	shrimp	fish	shrimp	fish	shrimp
lateral ventral		1.56 \pm 0.09 1.54 \pm 0.07 1.58 \pm 0.09 1.52 \pm 0.10	$1.50 \pm 0.08 \\ 1.44 \pm 0.11$	$1.50 \pm 0.08 \qquad 1.59 \pm 0.08 1.44 \pm 0.11 \qquad 1.57 \pm 0.10$	1.57 ± 0.10 1.34 ± 0.12	1.57 ± 0.10 1.54 ± 0.11 1.34 ± 0.12 1.66 ± 0.13	$1.68 \pm 0.09 \qquad 1.46 \pm 0.13$ $1.53 \pm 0.09 \qquad 1.50 \pm 0.17$	1.46 ± 0.13 1.50 ± 0.17

9.3.3 Variability of prey capture kinematics

Regardless of prey type, the species studied showed similar amounts of variation in their prey capture kinematics in lateral view (ANOVA on centroid distances, $F_{3,166} = 2.83$, P = 0.040; but Spjotvoll-Stoline *post hoc* test, P = 0.099 between the most distant species) and in ventral view (ANOVA, $F_{3,166} = 1.41$, P = 0.24). The experimental prey types also did not influence the variability of the kinematic patterns within each species. As shown in Table 3, the calculated average centroid distances of the PCA-scores (quantifying the amount of variability in strikes) for each prey type are not significantly different in either of the clarid species.

9.4 Discussion

separate PCAs for each species

The results of the present study generally support the hypothesis suggesting that trophic specialists have a reduced flexibility in their feeding mechanics in response to different prey types (or prey positions) compared to trophic generalists. Indeed, the species with the largest degree of trophic specialization in our study (C. apus and G. typus; Fig. 1), which have a narrow dietary range (Huysentruyt et al., 2004) and a morphologically modified jaw system (Herrel et al., 2002), show a reduced degree of modulation compared to the more generalist species (C. gariepinus and C. longicauda). specifically, prey type differences in prey capture kinematics could be demonstrated only for C. gariepinus and C. longicauda, but not for C. apus or G. typus (Table 2). However, all other estimates of modulatory capacity and variability of kinematics are similar for all the species studied: they all show the ability to modulate position during the strike by adjusting the degree of neurocranial elevation (Fig. 4), show a similar amount of variability in prey capture kinematics, and the degree of variability is not influenced by the offered prey types (Table 3).

Apparently, dietary breadth of trophic specialists and the possession of specialized morphological features are correlated with functional stereotypy in clariid catfishes. However, many previous studies failed to demonstrate differences in modulation capacity for trophic generalists and specialists (Liem, 1980; Liem 1984; Sanderson, 1988; Sanderson, 1990). In these studies, it was shown that species with morphological and dietary specialization still possess the ability to respond differently to a variety of prey types. This was the case, for instance, for the neuromuscular control of feeding in cichlid fishes (Liem, 1980; Liem, 1984), as well as for the muscle activity patterns (Sanderson, 1988) and jaw movements (Sanderson, 1990) of labrid fishes. On the other hand, and in accordance with our results, other experimental studies have confirmed the evolutionary hypothesis of reducing functional versatility with increasing degree of trophic specialization (Lauder, 1983a,b; Sanderson, 1991). A highly specialized snail-crushing sunfish, for example, showed a stereotyped muscle activity pattern of the pharyngeal jaws, also when processing prey other than snails (Lauder, 1983a). Consequently, independent evolution towards trophic specialization apparently leads to a reduced functional flexibility or versatility in certain groups of fishes, while not in others. However, this still leaves us with the question "why does this evolve in some groups, but not in others?"

Interestingly, the results of a study by Ralston and Wainwright on pufferfishes (1997) supported the expected relationship between trophic breadth and functional flexibility for buccal manipulation, but the ability to modulate prey capture mechanics in function of prey type was limited for both generalists and specialists. Apparently, differences in the degree of modulatary capacity among closely related species are harder to demonstrate for prey capture when compared to prey processing. In fact, apart from the present study, only a single study investigating prey capture relation to differences in trophic breath (or degree of specialization) found reduced modulatory capacity in specialized species when compared to closely related generalists (Sanderson, 1991, but see Liem, 1978, 1980; Sanderson, 1988, 1990; Norton, 1991; Ralston and Wainwright, 1997). In contrast, all studies focussing on prey processing found support for the hypothesis on the reduced functional flexibility of specialists (Lauder, 1983b; Ralston and Wainwright, 1997).

Possibly, prey capture demands a higher minimal degree of variability/flexibility compared to prey processing, even for specialized species. Many factors can vary during prey capture that potentially influence the appropriate prey capture behaviour, even when always capturing the same prey (prey movement, prey position relative to the predator and approaching speed of the predator, etc.). Indeed, Aerts (1990) even showed a relationship between the degree of bucco-pharyngeal expansion and the precise moment of prey uptake within the expansion phase of an insectivorous cichlid (Astatotilapia elegans) under identical feeding conditions (i.e. same prey and prey attachment method). Once the prey for which the species is specialized, is captured and held between the oral or pharyngeal jaws, the number of uncertainties in the system decreases. In this way, the evolution of a stereotyped and specialized pre-programmed prey processing pattern may be less constrained than developing a stereotyped and specialized initial prey capture pattern. This

may be a possible explanation to the observed dichotomy in the amount of studies that did, or did not find support for the hypothesis of reduced feeding flexibility in trophic specialists.

An evolutionary explanation of 'Liem's paradox' (referring specifically to cichlids with morphological specializations but still showing multiple, distinct prey capture mechanisms) has been proposed in population ecology (Robinson and Wilson, 1998). Based on optimal foraging theories, Robinson and Wilson (1998) suggested that species can develop specializations for non-preferred resources driven by competition, but still act as trophic generalists whenever the food availability rises. From this point of view, the flexibility of "specialists" would not be greatly compromised during evolution. The present result for Clariidae, in which the overall variability of prey capture kinematics is still very high in the most specialized species, in some way supports this theory. Due to the large variability in prey capture kinematics (regardless of prey type), even the specialized species will be able of performing successful prey captures on alternative, non-preferred prey. Yet, as the capacity to respond with altered capture kinematics in response to prey characteristics decreases, the specialized Clariidae will overall have a reduced prey capture success when feeding on a wide range of prey compared to the generalists. However, it is unknown how these differences in modulatory capacity affect the population ecology or competition in the natural environment of Clariidae.

The positional modulation by adjusting the magnitude of neurocranial elevation (Fig. 4) is an additional aspect of feeding versatility that has not been reported in previous studies. This capacity seems to be a general feature for Clariidae. Although it has been observed in other fishes that prey position (e.g., at the bottom, in midwater or at the water surface) can result in changes in capture kinematics (Liem, 1980; Lauder, 1981), prey were always suspended at the same distance from the bottom of the aquarium in the present study. However, they were not always approached in the same way. Prey were approached by the catfish with the head at the same level, underneath or slightly above the prey. By modifying the degree of neurocranial elevation, the catfish were capable of adjusting the position of the head during suction feeding. More neurocranial elevation was shown in strikes with the head positioned deeper underneath the prey during the approach, when compared to strikes in which the head was positioned at a higher level with respect to the prey (Fig. 4). Such positional modification through neurocranial elevation can be of great use, especially for predator species that need to locate prey from a short distance. While hunting, catfish mainly use tactile, chemical and electrical signals to locate the prey (Alexander, 1965; Bruton, 1979; Hossain et al., 1999; Hanika and Kramer, 2000; Pohlmann et al., 2001). Visual signals are also used, but are considered less important, as these catfishes have small eyes, and are mainly nocturnal predators. The exact position of the prey is detected by touching the food (active or passive) with the barbels that extend from the mouth in the form of a widening cone (Bruton, 1979). As this predatory strategy locates prey from a short distance, the ability to elevate the skull to a greater or lesser

extent (according to the position of the prey) during suction feeding, will most likely be important, and may beneficially influence prey capture success.

Finally, it should be noted that the range of prey used in the experiments of our study (Fig. 2) is inevitably, relatively narrow compared to the total diversity of prey included in the diet of some of the species studied (Fig. 1). We can therefore not conclude that the trophically specialized species *C. apus* and *G. typus* are completely unable of modulation in function of prey type. For example, modulation could still be observed if highly evasive prey had been included in our study. Nevertheless, the difference in shape, hardness and attachment strength between the prey used in the present study were enough to elicit modulation in the trophic generalists (*C. gariepinus* and *C. longicauda*), and thus provided a situation in which these catfish could distinguish both prey and adjust prey capture kinematics accordingly.

In conclusion, the present study on prey capture kinematics of a range of clariid species with increasing degree of specialization found a reduced flexibility in response to differences in prey type for the more specialized species. Modulation in function of prey position relative to the fish's head and the variability of prey capture kinematics, however, are independent of the level of trophic specialization. These result supports the notion that ecological and morphological specialization are linked with functional versatility of the feeding system in fishes, as hypothesised previously (see Liem 1984). In contrast to studies on prey processing, the present study is one of the few that was able to demonstrate the functional stereotypy of specialists compared to generalists when focussing on prey capture mechanics. The fact that the hypothetical relationship between the degree of trophic specialization and the degree of flexibility of the feeding behaviour is harder to observe for prey capture compared to prey processing, is possibly due to a higher demand on variability, needed for the initial capture of prey.

Chapter 10

Catfish strikes on land

Sam Van Wassenbergh – Anthony Herrel – Dominique Adriaens – Frank Huysentruyt – Stijn Devaere – Peter Aerts

Nature (in press)1

An important step towards our understanding of the evolution of terrestriality in vertebrates is to identify how the aquatic ancestors of tetrapods were able to exploit terrestrial prey resources. We discovered that the eel-catfish (*Channallabes apus*), an inhabitant of the muddy swamps of tropical Africa, possesses the remarkable ability to forage and capture prey on land. The animal's capacity to bend the head down towards the substrate while feeding terrestrially is shared with mudskippers (Sponder and Lauder, 1981), and therefore appears to be an essential feature for fishes to make the transition from an aquatic to a terrestrial feeding mode.

The acquisition of a terrestrial life-style, one of the key events in the evolution of vertebrates (Carroll, 2005), is particularly intriguing because of the vastly different physical demands on life in the terrestrial and aquatic environments. Although scientists have mainly focussed on adaptations of the locomotor system during the transition from water to land (Benton, 1997), early tetrapods were also confronted with serious constraints on foraging on land as aquatic vertebrates typically make use of a rapid rostro-caudal expansion of the buccal cavity to drag prey into the mouth (Lauder, 1980a,b). As air is about 800 times less dense than water, a suction-induced flow will no longer cause prey displacement. Consequently, early tetrapods were forced to develop alternative strategies to capture prey on land.

We discovered that eel-catfish, despite being typical suction feeders in water, can easily be persuaded to capture food on land. Accordingly, the natural diet of this species mainly

¹ The revised version differs slightly from this chapter and contains supplementary videos that will be published online on www.nature.com/nature.

consists of terrestrial insects (Huysentruyt et al., 2004). Our observations (Supplementary Methods, p.179) show that, after propelling its head onto the shore, the eel-catfish almost directly lifts the anterior part of the body and inclines the head downwards. Holding this posture, the catfish searches for food by scanning the substrate open-mouthed (Supplementary Videos, see p. 180-183). Once the animal makes contact with the prey, the mouth is opened and closed repeatedly until the prey is held firmly between the jaws. Finally, the catfish returns to the water where it further transports the prey. Interestingly, eel-catfish preserve the rostro-caudal expansion wave (mouth-opening followed by extensive hyoid-depression) during terrestrial feeding even though the resulting flow of air does not result in prey transport (Fig. 1). Consequently, terrestrial prey captures can be accomplished with relatively minor changes in the higher-level control circuits steering prey capture.

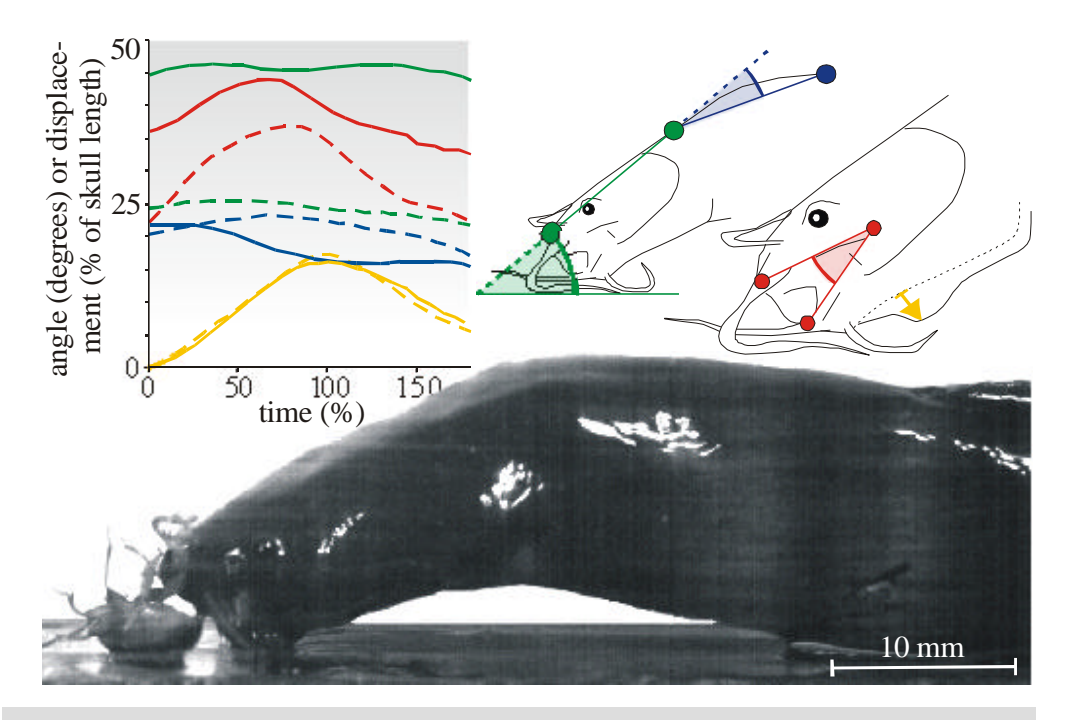


Figure 1: Average, time-scaled kinematic profiles of terrestrial prey capture (full lines, N=22) compared to aquatic bottom feeding (dashed lines, N=20), as measured in three *Channallabes apus* individuals. The drawings illustrate the measured head-to-body angle (blue), the head-to-substrate angle (green), the gape angle (red) and hyoid depression (yellow). A time of 100% represents the time until maximal hyoid-depression. Note that while the inclination of the head is much steeper during terrestrial compared to aquatic prey captures, the timing and range of mouth-opening and hyoid-depression are similar.

The ventrally inclined position of the head, which is also observed in mudskippers (Periophthalminae), seems essential for two reasons: the substrate prevents the prey from

being pushed forward, and the hyoid can freely depress which helps in opening the mouth further (*Chapter 2*). To maintain stability, this posture inevitably calls for dorsoventral flexion along the vertebral column. Interestingly, a recent study on the early tetrapod *Ichthyostega*, the oldest known terrestrial fossil, demonstrated that the animal's presacral vertebral column is adapted for dorsoventral flexion (Ahlberg et al., 2005). Our study suggests this may have allowed this animal to effectively capture prey on land. Our study also shows that having weight-bearing pectoral fins is not an obligatory pre-requisite for capturing prey on land in fish that have an eel-like body.

Supplementary Methods

Channallabes apus individuals (members of the Clariidae or air-breathing catfishes) were wild-caught in Northern Gabon. All animals were kept in a separate aquarium during the course of the recording period. High-speed video sequences (250 frames per second) were recorded of *C. apus* during aquatic bottom feeding and terrestrial feeding. Only those prey capture sequences that were perpendicular to the camera lens (Redlake Motionscope or Redlake MotionPro camera) were selected. For terrestrial feeding, this implied that only about one out of ten recordings could be retained for the analysis of feeding kinematics (see also Supplementary Video 1).

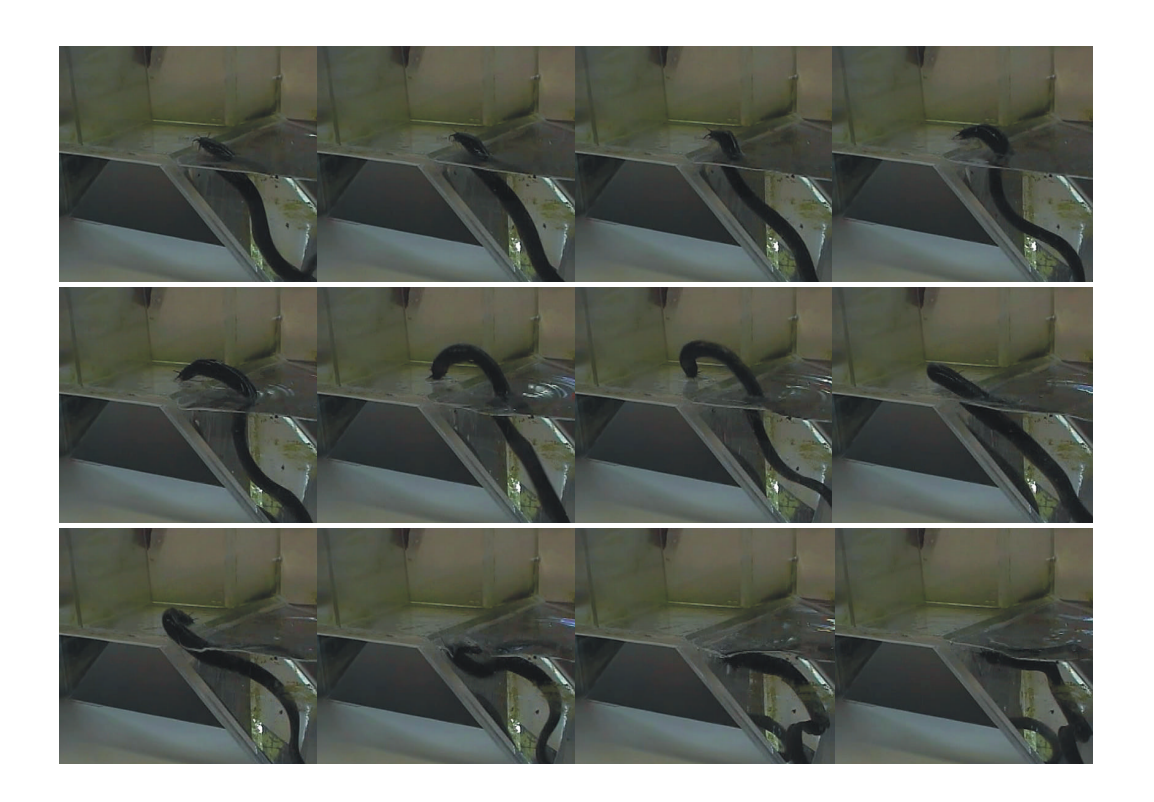
The following prey were used in the experiments: (1) pieces of cod fillet (*Gadus morhua*) of about 0.5 cm³ and (2) live beetles (*Tenebrio Molitor*). Prey were always presented at the bottom of the aquarium or lying on the terrestrial section of the aquarium (see Supplementary Video 1). We managed to analyse17 and 5 sequences of terrestrial prey capture on, respectively, the first and second type of prey. These terrestrial feeding sequences were obtained from three individuals (skull lengths of 17.7, 22.6 and 26.0 mm). The 20 aquatic bottom-feeding sequences included 10 prey captures (only cod as prey) for two individuals each (skull lengths of 17.7 and 24.5 mm).

Specific anatomical landmarks were digitised frame-by-frame using Didge (version 2.2.0, Alistair Cullum), including the tips of the upper jaw, the lower jaws, the hyoid and the rostral tip of the skull roof. As the precise positions of the caudal tip of the skull and the landmark on the dorsal side body at one skull length behind the skull (together with the skull's rostral tip used for calculating the head-to-body angle; see Fig. 1) are not directly discernable on the video frames, the entire dorsal contour of head and body was digitized. For each contour, the coordinates at one and two skull lengths behind the rostral tip were extracted using linear interpolations. Also two remote landmarks on the substrate were digitized in order to calculate the head-to-substrate angle. In order to account for strike-to-strike variability and to avoid the potential confounding effects on kinematic means, the time axis of each prey capture sequence was scaled to the total duration of hyoid depression of each sequence (Fig. 1).

Supplementary Videos

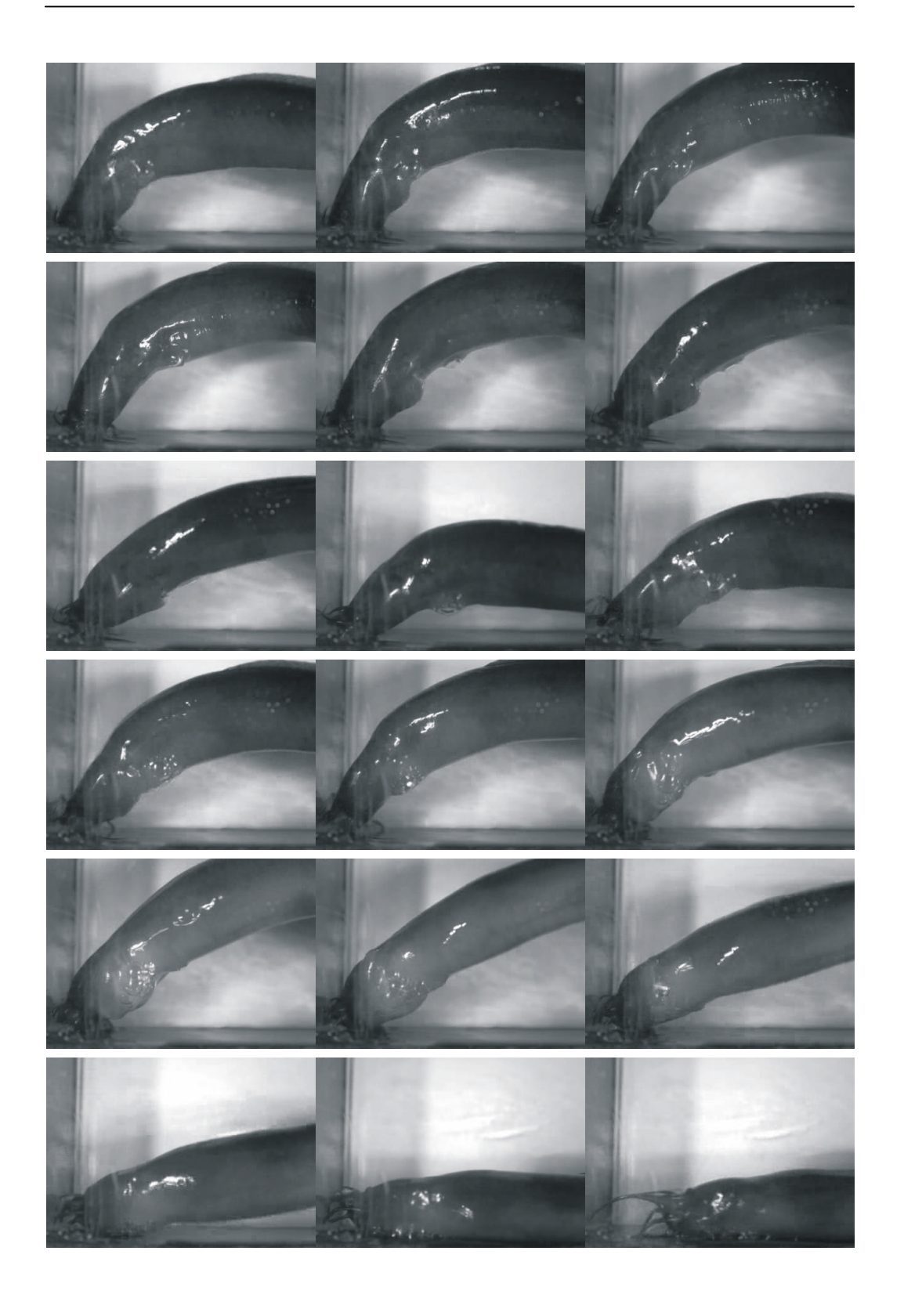
Video 1: This movie gives an overview of the terrestrial feeding behavior of *Channallabes apus*. A small piece of fish (indicated by the red arrow) is presented on the terrestrial section of the aquarium. Frames are shown each 0.06 second.





Video 2: A lateral view frame sequence from a high-speed video zoomed in on the moment of prey capture of *Channallabes apus* feeding terrestrially on a piece of fish. Frames are shown each 0.032 second.





References

- Adriaens, D. and Verraes, W. (1996) Ontogeny of cranial musculature in *Clarias gariepinus* (Siluroidei: Clariidae): The adductor mandibulae complex. *J. Morphol.* **229**, 255-269.
- Adriaens, D. and Verraes, W. (1997) Ontogeny of the hyoid musculature in the African catfish, *Clarias gariepinus* (Burchell, 1822) (Siluroidei: Clariidae). *Zool. J. Linn. Soc.* 121, 105-128.
- Adriaens, D. and Verraes, W. (1998). Ontogeny of the osteocranium in the African catfish, *Clarias gariepinus* Burchell (1822) (Siluriformes, Clariidae): ossification sequence as a reponse to functional demands. *J. Morphol.* 235, 183-237.
- **Adriaens, D., Aerts, P. and Verraes, W.** (2001). Ontogenetic shift in mouth opening mechanisms in a catfish (Clariidae, Siluriformes): a response to increasing functional demands. *J. Morphol.* **247**, 197-216.
- **Aerts, P. and Verraes, W.** (1984). Theoretical analysis of a planar four bar system in the teleostean skull: the use of mathematics in biomechanics. *Annls. Soc r Zool. Belg.* **114**, 273-290.
- Aerts, P., Osse, J. W. M. and Verraes, W. (1987). Model of jaw depression during feeding in Astatotilapia elegans (Teleostei: Cichlidae). Mechanisms for energy storage and triggering. J. Morphol. 194, 85-109.
- **Aerts, P.** (1990). Variability of the fast suction feeding process in *Astatotilapia elegans* (Teleostei : Cichlidae) : a hypothesis of peripheral feedback control. *J. Zool., Lond.* **220**, 653-678.
- **Aerts, P.** (1991). Hyoid morphology and movements relative to abducting forces during feeding in *Astatotilapia elegans* (Teleostei : Cichlidae). *J. Morphol.* **208**, 323-345.
- Aerts, P., Van Damme, J. and Herrel., A. (2001). Intrinsic mechanics and control of fast cranio-cervical movements in aquatic feeding turtles. *Amer. Zool.* 41, 1299-1310.
- **Agnese, J.-F. and Teugels, G.G.** (2005) Insight into the phylogeny of African Clariidae (Teleostei, Siluriformes): implications for their body shape evolution, biogeography, and taxonomy. *Mol. Phylogenet. Evol.* **36**, 546-553.
- Ahlberg, P. E., Clack, J. A. and Blom, H. (2005) The axial skeleton of the Devonian tetrapod Ichthyostega 437, 137-140.
- **Akster, H. A., Granzier, H. L. M. and Ter Keurs, H. E. D. J.** (1985). A comparison of quantitative ultrastructural and contractile characteristics of muscle fibre types of the perch *Perca fluviatilis L. J. Comp. Physiol.* **155**, 685-691.
- Albertson, R. C., Streelman, J. T. and Kocher, T. D. (2003). Directional selection has shaped the oral jaws of Lake Malawi cichlid fishes. P. Natl. Acad. Sci. USA. 100, 5151-5257.
- Alexander, R. McN. (1965). Structure and function in catfish. J. Zool. (London) 148, 88-152.
- **Alexander, R. McN.** (1970)a. Feeding. In *Functional design in fishes*. London, Hutchinson University Press. pp. 89-114.
- **Alexander, R. McN.** (1970)b. Mechanics of the feeding of various teleost fishes. *J. Zool., Lond.* **162**: 145-156.
- **Alexander, R. McN.** (2003). Principles of animal locomotion. Princeton University Press, Princeton.
- **Alfaro, M. and Westneat, M. W.** (1999). Motor patterns of herbivorous feeding: electromyographic analysis of biting in the parrotfishes *Cetoscarus bicolor* and *Scarus iseri*. *Brain. Behav. Evol.* **54**, 205-222.
- **Alfaro, M. E., Janovetz, J. and Westneat, M. W.** (2001). Motor control across trophic strategies: muscle activity of biting and suction feeding fishes. *Amer. Zool.* 41, 1266-1279.
- **Anker, G. Ch.** (1986). The morphology of joints and ligaments in the head of a generalized *Haplochromis* species: *H. elegans* trewavas 1933 (Teleostei, Cichlidae). I. The infraorbital apparatus and the suspensorial apparatus. *Neth. J. Zool.* **36**, 498-530.

- **Anker, G. Ch.** (1978). The morphology of the head muscles of a generalized *Haplochromis* species: *H. elegans* Trewavas 1933 (Pisces, Cichlidae). *Neth. J. Zool.* 28, 234-271.
- **Askew, G. N., Marsh, R. L. and Ellington, C. P.** (2001). The mechanical power output of the flight muscles of blue-breast quail (*Coturnix chinensis*) during take-off. *J. Exp. Biol.* **204**, 3601-3619.
- **Barel, C. D. N., Witte, F. and van Oijen, M. J. P.** (1976). The shape of the skeletal elements in the head of a generalized *Haplochromis* species: *H. elegans* Trewavas 1933 (Pisces, Cichlidae). *Neth. J. Zool.* **26**, 163-265.
- **Barel, C. D. N.** (1983). Towards a constructional morphology of cichlid fishes (Teleostei, Perciformes). *Neth. J. Zool.* 33, 357-424.
- Benton, M. J. (1997). Vertebrate Palaeontology, Chapman & Hall, London.
- **Bergert, B. A. and Wainwright, P. C.** (1997). Morphology and kinematics of prey capture in the syngnathid fishes *Hippocampus erectus* and *Syngnathus floridae*. *Mar. Biol.* **127**, 563-570.
- **Bixler, B. and Riewald, S.** (2002). Analysis of a swimmer's hand and arm in steady flow conditions using computational fluid dynamics. *J. Biomech.* **35**, 713-717.
- **Bone, Q. and Marshall, N. B.** (1986). Food and feeding, chapter seven. *In*: biology of fishes. Blackie, Glasgow. pp 130-147.
- **Bouton, N., Van Os, N. and Witte, F.** (1998) Feeding performance of Lake Victoria rock cichlids: testing predictions from morphology. *J. Fish Biol.* **53**, 118-127.
- Bouton, N., Witte, F., Van Alphen, J. J. M., Schenk, A. and Seehausen, O. (1999). Local adaptations in populations of rock-dwelling haplochromines (Pisces: cichlidae) from southern Lake Victoria. *Proc. R. Soc. Lond.* B 266, 355-360.
- Bruton, M. N. (1979). The food and feeding behaviour of *Clarias gariepinus* (Pisces: Clariidae) in Lake Sibaya, South Africa, with emphasis on its role as a predator of cichlid fishes. *Trans. Zool. Soc. Lond.* 35, 47-114.
- Bullen, R. D. and McKenzie, N. L. (2002). Scaling of bat wingbeat frequency and amplitude. J. Exp. Biol. 205, 2615-2626.
- Cabuy, E., Adriaens, D., Verraes, W. and Teugels, G. G. (1999). Comparative study on the cranial morphology of *Gymnallabes typus* (Siluriformes: Clariidae) and their less anguilliform relatives, *Clariallebes melas* and *Clarias gariepinus*. *J. Morphol.* 240, 169-194.
- Carrier, D. R., Walter, R. M. and Lee, D. V. (2001). Influence of rotational inertia on turning performance of theropod dinosaurs: clues from humans with increased rotational inertia. *J. Exp. Biol.* **204**, 3917-3926.
- **Carroll, A. M.** (2004). Muscle activation and strain during suction feeding in the largemouth bass *Micropterus salmoides. J. Exp. Biol.* **207**, 983-991.
- Carroll, A. M., Wainwright, P. C., Huskey, S. H., Collar, D. C. and Turingan, R. G. (2004). Morphology predicts suction feeding performance in centrarchid fishes. J. Exp. Biol. 207, 3873-3881.
- Carroll, R. L. (2005) Between water and land. Nature 437, 38-39.
- Cook, A. (1996). Ontogeny of feeding morphology and kinematics in juvenile fishes: a case study of the cottid fish Clinocottus analis. *J. Exp. Biol.* 199, 1961-1971.
- Cummins, K. W. and Wuycheck, J. C. (1971). Caloric equivalents for investigations in ecological energetics. *Int. Ass. of Theor. & Appl. Limn.* 18, 1-158.
- Cutwa, M. and Turingan, R. G. (2000). Intralocality variation in feeding biomechanics and prey use in *Archosargus probatocephalus* (Teleostei, Sparidae), with implications for the ecomorphology of fishes. *Env. Biol. Fish.* **59**, 191-198.
- Daniel, T.L. (1984). Unsteady aspects of aquatic locomotion. Amer. Zool. 24, 121-134.
- **Davenport, J.** (2003). Allometric constraints on stability and maximum size in flying fishes: implications for their evolution. *J. Fish Biol.* **62**, 455-463.
- De La Hoz, E. U. (1994). Aspectos cinemáticos del mecanismo de mordida premaxilar en los géneros Cauque, Basilichthys y Austromenidia (Teleostei, Atherinidae). *Investig. mar.* 22, 31-37.

- **De La Hoz, E. U., Cancino, C. A. and Ojeda E. J.** (1994). De capacidades de modulación y plasticidad funcional de los mecanismos de captura de alimento en *Atherinopsinae sudamericanos* (Teleostei, Atherinidae). *Invest. Mar.* **22**: 45-65.
- **De Visser, J. and Barel, C. D. N.** (1996). Architectonic constraints on the hyoid's optimal starting position for suction feeding of fish. *J. Morphol.* **228**, 1-18.
- **De Visser, J. and Barel, C. D. N.** (1998). The expansion apparatus in fish heads, a 3-D kinetic deduction. *Neth. J. Zool.* 48, 361-395.
- **Devaere, S., Adriaens, D., Verraes, W. and Teugels, G. G.** (2001). Cranial morphology of the anguilliform clariid *Channallabes apus* (Günther, 1873) (Teleostei : Siluriformes) : are adaptations related to powerful biting? *J. Zool. Lond.* **255**, 235-250.
- **Diogo, R. and Chardon, M.** (2000). Anatomie et fonction des structures céphaliques associées à la prise de nourriture chez le genre *Chrysichthys* (Téléostei : Siluriformes). *Belg. J. Zool.* **130**, 21-37.
- **Diogo, R.** (2005) Morphological evolution, aptations, homoplasies, constraints and evolutionary trends: catfishes as a case study on general phylogeny and macroevolution. Science Publishers, Inc., New Hampshire, USA.
- **Domenici, P.** (2001). The scaling of locomotor performance in predator-prey encounters: from fish to killer whales. Comp. Biochem. Phys. A **131**, 169-182.
- **Drost, M. R.and van den Boogaart, J. G. M.** (1986). A simple method for measuring the changing volume of small biological objects, illustrated by studies of suction feeding by fish larvae and of shrinkage due to histological fixation. *J. Zool., Lond.* **209**, 239-249.
- **Durie, C. J. and Turingan, R. G.** (2004). The effects of opercular linkage disruption on preycapture kinematics in the teleost fish *Sarotherodon melanotheron. J. Exp. Zool.* **301**, 642-653.
- Elshoud-Oldenhave, M. J. W. and Osse, J. W. M. (1976). Functional morphology of the feeding system in the ruff *Gymnocephalus cernua* (L. 1758) (Teleostei, Percidae). *J. Morphol.* **150**, 399-422.
- **Epstein, M. and Herzog, W.** (1998). Theoretical models of skeletal muscle. Biological and mathematical considerations. John Wiley & Sons, Chichester.
- Ferry-Graham, L. A. (1998) Effects of prey size and mobility on prey-capture kinematics in Leopard sharks *Triakis semifasciata*. *J. Exp. Biol.* **201**, 2433-2444.
- Ferry-Graham, L. A. and Lauder, G. V. (2001). Aquatic prey capture in Ray-finned fishes: a century of progress and new directions. *J. Morphol.* **248**, 99-119.
- Ferry-Graham, L. A., Wainwright, P. C., Hulsey, C. D. and Bellwood, D. R. (2001). Evolution and mechanics of long jaws in Butterflyfishes (Family Chaetodontidae). *J. Morphol.* **248**, 120-143.
- Ferry-Graham, L. A, Wainwright, P. C, Westneat, M. W. and Bellwood, D. R. (2001)

 Modulation of prey capture kinematics in the Cheeklined Wrasse Oxycheilinus digrammus (Teleostei: Labridae). J. Exp. Zool. 290, 88-100.
- Ferry-Graham, L. A., Wainwright, P. C. and Lauder, G. V. (2003). Quantification of flow during suction feeding in bluegill sunfish. *Zoology* **106**, 159-168.
- Ferry-Graham, L. A., Bolnick D. I. and Wainwright, P. C. (2002). Using functional morphology to examine the ecology and evolution of specialization. *Integ. Comp. Biol.* **42**, 265-277.
- **Flitney, F. W. and Johnston, I. A.** (1979). Mechanical properties of isolated fish red and white muscle fibres. *J. Physiol.* **295**, 49-50.
- Friel, J. P. and Wainwright, P.C. (1999) Evolution of complexity in motor patterns and jaw musculature of tetraodontiform fishes. *J. Exp. Biol.* **202**, 867–880.
- **Gans, C. and De Vree, F.** (1987). Functional bases of fiber length and angulation in muscle. *J. Morphol.* **192**, 63-85.
- Gibb, A. C. (1995). Kinematics of prey capture in a flatfish, *Pleuronichthys verticalis*. J. Exp. Biol. 198, 1173-1183.
- **Gibb, A. C.** (2003). Modeling the jaw mechanism of *Pleuronichthys verticalis*: the morphological basis of assymetrical jaw movement in a flatfish. *J. Morphol.* **265**, 1-12.

- Gibb, A. C. and Ferry-Graham, L. A. (2005). Cranial movements during suction feeding in teleost fishes: are they modified to enhance suction production? *Zoology* **108**, 141-153.
- **Gill, A. B.** (1997). The role of mouth morphology in determining threespine sickelback (*Gasterosteus aculeatus*) feeding behavior. *J. Morphol.* **232**, 258A.
- Gosline, W. A. (1971). Functional morphology and classification of Teleostean fishes. Honolulu, The University Press of Hawai.
- Granzier, H. L. M., Wiersma, J., Akster, H. A. and Osse, J. W. M. (1983). Contractile properties of white and red fibre type of the hyohyoideus of the carp (*Cyprinus carpio L.*). J. Comp. Physiol. 149, 441-449.
- **Groenewald, A. A. v. J.** (1964). Observations on the food habitats of *Clarias gariepinus* Burchell, the South African freshwater barbel (Pisces: Clariidae) in Transvaal. *Hydrobiologia* **23**:287-291.
- **Grubich, J. R.** (2000). Crushing motor patterns in drum (Teleostei : Sciaenidae) : Functional novelties associated with molluscivory. *J. Exp. Biol.* **203**: 3161-3176.
- Hanika, S. and Kramer, B. (2000). Electrosensory prey detection in the African sharptooth catfish, *Clarias gariepinus* (Clariidae), of a weakly electric mormyrid fish, the bulldog (Marcusenius macrolepidotus). Behav. Ecol. Sociobiol. 48, 218-228..
- Hernandez, L. P. (2000). Intraspecific scaling of feeding mechanics in an ontogenetic series of zebrafish, *Danio rerio. J. Exp. Biol.* 203, 3033-3043.
- Herrel, A., Adriaens, D., Verraes, W. and Aerts, P. (2002). Bite performance in clarid fishes with hypertrophied jaw adductors as deduced by bite modelling. *J. Morphol.* **253**, 196-205.
- Herrel, A., Van Wassenbergh, S., Wouters, S., Adriaens, D. and Aerts, P. (2005). A functional morphological approach to the scaling of the feeding system in the African catfish, *Clarias gariepinus. J. Exp. Biol.* 208, 2091-2102.
- Herrel, A., Van Wassenbergh, S., Wouters, S., Adriaens, D. and Aerts, P. (2005). A functional morphological approach to the scaling of the feeding system in the African catfish, *Clarias gariepinus. J. Exp. Biol.* **208**, 2091-2102.
- Hill, A.V. (1938). The heat of shortening and dynamic constants of muscle. *Proc. R. Soc. B* 126, 136-195
- Hill, A.V. (1950). The dimensions of animals and their muscular dynamics. Sci. Prog., Lond. 38, 209-230
- Hossain, M. A. R., Batty, R. S., Haylor, G. S., Beveridge, M. C. M. (1999). Diel rhythms of feeding activity in African catfish, *Clarias gariepinus* (Burchell 1822). *Aquac Res.* **30**, 901-905.
- **Hughes, W. F. and Brighton, J. A.** (1999). Schaum's outline of theory and problems of fluid dynamics, third edition. New York: Mcgraw-Hill.
- Hulsey, C. D. and Wainwright, P. C. (2002). Projecting mechanics into morphospace: disparity in the feeding system of labrid fishes. *Proc. R. Soc. Lond.* **269**, 317-326.
- Hunt Von Herbing, I., Miyake, T., Hall, B. K. and Boutilier, R. G. (1996). Ontogeny of feeding and respiration in larval Atlantic Cod *Gadus morhua* (Teleostei: Gadiformes). II Function. *J. Morphol.* 227, 37-50.
- Huskey, S. H and Turingan, R. G. (2001). Variation in prey-resource utilization and oral jaw gape between two populations of largemouth bass, *Micropterus salmoides*. *Env. Biol. Fish.* **61**, 185–104
- Hutchinson, J. R. and Garcia, M. (2002). Tyrannosaurus was not a fast runner. *Nature* 415, 1018-1021.
- Huysentruyt, F., Adriaens, D., Teugels, G. G., Devaere, S., Herrel, A., Verraes, W and Aerts, P. (2004). Diet composition in relation to morphology in some African anguilliform clarific catfishes. *Belg. J. Zool.* 134, 25-30.
- James, R. S., Cole, N. J., Davies, M. L. F. and Johnston, I. A. (1998). Scaling of intrinsic contractile properties and myofibrillar protein composition of fast muscle in the fish Myoxocephalus scorpius L. J. Exp. Biol. 201, 901-912.
- Janovetz, J. (2005) Functional morphology of feeding in the scale-eating specialist Catoprion mento. J. Exp. Biol. 208, 4757-4768.

- Jansen, G., Devaere, S., Weekers, P. and Adriaens, D. (2006). Phylogenetic and biogeographic analysis of air-breathing catfish (Siluriformes: Clariidae) inferred from ribosomal gene and spacer sequences, with an emphasis on anguilliformity. *Mol. Phylogenet. Evol.* 38, 65-78.
- **Jobson, J. D.** (1992) Principal components, factors and correspondence analysis. In: Fienberg S, Olkin I (eds) Applied Multivariate Data Analysis, Volume 2: Categorical and Multivariate Methods. New York, Springer-Verlag, pp 345-482.
- Johnston, I. A. (1982). Biochemistry of myosins and contractile properties of fish skeletal muscle. Mol. Physiol. 2, 15-30.
- **Johnston, I. A.** (1983). Dynamic properties of fish muscle, in: Webb, P. W, Wheis, D., (Eds.), Fish biomechanics, Preager, Cambridge, pp 36-67.
- **Johnston, I. A. and Brill, R.** (1984). Thermal dependance of contractile properties of single muscle fibres from antarctic and various warm water marine fishes including the skipjack tuna (*Katsuwonus pelamis*) and kawakawa (*Euthynnus affinis*). *J. Comp. Physiol.* **155**, 63-70.
- **Keast, A. and Webb, D.** (1966). Mouth and body form relative to feeding ecology in the fishes of a small lake, Lake Opinicon, Ontario. *J. Fish. Res. Board Can.* **25**, 1133-1144.
- Konow, N. and Bellwood, D. (2005). Prey-capture in *Pomacanthus semicirculatus* (Teleostei, Pomacanthidae): functional implications of intramandibular joints in marine angelfishes. *J. Exp. Biol.* **208**, 1421-1433.
- **Koolstra, J. H. and Van Eijden, T. M. G. J.** (1996). Dynamic properties of the human masticatory muscles on jaw closing movements. *Eur. J. Morphol.* **34**, 11-18.
- Koolstra, J. H. (2002). Dynamics of the human masticatory system. Crit. Rev. Oral. Biol. Med. 13, 366-376.
- Koolstra, J. H. and Van Eijden, T. M. G. J. (1997). Dynamics of the human masticory muscles during a jaw open-close movement. *J. Biomech.* **30**, 883-889.
- **Korff, W. L. and Wainwright, P. C.** (2004). Motor pattern control for increasing crushing force in the striped burrfish (Chilomycterus schoepfi). *Zoology* **107**, 335-346.
- **Lasher, W. C.** (2001). Computation of two-dimensional blocked flow normal to a flat plate. *J. Wind. Eng. Ind. Aerodyn.* 89, 493-513.
- **Lauder, G. V.** (1980)a. The role of the hyoid apparatus in the feeding mechanism of the Coelacanth *Latimeria chalumnae. Copeia* **1980**, 1-9.
- **Lauder, G. V.** (1980)b. Evolution of the feeding mechanisms in primitive Actinopterygian fishes: a functional anatomical analysis of *Polypterus*, *Lepisosteus*, and *Amia. J. Morphol.* **163**, 283-317.
- **Lauder, G. V and Norton, S. F.** (1980). Assymetrical muscle activity during feeding in the Gar, *Lepisosteus oculatus. J. Exp. Biol.* **84**, 17-32.
- **Lauder, G. V. and Liem, K. F.** (1980). The feeding mechanism and cephalic myology of *Salvelinus fontinalis*: form, function, and evolutionary significance. In: Balon E. K., editor. Charrs: Salmonid fishes of the genus *Salvelinus*. The Netherlands: Junk Publishers. pp. 365-390.
- **Lauder, G. V.** (1981). Intraspecific functional repertoires in the feeding mechanism of the characoid fishes *Lebiasina, Hoplias*, and *Chalceus. Copeia* **1981**, 154-168.
- **Lauder, G. V.** (1982). Patterns of evolution in the feeding mechanism of Actinopterygian fishes. *Amer. Zool.* **22**, 275-285.
- **Lauder, G. V.** (1983)a. Neuromuscular patterns and the origin of trophic specialization in fishes. *Science* **219**, 1235-1237.
- **Lauder, G. V.** (1983)b. Functional and morphological bases of trophic specialization in sunfishes (Teleostei, Centrarchidae). *J. Morphol.* **178**, 1-21.
- Lauder, G.V. (1983)c. Food capture. In Fish biomechanics (ed. P. W. Webb and D. Weihs), New York, Praeger., pp. 280-311.
- **Lauder, G. V.** (1985). Aquatic feeding in lower vertebrates. In: M. Hildebrand, D.M. Bramble, K.F. Liem and D.B. Wake, eds. Functional Vertebrate Morphology. The Belknap Press (Harvard University Press), Cambridge, Massachusetts. pp. 210-229.
- **Liem, K. F.** (1978). Modulatory multiplicity in the functional repertoire of the feeding mechanism in Cichlid fishes. I. Piscivores. *J. Morphol.* **158**, 323-360.

- **Liem, K. F.** (1980). Adaptive significance of intra- and interspecific differences in the feeding repertoires of cichlid fishes. *Amer. Zool.* **20**, 295-314.
- Liem, K. F. (1984). Functional versatility, speciation and niche overlap: are fishes different? In:

 Meyers DG, Strickler JR, editors. Trophic Interactions within Aquatic Ecosystems.

 Boulder, Colorado: Westview Press. pp. 269-305.
- Liem, K. F. (1985). Ventilation. In Functional Vertebrate Morphology, eds. M. Hildebrand, Bramble, D.M., Liem, K.F., Wake, D.B., Cambridge, Mass.: Harvard University Press. pp. 186-209.
- **Liem, K. F.** (1993) Ecomorphology of the teleostean skull. In: Hanken J, Hall BK (eds) The Skull, vol. 3, functional and evolutionary mechanisms. Chicago and London, The University of Chicago Press, pp. 422-452.
- **Magnhagen, C. and Heibo, E.** (2001). Gape size allometry in pike reflects variation between lakes in prey availability and relative body depth. *Funct. Ecol.* **15**, 754-762.
- Medler, S. (2002). Comparative trends in shortening velocity and force production in skeletal muscles. Am. J. Physiol. Reg. I 283, 368-378.
- **Moran, M. D.** (2003). Arguments for rejecting the sequential Bonferroni in ecological studies. *Oikos* **100**, 403-405.
- Motta, P. J. (1984). Mechanics and function of jaw protrusion in fishes: a review. Copeia 1984, 1-18.
- Muller, M., Osse, J. W. M. and Verhagen, J. H. G. (1982). A quantitative hydrodynamic model of suction feeding in fish. *J. Theor Biol.* **95**, 49-79.
- Muller, M. and Osse., J. W. M. (1984). Hydrodynamics of suction feeding in fish. *Trans. Zool. Soc. Lond.* 37, 51-135.
- **Muller, M.** (1987). Optimization principles applied to the mechanism of neurocranium levation and mouth bottom depression in bony fishes (Halecostomi). *J. Theor. Biol.* **126**, 343-368.
- **Muller, M.** (1996). A novel classification of planar four-bar linkages and its application to the mechanical analysis of animal systems. *Phil. Trans. R. Soc. Lond. B* **351**, 689-720.
- Munshi, S. R., Modi, V. J. and Yokomizo, T. (1999). Fluid dynamics of flat plates and rectangular prisms in the presence of moving surface boundary-layer control. J. Wind Eng. Ind. Aerodyn. 79, 37-60.
- Nagashima, T., Slager, G. E. C., Otten, E., Broekhuijsen, M. L. and Van Willigen, J. D. (1997). Impact velocities of the teeth after a sudden unloading at various initial bite forces, degrees of mouth opening and distances of travel. *J. Dent. Res.* **76**, 1751-1759.
- Narici, M. (1999). Human skeletal muscle architecture studied in vivo by non-evasive imaging techniques: functional significance and applications. *J. Electromyography Kinesiol.* 9, 97-103.
- Nemeth, D. H. (1997)a. Modulation of buccal pressure during prey capture in *Hexagrammos decagrammus* (Teleostei: Hexagrammidae). *J. Exp. Biol.* **200**,2145-2154.
- Nemeth, D. H. (1997)b. Modulation of attack behavior and its effects on feeding performance in a trophic generalist fish, *Hexagrammos decagrammus*. *J. Exp. Biol.* **200**, 2155-2164.
- **Norton, S. F.** (1991). Capture succes and diet of cottid fishes: the role of predator morphology and attack kinematics. *Ecology* **72**, 1807-1819.
- Norton, S. F. (1995). A functional approach to ecomorphological patterns of feeding in cottid fishes. *Env. Biol. Fish.* **44**, 61-78.
- Oliveira, C., Diogo, R., Vandewalle, P. and Chardon, M. (2001). Osteology and myology of the cephalic region and pectoral girdle of *Plotosus lineatus*, with comments on Plotosidae (Teleostei: Siluriformes) autapomorphies. *J. Fish Biol.* **59**, 243–266.
- Otten, E. (1982). The development of a mouth-opening mechanism in a generalized *Haplochromis* species: *H. elegans* Trewavas 1933 (Pisces, Cichlidae). *Neth. J. Zool.* **32**, 31-48.
- **Pasi, B. M. and Carrier, D. R.** (2003). Functional trade-offs in the limb muscles of dogs selected for running vs. fighting. *J. Evol. Biol.* **16**, 321-332.
- Peck, C. C., Langenback, G. E. J. and Hannam, A. G. (2000). Dynamic simulation of muscle and articular properties during human wide jaw opening. *Arch. Oral. Biol.* 45, 963–982.
- **Pohlmann, K., Grasso, F. W and Breithaupt, T.** (2001). Tracking wakes: the nocturnal predatory strategy of piscivorous catfish. *Proc. Natl. Acad. Sci. USA* **98**, 7371-7374.

- **Ralston K. R. and Wainwright, P. C.** (1997) Functional consequences of trophic specialization in pufferfishes. *Funct. Ecol.* 11, 43-52.
- **Reilly, S. M.** (1995). The ontogeny of aquatic feeding behavior in Salamandra salamandra: stereotypy and isometry in feeding kinematics. *J. Exp. Biol.* **198**, 701-708.
- **Richard, B. A. and Wainwright, P. C.** (1995). Scaling the feeding mechanism of largemouth bass (*Micropterus salmoides*): kinematics of prey capture. *J. Exp. Biol.* **198**, 419-433.
- **Robinson, B. W. and Wilson, D. S.** (1998). Optimal foraging, specialization and a solution to Liem's paradox. *Amer. Nat.* **151**, 223-235.
- **Robinson, M. P. and Motta, P. J.** (2002). Patterns of growth and the effects of scale on the feeding kinematics of the nurse shark (*Gynglymostoma cirratum*). *J. Zool., Lond.* **256**, 449-462.
- Roth, G. and Wake, D. B. (1989). Conservatism and innovation in the evolution of feeding in vertebrates. In: Complex organismal functions: integration and evolution in vertebrates. Wake, D.B. & G. Roth (editors). Wiley-interscience publication. pp. 7-22.
- Sanderson, S. L. (1988). Variation in neuromuscular activity during prey capture by trophic specialists and generalists (Pisces: Labridae). *Brain Behav. Evol.* 32, 257-268.
- Sanderson, S. L. (1990). Versatility and specialization in labrid fishes: ecomorphological implications. *Oecologia* 84, 272-279.
- **Sanderson, S. L.** (1991). Functional stereotypy and feeding performance correlated in a trophic specialist. *Funct. Ecol.* **5**, 795-803.
- Schael, D. M., Rudstam, L. G. and Post J. R. (1991). Gape limitation and prey selection in larval yellow perch (*Perca flavescens*), freshwater drum (*Aplodinotus grunniens*), and Black Crappie (*Promoxis nigromaculatus*). Can. J. Fish. Aquat. Sci. 48, 1919-1925.
- **Schilder, R. J and Marden, J. H.** (2004). A hierarchical analysis of the scaling of force and power production by dragonfly. *J. Exp. Biol.* **207**, 767-776.
- **Schmidt-Nielson, K.** (1984). Scaling: Why is animal size so important? Cambridge: Cambridge University Press.
- **Schondube, J. E. and Del Rio, C. M.** (2003). The flowerpiercers' hook: an experimental test of an evolutionary trade-off. *Proc. R. Soc. Lond.* B **270**, 195–198.
- Sibbing, F. A. and Nagelkerke, L. A. J. (2001). Resource partioning by Lake Tana barbs predicted from fish morphometrics and prey characteristics. *Rev. Fish Biol. Fisheries* 10, 393-437.
- Slager, G. E. C., Otten, E., Van Eijden, T. M. G. J. and Van Willigen, J. D. (1997).
 Mathematical model of the human jaw system simulating static biting and movements after unloading. J. Neurophysiol. 78, 3222–3233.
- Slager, G. E. C., Otten, E., Nagashima, T. and Van Willigen, J. D. (1998). The riddle of the large loss in bite force after fast jaw-closing movements. *J. Dent. Res.* 77, 1684-1693.
- Sokal, R. F. and Rohlf, F. J. (1995). Biometry. New York: W. H. Freeman and Comp.
- **Sponder, D. L. and Lauder, G. V.** (1981). Terrestrial feeding in the Mudskipper *Periophthalmus* (Pisces: Teleostei): A cineradiographic analysis. *J. Zool., Lond.* **193**, 517-530.
- Steans, S.C. (1992) The evolution of Life Histories. Oxford University Press, New York.
- Stiassny, M. L. J. (1996). Basal ctenosquamate relationships and the interrelationships of the myctophiform (scopelomorph) fishes. In *Interrelationships of fishes* (Eds. Stiassny, M. L. J., Parenti, L. R. and G. D. Johnson), London: Academic Press., pp. 405-426;
- Svanbäck, R., Wainwright, P. C. and Ferry-Graham, L. A. (2002). Linking cranial kinematics, buccal pressure, and suction feeding performance in Largemouth Bass. *Physiol. Biochem. Zool.* **75**, 532-543
- **Teugels, G. G.** (1986). Clariidae. In *Checklist of the fresh-water fishes of Africa (Cloffa) Vol. 2*. (ed. J. Daget, J. P. Gosse and D. F. E. T. Van Den Audenaerde), pp. 66-101. ISNB Brussels, MRAC Tervuren and ORSTOM Paris.
- **Teugels, G. G.** (1996). Taxonomy, phylogeny and biogeography of catfishes (Ostariophysi, Siluroidei): An overview. *Aquat. Living Resour.* **9** (Hors Série), 9-34.
- Teugels, G. G. and Adriaens, D. (2003). Taxonomy and phylogeny of Clariidae. An overview. In:

- Arratia, G., Kapoor, A. S, Chardon, M., Diogo, R., (Eds.), Catfishes Vol I., Science Publishers, Enfield, pp. 465–487.
- Toro, E., Herrel, A., Vanhooydonck, B. and Irschick, D. J. (2003). A biomechanical analysis of intra- and interspecific scaling of jumping and morphology in Caribbean *Anolis* lizards. *J. Exp. Biol.* 206, 2641-2652.
- **Turingan, R. G. and Wainwright, P. C.** (1993) Morphological and functional bases of durophagy in the queen triggerfish, *Ballistes vetula* (Pisces, Tetraodontiformes) *J. Morphol.* **215**, 101-118.
- **Turingan, R. G.** (1994). Ecomorphological relationships among Caribbean tetraodontiform fishes. *J. Zool., Lond.* **233**, 493-521.
- **Turingan, R. G., Wainwright, P. C. and Hensley, D. A.** (1995). Interpopulation variation in prey use and feeding biomechanics in Caribbean triggerfishes. *Oecologia* **102**, 296-304.
- Van Damme, R., Wilson, R., Vanhooydonck, B. and Aerts, P. (2002) Performance constraints in decathletes. *Nature* 415, 755-756.
- Van den Berg, C. (1994). A quantitative, three-dimensional method for analyzing rotational movement from single-view movies. *J. Exp. Biol.* **191**, 283-290.
- Van Dobben, W. H. (1937). Über den Kniefermechanismus der Knochenfishe. Arch. Néerl. d. Zool. 3, 1-72.
- Van Leeuwen, J. L. and Muller, M. (1983). The recording and interpretation of pressures in preysucking fish. *Neth. J. Zool.* 33, 425-475.
- Van Leeuwen, J. L. and Muller, M. (1984). Optimum sucking techniques for predatory fish. Trans. Zool. Soc. Lond. 37, 137-169.
- Van Meir, L. (2001). Functionele morfologie van cranial adaptaties bij *Clariallabes spec.* (Teleostei: Siluriformes). Licentiaatsthesis, Ghent University.
- Van Wassenbergh, S., Herrel, A., Adriaens, D. and Aerts, P. (2004) Effects of jaw adductor hypertrophy on buccal expansions during feeding of airbreathing catfishes (Teleostei, Clariidae). *Zoomorphology* 123, 81-93.
- Van Wassenbergh, S., Aerts, P., Adriaens, D. and Herrel, A. (2005) A dynamical model of mouth closing movements in clariid catfishes: the role of enlarged jaw adductors. *J. Theor. Biol.* 234, 49-65.
- Van Wassenbergh, S., Aerts, P. and Herrel, A. (2005). Scaling of suction-feeding kinematics and dynamics in the African catfish, Clarias gariepinus. *J. Exp. Biol.* **208**, 2103-2114.
- Van Wassenbergh, S., Herrel, A., Adriaens, D. and Aerts, P. (2005) A test of mouth-opening and hyoid-depression mechanisms during prey capture in a catfish. J. Exp. Biol. 208, 4627-4639.
- Van Wassenbergh, S., Aerts, P. and Herrel, A. (2006) Scaling of suction feeding performance in the catfish *Clarias gariepinus*. *Physiol. Biochem. Zool.* **79**, 43-56.
- Van Wassenbergh, S., Aerts, P. and Herrel, A. (in press) Hydrodynamic modeling of aquatic suction performance and intra-oral pressures: limitations for comparative studies. *J. R. Soc. Interface*.
- Van Wassenbergh, S., Herrel, A., Adriaens, D. and Aerts, P. (in press) Modulation and variability of prey capture kinematics in clariid catfishes *J. Exp. Zool. Part A*
- Van Wassenbergh, S., Herrel A., Adriaens, D., Huysentruyt, F., Devaere, S. and Aerts, P. (in press) Catfish strikes on land. *Nature*.
- Van Wassenbergh, S., Herrel, A., Adriaens, D. and Aerts, P. (submitted) Interspecific variation in sternohyoideus muscle morphology in clariid catfishes: functional implications for suction feeding. *J. Exp. Biol.*
- Van Wassenbergh, S., Herrel, A., Adriaens, D. and Aerts, P. (submitted) No trade-off between biting and suction feeding performance in clarific catfishes. *Funct. Ecol.*
- Van Willigen, J. D., Otten, E., Slager, G. E. C. and Broekhuijsen, M. L. (1997). Contribution of the digastric muscles to the control of bite force in man. *Arch. Oral. Biol.* **42**, 45-56.
- Vanhooydonck, B. and R. Van Damme (2001) Evolutionary trade-offs in locomotor capacities in lacertid lizards: are splendid sprinters clumsy climbers? *J. Evol. Biol.* 14: 46-54.

- Vogel, S. (1994). Life in Moving Fluids: The Physical Biology of Flow. Princeton University Press, Princeton, New York.
- Wainwright P. C and Lauder, G. V. (1986) Feeding biology of sunfishes: patterns of variation in the feeding mechanism. *Zool. J. Linn. Soc.* 88, 217-228.
- Wainwright, P. C. and Richard, B. A. (1995). Predicting patterns of prey use from morphology of fishes. *Env. Biol. Fish.* 44, 97-113.
- Wainwright, P.C. and Shaw, S. S. (1999). Morphological basis of kinematic diversity in feeding sunfishes. *J. Exp. Biol.* **202**, 3101-3110.
- Wainwright, P. C. and Friel, J. P. (2000). Effects of prey type on motor pattern variance in Tetraodontiform fishes. *J. Exp. Zool.* **286**, 563-571.
- **Wainwright, P.C.** (2002). The evolution of feeding motor patterns in vertebrates. *Curr. Opin. Neurobiol.* **12**, 691–695.
- Wainwright, P. C., Ferry-Graham, L. A., Waltzek, T. B., Carroll, A. M., Hulsey, D. C. and Grubich, J. R. (2001). Evaluating the use of ram and suction during prey capture by cichlid fishes. *J. Exp. Biol.* 204, 3039-3051.
- Wainwright, P. C., Alfaro, M. E., Bolnick, I. and Hulsey, D. (2005). Many-to-one mapping of form to function: a general principle in organismal design? *Integr. Comp. Biol.* 45, 256-262.
- Wakeling, J. M., Kemp, K. M and Johnston, I. A. (1999). The biomechanics of fast-starts during ontogeny in the common carp *Cyprinus carpio. J. Exp. Biol.* **202**, 3057-3067.
- Walter, R. M. and Carrier, D. R. (2002). Scaling of rotational inertia in murine rodents and two species of lizard. *J. Exp. Biol.* 205, 2135-2141.
- Waltzek, T. B. and Wainwright, P. C. (2003). Functional morphology of extreme jaw protrusion in neotropical cichlids. *J. Morphol.* **257**, 96-106.
- Ward, S. R. and Lieber, R. L. (2005). Density and hydration of fresh and fixed human skeletal muscle. *J. Biomech.* 38, 2317-2320.
- **Westneat, M. W.** (1994). Transmission of force and velocity in the feeding mechanism of labrid fishes (Teleostei, Perciformes). *Zoomorphology* **114**, 103-118.
- **Westneat, M. W**. (1990). Feeding mechanics of teleost fishes (Labridae; Perciformes): a test of four-bar linkage models. *J. Morphol.* **205**, 269-295.
- Westneat, M. W. (2004). Evolution of levers and linkages in the feeding mechanisms of fishes. Integr. Comp. Biol. 44, 378-389.
- Westneat, M. W. and Wainwright, P. C. (1989). Feeding mechanisms of *Epibulus insidiator* (Labridae; Teleostei): evolution of a novel functional system. *J. Morphol.* **202**, 129-150.
- Westneat, M. W. (1994). Transmission of force and velocity in the feeding mechanism of labrid fishes (Teleostei, Perciformes). *Zoomorphology* 114, 103-118.
- **Westneat, M. W.** (1995). Phylogenetic systematics and biomechanics in ecomorphology. *Env. Biol. Fish.* **44**, 263-283.
- Westneat, M. W. (2003). A biomechanical model for analysis of muscle force, power output and lower jaw motion in fishes. *J. Theor. Biol.* **223**, 269-281.
- White, F. M. (1991). Viscous Fluid Flow. 2nd ed. McGraw-Hill, New York.
- Winter, D. A. (2004). Biomechanics and Motor Control of Human Movement, 3rd edition. USA, John Wiley & Sons
- Woittiez, R. D, Huijing, P.A., Boom, H. B. K. and Rozendal, R. H. (1984). A three-dimensional muscle model: a quantified relation between form and function of skeletal muscles. *J. Morphol.* **182**, 95-113.
- **Wyckmans, M.** (2004). Dieet en kopmorfometrie van Afrikaanse katvissen met hypertrofe kaakspieren. Licentiaatsthesis (unpublished). University of Antwerp, Belgium.
- Yalçin, S., Akyurt, I. and Solak, K. (2001). Stomach contents of the catfish (*Clarias gariepinus* Burchell, 1822) in the river Asi (Turkey). *Turk. J. Zool.* 25, 461-468.
- Zar, J. H. (1996). Biostatistical analysis. London: Prentice-Hall International.

Nederlandse samenvatting / Summary in Dutch

Functionele consequenties van kaakspierhypertrofie voor de voedselopname bij clariide katvissen

Sam Van Wassenbergh

Binnen de familie van de luchtademende katvissen (Clariidae) zijn er een aantal soorten met zeer sterk ontwikkelde (hypertrofe) kaakspieren (*m. adductor mandibulae*), de spieren die de kaken doen sluiten. Het oppervlak van de hypertrofe kaakspieren in dwarse doorsnede is bij sommige soorten (b.v. *Channallabes apus*) wel tot 7 keer groter dan bij andere soorten (b.v. *Clarias gariepinus*: zie figuur p.7). Recent is ook gebleken dat deze hypertrofie minstens vier keer onafhankelijk is ontstaan in de evolutie binnen deze groep van katvissen (figuur p. 130). Waarom de kaakspieren zo sterk ontwikkeld zijn bij bepaalde Clariidae blijft voorlopig een open vraag. Zoals verwacht kon er reeds aangetoond worden dat er een verband bestaat tussen de grootte van de kaakspieren en de maximale bijtkracht van deze katvissen. Op zijn beurt lijkt deze verhoogde bijtkracht zich te vertalen in ecologische specialisatie, waarbij de soorten met hypertrofe kaakspieren een voorkeur blijken te hebben voor harde prooien, voornamelijk kevers.

De kaaksluiters vormen echter slechts één component van het complexe apparaat dat bij vissen voor een efficiënte voedselopname moet zorgen. Er komt bij de voedselopname dan ook meer aan te pas dan alleen maar bijtkracht uitoefenen op de prooi: vissen maken typisch gebruik van een plotse volumetoename van de mondholte om water en prooi naar binnen te zuigen. Voor cichlide vissen (Cichlidae) heeft men op basis van theoretische modellen aangetoond dat het vergroten van de kaakspieren nadelig zou kunnen zijn voor het expansieapparaat dat zuigkracht moet leveren. Centraal in deze thesis staat dan ook niet de meest voor de hand liggende functie (i.e. toename in bijtkracht), maar wel wat de mogelijke consequenties zijn van de kaakspierhypertrofie op de werking van het voedselopnameapparaat tijdens andere essentiële aspecten van de voedselopname. Dit kunnen zowel positieve consequenties (b.v. een toename in snelheid waarmee de kaken kunnen dichtklappen bij het happen naar een prooi) als negatieve consequenties inhouden (b.v. een afname in zuigkracht). Het identificeren van gekoppelde of conflicterende functies is vanuit

evolutionair oogpunt zeer belangrijk: het bepaalt in grote mate het ecologische potentieel van vissen (mogelijke nichebreedte) en kan ons daardoor belangrijk inzicht geven in de evolutionaire processen die aan de basis liggen bij het ontstaan van nieuwe soorten.

Vooraleer te starten met de vergelijkende studie naar de effecten van kaakspierhypertrofie binnen de Clariidae, werd er geopteerd om eerst twee hiaten in onze kennis over de mechanica van de voedselopname bij katvissen te behandelen: (1) hoe werkt het complexe systeem van onderling gekoppelde beentjes in de kop van katvissen tijdens de zuigvoeding en (2) wat zijn de effecten van lichaamsgrootte (scaling) op de werking van dit systeem. Hoewel dus niet direct van toepassing op de centrale vraag, zullen deze gegevens een onmisbaar werkmiddel blijken in het verdere verloop van deze thesis.

De werking van de het voedselopname-apparaat tijdens het openen van de mond en het verlagen van de mondboden (d.m.v. hyoiddepressie) werd bestudeerd op basis van highröntgenfilms Clarias van drie gariepinus individuen uitgerust Röntgenstralingabsorberende markeerpunten op welbepaalde posities in de kop. De beweging van deze markeerpunten werd gebruikt als input in vlakke vierstangensystemen, welke de gekoppelde beweging tussen de verschillende elementen tijdens de prooivangst beschrijven. Deze studie toonde aan dat het operculair mondopeningmechanisme de mondopening in gang zet, maar niet in staat is om de volledige mondopening te veroorzaken tijdens de prooivangst. Daarvoor krijgt het de hulp van de protractor hyoidei spier, die de retractie van het hyoid volgt en daardoor de mond opentrekt, en in een later stadium (tegen het einde van de mondopening) ook actief verkort. Het angulo-ceratohyal ligament, waarvan voorheen gedacht werd dat het een rol zou spelen in de mondopening, blijkt echter geen mondopening te veroorzaken. Dit ligament blijkt namelijk een functie te vervullen als hyoid-elevator tegen het einde van de mondsluitfase (zie figuur p. 31). Hyoiddepressie wordt uitsluitend vervuld door een vierstangensysteem dat de bewegingen van schedel (neurocraniale elevatie), schoudergordel (cleithrum retractie), sternohyoideus spier (verbindt cleithrum en hyoid) en, uiteraard, het hyoid met elkaar koppelt. Merkwaardig genoeg wordt de hyoiddepressie in dit gekoppelde systeem niet versterkt door samentrekking van de sternohyoideus spier, die in Clarias gariepinus zelfs in lengte wint tijdens de depressie van het hyoid.

Scaling van de prooivangst-kinematica werd bestudeerd in een reeks van individuen van de soort *Clarias gariepinus* met een verschillende lichaamsgrootte. Zowel de grootte van de prooi (een stukje kabeljauwfilet) als de grootte van het voedingsplatform werden aangepast in functie van de grootte van het proefdier, teneinde gestandaardiseerde condities te creëren waarbij enkel en alleen de scalingseffecten tot uiting worden gebracht. Na een periode van training en gewenning, die meestal 1 week in beslag nam, kon er gestart worden met de high-speed video opnames. In totaal werden er 17 individuen gefilmd met een totale lengte tussen de 11,1 en 92,3 cm. Op basis van deze beelden werden maximale excursies, snelheden en versnellingen van verschillende schedelelementen bepaald.

Digitalisatie van externe contouren van de kop tijdens expansie maakte het mogelijk om de expanderende katviskoppen te modelleren als een reeks van afgeplatte cilinders.

Vervolgens kon op basis van de wet van de continuïteit een spatietemporeel patroon van stroomsnelheden berekend worden dat opgewekt wordt binnenin het expanderende volume. Door te veronderstellen dat het water dat zich voor de mond bevindt naar binnen stroomt als een 'circulair vortex filament', werden stroomsnelheden buiten de mondopening berekend. Op deze manier werden de scalingseffecten op de zuigprestatie, kinematica en dynamica gekwantificeerd.

Nadat clariide katvissen prooien naar zich toe zuigen, worden de kaken toegeklapt. Snel kunnen happen is bijgevolg belangrijk om snelle prooien (zoals vissen) te vangen. Het experimenteel vergelijken van kaaksluitsnelheden van verschillende soorten met toenemende graad van ontwikkeling van de kaakspieren (*Clarias gariepinus*, *Clariallabes longicauda*, *Gymnallabes typus* en *Channallabes apus*) volstond echter niet om te evalueren of de kaakspierhypertrofie al dan niet een effect heeft op de maximale sluitsnelheid van de mond. Experimenteel onderzoek d.m.v. high-speed video opnames van deze soorten tijdens de prooivangst toonde namelijk aan dat de onderkaakrotatie sterk verschilt tussen de soorten: de soorten met kaakspierhypertrofie openen de mond verder en draaien de onderkaak slechts over een kleiner aantal graden tijdens het sluiten om de prooi tussen de tanden te klemmen in vergelijking met *Clarias gariepinus*, de soort met zwakst ontwikkelde kaakspieren. Hoewel op zich interessant, zorgt dit resultaat ervoor dat elke directe vergelijking van gemeten kaaksluitsnelheden weinig betekenis heeft.

Om dit probleem te omzeilen werd er een 'forward dynamic' kaaksluitmodel ontwikkeld dat werd getest met de experimentele gegevens. Dit wiskundige model simuleert kaaksluitbewegingen mits de invoer van een aantal morfologische en fysiologische eigenschappen van het hefboomsysteem verantwoordelijk voor de rotatie van de onderkaak. Dit model blijkt behoorlijk goede voorspellingen te geven van experimenteel gemeten kaaksluitbewegingen (zie figuur p.92). Vervolgens laat het model ons toe om de consequenties van variatie in morfologie te evalueren. De hypertrofie van de kaakspieren blijkt inderdaad een belangrijke bijdrage te leveren aan de kaaksluitsnelheid (figuur p.96). Het volledige kaaksysteem van de soorten met kaaksluiter-hypertrofie (Clariallabes longicauda, Gymnallabes typus en Channallabes. apus) zal echter alleen voor significant snellere kaaksluitbewegingen kunnen zorgen bij relatief korte mondsluitingen (beperkt aantal graden onderkaakrotatie tussen maximale mondopening en impact op de prooi). Het kaaksysteem in deze soorten is eveneens veel beter geschikt om de mond verder open te doen in vergelijking met Clarias gariepinus. Zulke wijde mondopeningen en relatief korte onderkaakrotaties werden daadwerkelijk vastgesteld tijdens in vivo analyse van de voedselopname-kinematica (figuur p.98). Dit lijkt vooral voordelig bij het grijpen van relatief grote prooien.

De hypertrofie van de kaakspieren blijkt eveneens consequenties te hebben voor de expansie-kinematiek van de schedel tijdens het zuigen. De sterke connectie van het

suspensorium met het neurocranium in de soorten die deze hypertrofie vertonen (Clariallabes longicauda, Gymnallabes typus en Channallabes apus) en de visco-elastische kaakspiermassa die het suspensorium overspant, zorgen er blijkbaar voor dat er minder laterale expansie (abductie) van het suspensorium en hyoid kan optreden. Deze vermindering in volumetoename in zijwaartse richting tijdens de craniale expansie lijkt echter geen effect te hebben op de maximale zuigprestatie bij de Clariidae: experimenten wezen uit dat gestandaardiseerde prooitjes (bolvormige stukje garnaalvlees die los op het einde een naald werden vastgemaakt) door de soorten met verhoogde bijtcapaciteit niet minder snel naar binnen gezogen werden (zie figuur p. 136). Aangezien de belangrijkste fractie van de totale volumetoename tijdens het zuigen bij deze vissen met dorsoventraal afgeplatte kop grotendeels in de ventrale richting gebeurt (mondbodemverlaging door onderkaak -en hyoiddepressie), lijkt alles erop te wijzen dat de verminderde expansiecapaciteit in laterale richting (suspensorium abductie) een te verwaarlozen aspect is (figuur p. 138). Een interessant gegeven hierbij is dat de hypertrofe groei van de kaakspieren weinig of geen veranderingen in de inwendige architectuur van het zuigapparaat heeft teweeg gebracht: het gereduceerde schedeldak (enkel nog een smalle band bij de extreem gehypertrofieerde soorten Gymnallabes typus en Channallabes apus) laat toe dat de kaakspieren dorsolateraal kunnen uitpuilen. De Clariidae hebben in de loop van hun evolutie dus blijkbaar een relatief eenvoudige manier 'gevonden' om een toename in bijtkracht te ontwikkelen, zonder daarbij in te boeten aan zuigkracht.

Niet alleen de kaakspieren, maar ook de sternohyoideus spier vertoont sterke variatie in massa en dikte bij de Clariidae. Deze spier bevindt zich aan de ventrale zijde van de kop en verbindt er de schoudergordel met het hyoid (zie figuur p. 145). Bij *Gymnallabes typus*, bijvoorbeeld, blijkt ze voor een gegeven schedellengte een meer dan dubbele fysiologische doorsnede te hebben in vergelijking met *Clarias gariepinus* (figuur p.150). Aangezien *Gymnallabes typus* ook de soort is waarvoor het hyoid de grootste verlaging van de mondbodem veroorzaakt, leek het niet onmogelijk dat deze soort in staat is om een ander verkortingspatroon te vertonen dan *Clarias gariepinus*, waar de relatief zwakke sternohyoideus (noodgedwongen?) uitrekt wanneer ze naar achter getrokken wordt door de schoudergordel en dus enkel als krachtoverdrager fungeert. Hoewel bij *Gymnallabes typus* initieel een korte fase van sternohyoideus verkorting optreedt in het begin van de expansiefase, volgt de spier nadien hetzelde patroon als bij de andere Clariidae (figuur p. 155). Door deze initiële verkorting slaagt de sterker ontwikkelde sternohyoideus van *Gymnallabes typus* er wel in om relatief minder uit te rekken tijdens de expansie, waardoor ze de retractie van de schoudergordel efficiënter omzet in hyoiddepressie.

Er werd voor deze soorten ook onderzocht of de bekwaamheid om hun prooivangstpatroon aan te passen in functie van verschillende prooitypen (stukje vis *versus* een ongepelde garnaal) verschilt. Het wordt namelijk verondersteld dat soorten die zich gradueel morfologisch gespecialiseerd hebben en zich toeleggen op een minder divers dieet, ook minder bekwaam zijn om hun prooivangstpatroon aan te passen in functie van verschillende prooitypes. Zoals verwacht neemt de capaciteit om de prooivangst

kinematiek aan te passen in functie van twee verschillende prooien inderdaad af in de meer gespecialiseerde soorten die een minder divers dieet vertonen. Terwijl *Clarias gariepinus* en *Clariallabes longicauda* respectievelijk de grootte van de mondopening en de grootte van de depressie van het hyoid-apparaat doen toenemen tijdens het grijpen van de garnaal in vergelijking tot het stukje vis, kan dit niet worden aangetoond bij *Gymnallabes typus* en *Channallabes apus* (tabel p. 170). Alle soorten vertonen echter een grote kinematische variabiliteit, ook tijdens het grijpen van één bepaald prooitype. De mogelijkheid om de koppositie aan te passen in functie van de positie van de prooi t.o.v. de kop (d.m.v. neurocraniale elevatie) blijkt een algemene eigenschap te zijn van de Clariidae, die voorheen nog niet beschreven werd voor andere visgroepen (zie p.171).

Recent werd door onderzoekers aan het Laboratorium voor Evolutionaire Morfologie van Vertebraten (Universiteit Gent) ontdekt dat Channallabes apus, de soort met de meest extreme kaakspierhypertrofie en een sterkt aalvormige lichaam, in staat blijkt te zijn om uit het water te gaan om voedselitems op het land te grijpen. Bovendien is uit maaganalyses van specimens uit Gabon gebleken dat het dieet van deze soort voor het grootste deel uit (terrestrische) kevers bestaat. Een high-speed video analyse van deze merkwaardige voedingsstrategie leverde interessante gegevens op: vanaf dat Channallabes apus zich uit het water lanceert, wordt het voorste deel van het lichaam opgeheven en de kop steil neergebogen richting de grond. Deze houding wordt aangehouden terwijl de katvis met open mond het substraat aftast. Wanneer Channallabes contact maakt met een prooi, wordt de mond herhaaldelijk geopend en gesloten tot de prooi stevig tussen de kaken geklemd is (zie figuur p. 182-183). Daarna laat de vis zijn lange lichaam zakken en keert hij terug in het water waar de prooi verder naar binnen gewerkt wordt. Aangezien de gebogen lichaamshouding ook bij slijkspringers -de bekendste groep van terrestrisch foeragerende vissen- voorkomt, lijkt dit een essentieel aspect voor vissen om op land efficiënt prooien te kunnen grijpen.

Dankbetuiging / Acknowledgements

In de eerste plaats wil ik (co-)promotor **Anthony Herrel** bedanken voor zijn steun bij zowat alles dat in deze thesis beland is. Hij leerde me de knepen van het vak in de experimentele functieanalyse van de voedselopname. Zijn onaflatend enthousiasme kon me telkens weer motiveren om het onderste uit de kan te halen. Zonder de projectaanvraag die hij in 2002 schreef, had waarschijnlijk enkel hoofdstuk 6 het licht gezien en was het nooit tot een doctoraatsverdediging gekomen.

Ik ben ook bijzonder veel verschuldigd aan promotor **Peter Aerts**. Hij leerde me de basisprincipes van de biomechanica en zijn ervaring in het wiskundig modelleren van de zuigvoeding kwam uitstekend van pas. Telkens ik hem een manuscript liet lezen, kwam hij wel met een idee dat mijn werk naar een hoger niveau kon brengen. Zijn inbreng is dan ook van onschatbare waarde, waarvoor ik hem graag wil bedanken.

Ook **Dominique Adriaens** van de Universiteit Gent was een belangrijke steun. Niet alleen reserveerde hij een deel van de aquaria in Gent voor mijn proefdieren, als coauteur was zijn expertise meer dan welkom; waarvoor dank! Ook zijn team van het vertebraten morfologie labo stonden altijd klaar als ik iets nodig had: **Stijn Devaere**, **Frank Huysentruyt**, **Natalie De Schepper** en **Tom Geerinckx**.

Jeannine Fret wil ik bedanken voor haar vakkundige hulp bij de EMG experimenten. Jammer dat de katvissen nadien elke vorm van medewerking weigerden. Ook haar administratieve hulp apprecieer ik ten zeerste.

Ik ben ook een deel verschuldigd aan **Sara Wouters** en **Marissa Wyckmans** voor het werk dat ze verzet hebben tijdens het maken van hun licentiaatsthesis.

Dank aan **Sandra Nauwelaerts**, ondermeer voor de discussies omtrent het kaaksluitmodel. Ook bedankt voor de reclame die je maakte voor mijn onderzoek bij de fish-feeding wetenschappers in de Verenigde Staten.

Rob James wil ik bedanken voor zijn fantastische ontvangst en inspanningen tijdens het onderzoeksverblijf in Coventry.

Jan Scholliers dank ik voor het assisteren bij enkele van mijn experimentele metingen en voor het zijn hulp bij het bouwen van proefopstellingen.

De ondergetekende dankt ook **Raoul Van Damme** en **Bieke Vanhooydonck** om me te helpen bij het oplossen van statistische problemen.

Verder dank ik uiteraard ook de rest mijn collega's van het laboratorium voor functionele morfologie Dave Verwaijen, Hans Scheers, Isabel Van Coppenolle, Evie Vereecke,

Kirsten Schoonaert, Kristiaan D'Août, Bart Adriaenssens, Ann Hallemans, Joke Bilcke, Katleen Huyghe, Jonathan Brecko, Vicky Schaerlaken en ook professor Frits De Vree.

Despite their relatively short stay at the lab in Antwerp, I would also like to thank **Jay Meyers** en **Keith Metzger**.

Dank aan de Universiteit Antwerpen (Dehousse-beurs), het Fonds voor Wetenschappelijk Onderzoek Vlaanderen, de Company of Biologists en de Society for Experimental Biology voor financiële steun.

Als leveranciers van vissen dank ik **Eddie Holsters, Frans Ollevier** en **Filip Volckaert** van de KULeuven, Fleuren-Nooijen katviskwekerij (Someren, Nederland) en Bassleer Biofish (Westmeerbeek).

Hartelijk dank aan mijn ouders die mij de kans gegeven hebben om deze weg in te slaan.

Waarschijnlijk nog het meest van al dank ik, uiteraard, mijn lieve vriendin **Karen Leyssens** voor alle liefde en nog zoveel meer dat ze aan haar Sammie gaf gedurende de voorbije vier jaar.

Sam Van Wassenbergh, 31 januari 2006

Curriculum Vitae



Sam Van Wassenbergh werd op 25 maart 1979 geboren in Beveren. Hij voltooide zijn middelbare studies in de richting Economie-Wiskunde aan de Sint-Maarten midden –en bovenschool te Melsele, waarna hij in 1997 Biologie ging studeren aan het Rijksuniversitair Centrum Antwerpen (RUCA). In 2001 studeerde hij af als licentiaat in de biologie aan de Universitaire Instelling Antwerpen (UIA) in de richting "Organismen en Populatiebiologie". Tijdens het laatste jaar koos hij ervoor om zijn licentiaatthesis te maken aan het Laboratorium voor

Functionele Morfologie onder begeleiding van dr. Anthony Herrel en prof. Peter Aerts en belandde zo in de wereld van de katvissen. Stevig vastgebeten in de problematiek van deze diergroep kreeg hij de kans om zijn onderzoek verder te zetten als doctoraatsstudent (2002 tot 2006). Het grootste deel van de resultaten van het uitgevoerde onderzoek staan beschreven in dit proefschrift.

